

AN ABSTRACT OF THE THESIS OF

Ning Li for the degree of Doctor of Philosophy in Horticulture presented on February 14, 1997. Title: Spectroscopy of Biophysical, Physiological and Pathological Responses of Plant Germplasm.

Abstract approved: _____

Larry S. Daley

Imaging spectra of plant tissues yield considerable potential and useful information for basic studies and agriculture practice. We constructed an imaging spectrophotometer with spectral range from 400 nm to 1100 nm, which was used to study various physiological events of plant germplasm: location of bundle sheath and mesophyll cells in sugar cane (*Saccharum officinarum* L.); chlorophyll b deficiency of ornamental perennial grass (*Millium effusum* L. var. aureum); respiration rate of soybean roots (*Glycine max* Merr. var. Yuusuzumi); concentration of azosulfamide dye of apple (*Malus domestica* Borkh. var. Red Rome) flower buds; sucrose concentration and invertase activity in stems of hazel (*Corylus avellana* L. var. Barcelona); *in vivo* effects of a fungal pathogen (*Pestalotiopsis microspora*) and its phytotoxin in the foliage of the rare nutmeg (stinking) cedar or yew of Florida (*Torreya taxifolia* Arn.) foliage; time course of water displacement by heavy water (deuterium oxide) in roselle (Jamaica sorrel, *Hibiscus sabdariffa* L.) leaves; water path estimation using mixtures of deuterium oxide.

A novel algorithm was found to measure the estimated quantum yield image (Y'). An imaging fluorometer based on this algorithm was constructed and tested for agriculture application: photoinhibition of photosynthesis, very early determination of freeze damage, herbicide effects and invasion by fungal pathogens in *Scrofularia nodosa* 'Variegata'. Excellent results were also obtained in testing four toxins: pestalopyrone, hydroxypestalopyrone, pestaloside, and triticone on three varieties (non soong, red sorrel, and altissima) on *Hibiscus sabdariffa* L. Triticone damage was still very obvious after 24 hours. Pestalopyrone effects disappear several hours after injection showing that photosynthetic function recovers rapidly from the pestalopyrone damage. Possibility of using chlorophyll protein complexes (CPX) *in vivo* for digital imaging storage, and the potential of the algorithm in remote sciences are also illustrated and discussed.

Using optical correlation interferometry, a novel method for plant sciences, we imaged *In vivo* the z-direction, perpendicular to the leaf surface, through *Tradescantia zebrina* leaves. Non-invasively we: determined the number of major cell layers, followed the time sequence of decrease in depth of the cells z-axes after exposure of tissues to high salt, and observed disruption of cells caused by freezing and thawing.

© Copyright by Ning Li
February 14, 1997
All Rights Reserved

**Spectroscopy of Biophysical, Physiological and Pathological
Responses of Plant Germplasm**

by

Ning Li

A THESIS

submitted to

Oregon State University

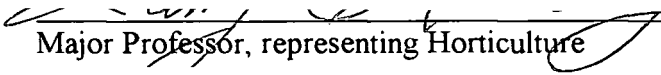
in partial fulfillment of
the requirements for the
degree of

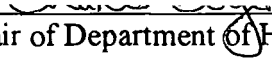
Doctor of Philosophy

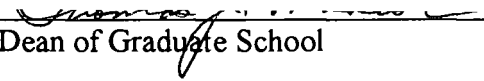
**Presented February 14, 1997
Commencement June 1997**

Doctor of Philosophy thesis of Ning Li presented on February 14, 1997

APPROVED:


Major Professor, representing Horticulture


Chair of Department of Horticulture


Dean of Graduate School

I understand that my thesis will become part of the permanent collection of Oregon State University libraries. My signature below authorizes release of my thesis to any reader upon request.


Ning Li, Author

ACKNOWLEDGEMENT

At this point, I would like to thank everyone who has been involved in this work. I would like to thank my wife, Wenqi Bao, for all her understanding and support.

I would like to thank my advisor, Larry S. Daley, for his moral and financial support during the course of my studies. I would like to thank Prof. James B. Callis, for his dedicated training on the topic of imaging spectroscopy methods. I would like to thank Prof. Gerald E. Edwards for his teaching and discussion on the subject of plant leaf fluorescence, which lead to the constructing the imaging fluorometer in the summer of 1994. I would like to thank Prof. Gary A. Strobel for his plant material and phytotoxin extractions.

I wish to express my appreciation to all who cooperated with me on my research over the years for arrangement of useful advice and discussions on a broad range of subjects, particularly: Prof. Bent Petersen for his idea on the digitizing and storing data (digits of π) on plant leaf; Walter J. Bowyer for his particular interest in the imaging fluorometer and exploration of phytotoxin bioassay; Annie M. Chozinski, Tamas Bubán, Anita Azarenko for their support and providing microphotographs of dye stained apple flower buds; E. H. Piepmeier for references on the subject of Rayleigh scattering, Zhao Lu for her help in using HP 8504A interferometer and MATLAB; Mr. Ozanich Rich for his initial work on imaging spectrophotometer on plant leaf; Prof. Sonia Anderson for her training in the course of biophysics methods; Prof. Chaur-fong Chen for his help and

suggestions in applying imaging fluorometer to remote sensing science; Mrs. Natalie Daley for her patient advice on improving my written English.

I would like to thank committee members: Prof. Tim Righetti, and Prof. Tom K. Plant, for their encouragement, interest in my research, advice, and careful planning of my study program. Thanks go also to Prof. Kelly Falkner for serving as Graduate Representative.

Funding for this research from Herman Frasch Foundation (Grant Number FRASCH 63-0738), OSU Agricultural Research Foundation, and Oregon Filbert Commission are gratefully acknowledged.

CONTRIBUTION OF AUTHORS

Ning Li was involved in the design, experimentation, analysis and writing of each manuscript. Dr. Larry S. Daley was involved in overseeing this work from its onset and in the design and analysis of experiments; and proofreading and editing of each manuscript. Although some of the other author's specific contributions are recognized in the acknowledgment section, the synergism, interaction and support of each member of this highly diverse and multidisciplinary group, although difficult to quantify and specifically assign credit, was essential to the production of this body of work. The diversity of the disciplines and the broad sweep of the experimental topics successfully addressed demonstrates the advantages and contributions of such a multidisciplinary group.

TABLE OF CONTENTS

	<u>Page</u>
CHAPTER 1: Introduction	1
CHAPTER 2: Construction Of An Imaging Visible Spectrophotometer And Its Application To Plant Sciences	15
CHAPTER 3: Five Novel Applications Of Imaging Visible And Short Near Infrared Spectrophotometry And Fluorometry In The Plant Sciences	48
CHAPTER 4: Spectroscopic Imaging Of Water In Living Plant Leaves, "Rayleigh" Corrections, And Significance For Beer's Law Based <i>In Situ</i> Quantification	113
CHAPTER 5: Imaging Fluorometer To Detect Pathologic.al And Physiological Change In Plants	174
CHAPTER 6: <i>In Vivo</i> Plant Leaf Photosynthetic Apparatus Can Store Digital Information As Fluorescence Signal	203
CHAPTER 7: <i>In Vivo</i> Imaging Of The Interior Of Tradescantia Zebrina Leaves By Optical Cross Correlation Interferometry	234
CHAPTER 8: Conclusion	252
BIBLIOGRAPHY	260

LIST OF FIGURES

<u>Figure</u>	<u>Page</u>
1.1 Cover from the journal <i>Applied Spectroscopy</i> (Volume 49 (10), October, 1995) illustrating the Photo-induced image on <i>Ginkgo</i> tree leaf	6
1.2 Cover from the journal <i>Spectroscopy</i> (Volume 11 (3), March/April, 1996) illustrating the <i>in vivo</i> measurement of water in slices of living <i>Aloe miltotii</i> leaves	10
2.1 Schematic of CCD based imaging spectrophotometer	29
2.2 Electron micrograph of bundle sheath cells and mesophyll cells and their chloroplasts	30
2.3 Spectra and chlorophyll protein complex structure	33
2.4 Spectra images of sugar cane leaf	35
2.5 Image spectra of sugar cane leaf and chlorophyll b-deficient oil yellow-yellow green (OY-YG) maize leaf	39
2.6 Respiration activity of soybean root	42
3.1 Application one: uptake of azosulfamide dye in apple flower buds	63
3.2 Model for biochemical histological changes	70
3.3 Application two: biochemical histology of invertase	73
3.4 Analysis of and calibration of spectra for fungal pathogen detection	79
3.5 Absorbance bands of water and deuterium oxide mixtures in the range of 700-850 nm	83
3.6 Application three: imaging of pathogen advance in a leaf <i>In vivo</i>	86
3.7 Application four: determination of water in a living leaf	89
3.8 Application five: demonstration of fluorescence configuration used to determine differences in photosynthetic efficiency	92

LIST OF FIGURES (CONTINUED)

<u>Figure</u>	<u>Page</u>
3.9 Data on differences in orientation of leaves of canopy and its effect on apparent quantum efficiency of photosynthesis	96
4.1 Experimental plant material	131
4.2 “Raleigh” scattering correction	134
4.3 Spectra of deuterium oxide (D-O-D), water (H-O-H) mixtures in visible and very short NIR	139
4.4a Reconstruction of spectra of deuterium oxide diluted water compared to observed data	141
4.4b Reconstruction of a series of water/deuterium oxide mixtures using the simplified method	143
4.5 Demonstration of water peak in solid substrate	147
4.6 Utility of normalization of water in wet and living substrate	149
4.7 <i>In vivo</i> tests of water content and general distribution of chlorophyll-protein complexes in leaf sections of <i>Aloe milotii</i> and a section of living leaves of <i>Scrofularia nodosa</i> ‘Variegata’	152
4.8 Mapping light harvesting (LH) chlorophyll-protein complexes (CPX) in the living leaf	159
4.9 Mapping photosystem I (PSI) chlorophyll-protein complexes (CPX) in the living leaf	162
5.1 Schematics comparing CCD based imaging fluorometer	184
5.2 Flowchart of the software used to run the instrument	187
5.2 Example of leaf fluorescent transients associated with photosynthetic apparatus	188
5.4 Y’ (Empirical estimation of quantum yield) images of freezing damaged, DCMU treated and fungal pathogen infected leaves	193

LIST OF FIGURES (CONTINUED)

<u>Figure</u>	<u>Page</u>
5.5 Imaging fluorometer used at a distance of 7 meters	196
6.1 Demonstrating the sensitivity of the imaging fluorometer: photo-induced "Birth of Venus" image on a living tobacco leaf	216
6.2 The mask used to code 100 digits of π apparent quantum efficiency of photosynthesis	221
6.3 The process of preparation of the image for machine reading	224
7.1 Optical cross correlation interferometer response in model system	240
7.2 Optical image fit to optical cross correlation interferometer response of <i>Tradescantia zebrina</i> leaves	243
7.3 Time sequence histogram of optical cross correlation images (z-axis) as a silver section of the leaf immersed in 15% sodium chloride solution	245
7.4 Optical cross correlation images (z-axis) of a silver section of the leaf before and after freezing, and then when thawed	248

DEDICATION

To my beloved father:

Chuei-Tong Li

SPECTROSCOPY OF BIOPHYSICAL, PHYSIOLOGICAL AND PATHOLOGICAL RESPONSES OF PLANT GERMPLASM

CHAPTER 1

INTRODUCTION

To achieve the goal of the germplasm characterization by *In vivo* methods, it was necessary to develop new spectroscopic equipment to explore the biochemistry, physiology and pathology of the plant germplasm.

Photosynthetic processes of the plant leaf supports essentially all life on Earth. The light gathering part of the photosynthetic processes has strong signals in the visible and near IR range. These signals have a rich and complex structures which change to reflect the health of the leaf and the plant's adaptation to environmental conditions (Greene *et al.* 1988, Osmond *et al.* 1990, Mawson *et al.* 1994). The signals are not distributed evenly across the leaf, but vary spatially in ways that are diagnostic of leaf health, function and insect predation (Mawson *et al.* 1994). Thus, two or three dimensional spectroscopy would be very useful to distinguish these localized signals.

One of the most readily accessible and useful absorbance (and fluorescence) signals arising from plant tissues is that of the chlorophyll protein complexes of the photosynthetic apparatus. Daley *et al.* (1986) has combined his work with the data of others to interpreting the second and fourth derivative visible spectrum in terms of chlorophyll protein complexes (CPX) and to relate this to selected aspects of plant pathology and physiology, and applied agricultural concerns (Eskelsen *et al.* 1994).

Imaging acquisition and analysis are powerful analytical tools to determine the chemical concentrations distributed in two-dimensional space. Imaging instruments have been built to study the physiology of whole body systems (Wolf *et al.* 1992), biophysics of DNA (Jordan *et al.* 1992), and the biochemistry of calcium (Borst and Egelhaaf 1992). For remote sensing, the Airborne Visible/Infrared Imaging Spectrometer was built to acquire images over large areas using the full solar spectrum; data from this spectrophotometer proved to be very useful in ecology, hydrology, oceanography, atmospheric sciences (Vane and Goetz 1993), and biology (Elvidge *et al.* 1993, Hamilton *et al.* 1993).

Some years ago Callis and Burkner experimented with various designs for an imaging spectrophotometer (Callis and Burkner 1983). They concluded that the combination of a continuously tunable monochromatic light with a thermoelectric-cooled CCD detector offered the best approach (Gianelli *et al.* 1983). This configuration had been used for quantitative estimation of analyses on thin layer chromatography plates. The data obtained could be represented as a stack of monochromatic images and could be processed in a number of ways (Burns *et al.* 1986) and plotted as composite, false colored images or as spectra associated with a specific spatial address on the plate. Later, a field portable version of this instrument was constructed for the USDA for determination of sulfonamide drugs used in slaughter houses (Aldridge *et al.* 1990). Application of this same principle lead to the development of a multi-wavelength "imager" to analyze the depth and extent of burn wounds in humans (Afromowitz *et al.* 1988).

N.J.C. Müller (1874) visually observed chlorophyll fluorescence changes in green leaves using a combination of colored glasses (Bolhar-Nordenkamp and Oquist 1993).

By the 1920s, fluorescence microscopy allowed practical investigations of fluorescence excited by UV-A or blue light. When thin slices of leaves were examined their photosynthetic tissues emitted red fluorescence. Kautsky and Hirsch (1934) exposed dark-adapted leaves to light and generating time dependent fluorescence transients.

Photosynthetic processes absorb broadly across the visible range. Photosystems 'funnel' light to their reaction centers (RC) (Taiz and Zeiger 1991, Bolhar-Nordenkamp and Oquist 1993). When RC are maximally available (open) and when the light intensity is limited, about 97% of absorbed light is used for photochemistry, 2.5% is transformed to heat, only 0.5% re-emitted as red fluorescence (Bolhar-Nordenkamp and Oquist 1993). If RC are not available (closed) 90-95% of absorbed light may be 'deactivated via heat' and 2.5-5% via fluorescence (Bolhar-Nordenkamp and Oquist 1993). Darkening the leaf before fluorescent measurements assures open RCs; then on illumination complex, time and wavelength variable, fluorescence is produced (Bolhar-Nordenkamp and Oquist 1993). These complex fluorescence signals in a given plant are functions of the structure and potential for activity of the photosynthetic apparatus, the demands of the "dark reaction", the health of the leaf and the plant's adaptation to environmental conditions and vary across the leaf lamina in ways diagnostic of leaf function (Havaux and R. Lannoye 1984, Omasa *et al.* 1987, Bolhar-Nordenkamp and E.G. Lechner 1988, Daley *et al.* 1989, Ghirardi *et al.* 1988, Osmond *et al.* 1990).

Fluorescence is photochemical quenched when the light is used to drive the electron transport chain of the photosynthetic "light reaction" (Papageorgiou 1975). Thus, fluorescence intensity from Photosynthesis System II (PSII) increase when high

temperatures, chilling, freezing, drought or excess radiation (Havaux and Lannoye 1984, Smillie 1979, Powles 1984) decrease photosynthesis.

Fluorescent and absorption spectroscopy of leaves reveal different aspects of leaf structure and function. Both methods are useful and their capabilities overlap. However, fluorescence is most frequently used to measure transitory photosynthetic functions (Daley *et al.* 1989), while absorption (here 3D attenuation) more readily measures the more permanent structures of the photosynthetic system (Daley 1990).

Fluorescence imaging devices for plant leaf function have been known for at least 7 years (Daley 1989, Fenton and Crofts 1990). Fluorescence imaging can screen photosynthetic bacteria seeking highly fluorescent, low photosynthetic efficiency mutants (Fenton *et al.* 1990, Youvan *et al.* 1983). Imaged chlorophyll fluorescent transients diagnose effects of herbicides and industrial pollutants on leaves (Omasa *et al.* 1987).

Non-photochemical quenching (qn) could be empirically estimated in image level (P.F. Daley 1989). This parameter is useful because (1-qn) can positively correlate photosynthesis rate (Weis and Berry 1987, Horton and Hague 1988). However, when the leaf is under stress this correlation to photosynthetic rate may not hold. For example, after treatment with the powerful herbicide DCMU (3-(3,4- dichlorophenyl)-1,1-dimethyl urea) treatment, qn is low, therefore (1-qn) is high; yet we know that high (1-qn) does not predict high photosynthesis, after all DCMU is a herbicide that interrupts photosynthesis.

In important crop plants with C-4 metabolism, fluorescence can also measure the "dark reaction". This is because in C-4 plants most electron flow through PSII is used, via PSI, to make the NADPH for the "dark reactions" of carbon assimilation. Thus, PSII quantum yield can be closely correlated to the CO₂ fixation (Edwards and Baker 1993).

That means if we could measure the PSII quantum yield in two-dimensional level, we could visualize photosynthesis rate on leaf. During a summer in Professor Gerry Edwards' laboratory, (Washington State University, Pullman, Washington), it was found that PSII quantum yield can be imaged. This value estimates of the true quantum yield as empirical estimated quantum yield(Y'). Excellent results were obtained by introducing this new physiological parameter. Y' is very sensitive to freeze damage, herbicide exposure, fungal disease and other plant stress. Since previous light could decrease the quantum yield, we were able to record photo-induced image on a leaf (figure 1.1).

The changes in depth of the leaf (z-axis) is also important because leaf cell biochemistry is most frequently specialized in tissues perpendicular to this axis. Many approaches are available to image along the z-axis as well as the conventional x and y axes.

To mechanically slice the sample into sections perpendicular to the z-axis is destructive and thus, reveals data from only one instant in time for each set of tissue slices. This, because of biological variability between tissue samples, introduces unwanted variables into the composite time sequences generated from the pooled samples. In optical tomography (e.g. Burns 1994), straight forward use of parallel sheets of light becomes problematic for small objects. Therefore, using a microscope, one captures a series of optical slices by simple varying the focal distance; then one corrects the images for above and below plane out of focus contributions (Castleman 1979). The resulting stack of 2-D images can then be rendered into 3-D images using the same techniques that magnetic resonance imaging (MRI, see Treado *et al.* 1994) uses to make 3-D images. Thus, complete optical characterization of leaves requires z-direction data.

Figure 1.1. Cover from the journal *Applied Spectroscopy* (Volume 49(10), October, 1995) illustrating the photo-induced image on *Ginkgo* tree leaf. Strong light also leaves “memory” images, as illustrated, where a transparency mask, prepared with a color copier, was placed over a *Ginkgo biloba* leaf. The leaf was illuminated through the mask for three minutes. The mask was removed and then the leaf’s pattern of estimated quantum efficiency (Y’) was determined by the fluorometer, as described in the paper “Imaging Fluorometer to Detect Pathological and Physiological Change in Plants”, by Ning, Daley, Edwards, Strobel, and Callis (Ning et al 1995b).

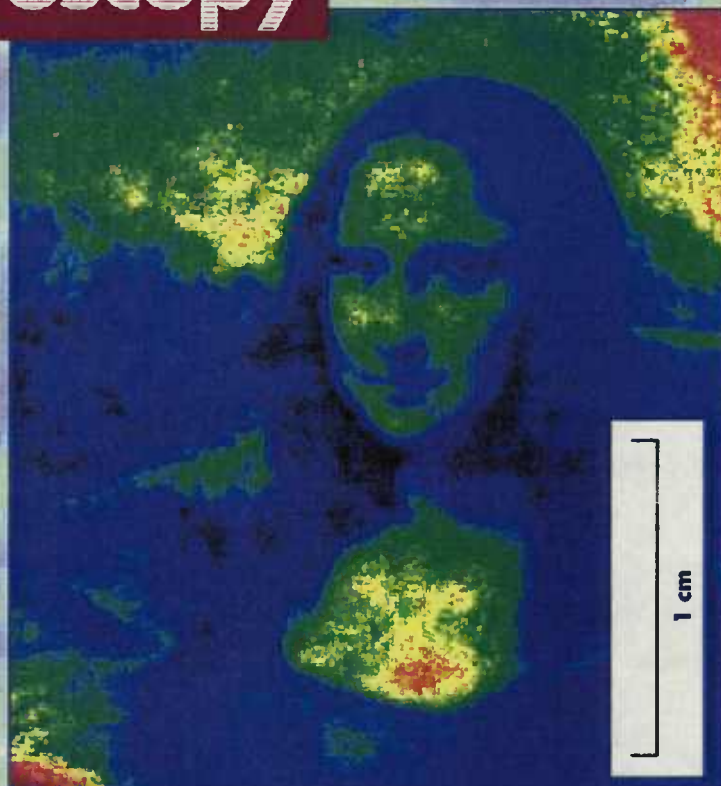
applied spectroscopy

49/10OCTOBER 1995
ISSN: 0003-7028

An International
Journal of Spectroscopy



FOCAL POINT:
IPC Emission
Spectrometers:
1995 Analytical
Figures of Merit



Photon-induced Image on *Ginkgo* Tree Leaf

Official Publication of the Society for Applied Spectroscopy

One can get z-axis data by tracing photon flow through samples. A way to do this is to give a pulse of light and time photon arrival. This requires super fast electronics to measure small objects, i.e. to resolve one micron requires 4×10^{-15} s timing. Light pulses of a duration this short require very expensive, and not easily portable, laser technology (Savikhin *et al.* 1994). There is an alternative way: non-monochromatic light undergoes random fluctuations on a time scale set by the inverse bandwidth of the light source (Chamberlain *et al.* 1979). These fluctuations can be characterized by their correlation time τ given by the equation: $\tau = \lambda^2 / (\pi \Delta \lambda c)$, Here λ is wavelength, $*$ indicates multiplication, and c is the speed of light, which in a vacuum is 2.998×10^8 meters per second, approximated here as $3 \times 10^8 \text{ m} \cdot \text{s}^{-1}$. Thus, for a center wavelength of 450 nm, and a band width of 90 nm, $\Delta \lambda = 90 \text{ nm}$; we can approximate: τ as $(450 \text{ nm})^2 / (\pi \cdot 90 \text{ nm} \cdot 3 \times 10^8 \text{ m} \cdot \text{s}^{-1}) = 2.38 \times 10^{-15} \text{ s}$, which is enough time resolution for a spatial resolution of better than a micron.

A fluctuating light source can replace pulse light as the probe. From linear systems theory (Yu 1973), it can be shown that one can do the equivalent to an impulse response experiment, by cross correlating the random probe beam with the output beam. It is not yet possible to perform the cross correlation in the time domain because detectors of sufficiently wide bandwidth and means to record the waveforms do not exist. Instead we use the spatial domain with a Michelson interferometer (Chamberlain *et al.* 1979) as an analog computer of the cross correlation function. This device, developed to test fiber optic instrumentation, had been used to profile human skin in depth (Schmitt *et al.* 1993).

The specific aims of this thesis are:

1. Construct an imaging spectrophotometer, employing a charge-coupled device (CCD) camera to provide high quality spectral images of leaf samples (Ning *et al.* 1994). The instrument will be tested to detect the sugar cane (*Saccharum officinarum* L.) bundle sheath cells from mesophyll cells; obtain spectra of a full sun tolerant, chlorophyll b deficient ornamental perennial grass (*Milium effusum* L. var. aureum); estimate the relative respiration rate of plant roots; study the xylem development in apple (*Malus domestica* Borkh. var. Red Rome) flower buds; determine (in situ) sucrose and invertase activity in stems of hazel (*Corylus avellana* L. var. Barcelona); detect *In vivo* effects of a fungal pathogen (*Pestalotiopsis microspora*); test phytotoxin in the foliage of the rare nutmeg (stinking) cedar or yew of Florida (*Torreya taxifolia* Arn.) foliage; trace the water displacement by heavy water (deuterium oxide) in roselle (*Jamaica sorrel*); determine the water in living plant tissues (figure 2.1); estimate biochemically active path length of light in plants; compare chlorophyll-protein complex structure and function between different hue-domains of variegated leaves.

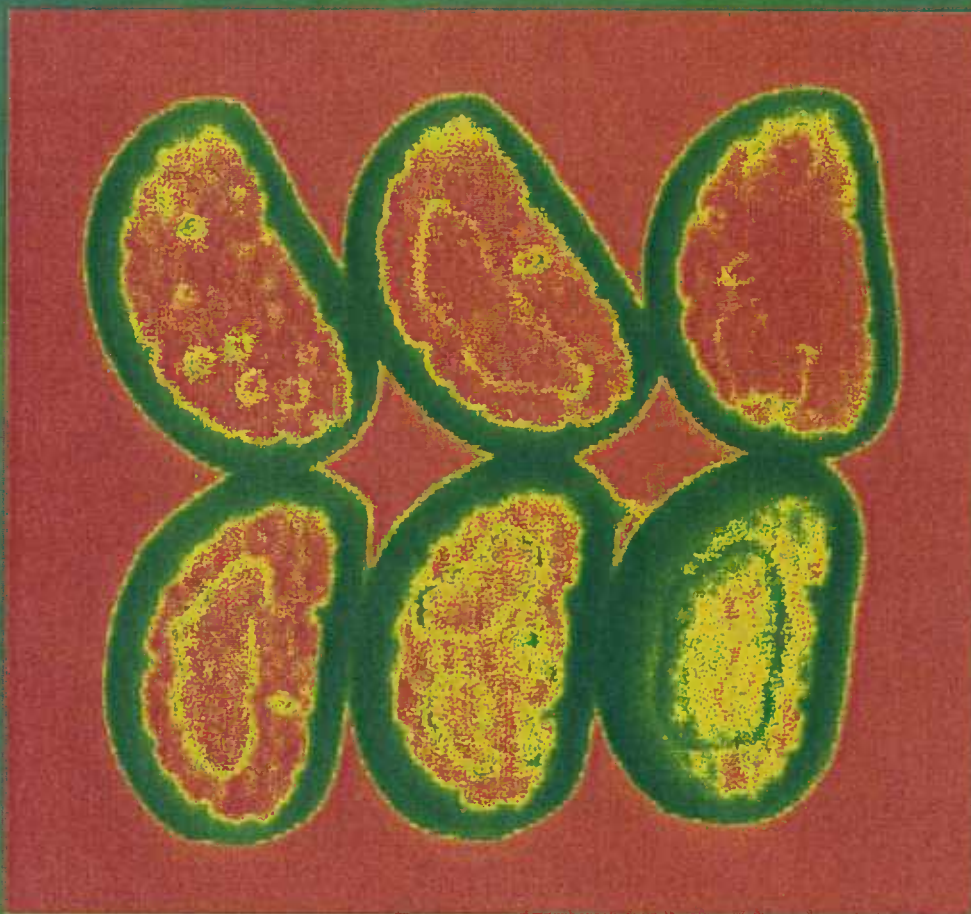
2. Built an imaging fluorometer to measure the estimated quantum yield (Ning *et al.* 1995). This instrument could be used in research laboratory and agriculture, and will demonstrated: very early determination of freeze damage, herbicide effects and invasion by fungal pathogens. In an extension of this application, the instrument will be used to explore the potential value of biological media for digital storage, and to investigate the possible application in remote sensing science.

3. Image the z-direction, by an optical correlation interferometry, through *Tradescantia zebrina* leaves. With a HP reflectance interferometer, the structure and the changes of major cell layers will be studied, after high salt, freezing and thawing treatment.

Figure 1.2. Cover from the journal *Spectroscopy* (Volume 11 (3), March/April, 1996) illustrating the *in vivo* measurement of water in slices of living *Aloe miltotii* leaves. The middle area of each leaf slice shows the so called water cells characteristic of these plants (see Chapter 4).

MARCH/APRIL 1996 Volume 11 Number 3

Spectroscopy



Special Issue:
***Imaging and
Microspectroscopy***

U.S. \$12
AN ADVANTAGE PUBLICATION

REFERENCES

- Afromowitz M.A., J.B. Callis, D.M. Heimbach, L.A. Desoto, and M.K. Norton, 1988, *IEEE Transactions on Biomedical Engineering* 35:842.
- Aldridge P.K., J.B. Callis, and D.H. Burns, 1990, *J. Liq. Chrom.* 13:2829.
- Bolhar-Nordenkamp H.R. and E.G. Lechner, 1988, "Winter Stress and Chlorophyll Fluorescence in Norway Spruce (*Picea abies* (L.) Karst)", in *Applications of Chlorophyll Fluorescence*, (H.K. Lichtenthaler Ed.), Kluwer Academic Publ., Dordrecht, Holland, pp. 173:180.
- Bolhar-Nordenkamp H.R. and G. Oquist, 1993, "Chlorophyll Fluorescence as a Tool in Photosynthesis Research," in *Photosynthesis and Production in a Changing Environment, a Field and Laboratory Manual*, (D.O. Hall, J.M.O. Scurlock, H.R. Bolhar- Nordenkamp, R.C. Leegood and S.P. Long, Eds.), Chapman and Hall, London, Chap. 12, pp. 193:206.
- Borst A., and M. Egelhaaf, 1992, *Proc. Natl. Acad. Sci. USA* 89:4139.
- Burns D.H., J.B. Callis, and G.D. Christian, 1986, *Anal. Chem.* 58:2805.
- Burns, D. H, 1994, *Appl. Spectrosc.* 48(5):12A.
- Callis J.B., and A.P. Burkner, 1983, *ACS Symp. Ser.* 236:233.
- Castleman K.R., 1979, *Digital image processing*, Prentice-Hall, Inc, Englewood Cliffs, NJ.
- Chamberlain J., 1979, *The principals of interferometric spectroscopy*, John Wiley, New York, NY.
- Daley L.S., 1986, *Scientia Hort.* 28:165.
- Daley L.S., 1990, *Plant Physiol. Biochem.* 28(2):271.
- Daley P.F., K. Raschke, J.T. Ball, and J.A. Berry, 1989, *Plant Physiol.* 90:1233.
- Daley P.F., K. Raschke, J.T. Ball, and J.A. Berry, 1989, *Plant Physiol.* 90:1233.

- Edwards G.E., and N.R. Baker, 1993, *Photosynthesis Research* 37:89.
- Elvidge C.D., Z. Chen, and D.P. Groeneveld, 1993, *Remote Sens. Environ.* 44:271.
- Eskelsen S.R., G.D. Crabtree, R.B. Boone, G.M. Volk, L. Ning and L.S. Daley, 1994, *Spectroscopy* 7(2):34.
- Fenton T.J., and A. R. Crofts, 1990, *Photosynth. Res.* 26:59.
- Ghirardi M.L., and A. Melis, 1988, *Biochim. Biophys. Acta* 932:130.
- Gianelli M.L., D.H. Burns, J.B. Callis, G.D. Christian, and N.H. Andersen, 1983, *Anal. Chem.* 55:1858.
- Greene B.A., L.A. Staehelin, and A. Melis, 1988, *Plant Physiol.* 87:365.
- Hamilton M.K., C.O. Davis, W.J. Rhea, S.H. Pilorz, and K.L. Carder, 1993, *Remote Sens. Environ.* 44:217.
- Havaux M., and R. Lannoye, 1984, *Photosynthetica* 18:117.
- Horton P., and A. Hague, 1988, *Biochem. Biophys. Acta* 932:107.
- Jordan E.G., O.V. Zatsepina, and P.J. Shaw, 1992, *Chromosoma* 101(8):478.
- Kautsky H. and A. Hirsch, 1934, *Biochem. Zeitschrift* 274:423.
- Mawson B.T., P.J. Morrissey, A. Gomez and A. Melis, 1994, *Plant Cell Physiol.* 35:341.
- Müller N.J.C., 1874, *Jahrbuch wiss Botanik* 9:42.
- Ning L., G. E. Edwards, G.A. Strobel, L.S. Daley, and Callis, J. B., 1995, *Applied Spectroscopy*, 48:1381.
- Ning L., R. Ozanich, L.S. Daley and J.B. Callis, 1994, *Spectroscopy* 9(7):41.
- Omasa K., K. Shimazaki, L. Aiga, W. Larcher and M. Onoe, 1987, *Plant Physiol.* 84:748.
- Osmond C.B., J.A. Berry, S. Balachandra, C. Buchen-Osmond, P.F. Daley, and R.A. Hodgson, 1990, *Bot. Acta* 103:226.
- Papageorgiou G., 1975, "Chlorophyll Fluorescence: an Intrinsic Probe of Photosynthesis," In *Bioenergetics of Photosynthesis*, (Govindjee ed.), Academic Press, New York, p. 319-371.

- Powles S.B., 1984, *Ann. Rev. Plant Physiol.* 35:14.
- Savikhin S., Y. Zhu, S. Lin, R.E. Blankenship, and W.S. Struve, 1994, *J. Phys. Chem.* (in press).
- Schmitt J.M., A. Knuttell, and R.F. Bonner, 1993, *Applied Optics*, 32:6032.
- Smillie R.M., 1979, "The Useful Chloroplast: a New Approach for Investigating Chilling Stress in Plants", in *Low Temperature Stress in Crop Plants*, (J.M. Lyons, D. Graham and J.K. Raison ed.), Academic Press, New York, p. 187-202.
- Taiz L. and E. Zeiger, 1991, *Plant Physiology*, Benjamin/Cummings Pub. Co., Inc., Redwood City, California, Chap. 8-10, p. 177.
- Treado P.J., I.W. Levin and E.N. Lewis, 1994, *Appl. Spectrosc.* 48(5):607.
- Vane G., and A.F.H. Goetz, 1993, *Remote Sens. Environ.* 44:117.
- Weis E., and J.A. Berry, 1987, *Biochim. Biophys. Acta* 894:198.
- Wolf R.F.E., K.H. Lam, E.L. Mooyaart, R.P. Bleichrodt, P. Nieuwenhuis and J.M. Schakenraad, 1992, *Laboratory Animals* 26(3):222.
- Youvan D.C., J.E. Hearst and B. L. Marrs, 1983, *J. Bacteriol.* 154:748.
- Yu F.T.S., 1973, *Introduction to diffraction, information processing and holography*, MIT Press, Cambridge, MA.

CHAPTER 2

CONSTRUCTION OF AN IMAGING VISIBLE SPECTROPHOTOMETER
AND IT APPLICATION TO PLANT SCIENCES

Ning, L.¹, Ozanich, R.², Daley, L. S.¹ and Callis, J. B.³

¹Department of Horticulture, ALS 4017, Oregon State University, Corvallis, OR 97331.

²Earth and Environmental Sciences Center, Battelle, Pacific Northwest Laboratories, Richland, WA 99352.

³Department of Chemistry, University of Washington, Seattle, WA 98195.

Published in *Spectroscopy*,
Advanstar Communications, Eugene, O.R.
September 1994, 9(7):41-48.

CONSTRUCTION OF AN IMAGING VISIBLE SPECTROPHOTOMETER AND IT APPLICATION TO PLANT SCIENCES

Ning, L.¹, Ozanich, R.², Daley, L. S.¹ and Callis, J. B.³

¹Department of Horticulture, ALS 4017, Oregon State University, Corvallis, OR
97331.

²Earth and Environmental Sciences Center, Battelle, Pacific Northwest Laboratories,
Richland, WA 99352.

³Department of Chemistry, University of Washington, Seattle, WA 98195.

Visible spectra of plant leaves yield information with considerable potential for improving agricultural production. Since the related spectral information contained in leaves is distributed unevenly across the surface of the leaf, we constructed an imaging spectrophotometer. This instrument employs a charge-coupled device (CCD) camera, which can acquire spectra for 31,680 positions per sample. Fully computer interfaced, it provides high quality spectral images of leaf samples. The instrument was tested using *in vivo* spectra of plants, since *in vivo* absorbance between 600 and 750 nm are associated with photosynthetic light gathering systems. In sugar cane (*Saccharum officinarum* L.), a C-4 plant, patterns consistent with resolving bundle sheath cells from mesophyll cells were found using equation: $((A_{684\text{nm}} - A_{700\text{nm}}) - (A_{650\text{nm}} - A_{638\text{nm}})) / A_{680\text{nm}}$, where each component represents attenuance ($\sim A$) at each wavelength. Difference spectra of leaf areas showing these different cell types were obtained and compared to spectra of a full

sun tolerant, chlorophyll b deficient ornamental perennial grass (*Millium effusum* L. var. aureum) and the published spectra of chloroplasts of OY-OG chlorophyll b deficient mutant of *Zea mays* L. Excellent results were also obtained when the relative respiration rate of plant roots was determined by measuring pH dependent absorbance of a dye impregnated agar matrix around the roots. The pH sensitive dye, resazurin (7-hydroxy-3H-phenoxazin-3-one 10-oxide), changed color to reveal the localized pH changes around soybean (*Glycine max* Merr. var. Yuusuzumi) root. These pH changes are consistent with the expected respiratory activities of the different parts of the root.

INTRODUCTION

We constructed an imaging spectrophotometer to quantify the interaction between spatial and spectroscopic characteristics of leaves so as to generate quantified images. These quantified images detect changes related to function and pathology of plants. These changes have considerable applied and scientific interest. The purpose of this instrument is to support scientific research in plant physiology and biophysics and help improve present agricultural practices.

Plant leaves, using their photosynthetic apparatus, convert light into chemical energy used to make food, and in the process generate oxygen from water. Through these photosynthetic processes the plant leaf supports essentially all life on Earth. The light gathering part of the photosynthetic processes has strong signals in the UV-visible range. These signals have a rich and complex structures which change to reflect the health of the leaf and the plant's adaptation to environmental conditions¹⁻³. The signals are not

distributed evenly across the leaf, but vary spatially in ways that are diagnostic of leaf health, function and insect predation³.

Imaging acquisition and analysis are powerful analytical tools to determine the chemical concentration distribution in two-dimensional space. Imaging instruments have been built to study the physiology of whole body systems⁴, structure and function of DNA⁵, and the dynamics of calcium accumulation⁶. For remote sensing purposes, the Airborne Visible/Infrared Imaging Spectrometer was built to acquire images over large areas using the full solar spectrum; data from this spectrophotometer proved to be very useful in ecology, hydrology, oceanography, atmospheric sciences⁷, and biology^{8,9}. Fluorescent imaging devices for plant leaf function have been known for at least 5 years^{10,11}. Fluorescent and absorption spectroscopy of leaves reveal different aspects of leaf structure and function. Both methods are useful and their capabilities overlap. However, fluorescence is most frequently used to measure transitory photosynthetic functions¹⁰, while absorption (here attenuation) more readily measures the more permanent structures of the photosynthetic system¹². We expect that eventually hand held instrumentation to examine the living leaf will incorporate both of these imaging technologies plus others such as light scattering and refractive index, or even imaging NMR¹³⁻¹⁵. This may at first seem far fetched science fiction as in the omnipotent "tricorder" of Star Trek fame. However, we already have hand-held spectroscopic devices of many sorts¹⁶ that perform such functions as determination of chlorophyll, wheat protein, blood glucose or body fat *in vivo* or determine gasoline octane. Development of hand held instruments with more elaborate abilities and which will display images of complex biological functions are expected in the relatively near future.

The *in vivo* spectra of leaves is interpretable in terms of pigments and pigment complexes, e.g., electronic transitions of chlorophylls, cytochromes, carotenoids and various accessory pigments^{12,17-33}. We have combined our work with the data of others to interpreting the second and fourth derivative visible spectrum in terms of chlorophyll protein complexes (CPX) and to relate this to selected aspects of plant pathology and physiology¹², and applied agricultural concerns³³.

Events that alter leaf condition, usually have accompanying spatial as well as spectroscopic changes. Thus each spectroscopic change has a spatial distribution which may differ at various wavelengths. For example a fungal attack may present itself as a series of small black dots (necrotic areas), each surrounded by a ring of localized resistance³⁴; viral infection as a series of splotches across the leaf^{3,34}; fertilizer deficiency may show symptoms localized only along leaf veins or leaf margins³⁴, etc. To detect such differences an instrument must be capable of recording the spectrum over two-dimensional space.

BRIEF INTRODUCTION TO CO₂ FIXATION FOR SPECTROSCOPISTS.

Spectroscopy is beginning to be used, not only to analyze chemical components in harvested crops, but in the field to direct agricultural sprays³⁵. Spectroscopists seeking to advance these applications face massive amounts of complex data on plants not yet well resolved into coherent concepts and principals as is common in chemistry and physics. Plants have at least three general paths of carbon metabolism (C-3, C-4 and CAM)³⁶, but there may be others³⁷. The C-3 and C-4 refer to the number of carbons in first

carboxylation product and CAM to Crassulacean Acid Metabolism. This division into C-3, C-4 and CAM is not only of academic interest, but is very important in agriculture. Major crops are usually C-4, such as corn (maize) or sugar cane or C-3 such as grapes, lettuce, potatoes, rice, soybeans, rice, wheat. Economically important weeds are usually C-3 or C-4 also. In many cases C-3 weeds grow in C-4 crops and C-4 weeds grow among C-3 crops. These paths of carbon metabolism are fueled by the light gathering capacity specially adapted arrays of CPX, that vary in spatial distribution and thus are important when imaging spectra of leaves. Differences in spatial distribution of CPX in C-4 plants arises from the two different ways of gathering CO₂ from the atmosphere. C-3 plants carboxylate almost entirely using the less efficient, but more directly usable, carboxylating enzyme ribulose biphosphate carboxylase (RuBPCase); although they do have phosphoenolpyruvate carboxylase (PEPCase) activities. Both C-4 and CAM perform a preliminary enrichment process using PEPCase and the products of this carboxylation are then decarboxylated under more enclosed conditions to enrich and increase the carboxylation productivity of RuBPCase. CAM plants keep these two carboxylating processes separate by using PEPCase at mainly at night and RuBPCase in the day. C-4 plants physically separating most these activities in different parts of the tissue: PEPCase function is enhanced in the mesophyll and RuBPCase function in bundle sheath (Kranz) cells. C-3 plants limit these enrichment type processes mainly to the guard cells that control gas exchange in a single cell type CAM like process³⁸.

A rule of thumb that helps a spectroscopist mentally organize the complexities and distinctions among the C-3, CAM and C-4 metabolic paths is to view CAM as the ancient original path, then C-3 is CAM with the PEPCase function curtailed to guard cells or lost

and C-4 is a specially adapted, very low CO₂ tolerating, CAM where space rather than time separates functions. This ancient CAM path is considered here in this rule of thumb, although not in the principle dogma of the field³⁹, to be coded in to the DNA of all higher plants, but variable activated: limited to stomatal guard cells in C-3³⁸, as full blown CAM in CAM plants, or as modified and split spatially into two cell types in C-4 plants.

This rule of thumb is an expansion of the Cockburn hypothesis³⁸, and is consistent with: (a) arguments of facilitation that recognize that evolution of CAM predates C-4 evolution⁴⁰. (b) Existence of CAM or CAM like metabolism in early primitive plants such as Isoetes, Pyrrosia (ferns), Welwischia (gymnosperm)^{41,42}. (c) The much better adaptation of CAM plants, vs C-3 or C-4 plants, to the expected primeval Silurian land conditions: high atmospheric CO₂, frequent drought due to the low water retaining capacity of the undeveloped primeval soils or rigolith, and high salt environments⁴³⁻⁴⁵ close to the primordial sea. (d) This view avoids the need to postulate multiple, separate, initiation of converging evolution of CAM in many unrelated species³⁹, and (e) can much more readily explain why guard cells of C-3 plants, found in the desert like microenvironment⁴¹ on the exposed surface of the leaf, express CAM like metabolism. Therefore this view, or rule of thumb, is a simpler hypothesis and therefore the more likely to be correct (Ockham's Razor^{46,47}, William of Ockham).

Spectroscopically the C-4 plant leaf can be looked at as a striped mosaic in which different groups of cells carry out different parts of CAM. Because of the different energy requirements of their different carboxylation processes the different groups of cells derive their energy from light trapped by different proportions of CPX. The different proportions of CPX then yield different proportions of spectral signals which will be shown to be

detectable by our imaging instrument. Thus, this phenomenon then has the potential to be used in applied agricultural sensing to distinguish C-3 crops from C-4 weeds and vice versa.

Today less precise evaluation of these leaf signals and other indicators of plant health is done by eye by a trained observer in an expensive and time consuming process called field scouting. Most US crops have tentative spray, irrigation and fertilizer schedules that suggest amounts and timing for the application of agricultural inputs, such as fertilizer, water and pesticides. Scouting provides information to modify these schedules to attempt to maximize productivity of individual growers. Scouting may be supplemented by more precise analyses in distant laboratories. Then the modified schedule is carried out by applying agricultural inputs uniformly on entire fields.

Yet today already possible to locate and spray weeds outside of rows³⁵. However, much more could be done in the future, since automated interpretation of leaf function and health from leaf images has great potential in robotic agriculture. Robotic agriculture allows supply of an individual mix of agricultural inputs to each plant in every part of the field. For example: pesticides can be applied rapidly just to the affected plants, killing pests before they spread; or fertilizer mix and water can be supplied only as is required by each plant. This drastically reduces amounts of pesticides used, could reduce run off of excess fertilizer, and reduces amount of water required. However, to do this a robot must receive and process information on the conditions of each plant. This is where an imaging spectrophotometer is potentially useful. Plants adapt to their environment, and as each plant adapts to constantly changing conditions, such as availability of each nutrient

(fertilizer) in soil, water potential, and light environment, pest attack and pathogen infection, etc., the leaf spectra changes. Weeds and crop plants with different metabolism could be distinguished. Thus, interpretation of leaves spectra of each individual plant could guide robots dispensing agricultural inputs to each plant or group of plants as needed.

Some years ago Callis and Burkner experimented with various designs for an imaging spectrophotometer⁴⁸. They concluded that the combination of a continuously tunable monochromatic light with a thermoelectric-cooled CCD detector offered the best approach⁴⁹. This configuration had been used for quantitative estimation of analyses on thin layer chromatography plates. The data obtained could be represented as a stack of monochromatic images and could be processed in a number of ways⁵⁰ and plotted as composite, false colored images or as spectra associated with a specific spatial address on the plate. Later, a field portable version of this instrument was constructed for the USDA for determination of sulfonamide drugs used in slaughter houses⁵¹. Application of this same principle lead to the development of a multi-wavelength "imager" to analyze the depth and extent of burn wounds in humans⁵².

INSTRUMENTATION AND PLANT MATERIALS

Hardware We constructed an imaging spectrophotometer based on Callis and Burkner's design⁴⁹. A block diagram (Figure 1) shows the prototype instrument. The light sources is a 500 W, 120 volt projector lamp (model CZX/DAD, GTE Products Inc. Winchester, KY). In the configuration, light from the monochromator is focused on to

one end of an optical fiber bundle (12mm outside bundle, 1m in length). The other end of the fiber is mounted 15 centimeters away from the sample. The transmitted light through the sample is focused on to a CCD chip for spectra readout. We used a thermoelectric cooled 12 bit CCD camera (Lynxx PC, CCD Digital Imaging System, SpectraSource Instruments, Westlake Village, CA), and a CCD with a spatial resolution of 165*192 (31,680 pixels). An IBM/PC compatible computer (Pentium^R chip, 90 MHz) controlled the CCD camera through an interface board (Lynxx PC, SpectraSource Instruments). The computer also controlled the movement of a step motor (model HY 200, Oregon Microsystems, Beaverton, OR) used to drive the monochromator (Jarrell Ash single monochromator, model No. 82-410, Scientific Measurement Systems, Grand Junction, CO). Collected image data were stored as image files in removable 88 Mbytes SyQuest cartridge (Model SQ800 on the corresponding internal drive, SyQuest technology, Fremont, CA) for easy access. Standard *in vivo* leaf spectra were obtained from leaf samples with a Shimadzu 3100 (Shimadzu Scientific Instruments, Columbia, MD) using an integrating sphere to minimize optical artifacts (e.g. Eskelsen),

Software The program controlling the instrument was written using Borland C++ 4.0. The program, which is available from one of us (L.N), can be modified to achieve optimal analysis time. Data were retrieved and processed using a numerical software package called MATLAB (The MathWorks, Inc., Natick, MA).

Acquiring spectral images It takes four steps to get an imaging spectra. First we set parameters. For example, the imaging spectrophotometer is set to take a series of images from 750 nm to 600 nm at one nm intervals, this takes an acquisition time of approximately 15 minutes for physiological quality images. We set the exposure time to 6

seconds, taking care to avoid overexposure, because we use a 12 bit CCD, that will saturate if the intensity is more than 4095 counts. Each image is acquired 10 times, and the average image stored, higher absorbing leaves require more acquisitions. Second we obtain 'dark current' background. The CCD has a background of approximately 150 counts per 6 seconds, independent of the input light wavelength. Third we obtain the transmitted light intensity data, from this the attenuance ($\sim A$) of the sample can be calculated as described below.

After images are acquired, the CCD files were translated into MATLAB files and then processed. MATLAB functions were developed so that the spectra of one pixel of a selected area of pixels could be retrieved. For quicker processing, data structure was changed. The data was stored, on SyQuest removable drives, as spectra data at specified pixels (e.g. the matrix dimension: absorption at 151 wavelengths for each of 31,680 pixels), instead of frame data (151 frames taken at a specific wavelength, each frame 31,680 pixels). The new structure increased spectra extraction speed ten fold. This is important when average spectra of thousands of pixels is required.

Calculation of attenuance The data collected by the imaging spectrophotometer consist of an ordered sequence of transmission images of the sample, each at a specific wavelength. The resultant data may be represented as a three-dimensional array, T^{trans} :

$$T^{\text{trans}} = \{I^{\text{trans}}_{xyk} - I^{\text{dark}}_{xy}\} \quad (i)$$

where I^{trans}_{xyk} is the array element that corresponds to intensity of the light transmitted through the sample located at position x ($1 < x < 165$), y ($1 < y < 192$) at wavelength k ; and I^{dark}_{xy} is the array element that measures intensity of the CCD "dark current".

To find absorbance of the sample, we calculate input light intensity array T^{in} .

$$T^{in} = \{I_{xyk}^{in} - I_{xy}^{dark}\} \quad (ii)$$

where I_{xyk}^{in} is the array element that corresponds to the intensity of the input light (blank).

The absorbance array A is: $A = A_{xyk}$;

$$A_{xyk} = -\log_{10} [T^{trans}/T^{in}] \quad (iii)$$

where T^{in} is the intensity of the blank, and the T^{trans} is the corresponding intensity transmitted through a sample.

‘Reference beam’ Most modern UV-visible spectrophotometers use a second light path (‘reference beam’) system to correct for instrument fluctuations such as small changes in detector sensitivity or light source output. In the traditional instrument the use of the reference beam greatly increases the reproducibility and sensitivity of the instrument; however, frequently instrument design makes it necessary to acquire sample and reference beam data at rapidly alternating intervals. Using a CCD it is relatively simple to assign a number of pixels to this ‘reference beam’ use, and the sample and reference beams are measured simultaneously. Here this was done simple by using as a reference part of image area uncovered by the leaf. After the image was acquired this area was averaged and subtracted from the image. This resulted in a less noisy base line and smoother derivatization of spectra.

Debye transform To smooth background, as in root respiration, we further transformed data to a truncated Debye format^{53,54} as $1 - \sin^2 A + \sin^4 A - \sin^6 A$, where A is the attenuance at a given wavelength. This transformation increases (*in vivo*)/(*in vitro*) R^2 and decreases background of *in vivo* images⁵⁵. Care must be taken to normalize the data so as to avoid the cyclic downturn of the sine transform.

Plant materials Sugar cane (*Saccharum officinarum* L.) clone 51 NG 97 which has temperature dependent responses to helminthosporoside describable by *in vivo* spectroscopy³⁸ and *Millium effusum* L. var. aureum, a sun tolerant, ornamental, perennial grass which is shown here to lack light harvesting chlorophyll protein signal near 650 nm, were grown in a greenhouse. Soybean (*Glycine max* Merr. var Yuusuzumi) seeds were germinated in the dark at room temperature (approx. 25°C). Five days later, these roots were used for the respiration study.

Root respiration measurements One gram of agar (type A 7002 from Sigma Chemical Co., St. Louis, MO) was dissolved in 100 ml of boiling water, then ten ml of 0.1% resazurin (7-hydroxy- 3H-phenoxazin-3-one 10 oxide sodium salt, ACS registry number 62758-13-8, Sigma Chemical Co.) was added to the solution. This dye, orange at pH 3.8 and violet at pH 6.5, has a maximal absorption at 595 nm at low pH. When the solution cooled to 50 °C, the gel was poured onto a culture plate. Germinated soybeans were embedded into the gel. Once the gel solidified the plates were mounted in the imaging spectrophotometer. The monochromator was set to 595 nm. The absorption measurements were recorded from five to sixty minutes at five minute intervals. Control soybeans were boiled for 5 minutes, after germination and before embedding in agar.

RESULTS AND DISCUSSION

Plants, unlike animals, have few distinct functional areas or organs, but are constituted of complex plant structures such as roots, stems, and leaves. Distributed in complex patterns within each structure plants are areas containing groups of cells

specialized in different physiological functions. This imaging spectrometer is designed to distinguish spectral differences that map these closely adjacent areas of physiological importance in plants.

The figures in this paper present five points. Figure 2.1 presents instrument design. Figure 2.2 presents electron micrographs illustrating two groups of cells important in C-4 type of photosynthesis: the mesophyll and bundle sheath cells. We will later test the location of these cell types spectroscopically; however first, in Fig. 2.3 we test the level of spectroscopic quality required for this task. Figure 2.4 shows spectral images first taken at discrete wavelengths, and then combined algebraically to distinguish mesophyll and bundle sheath areas of the leaf. Figure 2.5 compares the results obtained to known plant material spectra to verify what we observe in Fig. 2.4 c. Then, in Fig. 2.6 we examine another physiological activity, respiration, as it is distributed unevenly across and along the plant root.

Figure 2.1 shows a schematic of the CCD based imaging spectrophotometer. Notice that there little need for a heat filter, because using attenuance measurements, unlike fluorescent analysis¹¹, the temperature limits relate to the physiology of the plant not the variability of the fluorescent response. Omitted for clarity is the enclosed light excluding box that contains the sample in its holder and strongly reduces stray light problems.

Figure 2.2a shows scanning electron micrographs demonstrating the location of mesophyll and bundle sheath cells in the leaf of sugar cane. At this level the spatial distinction between these types of cells is apparent. It is also important to note that the spectrophotometer, as opposed to electron microscope observes the leaf *in vivo*. Figure

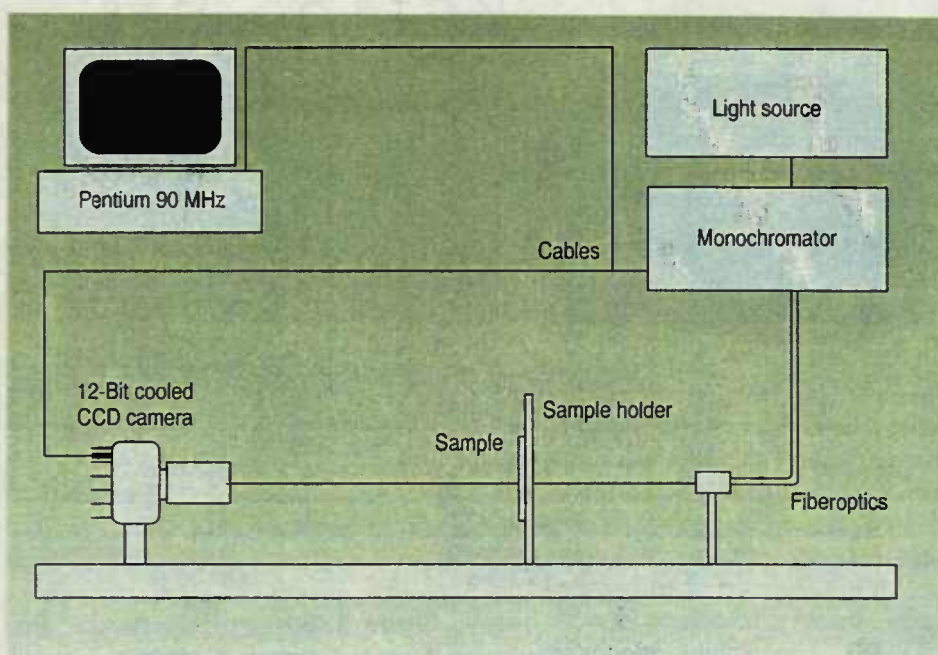
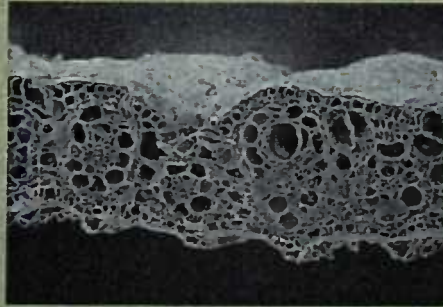


Figure 2.1. Schematic of CCD based imaging spectrophotometer.

Figure 2.2. Electron micrograph of bundle sheath cells, mesophyll cells and their chloroplasts. [a] Scanning electron micrographs demonstrating the location of mesophyll (MC) and bundle sheath (BSC) cells in the leaf of sugar cane (250X). [b] Transmission electron micrograph of midvein bundle sheath chloroplasts (1 mm=29 nm). [c] Transmission electron micrograph of secondary vein bundle sheath chloroplasts (1 mm=38 nm). [d] Transmission electron micrographs of mesophyll chloroplasts (1 mm=23 nm).

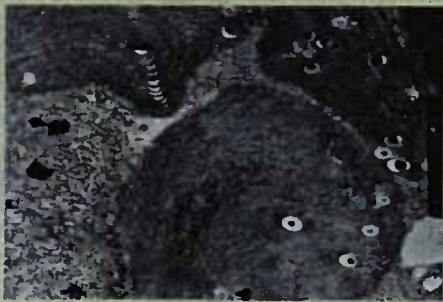
A



B



C



D



FIGURE 2.2

2.2b shows transmission electron micrograph of midvein bundle sheath chloroplasts; Figs. 2.2c and 2.2d show corresponding micrograph of secondary vein bundle sheath chloroplasts and mesophyll chloroplasts respectively. Note the differences in the complex layered membrane structures, that resemble a side view of the pages of well leafed phone directory, these are the thylakoid membranes³⁶. The thylakoid membranes contain the CPX. When they are stacked in multiple layers the thylakoid membranes are known as grana lamellae; the more exposed and less layered membranes are called stroma lamellae. Photosystems I (max. ~ 684 nm) and II (max. < 678 nm) are found in the stroma (and edges of the grana lamellae) and in the grana lamellae respectively. The ratio of these two photosystems is a function of adaptation of the plant to its environment^{1,3}. The light harvesting chlorophyll protein complex (max. ~ 650 nm) is mobile; when phosphorylated this CPX migrates to the stroma lamellae, reduces energy delivered to photosystem II, and diverts more energy to photosystem I.

Figure 2.3a demonstrates resolution of the principal chlorophyll protein complexes by the imaging instrument in leaves of sugar cane. The smoother less abrupt line is the attenuation (approx. absorption) trace; the more abruptly fluctuating line is the second derivative trace. Note in this figure the position of the light harvesting chlorophyll b complexes (~ 650 nm, a shoulder in the attenuation spectra and a peak in the second derivative trace), and the peak corresponding to the chlorophyll a in the antenna of the longer wavelength photosystem I (~ 684 nm). Photosystem I antenna gathers light for processing in its reaction center at about 705 nm, this point is barely perceptible as a slight inflection in the second derivative curve as it usually requires flash- or chemically-induced difference spectra³⁰ or fourth derivative analyses¹² to be seen clearly. Photosystem II

Figure 2.3. Spectra and chlorophyll protein complex structure . [a] Spectra demonstrating resolution of the principal chlorophyll protein complexes by the imaging instrument in leaves of sugar cane. The smoother less abrupt line is the attenuance (approx. absorption) trace; the more abruptly fluctuating line is the second derivative trace. The second derivative trace is inverted to permit more ready comparison with the attenuance trace. Note in this figure the position of the light harvesting chlorophyll b complexes (maxima ~650 nm) and the peak corresponding to the chlorophyll a in the antenna of the longer wavelength photosystem I (maxima ~684). Photosystem I antenna gathers light for processing at reaction center I (~705 nm). Photosystem II antenna gathers light for processing at reaction center II (~678nm). Second derivative peak analysis, unlike fourth derivative analysis does not completely resolve chlorophyll a structures of the shorter wavelength photosystem II, which appears here as a shoulder on the shorter wavelength side of the main peak. [b] Corresponding spectra taken with a standard research spectrophotometer.

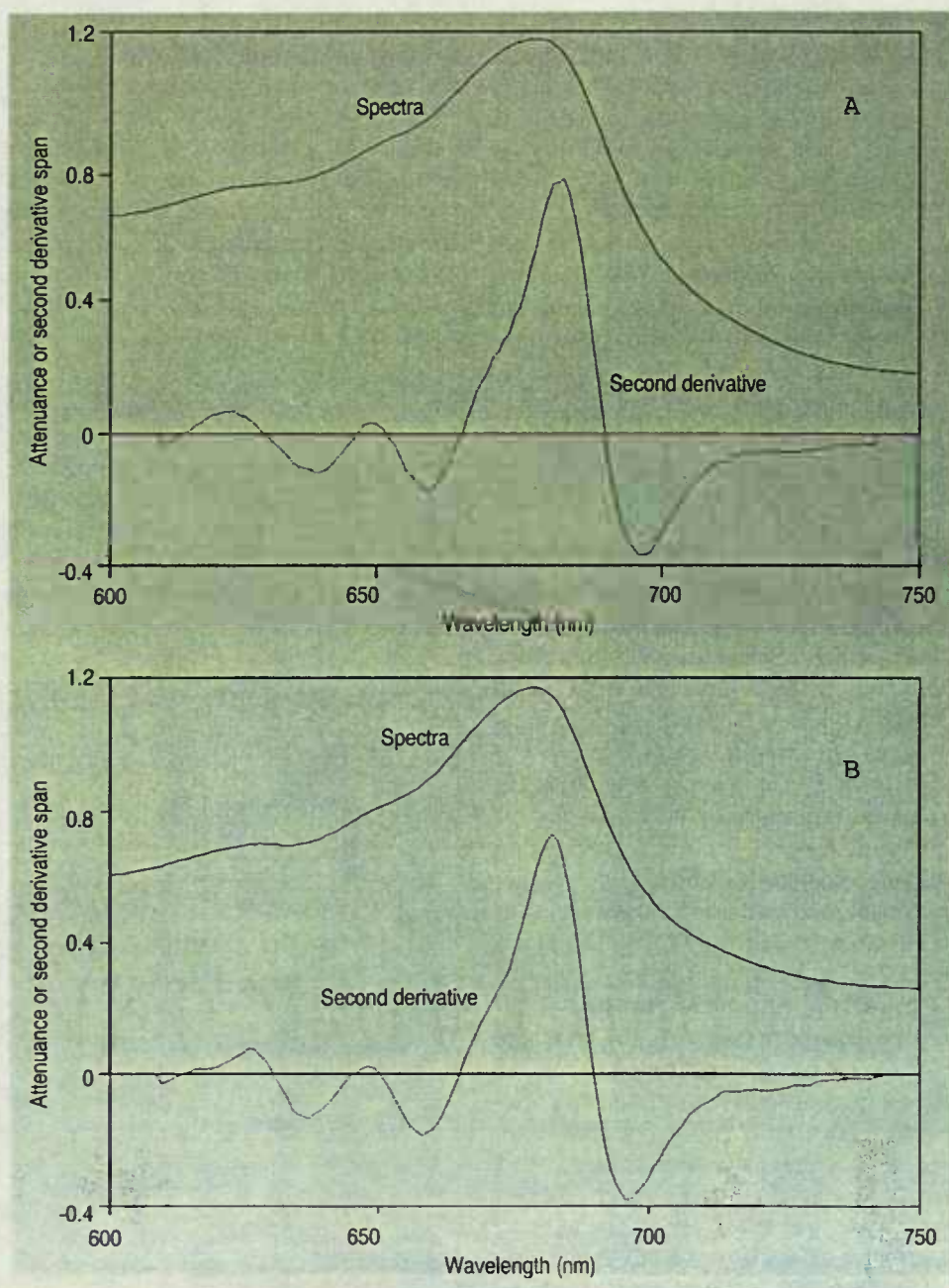


FIGURE 2.3

Figure 2.4. Spectra images of sugar cane leaf. [a] Sugar cane leaf image taken at 684 nm. [b] sugar cane leaf image taken at 648 nm. [c] Sugar cane leaf image taken at 700 nm. [d] Segregation of strips of containing bundle sheath cells using equation $((A_{684nm} - A_{700nm}) - (A_{650nm} - A_{638nm})) / A_{680nm}$, where each component represents attenuance ($\sim A$) at each given wavelength.

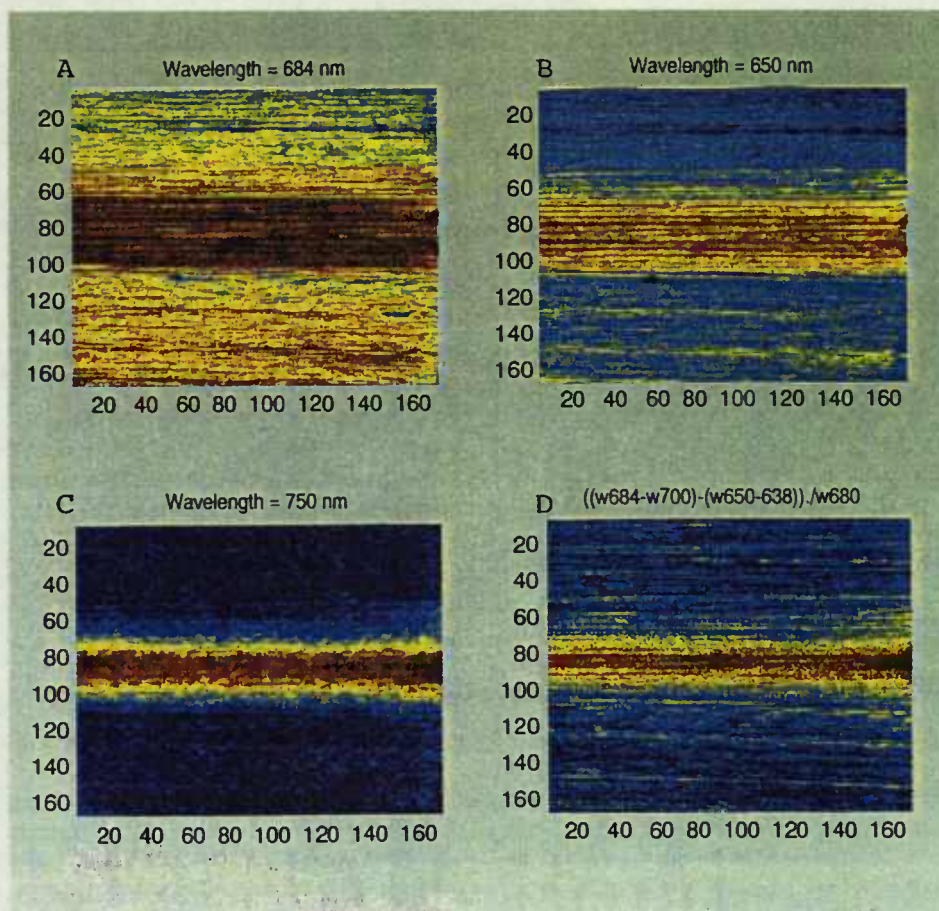


FIGURE 2.4

antenna gathers light for processing at its reaction center at about 680 nm, which is rarely seen *in vivo*³³. Second derivative peak analysis, unlike fourth derivative analysis does not completely resolve chlorophyll a structures of the shorter wavelength photosystem II, which appears here as a shoulder on the shorter wavelength side of the main peak. Figure 3b shows corresponding spectra taken with a standard research spectrophotometer. Notice that in the range of attenuance used the spectra of imaging instrument is almost as good as that of the standard research spectrophotometer.

Figure 2.4 shows images taken at different wavelengths. Figure 2.2a shows sugar cane leaf image taken at 684 nm. In the upper right of Fig. 2.2a shows a dark blue line indicating a fungal infection not described here; this figure is dominated by the red trace of main leaf vein, on a background of yellow leaf lamina. Figure 2.2b shows sugar cane leaf image taken at 650 nm. This figure shows yellow traces in the lower half of the figure corresponding to the position of bundle sheath cells. However, Figure 2.2b does not show these traces clearly in the upper half of the figure, where the fungal infection dominates the image. At 700 nm (Figure 2.4c), a wavelength with low attenuance close to the reaction center of photosystem I, little detail appears in the leaf lamina. Yet when these various wavelength images are combined in Fig. 2.4d the resolution of cell types is readily interpretable, if we know what we are looking for.

Sugar cane gathers CO₂ used to make sugars by the efficient, warm temperature adapted, C-4 path³⁶. In C-4 plants the CO₂ is first fixed in the mesophyll cells, then the fixed carbon is then transferred for further processing in bundle sheath cells. The mesophyll cells are found just beneath the surface of the leaf, while the bundle sheath cells are deeper in the leaf close to the leaf veins. Manipulating the different wavelengths

allows (Fig. 2.4d) segregation of areas with bundle sheath structures using equation $((A_{684nm}-A_{700nm})-(A_{650nm}-A_{638nm}))/A_{680nm}$, where each component represents attenuance ($\sim A$) at each wavelength. Using this equation (Fig. 2.4d) locations of bundle sheath cells appear as yellow stripes, while the mesophyll cell locations are shown in blue. The midvein is paralleled by these yellow stripes in a way consistent with the location of abundant bundle sheath cells in this area as shown in the electron micrographs of Fig 2.3.

However, the question arises are we really seeing CPX differences in the yellow and blue areas. Figure 2.5 shows the consistent spectral difference between different areas of the leaf. Figure 2.5a compares image spectra from areas of sugar cane leaf with and without bundle sheath cells. The difference spectra is also shown. Figure 2.5b compares of image spectra of *Millium effusum* L. var aureum which lacks the light harvesting chlorophyll b structures and the chlorophyll b-deficient oil yellow-yellow green (OY-YG) mutant of maize with the difference spectra obtained by imaging the different areas of the leaf. In Fig. 2.5b difference spectra between the mesophyll and bundle sheath cells, note the lack of the shoulder at or near 650 nm. This corresponds to the chlorophyll b signal of the light harvesting chlorophyll protein. The comparisons in this figure shows that the differences between the areas are attributable to differences between the CPX of different areas. This strongly supports the idea that we are observing differences between the CPX of mesophyll and bundle sheath areas in this C-4 plant. The applied advantages of distinguishing C-4 crop plants from C-3 weeds and vice versa are significant.

Figure 2.6 explores a different biochemical phenomena respiration. Figure 2.6a shows images of soybean roots in resazurin agar gel. Left root, showing yellow and red is a living root. Right root, barely perceptible as dark blue against the blue of the

Figure 2.5. Image spectra of sugar cane leaf and chlorophyll b-deficient oil yellow-yellow green (OY-YG) maize leaf. [a] Comparison of triple replicated portions of image spectra (size 400 pixels) of sugar cane leaf with and without bundle sheath cells and difference spectra. The upper, middle and lower three traces are respectively bundle sheath, mesophyll and difference spectra. Difference spectra was obtained by subtracting the spectra of mesophyll cells from the spectra of bundle sheath cells, and multiplying this spectra by four. [b] Comparison of image spectra of *Millium effusum* L. var. aureum which lacks the light harvesting chlorophyll b structures and the chlorophyll b-deficient oil yellow- yellow green (OY-YG) mutant of maize with the difference spectra obtained by imaging. In Fig. 2.5b the spectra are normalized for more ready comparison.

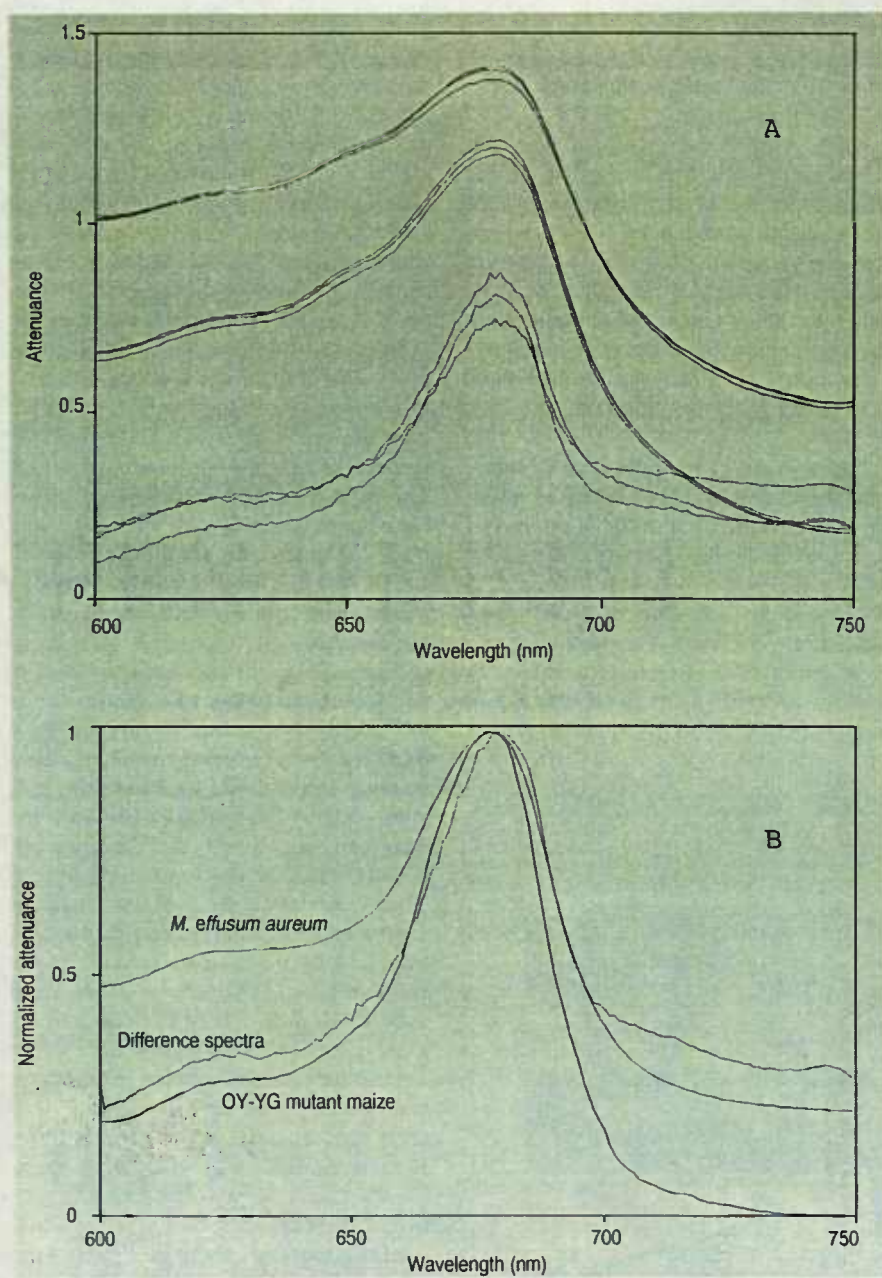


FIGURE 2.5

surrounding gel) is the dead root. Background is suppressed using a modified Debye transform (see Instrumentation and Plant Materials section). The living root (left) was actively releasing CO₂ as indicated by the dye resazurin measured at 595 nm, here converted to false color for contrast. This indicates a significant pH change as the CO₂ respired converts to bicarbonate in the agar. The boiled root (on the right) only produced slight changes at 595 nm absorbance in the surrounding area. Figure 2.6 shows only the upper two centimeters of the root and is consistent with what is known of root respiration especially with regard to the location of maximal respiration. The very slight changes associated with the boiled root are believed to be caused by metabolites, such as organic acids, released from the dead root into the agar because root cell membrane damage during boiling. Although we have not done so here, these colors and color areas can easily be quantified for experimental purposes.

CONCLUSION AND FUTURE DIRECTIONS

It is possible to build a high resolution imaging spectrophotometer capable of recording leaf spectrum over two-dimensional space. Excellent quality images can be obtained by applying signal averaging. Since we average 10 images, we calculate absorbance differences of 0.05 A can be measured. This resolution could be critical in the prediction of plant stresses or diseases. In the future, using multivariate calibration such as partial least squares, calibration models of spectral properties of discrete components taken from the literature can be used to target important parameters *in vivo*. Among the suitable subjects for this kind of investigation are the many different kinds of chlorophylls-

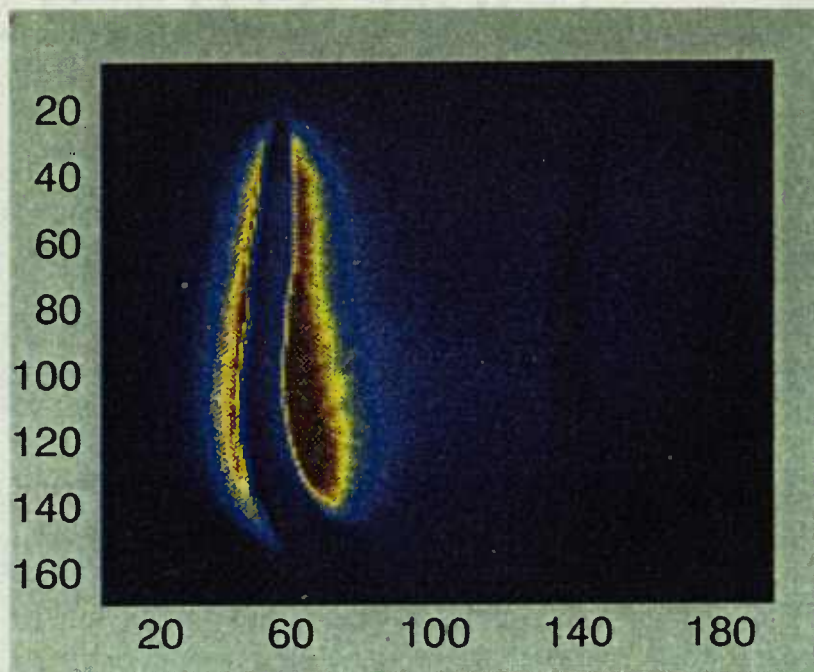


Figure 2.6. Respiration activity of soybean root. The first two centimeters of two soybean roots embedded in resazurin agar gel. Left root, red and yellow, is a living root. Right root, a dark blue barely detectable against background of dyed gel is the dead root.

protein complexes which have published spectral properties and are known to change in proportions during light adaptation, nutritional availability and disease. Since, this optical method is non-invasive it allows continuous examination of physiological change in the same sample. This greatly simplifies these kinds of experiments. Thus, it is possible that imaging spectroscopy will become a routine laboratory tool to measure plant physiological parameters and histochemical change, in addition to its potential in applied robotic agriculture³⁵.

We plan to upgrade the CCD to improve spatial resolution and dynamic range. The latter will be especially critical for study of weak absorbances in the near-IR region. Expanding the measurable spectral region to 900-1700 nm will make possible quantitative analyses of water, starch and protein.

AUTHORS

Li Ning is a Graduate Research Assistant in Department of Horticulture at Oregon State University (OSU), Corvallis. He received an M.S. (1987) in the Department of Horticulture from Beijing Agriculture University, China, and a B.S. (1983) in Biology from Peking University, China. Ning's Ph.D. thesis will include the construction and application of the imaging spectrophotometer.

Richard Ozanich does research at Battelle, Pacific Northwest laboratories. He received a Ph.D. (1992) in Chemistry from the University of Washington and a B.S. from Washington State University. Ozanich's research interests include near-IR spectroscopy.

Alfred H. Soeldner is senior instructor in the Department of Botany and Plant Pathology at OSU, where he received his PhD in 1967. He runs the electron microscope facility and x-ray energy spectrometer facility at OSU. Soeldner provides instruction in the use of these instruments, interprets electron micrographs, and cooperates in the research of other scientists on campus.

Larry S. Daley is an Associate Professor of Horticulture at Oregon State University. He received a Ph.D. (1975) from the University of California at Davis in the Biochemistry and Biophysics department. His research interests include the biochemical and biophysical interpretation of *in vivo* leaf spectra, and its relationship to germplasm research.

James B. Callis is a professor of Chemistry and adjunct professor of Bioengineering at the University of Washington, Seattle. He received a Ph.D. (1970) in Chemistry from the University of Washington. His research interests include the development of instruments such as the video fluorometer, flash calorimeter, imaging spectrophotometer, lap-top computerized instruments. Callis's currently interests include development of instrumentation for ecological surveys and *in vivo* interferometry.

ACKNOWLEDGMENTS

We gratefully acknowledge support from the Herman Frasch Foundation (grant number: FRASCH 63-0738). This paper is Oregon Agricultural Experiment Station Technical paper #10550.

REFERENCES

- (1) Greene, B.A., L.A. Staehelin, and A. Melis, *Plant Physiol.* 87, 365- 379 (1988).
- (2) C.B. Osmond, J.A. Berry, S. Balachandra, C. Buchen-Osmond, P.F. Daley, and R.A. Hodgson, *Bot. Acta* 103, 226 (1990).
- (3) B.T. Mawson, P.J. Morrissey, A. Gomez and A. Melis, *Plant Cell Physiol.* 35, 341 (1994).
- (4) R.F.E. Wolf, K.H. Lam, E.L. Mooyaart, R.P. Bleichrodt, P. Nieuwenhuis and J.M. Schakenraad, *Laboratory Animals* 26(3), 222 (1992).
- (5) E.G. Jordan, O.V. Zatsepina, and P.J. Shaw, *Chromosoma* 101(8), 478 (1992).
- (6) A. Borst and M. Egelhaaf, *Proc. Natl. Acad. Sci. USA* 89, 4139 (1992).
- (7) G. Vane and A.F.H. Goetz, *Remote Sens. Environ.* 44, 117 (1993).
- (8) C.D. Elvidge, Z. Chen, D.P. Groeneveld, *Remote Sens. Environ.* 44, 271 (1993).
- (9) M.K. Hamilton, C.O. Davis, W.J. Rhea, S.H. Pilorz, and K.L. Carder, *Remote Sens. Environ.* 44, 217 (1993).
- (10) P.F. Daley, K. Raschke, J.T. Ball, and J.A. Berry, *Plant Physiol.* 90, 1233 (1989).
- (11) T.J. Fenton and A. R. Crofts, *Photosynth. Res.* 26, 59 (1990).
- (12) L.S. Daley, *Plant Physiol. Biochem.* 28, 271 (1990).
- (13) M. Faust, D. Liu, M.M. Millard and G.W. Stutte, *HortSci* 26,887 (1991).
- (14) A.A. Gardea, L.S. Daley, R.L. Kohnert, A.H. Soeldner, L. Ning, P.B. Lombard, and A.N. Azarenko, *Spectroscopy* 8(1): 27-35 (1993).
- (15) A.A. Gardea, L.S. Daley, R.L. Kohnert, A.H. Soeldner, L. Ning, P.B. Lombard, and A.N. Azarenko, *Scientia Hort.* 56: 339-358 (1994).
- (16) R.D. Rosenthal, Futrex inc., Gaithersburg, Maryland, personal communication.
- (17) J.S. Brown, *Photosynth. Res.* 4, 375 (1983).
- (18) J.S. Brown and S. Schoch, *Biochim. Biophys. Acta* 63, 201 (1981).

- (19) C. Chen, J.S. Cameron, and S.F. Klauer, *HortScience* 25, 1166 (1990).
- (20) C. Chen, L.S. Daley, and W.E. Kronstadt, *Plant Physiol. Biochem.* 28(2): 259-269 (1990).
- (21) W.W. Cure, *Proc. Amer. Soc. Photogrammetric Eng.* 3, 181 (1989).
- (22) L.S. Daley, M.M. Thompson, W.M. Proebsting, J. Postman, and B.R. Jeong, *Spectroscopy* 1(7), 28 (1986).
- (23) L.S. Daley, and K.C. Nichols, *Plant Physiol. Biochem.* 25: 467-476 (1987).
- (24) L.S. Daley, P.J. Breen, and P. Mohanty, *Spectroscopy* 2(3): 32-35 (1987).
- (25) L.S. Daley, O. Jahn, and C. Guttridge, *Photosynth. Res.* 11: 183-188 (1987).
- (26) L.S. Daley, R.A. Menendez, and R.L. Stebbins, *J. Environ. Hort.* 5, 25 (1987).
- (27) L.S. Daley, J.M. Montano, R.A. Menendez, A.H. Soeldner, and R.B. Boone, *Spectroscopy* 2(9): 32-36 (1987).
- (28) L.S. Daley, J.R. Powell, G.A. Strobel, R.B. Boone, J. Postman, M. Willie, and J.H. Brown, *Plant Physiol. Biochem.* 26: 683-694 (1988).
- (29) C.S. French, J.S. Brown, and M.C. Lawrence, *Plant Physiol.* 48, 421 (1972).
- (30) T. Hiyama and B. Ke, *Biochim. Biophys. Acta*, 267, 160 (1972).
- (31) W. Ruhle and A. Wild, *Planta* 146, 551 (1979).
- (32) Yoder B.J. and L. S. Daley, *Spectroscopy* 5(8): 44-50 (1990).
- (33) S.R. Eskelsen, G.D. Crabtree, R.B. Boone, G.M. Volk, L. Ning, and L.S. Daley, *Spectroscopy* 8(3), 34 (1994).
- (34) R.M. Pratt, *Agric. Exp. Stat.*, (Gainesville, Florida, 1958).
- (35) J. Beck, Patchen California Inc., Los Gatos, CA, personal communication, 1994.
- (36) L. Taiz and E. Zeiger, *Plant Physiology* (Benjamin/Cummings Pub. Co., Inc., Redwood City, California, 1991).
- (37) P.S. Sinadze, National Academy of Sciences, Tbilisi, Georgia, personal communication, 1977.

- (38) W. Cockburn, *Plant Cell. Envir.*, 4, 417 (1981).
- (39) J.R. Ehleringer and R.K. Monson, *Ann. Rev. Ecol. Sys.*, 24, 411 (1993).
- (40) H. Griffiths, *Plant Cell. Envir.*, 15, 1051 (1992).
- (41) C.C. Black, Biochemistry Department, University of Georgia, personal communication, 1994.
- (42) I.P. Ting, Botany Department, University of California, Riverside, personal communication, 1994.
- (43) S.P. Slocombe, G.C. Whitelam and W. Cockburn, *Plant Cell. Envir.*, 16, 403 (1993).
- (44) U. Luttge, *New Phytol.* 125, 59 (1993).
- (45) D.M. Vernon, J.A. Ostrem and H.J. Bohnert, *Plant Cell. Envir.*, 16, 16,437 (1993).
- (46) R. Hunt, *Plant Growth Curves* (Edward Arnold Ltd, London, 1982), p.115.
- (47) C. Borggaard and H.H. Thodberg, *Anal. Chem.* 64, 645 (1992).
- (48) J.B. Callis and A.P. Burkner, *ACS Symp. Ser.* 236, 233 (1983).
- (49) M.L. Gianelli, D.H. Burns, J.B. Callis, G.D. Christian, and N.H. Andersen, *Anal. Chem.* 55, 1858 (1983).
- (50) D.H. Burns, J.B. Callis, and G.D. Christian, *Anal. Chem.* 58, 2805 (1986).
- (51) P.K. Aldridge, J.B. Callis, and D.H. Burns, *J. Liq. Chrom.* 13, 2829 (1990).
- (52) M.A. Afromowitz, J.B. Callis, D.M. Heimbach, L.A. Desoto, and M.K. Norton, *IEEE Transactions on Biomedical Engineering* 35, 842 (1988).
- (53) P. Debye, *J. Phys. Colloid. Chem.* 51, 8 (1947).
- (54) P.J. Wyatt, *American Lab.* 1994 (March), 25 (1994).
- (55) L. Daley, unpublished data (1994).

CHAPTER 3

FIVE NOVEL APPLICATIONS OF IMAGING VISIBLE AND
SHORT NEAR INFRARED SPECTROPHOTOMETRY AND
FLUOROMETRY IN THE PLANT SCIENCES

Li Ning¹, Walter J. Bowyer², Annie M. Chozinski¹,
Tamas Buba³, Anita Azarenko¹, Gerald E. Edwards⁴,
Larry S. Daley^{1*}, James B. Callis⁵ and Gary A. Strobel⁶

¹Department of Horticulture, ALS 4017, Oregon State University, Corvallis, OR 97331.

²Department of Chemistry, Hobart and William Smith Colleges, Geneva, NY
14456-3397.

³Gyümölcs és Dísznövénytermesztési Fejlesztő Vállalat Allomása (Fruit and Pork
Production Development Station), Újfehértó, Hungary.

⁴Botany Dept., Washington State Univ., Pullman, WA 99164

⁵Department of Chemistry, University of Washington, Seattle, WA 98195.

⁶Department of Plant Pathology, Montana State University, Bozeman, MT 59717.

*Author to whom correspondence should be addressed.

Published in *Spectroscopy*,
Advanstar Communications, Eugene, O.R.

FIVE NOVEL APPLICATIONS OF IMAGING VISIBLE AND SHORT NEAR INFRARED SPECTROPHOTOMETRY AND FLUOROMETRY IN THE PLANT SCIENCES

Li Ning¹, Walter J. Bowyer², Annie M. Chozinski¹, Tamas Buba³, Anita Azarenko¹, Gerald E. Edwards⁴, Larry S. Daley^{1*}, James B. Callis⁵ and Gary A. Strobel⁶

¹Department of Horticulture, ALS 4017, Oregon State University, Corvallis, OR 97331.

² Department of Chemistry, Hobart and William Smith Colleges, Geneva, NY 14456-3397.

³Gyümölcs és Dísznövénytermesztési Fejlesztő Vállalat Allomása (Fruit and Vegetable Production Development Station), Újfehértó, Hungary.

⁴Botany Dept., Washington State Univ., Pullman, WA 99164

⁵Department of Chemistry, University of Washington, Seattle, WA 98195.

⁶Department of Plant Pathology, Montana State University, Bozeman, MT 59717.

*Author to whom correspondence should be addressed.

Visible (and near infrared) spectra of plant tissues yield information with considerable potential for basic studies, and to test advanced concepts for their later application to agricultural robotics and remote sensing. Imaging plant tissues in this spectral range can be done with a new, CCD (charge coupled device) equipped, instrument (Ning, *et al.*, *Spectroscopy*, 9 (7), 41 1994), which can also be reversible and rapidly reconfigured as an imaging fluorometer (Ning *et al.*, *Applied Spectroscopy*

48(10):138, 1995). Here we present five diverse applications of this instrument. Four applications involve attenuance (~absorbance, A) spectroscopy: (i) extraction of data from microphotographs of apple (*Malus domestica* Borkh. var. Red Rome) flower buds, (ii) in situ determination of sucrose and invertase activity in stems of hazel (*Corylus avellana* L. var. Barcelona), (iii) *in vivo* effects of a fungal pathogen (*Pestalotiopsis microspora*), and its phytotoxin in the foliage of the rare nutmeg (stinking) cedar or yew of Florida (*Torreya taxifolia* Arn.) foliage, (iv) time course of water displacement by heavy water (deuterium oxide) in roselle (Jamaica sorrel), *Hibiscus sabdariffa* L., leaves. The fifth application (v) is generation of quantum yield fluorescence (Ning *et al.*, 1995) leaf maps in the multi-hued ornamental and potential drug source *Scrofularia nodosa* 'Variegata'. Uses and limitations of the instrument in remote fluorescence techniques are illustrated and discussed. Applications are supported by additional data and models of solid matrix biochemistry and multivariate analyses. The data generated helps supports conclusions to be published separately: on (i) xylem development in apple flower buds, (ii) relationships, in hazel varieties, between stem sugar content and susceptibility to *Anisogramma anomala*, a lethal and spreading fungal pathogen, that causes Eastern filbert blight, (iii) methods to detect pathogens and toxin damage in plants before symptoms become visible, (iv) detection of water in living plant tissues, and use of plant water to determine biochemically active path of light in plants, and (v) comparisons of chlorophyll-protein complex structure and function between different hue-domains of variegated leaves.

INTRODUCTION

We constructed an imaging spectrophotometer (1), which can also be rapidly and reversibly reconfigured to image, by fluorescence, photosynthetic quantum yield (2). The purpose of this instrument is to support scientific research in plant physiology and biophysics and help improve present agricultural practices. This instrument allows quantification of the interaction between spatial and spectroscopic characteristics of plant tissue so as to generate quantified images. The instrument's design and data processing (1,2) allows determination of a linear response to absorbance up to about 2 absorbance units (A), a narrow wavelength resolution (<1 nm) and a 400-1000 nm detection range. Separate detection on each of the 31,680 pixels of the CCD (Charge Coupled Device) reduces the distribution error found when collecting signals from areas of unequal absorbance in a single detector. This instrument allows chemometric statistical analyses of complex plant chromophores, and it has the sensitivity necessary to quantify many low absorbing or low concentration chromophores. The quantified images generated detect changes related to function and pathology of plants. These images have considerable potential for applied and scientific uses.

Plant leaves (3-37), stems (38) and flowers (39) have strong signals in the UV-visible range. These signals have rich and complex structures which change to reflect the health of the leaf and the plant's adaptation to environmental conditions (40-53). Leaf chromophore changes are not distributed evenly across the tissues, but vary spatially in ways diagnostic of leaf health, function and insect predation (54-56).

In vivo visible spectra of leaves, stems and flowers are interpretable in terms of pigments and pigment complexes, e.g. electronic transitions of chlorophylls, cytochromes, carotenoids and various accessory pigments (27,31,57-62). Our work combined with the data of others allows interpretation of second and fourth derivative visible spectra in terms of chlorophyll protein complexes (CPX) and relates this to selected aspects of plant pathology and physiology (1,2,27,55,56), and applied agricultural concerns (63-66).

The *in vivo* spectra of hydrated and biochemically active plant material in the short near infrared spectra between 750 and 1000 nm is less explored (67-74). A good discussion of the molecular mechanisms of absorbance in this spectral range is found in Murray and Williams (75).

Events that alter a plant's biochemistry condition, usually have accompanying spatial as well as spectroscopic changes. Thus, each spectroscopic change has a spatial distribution which differs with wavelength. For example, a fungal attack may present itself as a series of small black dots (necrotic areas), each surrounded by a ring of localized resistance (e.g. 54); viral infection as a series of splotches across the leaf (e.g. 54,56); fertilizer deficiency may show symptoms localized only along leaf veins or leaf margins (e.g. 54), etc. To detect such differences an instrument must be capable of recording the spectrum over two-dimensional space (1,2,55,56,74).

At present less precise evaluation of these signals, their position on the plant, and other indicators of plant health is done by eye by a trained observer in an expensive and time consuming process called field scouting. Agricultural scientists have prepared generalized, irrigation and fertilizer schedules for most US crops. Optimal amounts and application timing of each agricultural input, such as fertilizer, water and pesticides, at

each crop site varies. Scouting provides information to individual growers, on how to modify these schedules to attempt to maximize productivity at each site. Scouting may be supplemented by chemical analyses. Then the modified schedule is carried out by applying agricultural inputs uniformly on entire fields. However, the conditions in each part of the fields are not uniform. Excess application of inputs, to a part of the field where it is not needed, causes waste.

Already equipment exists today that uses spectroscopy to locate and spray weeds in the bare batches between crop rows (64). Much more will be done in the future, since automated interpretation of plant function and health from leaf, flower and stem images has great potential in robotic agriculture. Robotic agriculture would allow supply of an individual mix of agricultural inputs to each plant in every part of the field. For example: pesticides could be applied rapidly just to the affected plants, killing pests before they spread; or fertilizer mix and water could be supplied only as is required by each plant. This would drastically reduce amounts of: pesticides used, run off of excess fertilizer, and when used to control irrigation, water wasted. To do this instrumentation to detect pathologies and plant health will be needed. This instrument could serve to study these uses.

Fluorometry of the plant's photosynthetic system not only allows measure of this most important function of plants, but also allows determination of many interaction of the plant with its environment (reviewed in 2). Fluorescence measurement of photosynthesis involves matters of some complexity (2). Plants gather energy from photons. Photons, of course move at the speed of light, so somehow plants photosynthetic systems must hold and trap this photonic energy long enough and in the appropriate forms to do biochemical

work. Quantum efficiency is a measure of how well the photosynthetic system functions. In plants photosynthetic function is closely regulated by the interaction of each plant's genetically coded germplasm variables with the environmental variables that act on the plant. Thus, imaging of estimates of quantum yield by this method allows imaging of many plant germplasm/environmental interactions (reviewed in 2). For these reason access to fluorescence data from field plants has considerable research interest.

INSTRUMENTATION, MATERIALS AND METHODS

Hardware We used an imaging spectrophotometer /fluorometer described previously (1,2). The imaging fluorometer configuration has a simpler design than previous instruments. It has only one light source, a 500 W, 120 volt projector lamp (model CZX/DAD, GTE Products Inc. Winchester, KY). Two filters are used, one filter removes long wavelength light from the excitation beam and the other short wavelength light from the detecting system. Time sequenced image data is collected, as in the imaging spectrophotometer, on a thermoelectric cooled 12 bit CCD camera (Lynxx PC, CCD Digital Imaging System, SpectraSource Instruments, Westlake Village, CA), with a spatial resolution of 165*192 (31,680 pixels). An IBM/PC compatible computer (Pentium^R chip, 90 MHz, Intel Corp., Palo Alto, CA) controls the CCD camera through an interface board (Lynxx PC, SpectraSource Instruments). Collected image data are stored, for easy access, as image files in removable 88 MByte SyQuest cartridge (Model SQ800 on the corresponding internal drive, SyQuest technology, Fremont, CA). Adaptation to test remote sensing applications was done simply by adjusting the CCD camera, and the light

source's lenses, to focus on the distant plant. Since the plant's leaves need to be in the dark before the experiment, it is necessary to do these measurements, at night or in an enclosed space with little or no external light.

Acquiring fluorescence images Fluorescence quantum yield (Y) is estimated as Y' (2). To obtain Y' a background, "dark", signal plus two selected fluorescence signals are required. The detector, here the CCD camera, captures a timed series of signal samples which represent points along the complex time dependent fluorescence transients of the Kautsky curve (2,7). From the first ten signals the brightest is selected as F_m . After a signal at 150 seconds F_s , is collected to represent the terminal signal. The background signal F_{dark} is acquired with the exciting lamp off. F_s is used to estimate the initial fluorescence signal (F_o), which occurs and changes too rapidly to detect with most equipment (76). This is done because we found that, under saturating light (2) and with most usual treatments, $F_s \cong F_o$. Thus, from equations in previous paper (2), an estimate of quantum yield (Y') determined empirically as:

$$Y' \cong \{(F_m - F_s) / (F_m - F_{dark})\} \quad (i)$$

The data collected from the CCD consists of a time ordered sequence of fluorescence images (FI) of the sample, each taken at a different time. Images were taken with an exposure time of 0.1 s, however, it took about 0.6 s to completely digitize and store one image. The image of estimated quantum yield (FI_Y) is processed by equation ii (below) which is an image matrix version of equation (i). The first ten images collected by the instrument are evaluated for greatest intensity, the most intense is called FI_m for peak fluorescence image; the image taken at 150 seconds is FI_s , the estimated of terminal fluorescence; the dark current or background fluorescence, taken without illumination, at

end of experiment is symbolized by FI_{dark} . The images FI_n , FI_s , and FI_{dark} are processed by equation ii to the yield estimated quantum yield image (FI_Y) thus:

$$FI_Y = \{(FI_n - FI_s) / (FI_n - FI_{\text{dark}})\} \quad (\text{ii})$$

After images are acquired, the CCD files were translated into MATLAB files and then processed. MATLAB functions were developed so that the Y' value of one pixel of a selected area of pixels could be retrieved.

Software for image acquisition, processing and developing correlations Image acquisition and processing software have been described previously (1,2). The program controlling the instrument was written using Borland C++ 4.0. This program, which is available from one of us (L.N.), can be modified to achieve optimal analysis time. Data were retrieved and processed using a numerical software package called MATLAB (The MathWorks, Inc., Natick, MA). The partial least-squares (PLS) program we used was provided by Bruce Kowolski, CPAC, Department of Chemistry, University of Washington.

Other instruments Sucrose determinations on solid matrices were done using an "One Touch II" blood glucose meter (Johnson and Johnson, Inc., Milpitas, California). The non-imaging spectrophotometer used was a Shimadzu 3100 (Shimadzu Scientific Instruments, Columbia, Maryland).

Plant materials Apple (*Malus domestica* Borkh. var. Red Rome) stems with vegetative and flower buds attached were cut in the field in Hungary from January through March, and kept in refrigeration until forced. Hazelnut stems (*Corylus avellana* L. var. Barcelona) were collected by David Smith from the orchards maintained at Oregon State University by Shawn Mehlenbacher for his breeding program. *Digitalis purpurea* L.,

Hibiscus sabdariffa L. and *Scrofularia nodosa* 'Variegata' were grown in pots containing OSU mix and kept in OSU greenhouses. Nutmeg trees (*Torreya taxifolia* Arn., common names: nutmeg cedar, nutmeg yew, stinking cedar or stinking yew) were provided by Mark Schwartz (Univ. Calif., Davis) and were originally acquired from the Nature Conservancy of Northern Florida. Pathogen infected and control yew leaves were shipped chilled by overnight mail from Montana to Oregon for analyses.

Pathogen isolation, identification and inoculation The pathogen *Pestalotiopsis microspora* was isolated from the nutmeg tree stems using a plating technique involving stem surface sterilization with 70% ethanol followed by placement of stem pieces on water agar. Identification of the pathogen (77) is based on very characteristic conidiospore appendages and brown color (78,79). The conidiospore of *P. microspora* has five cells; the three central cells are brown; the lower cell has a lance like appendage; the top has appendages that resemble helicopter rotors. The pathogenicity of *P. microspora* has been established by fulfillment of Koch's postulates (77). Tissue damage, in the needles of this Florida *Torreya*, is caused by phytotoxins which spread ahead of the fungus (80). *T. taxifolia* stems were inoculated, in a greenhouse setting, with agar blocks containing *P. microspora* and allowed to incubate for three weeks at which time the stem was harvested for spectroscopic examination. Control plants received only plain water agar blocks as inoculum. Examination was done on the terminal leaves 10-12 cm removed from the site of inoculation.

Test of xylem function Xylem function was tested by uptake of azosulfamide dye (4-sulfamylphenyl-2-azo-7-acetamido-1-hydroxy-naphthalene 3,6-disulfonic acid, disodium salt, Chemical abstracts (CAS) registry number 133-60-8, purchased from Sigma

Chemical Co., St. Louis, MO). If azosulfamide moves up the stem and into the buds, this demonstrates vascular continuity (81,82). Stem sections with leaf and flower buds were placed in water containing azosulfamide (17 mM) to take up dye. The buds were "forced" to develop by placing them at 20°C in the dark from early January to late March. Flower buds, replicated three times per cultivar, were excised at weekly intervals, longitudinal sections were taken and microphotographed. However, since we here wish to document and illustrate horticultural applications of image spectroscopy, not developmental morphology, we present only one image of one replicate taken at one time, January 17, from one cultivar, Red Rome. Developmental morphology studies and their application to horticulture will be presented elsewhere.

Determination of invertase and sucrose In tissues of hazelnut varieties, glucose oxidase-peroxidase-dye reaction was used to determine sucrose, as glucose after invertase treatment. Invertase activity was also determined by first removing endogenous sucrose and then adding known amounts of sucrose. The yeast invertase (b-D-fructofuranoside fructohydrolase, EC 3.2.1.26) had an activity of approximately 400 units per milligram solid, was prepared from *Candida utilis*, and was purchased from Sigma Chemical Co. One unit of invertase can hydrolyze 1 mmole of sucrose per min at pH 4.5 and 55 °C. The Touch^R test strips were donated by Johnson and Johnson Inc. Each of these strips contains: glucose oxidase [17 international units (I.U.)], peroxidase (12 I.U.), 3-methyl-2-benzothiazolinone hydrazone hydrochloride (0.06 mg) and 3-dimethylaminobenzoic acid (0.13 mg). To prepare the color reaction solution 21 strips were mixed in 0.8 ml of buffer. The buffer, unless otherwise specified, was 50 mM acetate pH 4.6. For the pH curve the following buffers, purchased from Sigma Chemical

Company, were used (2 mM each): 2-[N-morpholino]ethane sulfonic acid (MES), N,N-bis[2-hydroxyethyl]-2-aminoethanesulfonic acid (BES), 3-[N-morpholino]propanesulfonic acid (MOPS), N-tris[hydroxymethyl]methylglycine (Tricine), 2-[N-cyclohexylamino]ethanesulfonic acid (CHES) and 3-[cyclohexylamino]-1-propanesulfonic acid (CAPS). These buffers have, respectively, $pK_a(25^\circ\text{C})$ of 6.1, 7.1, 7.2, 8.1, 9.3, 10.4 (83-85). The buffers were taken to pH 9.0 with K_2HPO_4 , then back titrated with 0.2 M acetic acid to appropriate pH. Mixing buffers avoids discontinuities in pH vs. activity curves. These discontinuities are relatively common when different, unmixed, buffers are used to generate pH activity curves. The discontinuities are attributed to secondary biological effects, caused by the different buffers (85), on enzyme activity.

Preliminary assays were done using the One Touch II blood glucose meter. Cell wall material was prepared in a manner conceptually similar to that used by Barnett (86) and Daley *et al.* (87). The stems were cut into sections and crushed on to filter paper, as is more commonly done for metabolite studies (e.g. 88). Disks (0.385 cm^2) are punched out of the filter paper and washed gently but thoroughly six times with distilled water. Components of system are: sucrose in 50ul appropriate buffer, 50ul of color reaction solution and 5ul of 5mg/ml invertase (about 10 units, prepared in acetate buffer described above). Sucrose is not added when determining sucrose; invertase is not added when determining invertase. Boiled disks served as controls, sucrose in the absence of invertase did not react. When measuring sucrose, enzyme levels in reagents and added invertase were saturating, as is appropriate, since there was no time dependence of the reaction after one minute. When measuring invertase, invertase was limiting, as is appropriate, since the

reaction was linear for 15 min. Components are added to disk, which is then incubated at room temperature for an hour, after which the color is measured by the blood glucose meter.

In vivo stem reactions are measured, at 595 nm, using the imaging spectrophotometer. Sucrose is determined by applying the reaction mix without sucrose, but with added invertase, directly to the stem. Reagent enzyme concentrations were appropriate since after about one minute this reaction was not time dependent. Bound invertase is determined by washing the stem thoroughly with water to remove endogenous sucrose, then applying the reaction mixture with sucrose, but without invertase. The tissue invertase reaction is time dependent for about 15 minutes under our conditions.

RESULTS AND DISCUSSION

Plants are constituted of complex structures such as roots, stems, and leaves. Distributed in complex patterns within each plant structure are groups of cells specialized in different physiological functions. Our imaging spectrophotometer/fluorometer can distinguish spectral differences between these closely groups of cells. Thus different, but adjacent, areas of physiological and pathological importance are resolved. Absorbance (here attenuation), rather than reflectance is used. Since reflectance, but not attenuation, measurements have been found to be biased towards surface data (89); and spectra from attenuation measurements of leaves are more highly resolved than reflectance spectra (14). This instrument is capable of imaging leaf CPX spectra (1,74) at room temperature. This avoids use of cryogenic conditions which increase spectral resolution (59), but cause cell

disruption. The instrument was also used in its fluorescence mode to approximate photosynthetic quantum yield efficiency.

To interpret our image data certain conventions are used. The instrument's CCD array covers two dimensions, commonly the x-y plane of the leaf lamina. The intensity of the instruments response, a third dimension, is represented as a color gradient. Thus, the variable coloring of the two-dimensional space of the figure, represents the intensities of the instrument's signal or signal equation. For instance a gradient of increasing absorbance is commonly represented in colors, smoothly increasing wavelength from the blue, through the yellow, and on to the red range of the visible spectrum. To make this convention clearer to the reader a color gradient bar is usually included adjacent to the figure. For example in Fig. 3.1, the darkest, most intensely red, color indicates highest dye levels, which fades through orange to yellow areas to indicate decreasing levels, and then to light blue (turquoise) and deep blue indicating the areas with the little or no dye. Stretching color images is accomplished by mathematical manipulations of image generating equations.

Application 1, enhancement of histological photographs The original image (Fig. 3.1a), shows a section of apple bud, total length about 2.6 mm, after the bud was treated with a tracer dye. This image (Fig. 3.1a) was acquired by true color image technology e.g. a color photograph (micrograph) taken through a microscope. However, color photography did not allow a visual distinction between the dyed areas and the plant's own pigmented tissues. Thus these micrographs, taken with considerable expenditure of effort in 1989, were unusable in their original state.

Figure 3.1a shows the original micrographs as received from Hungary. The presence of the azosulfamide dye color is imperceptible. To make apparent the presence of the dye it was necessary to enhance (stretch) the color differences using the false color imaging capabilities of the instrument to detect and locate in situ azosulfamide in the presence of natural pigments (Fig. 3.1b). This is done taking advantage of the wavelength resolution ($<2\text{nm}$ at half peak height) of the instrument and by mathematically stretching the false color images to distinguish the dye signal from the background. Figure 3.1b shows the enhanced image, obtained by imaging the attenuation of the photographic positive, which is on thin paper. To do this, we subtract the attenuation ($\sim A$) at 650 nm from the attenuation at 553 nm ($A_{553}-A_{650}$).

In the false color image (Fig. 3.1b) one can clearly observe the xylem transportable dye. The movement of azosulfamide dye from one part of a plant to another part is a measure of vascular connection between the two parts (81,82). By the time of the season this image was taken, January 17 1989, the vascular traces have extended into the bud. Figure 3.1c, a schematic generated by Photofinish (Softkey International, Cambridge, Massachusetts) software, shows where the diverse bud parts and tissues in the bud are located. Bud tissues and parts of interest are: bracts (A), flower primordia (B), receptacle (C), and the vascular tissue (D). Notice, in Fig 3.1b, how the dye accumulates mainly in or near the flower primordia (B), and how little dye there is in the bracts (A). This suggests that staining intensity relates, at least, indirectly to metabolic activity. The vascular tissues (D) through which the dye reached the bud from the stem also contain significant amounts of dye.

Figure 3.1. Application one: uptake of azosulfamide dye in apple flower buds.

Enhancement of micrographs Figures 3.1a, 3.1b and 3.1c illustrate effect of uptake of azosulfamide dye in apple flower buds and describe use of the imaging spectrophotometer to enhance photographic data. The x and y axis numbers correspond to pixels in the image; Fig. 3.1a, a photographic image, does not require these numbers. Figure 3.1a shows the original field microphotographs as received from Hungary. Bud length is 2.6 mm. Notice the interference from natural pigments of the tissues and the green of the chlorophyll of the bracts. Figure 3.1b shows the photometrically enhanced image, obtained by subtracting the attenuance ($\sim A$) at 650 nm from the attenuance at 533 nm. The false color images in this figure follow the convention red greatest intensity, yellow less and blue little of activity measured. Figure 3.1c is a schematic silhouette, generated by the software showing flower but features of interest: (A) bracts, (B) flower primordia, (C) receptacle and (D) vascular tissue. Comparing Fig. 3.1b with Fig. 3.1c, notice the staining of the vascular tissue (D) demonstrates continuity with the vascular tissue of the stem; apparently the flower primordia (B) is a sink where the dye accumulates at greatest intensity (deepest red).



FIGURE 3.1a

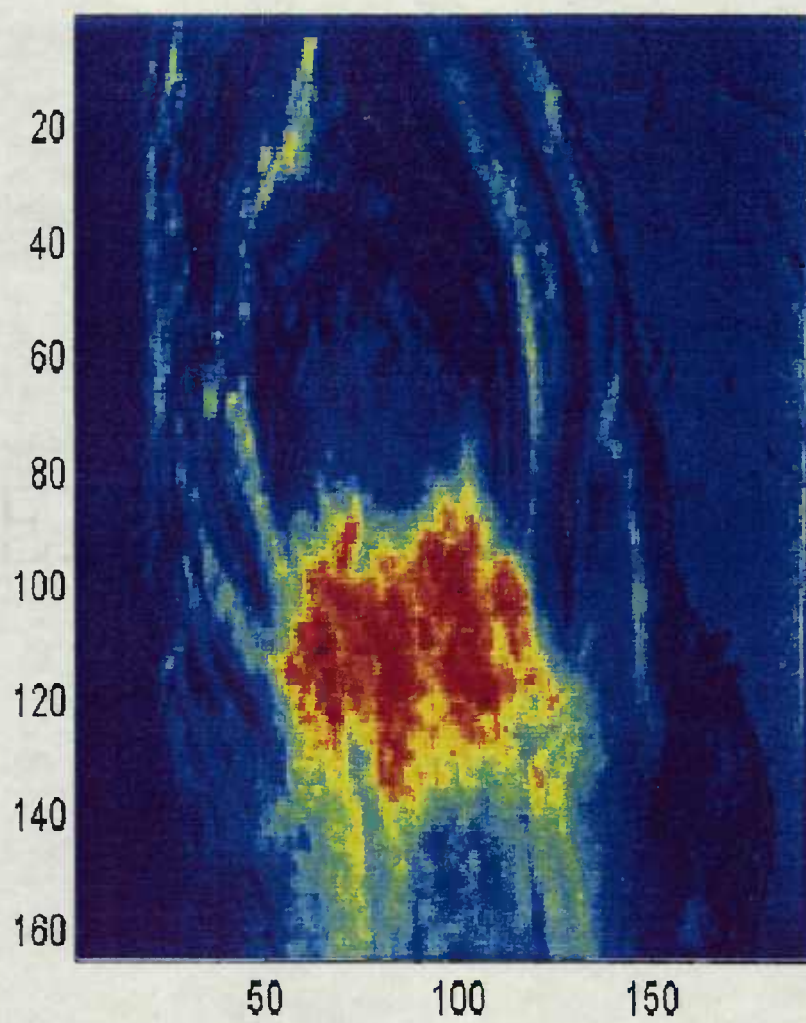


FIGURE 3.1b

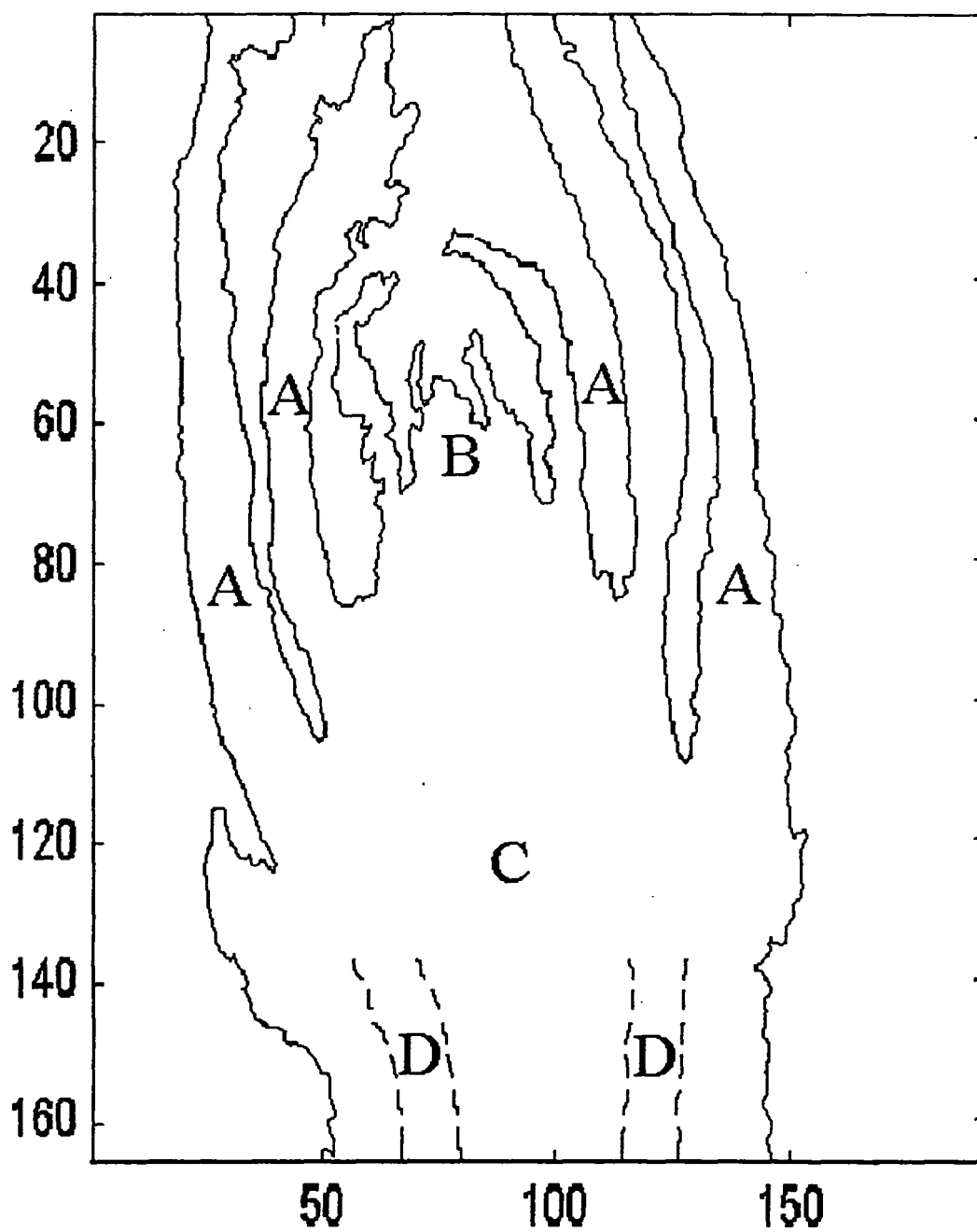


FIGURE 3.1c

A large number of micrographs of flower buds from several apple cultivars, taken at set intervals in the Spring of 1989, were spectroscopically enhanced. In these enhanced images, as opposed to the original photographs, it could be clearly seen that the dye movement was correlated to development of vascular tissues and buds. Documentation of the flower buds' developmental succession and discussion of its horticultural implications will be presented separately. However, we can state that we successfully demonstrated that as the bud starts to develop vascular connections are established, and the dye taken up through the stem xylem reaches the bud's primordia. This allows determination of the time in the Spring when each apple cultivar makes vascular connections between the stem xylem and the bud. This is a matter of interest to students of plant dormancy (~rest).

Application 2, *in vivo* biochemical histology The histological tradition uses reagents which react with specific tissue components to prepare colored slides (e.g. 90), which traditionally are recorded photographically as micrographs. It is so accepted in histology that relative, not absolute, measurements are made that this is not even mentioned in most texts (e.g. 91) and the differences between paths of light in different parts of the complex image is also not discussed. Although in the spectroscopic tradition pathlength is very frequently considered (e.g. 74), much useful histological data can be obtained without normalizing images for pathlength.

In our first application, since we used a non-reactive dye, we could be reasonable sure that dye intensity related to dye concentration. However, in the second application with our sucrose/invertase detecting enzymic dye system (Instrumentation, Materials and Methods section), we need to first established the range of sucrose concentration in which invertase response was linear, and at the same time explore higher sucrose concentrations

that inhibited the invertase reaction. It was also necessary, to verify that the invertase activity observed was due to enzyme activity. Invertase enzyme activity can be demonstrated by determining substrate dependency (K_m), pH optima and using boiled controls. However, a test of activity of an enzyme bound to an insoluble substrate is not readily done by continuous assay in a stirred cuvette. Since stirring, necessary to suspend cell wall particles for measurement, interferes with spectrophotometric measurements. *In vivo* determination of K_m and pH optima using complex plant tissues are difficult because invertase activity is not uniformly distributed through the tissue. We needed a uniformly distributed enzyme activity on a solid matrix to do these tests.

Thus, before imaging invertase in the complex tissues of the plant stem, we first demonstrated (Fig. 3.2) the staining procedure in a model system with relatively uniformly distributed enzyme activity. We crushed hazel (*Corylus avellana* L.) stems onto filter paper taking care to distributing the stem invertases uniformly. This model system takes advantage of the fact that filter paper is made from plant cell walls from which all enzymic activities have been removed.

The invertase (b-fructosidase, saccharase, b-D-fructofuranoside fructohydrolase, EC 3.2.1.26 (92)) activity we measured is the matrix bound, usually considered to be cell wall bound, invertase activity usually considered related to carbohydrate transport (e.g. 90). This activity has not, to our knowledge, been previously described in hazel cell walls. The soluble material from the crushed stems is washed away. Then the washed, hazel stem cell wall material, on its filter paper support matrix, is analyzed for invertase using the "One Touch II" meter. What is measured is the hydrolysis by cell wall invertase of

Figure 3.2. Model for biochemical histological changes. This figure illustrates the determination of invertase activity in stems of hazelnut trees crushed onto filter paper. Each data point represent the mean of at least ten separate assays. This data was obtained using a One Touch II blood glucose meter (Johnson and Johnson, Co.). Figures 3.2a, 3.2b and 3.2c show the dependence of the reaction in the solid matrix, when crushed on paper on substrate and pH. Figures 3.2a and 3.2b were done at pH 4.6 for 0.5 h. In 3.2b, the calculation of K_m is done, as is appropriate, omitting the data at 800 mM where substrate inhibition is apparent; the lines running almost parallel to the regression trace are the 95% probability traces. Figure 3.2c, the pH curve was determined using saturating (400 mM) sucrose which allowed the reaction to proceed for five hours to enhancing minor pH forms without depleting sucrose for major pH forms. The thinner trace in Fig. 3.2c is the quasi cubic spline fit (Statgraphics Plus, Manugistics Inc., Rockville, MD) which in this use predicts the most probable optima of the different activities.

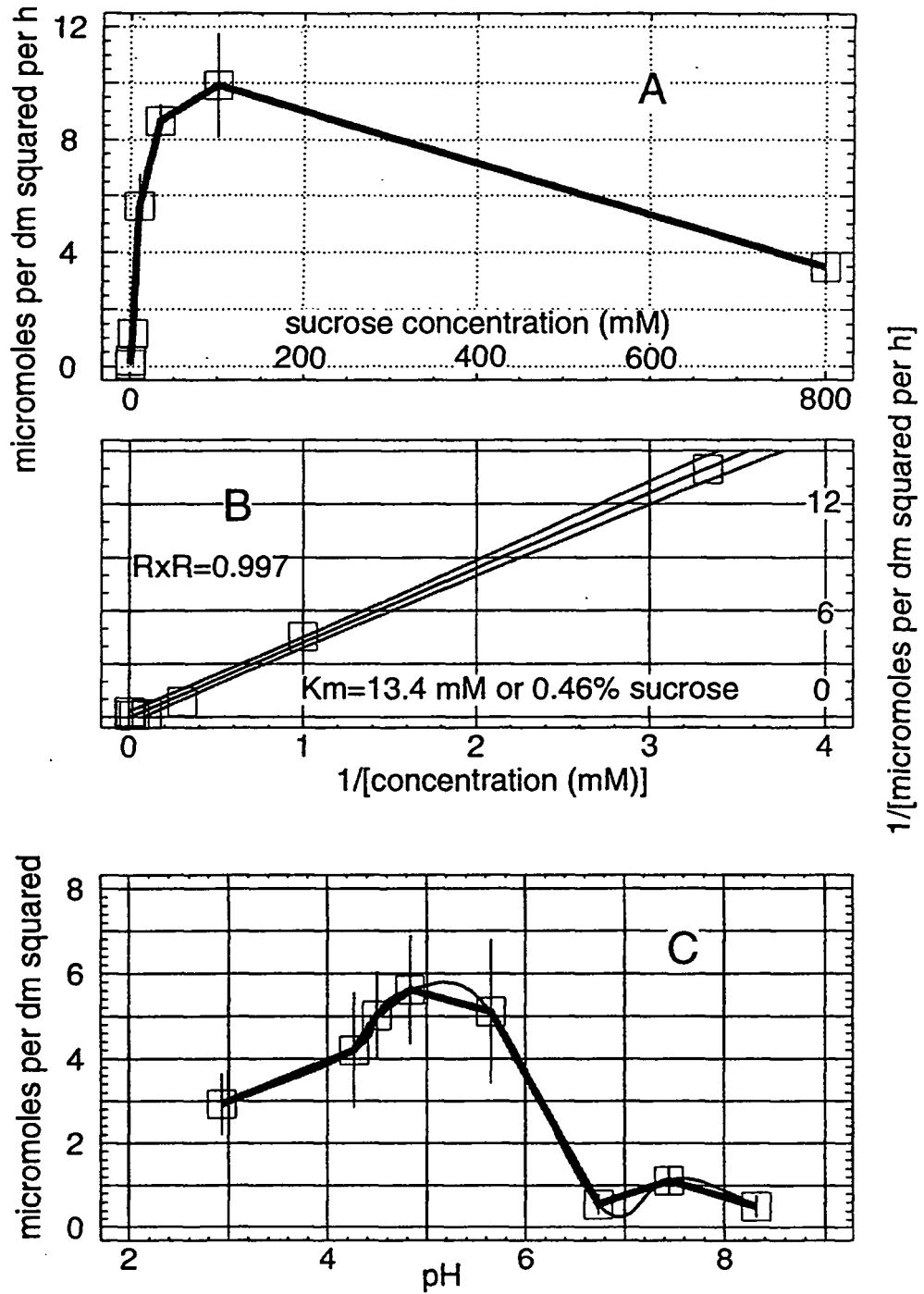


FIGURE 3.2

sucrose, not detectable by the meter, to glucose, detectable via the peroxidase and dye coupled glucose oxidase reaction (Instrumentation, Materials and Methods).

Figures 3.2a, 3.2b and 3.2c show the dependence of the cell wall invertase reaction, on substrate and pH. In Fig. 3.2a we measure the rate of the reaction as it varies with added sucrose substrate. In Fig. 3.2b we measure K_m by the double reciprocal (Lineweaver-Burk plot) (e.g. 93). The Michaelis constant, K_m , is an approximate measure of affinity of the enzyme (invertase) to its substrate (sucrose) that is essentially independent of the amount of enzyme assayed.

K_m is expressed as a substrate concentration, and is used in physiological evaluations of biochemical data. In this use K_m for a given enzyme found in a given tissue is compared to the levels of the substrate found in that tissue. Usually for a enzyme to be considered a plausible part of a process in a given tissue the K_m of the enzyme for that substrate must be less than the substrate levels found in the tissue. The K_m for invertase at pH 4.6 is about 13 mM sucrose (Fig. 3.2b). This works out to be 4.4 g/L or 0.44% sucrose a level far below that found in many plant tissues (reviewed in 74). Therefore the invertase activity measured is plausible physiologically by the K_m criteria.

The pH curve (Fig. 3.2c) shows the acid invertase activity quite clearly and there is a strong suggestion of a neutral invertase. This is also what would be expected in for a plausible invertase reaction.

Table 1 documents the invertase reaction in the stem materials embedded in filter paper. The unwashed disks generate 'net rate' ($\text{mmoles h}^{-1} \text{ dm}^{-2}$) (Table 1, column 4), obtained by subtracting sucrose additions (Table 1, column 3), that was considerably less than the 'net rate' of washed disks. This suggests that endogenous sucrose slows invertase

rate. The apparent effect of endogenous sucrose on invertase rate, together with the specificity of the enzyme reactions, strongly suggests that adding exogenous sucrose to that already there causes a situation of substrate inhibition similar to that shown in the model system (Fig. 3.2a).

Once the enzymic parameters of the staining procedure were worked out we examined sliced, but not crushed, stems (Fig. 3.3a and 3.3b). Now sucrose and invertase are measured by the imaging instrument at the most useful wavelength (595 nm). Uncrushed stem slices are prepared for imaging in the same way as in the model system. The reagent mix lacks added sucrose when measuring sucrose and lacks added invertase when measuring invertase.

Invertase typically acts as a β -fructosidase hydrolyzing sucrose to fructose and glucose. However, invertase also reacts with other substrates such as raffinose that contain a terminal unsubstituted β -D-fructofuranosyl residue and participates in transferase reactions, although not with α -fructofuranosides, fructopyranosides, β -L-sorbofuranosides, β -D-xyloketofuranosides (92). Thus, it is possible that what we observe as a invertase function, may be doing something else *in vivo*. However, given the K_m evaluation (above), the presence of sucrose in the stem (Fig. 3.3a), and that these other invertase reactions are considered have much less metabolic importance (92), it is most logical to assume that what we are observing in Fig. 3.3a and 3b is sucrose content and invertase activity on sucrose respectively.

Figures 3.3a and 3.3b are images of living, not fixed, stem tissue. Figure 3.3a illustrates distribution of sucrose in stem cross section. Notice accumulation (red and yellow) of sucrose in the pith and under the encircling dark blue, almost black, image of

Figure 3.3. Application two: biochemical histology of invertase. This figure shows the histological type data from a dye coupled enzyme staining procedure. Figure 3.3a shows the distribution of sucrose in a slice of hazel tree (*Corylus avellana* L. cv. Barcelona). Figure 3.3b shows the presence of invertase activity in a different slice of stem.

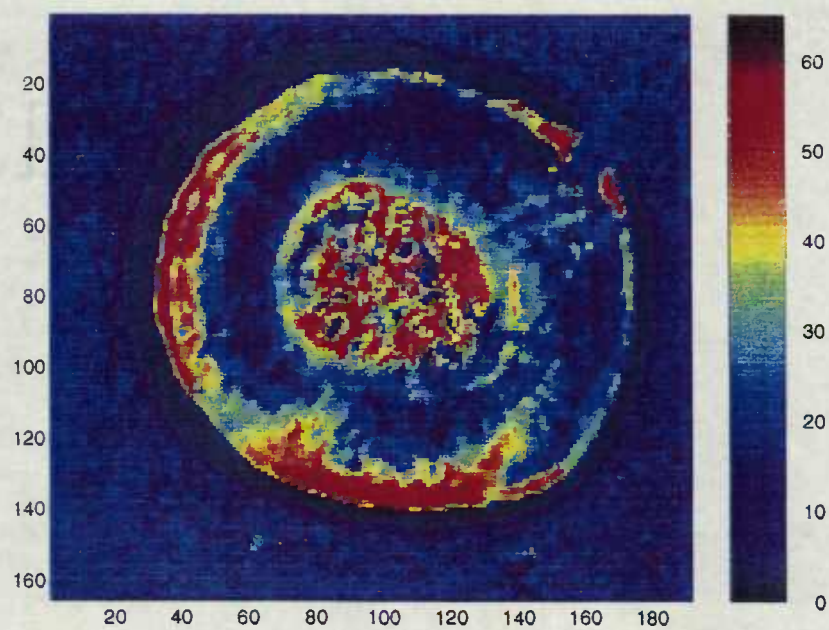


FIGURE 3.3a

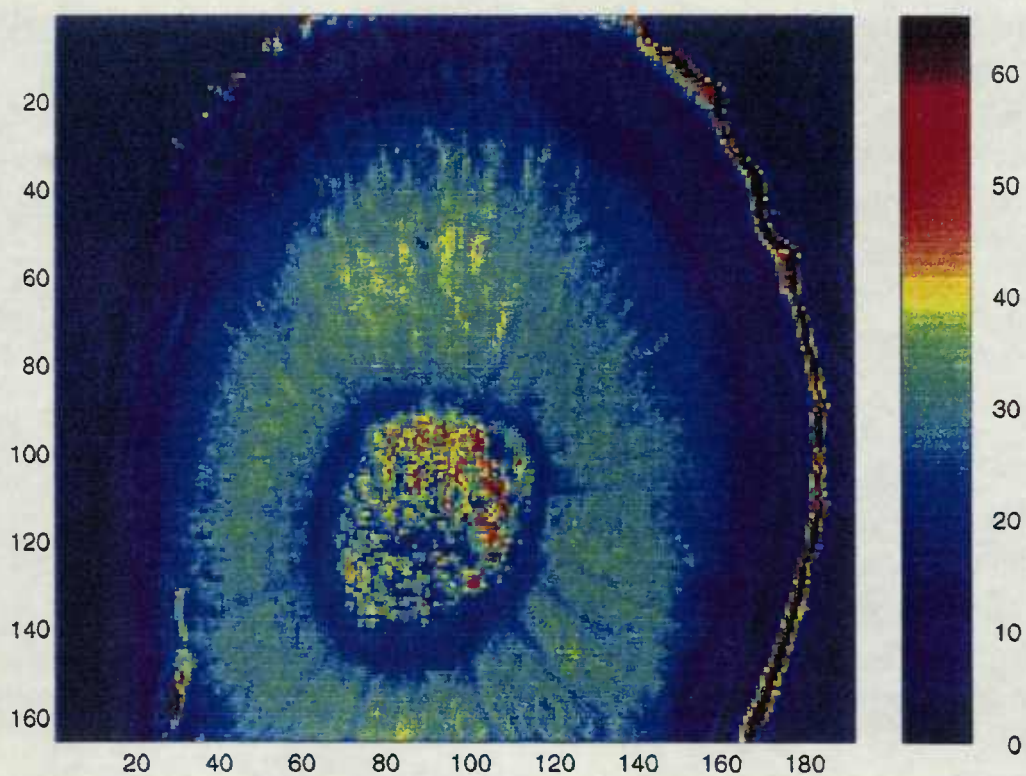


FIGURE 3.3b

the stem's bark. Notice also the asymmetric, sometimes doubled layered (at 8 to 11 clock position), high sucrose bands under the bark.

Figure 3.3b shows the distribution of cell wall bound invertase. The invertase is also distributed in two parts of the stem, but the distribution is different from that of sucrose. The red and yellow areas richest in bound invertase, putative "ray parenchyma", are below (or encircled) by the sucrose rich tissues. The ray-like pattern of the bound invertase activity in this area could be interpreted as the outline of sucrose transport system. Since the "ray parenchyma of woody plants is specialized for seasonal storage, mobilization and translocation of assimilates" (94). The central area, the pith, is also rich in invertase. However, if what we image is a transport system, the connections between sucrose rich "ray parenchyma" area under the bark, and in the pith are not easily apparent, because a dark blue, low invertase, ring like area separates the invertase rich areas of the pith and the "ray parenchyma". The mottled pattern of bound invertase and sucrose in the pith may suggest cell specialization in pith.

This stem sucrose and invertase may have economic and germplasm significance. Sucrose content in stems correlates to varietal, germplasm, susceptibility to Eastern filbert blight (95). The fungal pathogen that causes Eastern filbert blight is *Anisogramma anomala* (Peck) E. Müll. (Diaporthales, Gnomoniaceae). "Sucrose was the only carbon source of 19 carbohydrates tested that supported prolonged growth" of this fungus on artificial media (96).

In the histological approach, for reasons related to effective pathlength, explained here and in detail in previous work (74) the tissue content of sugar and invertase is imperfectly quantified. However, the basic relation of stain to sucrose or invertase is

linear (Fig. 3.2). Thus, the image data of Fig 3.3 can be, as in standard histological work, readily interpreted to explore tissue relationships. However, distinct from histological fixed samples, with our imaging instrument we can examine living tissues. Since, the sucrose detection reactions can be adjusted to be much faster than the plant reactions we could use this method to investigate events in sucrose metabolism in real time. In addition, as was done in early designs (unpublished), our instrument can be adapted to microscopic work.

An alternative to the histological assumption of equal effective pathlength is to choose to determine absolute sucrose concentrations (or invertase activities) by wet chemistry analyses of tissue subsets. However in complex tissues, wet chemistry analyses limit experimental opportunities. Limits of wet chemistry sample calibration arise because: (a) the large number of wet chemistry samples required to properly calibrate all the different tissues found in the complex 31,680 pixel image. (b) To excise these samples would require a large number of cumbersome micromanipulations. (c) Once samples are excised, tissue cell integrity is compromised and extensive degradation of the tissue rapidly ensues. This kind of destructive analyses, where a substantial portions of the tissues are disrupted to remove tissue for wet chemistry analyses, limits time course studies on single samples. This is troublesome since time course studies on single samples eliminate much biological variation.

Thus, in complex tissues, the histological approach using assumptions of equal effective pathlength, is a more practical than wet chemistry spot sampling. We are working on other ways to solve this problem (74). However for now in practical use we can, in first approximation, consider the different pseudo colors of the Fig. 3.3a and 3.3b

to represent relative sucrose concentrations (or invertase activities) from increasing from blue, through yellow, to red.

Application 3, *in vivo* effects of a fungal pathogen One way to calibrate absolute concentrations, non-invasively, is to use Beer's law to determine the effective path of the absorbance of water. This can be done using the absorbance bands of water since in biological systems biochemically active constituents are found in relatively constant water concentrations (74). This approach is appropriate when one is investigating the biochemistry of plant tissues under normal and approximately steady state conditions. However, we should be aware that the amount of water in the light path of spectrophotometrically examined tissues can be changed by a number of plant pathologies (e.g. 97). Spectroscopic changes that apparently arise from pathological changes in water content are also found in the following application (Fig. 3.4, 3.5).

Figure 3.4 illustrates a multispectra analysis used to examine a complex of host-parasite interaction. This interaction has maximal response at about 750 nm, a wavelength which strongly suggests a pathogen mediated water content change. The filamentous fungus *Pestalotiopsis microspora* has an endophytic-pathological relationship with the Florida Torreya or nutmeg cedar (*Torreya taxifolia* Arn.). The Florida Torreya is rare and in decline. And pathogen infection can be demonstrated by taking surface-disinfected (70% ethanol) nutmeg cedar stems with chlorotic (yellowing) leaves and plating out the pathogen on water agar.

This kind of pathogen spreads through the tissue in a way directly related to the distance from the most severely infected sites. For brevity we equate the term disease stage to distance from the severe infection, although we recognize that in a plant

Figure 3.4. Analysis and calibration of spectra for fungal pathogen detection. This figure illustrates a multivariate approach to spectroscopic examination for pathogenic fungus *Pestalotiopsis microspora* on *Torreya taxifolia* Arn. leaves (needles). The upper left panel, shows a three dimensional plot of attenuance, wavelength and disease stage. Panels on upper right and lower left compress this data into two dimensions in plots designed to find the location of the unaffected wavelength at the "isobestic" point. The upper right panel shows raw data and the lower left panel shows the same data data normalized at "isobestic point". The lower right panel shows a plot of a specialized multivariate analysis (PLS). Notice in Fig. 3.4 lower right: minima correlation attributed to interference near 680 nm, the transition through zero correlation at the 715 nm isobestic point, and maximal correlation at 750 nm.

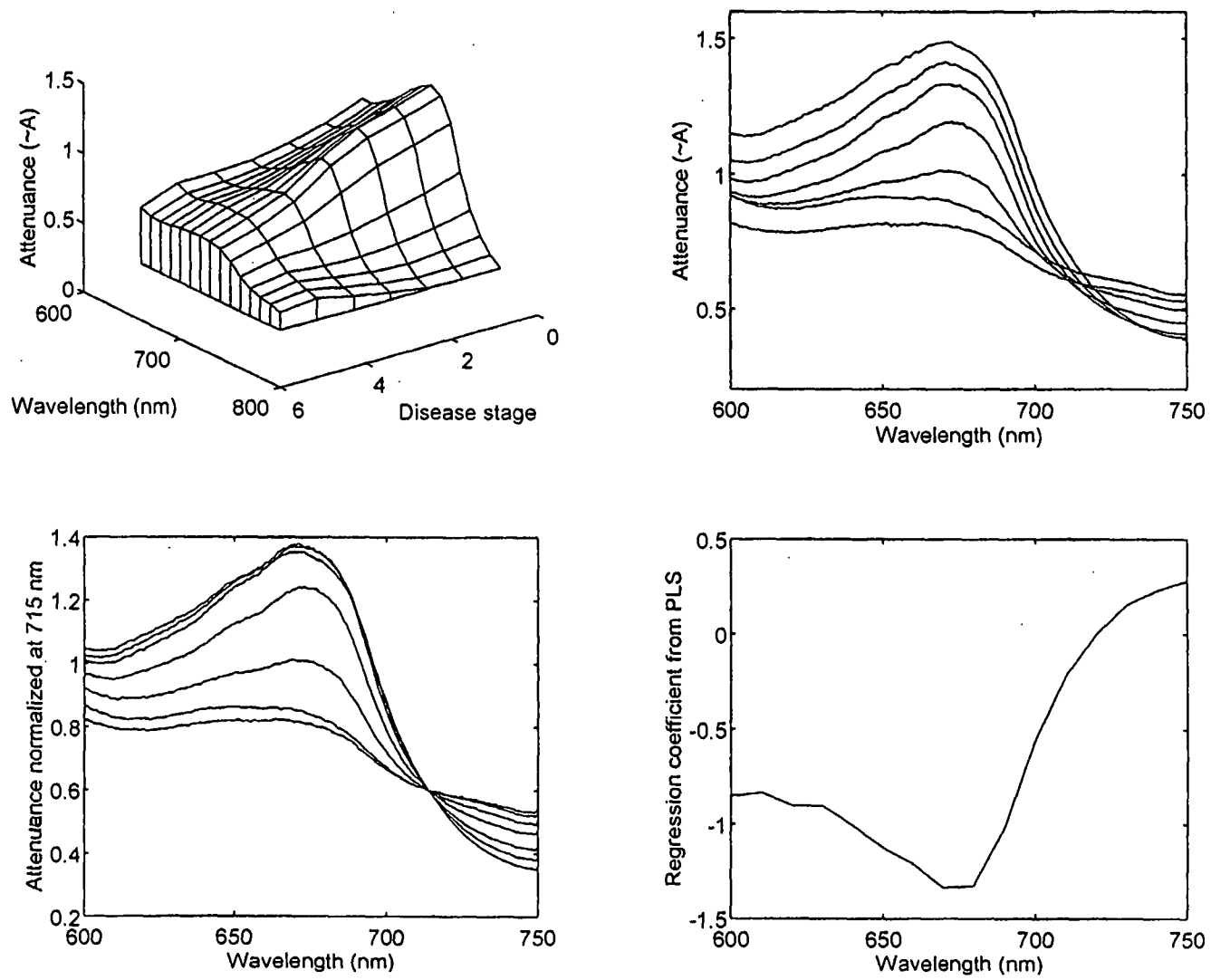


FIGURE 3.4

pathological sense this term is imprecise. However, it is this relationship of severity of infection to distance that allows statistical analyses. Here we used the partial least-squares regression method (PLS). PLS is gaining importance in many fields of chemistry; analytical, physical, clinical chemistry and industrial process control. PLS is a good alternative to the more classical multiple linear regression and principal component regression methods because it is more robust (98-100). PLS is robust because model parameters do not change very much when new calibration samples are taken from the total population.

Figure 3.4 illustrates how PLS was used to find the most appropriate wavelength relationships that maximize spectroscopic imaging of the pathogen in *T. taxifolia* as shown below. Figure 3.4, upper left, shows relationships between attenuance (~absorbance, A), wavelength and distance from spreading front of disease. The relationships between these three parameters is complex and its usefulness is not readily apparent; although one can see apparent correlation between attenuance and disease stage has a minima between 700 and 750 nm.

Figure 3.4, upper right, shows the same data in a two dimensional format, using separate traces for each disease stage. This plot is useful because it signals an apparent isobestic point at about 715 nm. Attenuance then can be normalized at this apparent isobestic point as shown in Fig. 3.4, lower left.

To prepare the PLS plot spectra of diseased and healthy leaflets (needles) were acquired from 600 nm to 750 nm at 1 nm intervals. PLS analysis (100) was performed at all measured wavelengths between 600 and 750 nm. Then a PLS plot of the attenuance at these diverse wavelength against disease stage was generated from the data shown in Fig.

3.4, upper left. Figure 3.4, lower right, shows the PLS regression coefficient curve (100). Please note this is not the standard type regression coefficient since it can exceed +1 and be less than -1.

Notice from the PLS plot (Fig. 3.4, lower right) that the maximal PLS value is at or a little beyond 750 nm. Now we can interpret the other data of this figure with the PLS plot. Comparisons of the attenuance spectra (Fig. 3.4 upper right) to the PLS analyses (Fig. 3.4 lower right) show them to be, in good approximation, mirror images of each other. The PLS minima (Fig 3.4, lower right), corresponds to the attenuance maxima of leaf (needle) absorbance (Fig 3.4, upper right).

PLS regression analysis plots have complex interpretations. In a PLS plot, negative regression coefficient means interference exists at these wavelengths. Figure 3.4, upper right, shows that the 680 nm region is the *in vivo* maxima, the wavelength maxima of photosynthetic system between 600 and 750 nm *in vivo* (e.g. 26,27). Thus it is logical to attribute the PLS minima (Fig. 3.4, lower right) to maximal absorbance of these chlorophyll protein complexes.

The apparent isobestic point (715 nm) (Fig. 3.4 upper right, and lower left) has a PLS correlation coefficient of zero (Fig. 3.4, lower right). When the PLS regression coefficient is close to zero, data at this wavelength does not provide information to the regression model. Thus it is appropriate to use A715 nm, which is also the apparent isobestic point (Fig. 3.4 upper right and lower left) as a baseline for image equations.

We sought a chromophore that could rationally explain the PLS maxima near 750 nm. Water has an absorbance in this range (Fig. 3.5). Since water is present in biochemically active plant material at about 50 M (74), and plant pathology frequently

Figure 3.5. Absorbance bands of water and deuterium oxide mixtures in the range of 700-850nm. Preparation for application 3; demonstration of probable chromophore. This figure demonstrates the minor absorbance bands of water and deuterium oxide mixtures in the range of 700-850 nm.

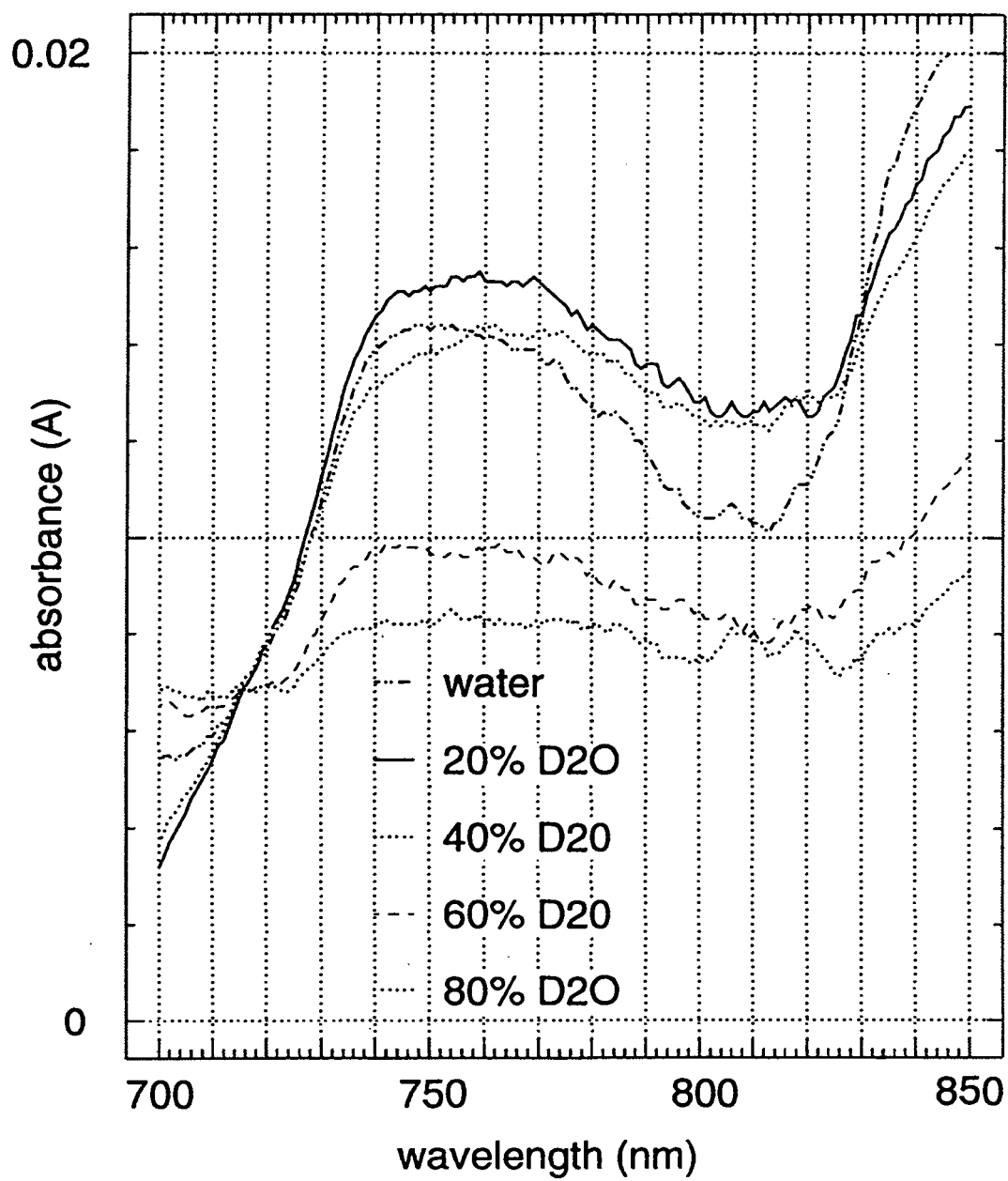


FIGURE 3.5

alters plant tissue water content (e.g. 97) it is most probable that the chromophore responsible for the PLS maxima is the water signal maxima at about 750 nm (Fig. 3.5).

To demonstrate this water chromophore, Fig. 3.5 was generated in a non-imaging spectrophotometer, using deuterium oxide/water mixes (74). In this wavelength region (700-850 nm), the contributions of the mixed species D-O-H, D₂O and water (H₂O, H-O-H) to total absorbance is complex. The data indicates the possibility that D-O-H absorbance is proportionally greater [$A_{D-O-H}^3(A_{H-O-H}/2)$] than is found in the 970-980 nm range (74). This caused difficulty in establishing Beer's law concentration to absorbance correlations in D₂O/water mixes. However unless the water band of Fig. 3.5 demonstrates an unknown, or little known, exception, it is still most logical that this weak water band will follow Beer's law. If this water band follows Beer's law, then it will have an absorbance proportional to its concentration; since water, H-O-H, is the only component absorbing at these wavelengths that is present in significant concentrations *in vivo* (Fig. 3.4 and 3.6).

Using both A715 and A760 nm data we were able to readily distinguish infected from healthy needles of *T. taxifolia* in three populations of needles. This was independently verified by imaging change in fluorescence quantum yield of photosynthetic system caused by pathogen in a fourth population of needles (2).

Figure 3.6 shows a false color image of the progress of damage caused by the toxins of the pathogen *P. microspora* as it spreads through the yew *Torreya taxifolia* Arn. To obtain Fig. 3.6, first we combined the wavelength of the PLS maxima (750 nm) corrected using A715 nm, the isobestic point, as a baseline. However, equations using A760 nm yielded somewhat superior images than those using A750. The reason for this is

Figure 3.6. Application three: imaging of pathogen advance in a leaf *in vivo*. This figure shows, by imaging absorbance spectroscopy, effects of *Pestalotiopsis microspora*. pathogen attack on *Torreya taxifolia* Arn. leaves (needles). Red indicates healthy tissue, yellow indicates pathogen damage. The upper four needles are healthy, the lower four needles are infected at their tips. The equation used for the image is $[80 \cdot (A_{715} - A_{760}) + 38]$, the factors 80, and 38 are explained in text.

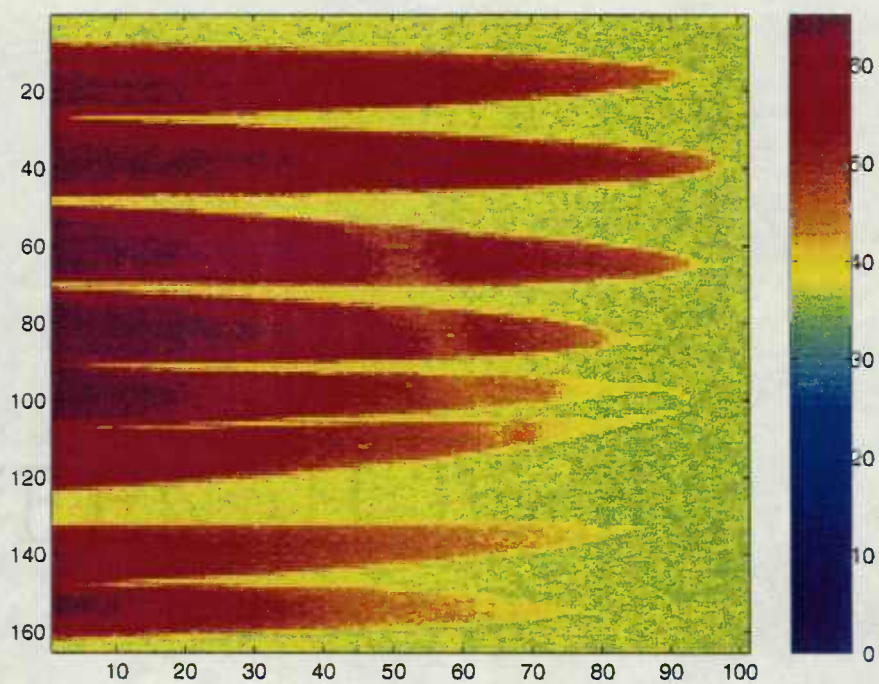


FIGURE 3.6

not clear, but from trends in Fig. 3.4 lower right do suggest that 760 nm may be closer to the "true" PLS maxima; and the water peak maxima in this region (Fig. 3.5) is broad enough to readily justify this use of A760 nm.

Figure 3.6 shows, by imaging absorbance spectroscopy, the progress of *P. microspora* pathogen attacking the endangered species *T. taxifolia* needles. Red color indicates healthy tissue, yellow indicates pathogen damage. The upper four needles are healthy, although there is a line indicating folding in shipping. The lower four needles are infected at their tips. The equation used for the image is $[80 \cdot (A_{715} - A_{760}) + 38]$. The notation A indicates attenuance, A760 the PLS maxima (Fig. 3.4) is close at the maxima for water absorbance in this wavelength range (Fig. 3.5), A715 is the wavelength of the isobestic point (Fig. 3.4 upper right and lower left). The numbers 80 and 38 are used to present the image in the appropriate color format.

The ecological significance of Fig. 3.4 and 3.6 is that they describe *in vivo* the progress pathogen attack on an endangered tree species. The visual appearance of symptoms at three weeks is very weak and essentially undetectable except by this method or by fluorometry (2). Furthermore, symptom expression seems to be related to the phytotoxin rather than a direct effect of the pathogen on host cells, because spectral differences appear in advance of spreading fungus.

Application 4, following changes in water *in vivo* Figure 3.7 shows the successive loss of water, as it is replaced by deuterium oxide, in a leaf of *Hibiscus sabdariffa* L. The significance of this data is we can measure water levels directly in plant tissue using the band near 970 nm. The band near 970 nm is stronger and less affected by the presence of deuterium oxide (74) than the water band near 750 nm (Fig. 3.5). As explained previously

Figure 3.7. Application four: determination of water in a living leaf. This figure shows, in a leaf of *Hibiscus sabdariffa* L, the successive loss of water which absorbs at 970 nm, as it is replaced by deuterium oxide which has essentially no absorbance at 970 nm. The "chicken track" traces are the vascular tissue (veins) of the leaf. The upper left, upper right and lower left show the images of $A_{970}-A_{790}$ at 0, 36 and 72 hours respectively. The lower right panel shows the difference spectra between the upper, and lower left panels; this panel represents the levels of water in the original leaf.

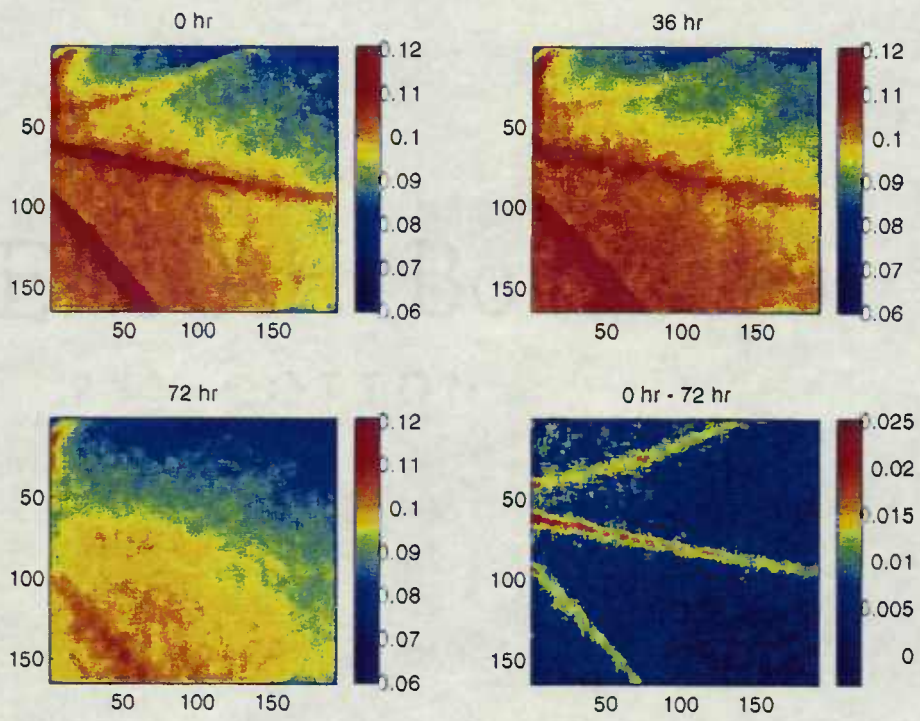


FIGURE 3.7

(74) the water concentration of healthy plant tissue remains quite constant. The importance of this particular use is that the plant *H. sabdariffa* is a good test system for phytotoxins, which, as described above, may be related to changes in water content. In addition unpublished work using this approach has demonstrated spectral signal strength sufficient to follow, in situ the effects of progressive hydration, dehydration or pathology of plants, and thus may have considerable applied use in agriculture (101).

Application 5, estimation of quantum yield of photosynthetic fluorescence in variegated leaves Figure 3.8, demonstrates a quite different application, fluorometry which is done when the instrument is reconfigured into an imaging fluorometer (2). In this configuration the instrument measures, in good approximation, the quantum yield of photosynthesis.

Photosynthetic fluorescence is quite complex (2,7,11,31,43,47,102). Absorbing broadly across the visible range, the plants' photosystems 'funnel' light to their reaction centers (RC) (47,53,60,102). When RC are ready for use about 97% of absorbed light is used for photochemistry, 2.5% is transformed to heat, and fluorescence is quenched with only 0.5% re-emitted as red fluorescence (47). If RC are not ready 90-95% of absorbed light may be lost through heat deactivation and 2.5-5% through fluorescence (47).

Darkening the leaf ensures open RCs; then, on illumination, complex time and wavelength variable, fluorescence signals are generated (e.g. 2,7,47). The intensity and timing of these complex fluorescence signals strongly reflect the structure and potential for activity of the photosynthetic apparatus, the demands of the "dark reaction", the health of the leaf and the plant's adaptation to environmental conditions (2,31,42,43,47,48,50,53,55,56,

Figure 3.8. Application five: demonstration of fluorescence configuration used to determine differences in photosynthetic efficiency. This figure shows data obtained by the instrument when it is configured to measure photosynthetic fluorescence and the image is acquired perpendicular to the plane of the leaf and at close range. The leaves of *Scrofularia nodosa* 'Variegata' plant have hue domains, x-y oriented areas where the concentrations of chlorophyll are relatively uniform. In this leaf are three domains, high chlorophyll, low chlorophyll and very low chlorophyll. The area immediately adjacent and parallel on both sides to the central vein is the high chlorophyll area. The very low chlorophyll area is at the extreme edges of the leaf. The low chlorophyll area fills the space between the other two domains. These hue-domains have relatively abrupt transitions between them. The panels at the upper left, upper right, lower left and lower right show respectively: response at the time of maximal fluorescence (F_m); response at time of minimal fluorescence (F_s); response ($F_m - F_s$); and response for quantum yield estimate $Y' = (F_m - F_s) / (F_m - F_{\text{dark}})$. Panel legends show these equations, however, the imaging program does not allow for subscripts.

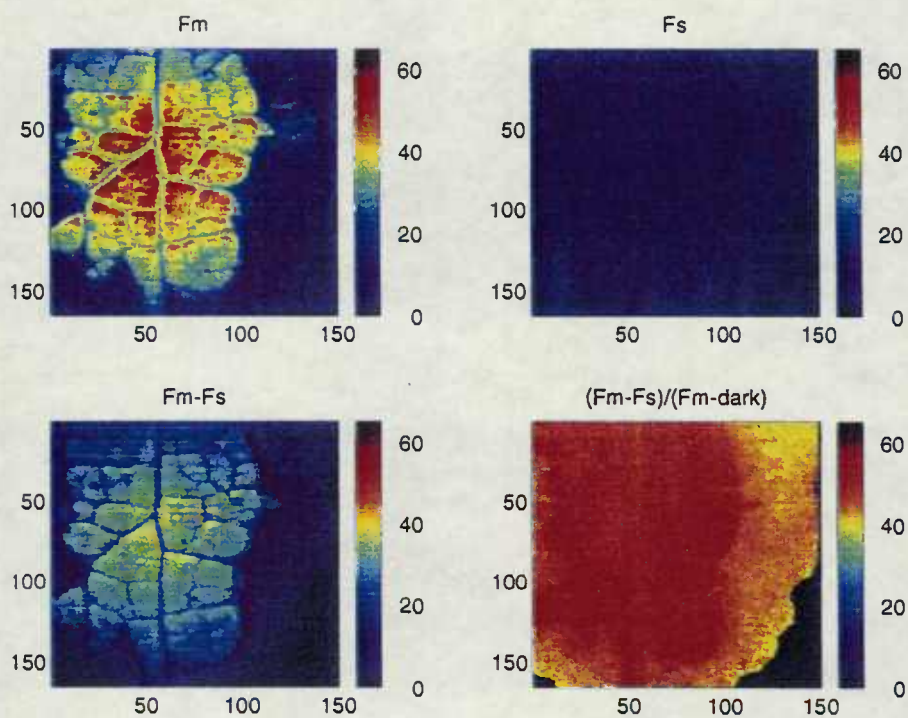


FIGURE 3.8

103,112,118). Fluorescence signals vary in ways diagnostic of leaf function (e.g. 2,55,112), leaf environmental history and damage (103-109).

In intact leaves (e.g. 2, 37,55) functional photosynthetic tissues generate changing patterns of fluorescence immediately after these tissues (usually leaves) are illuminated. The selected fluorescence maxima (F_m) and the time estimated minima (F_s) can be used empirically estimate quantum yield of photosynthesis (2) and thus are very sensitive indicators of changes in plant photosynthetic function. Fluorescence and absorbance spectra of leaves reveal useful information about leaf photosynthesis and their capabilities overlap. Fluorescence imaging is used mostly to detect photosynthetic functions (55); absorbance imaging more readily describes photosynthetic structure changes (1,74). Since plant photosynthetic function relates to crop yield, fluorescence imaging (2,28,55,110-113) measurements are important to agricultural research.

Notice in Fig. 3.8, how in this leaf the distribution of maximal fluorescence (F_m), upper left, is mottled demonstrating the relative distribution of chlorophyll. The terminal fluorescence (F_s), upper right, is of low intensity, yielding a dark image in which details are hard to see. The difference between maximal fluorescence and minimal fluorescence ($F_m - F_s$) still retains the effects of chlorophyll content. However, the image equation, lower right, for estimate quantum yield Y' , $(F_m - F_s)/(F_m - \text{dark})$ shows the quantum efficiency hue-domains quite clearly. Comparing the upper left image with the lower right image, one can see how the Y' equation presents relatively uniform surfaces for the different hue-domains.

Figure 3.8 demonstrates the differences in estimate of fluorescence quantum yield in the different hues parts, hues-domains, of a *S. nodosa* 'Variegata' leaf. This is

significant to us because we have already demonstrated that differences in CPX exist between the different and well resolved hued domains found on the leaf of this plant. Thus we can related structure to function, and show the lesser photosynthetic efficiency of the more lightly pigmented CPX domains on the leaf. Since these differences are within leaves grown in exactly the same conditions we can surmise that genetic effects dominate over environmental factors in this situation.

Demonstration of challenges to remote fluorescence measurement of photosynthesis of whole plants Figure 3.9 shows photosynthetic fluorescence taken at a distance (7 m). Fluorescence imaging would best serve agriculture and Earth sciences if it could be done at a distance. Figure 3.9 illustrates the challenges faced by remote fluorescence sensing. Remote fluorescence sensing commonly uses laser illumination (e.g. 114-118); thus it is known as Lidar (Laser distance fluorescence). Leaves are oriented on the plant to gather solar radiation. Solar radiation, because it is scattered, by its passage through the atmosphere does not act only as a point source. This relates to the classical reason Lord Rayleigh gave why the sky is blue, since blue light is more intensely scattered than red light (e.g. 119). Thus plants receive light from different directions: as direct solar radiation from the sun's position, as diffuse radiation from scattering in the sky and as reflected light from other foliage and the ground (e.g. 120). In addition, as the Earth moves, the relative position of the sun changes. Thus to function optimally for photosynthesis leaves are placed non-randomly, but complexly, on a plant, where the leaves, and commonly those of other plants, form a leaf canopy (e.g. 121).

In remote sensing of vegetation the canopy, not individual leaves, need to be investigated (e.g. 33,35,46,52,63,65,66). When we perform experiments with a point

Figure 3.9. Data on differences in orientation of leaves of canopy and its effect on apparent quantum efficiency of photosynthesis. This figure shows data obtained by the instrument when it is configured for fluorescence and used at a distance of 7 meters, and the leaves are not all perpendicular to the light source direction. This figure images fluorescent parameters of potted *Digitalis purpurea* L. plant. The panels at the upper left, upper right, lower left and lower right show respectively: response at the time of maximal fluorescence (F_m); response at time of minimal fluorescence (F_s); response ($F_m - F_s$); and response $Y' = (F_m - F_s) / (F_m - F_{dark})$. In the upper left panel (F_m), one can also distinguish the faint, very dark blue, outline of the pot that contains the plant. In the upper right panel (F_s) the remaining fluorescence at 150 s is shown, notice how there are less red areas. Subtracting F_s from F_m , lower left panel, shows that under these conditions of relatively weak illumination the decay time of the fluorescence is prolonged. The normalization procedure of the lower right panel [$Y' = (F_m - F_s) / (F_m - F_{dark})$] does not yield a uniform false color, such as is found within each of the different hue domains of Fig. 3.8. These image reflect the complex orientation of leaves in the plant's canopy and weaker illumination. This illustrates the challenges of remote fluorescence sensing of photosynthetic parameters. However, it is still possible to detect photosynthetic activity in the leaves that have their x-y plane perpendicular to the direction of the light

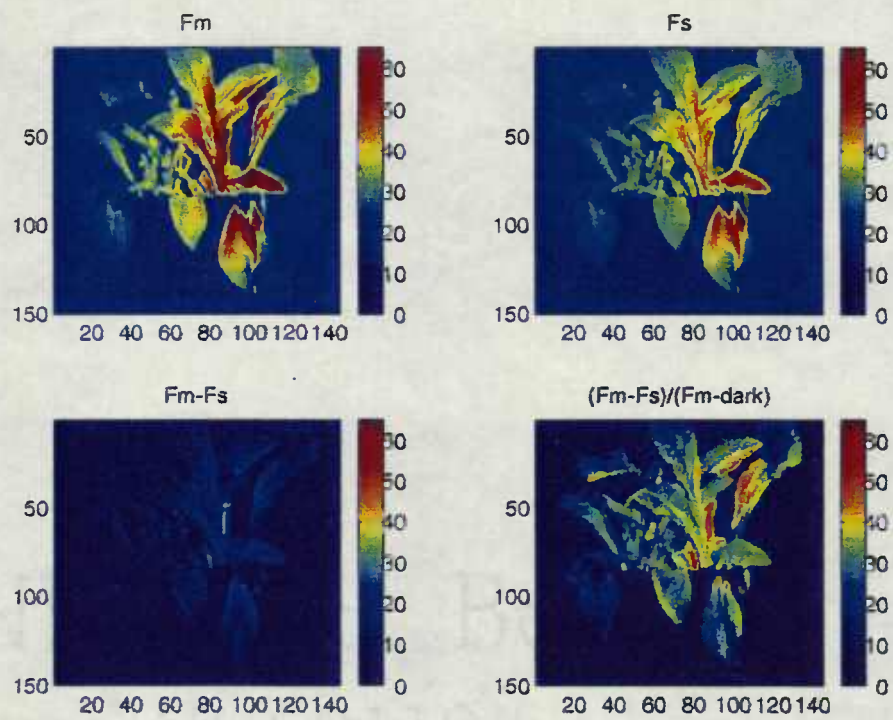


FIGURE 3.9

source of light, we note two classes of leaf positions: position (I) when the x-y plane of the leaf lamina is perpendicular to the light beam the best, strongest, most informative, images are obtained. Thus it is common in preliminary work to place or hold the leaves in position I (e.g. 2,118). Even when light intensity is not saturating, the images of leaves in position I can provide much useful data (2).

We can think of position I as the sun illuminating the equatorial regions of Earth. In this case the light reaches the Earth perpendicular to the surface and yields the highest solar light flux per unit area. Position II where the x-y plane of the leaf is not perpendicular to the light beam can be thought of as similar to sun illuminating the polar regions in winter. In the polar regions the sun's light strikes obliquely and thus yields much less solar light flux per unit area.

Is possible to illuminate leaf canopies at short range with lasers sufficiently powerful so that effects of leaf position in canopies can be neglected (e.g. 52). However, in the future remote photosynthetic sensing will probably be done with lasers illuminating from orbit. Laser broadening and atmospheric scattering over the great distances involved will make it difficult to light saturate the photosynthetic system of all canopy leaves. Thus, position (II) leaves, since they do not present their leaf x-y plane perpendicular to the direction of the exciting light, will yield much weaker and provide less informative signals.

In Fig. 3.9, since we are not using a coherent laser light source, at 7 m the exciting light reaching the plant is not saturating, even when the leaf lamina plane is perpendicular to the exciting light. Therefore, the leaf is "hungry for light", most of the light is used, and

fluorescence signals are weak. Consequently the apparent quantum yield is less (Fig. 3.9) than that observed when leaves are illuminated from a shorter distance (Fig. 3.8).

This could be easily remedied in the laboratory, using a more powerful light source or a laser. However, we choose to use this situation to show the influence of leaf orientation on apparent quantum yield. In Fig. 3.9 image equations F_m and F_s (upper left and right respectively) are relatively well defined. However these images, as discussed for Fig. 3.8, are still dependent on chlorophyll concentration. The F_m-F_s image (lower left) is very weak because the fluorescence decays much slower under low light. The lower right image of Y' approximation of quantum yield image [$Y'=(F_m-F_s)/(F_m-F_{dark})$], shows photosynthetic activity of position I leaves, without the confusing influence of variable chlorophyll concentrations. This last image clearly illustrates the effect of leaf position on fluorescence due to uneven, weak, illumination. For instance in Fig. 3.9, lower right panel, observe an upright leaf at about the 1 o'clock position. In this leaf, one half on the upper side of the mid vein is much less illuminated than the lower half. Yet these two sides of the leaf are essentially identical.

This demonstrates a potential advantage of the Y' equation for Lidar applications. Quantum yield estimates give a relatively uniform field when the leaves are in position I (2), but not when leaves are in position II (Fig. 3.9). Therefore in theory, if the canopy is illuminated with coherent light from a laser, or even relatively well focused light from a point source, potentially useful data can be obtained from the subset of canopy leaves, or parts of leaves, in position I (lamina's x-y plane approximately perpendicular to the exciting light). This position I subset potentially determines the maxima of quantum yield if the strength of the exciting light reaching the leaf is sufficient to saturate the

photosynthetic system. The fluorescence from leaves in position II weaker, and with lower apparent quantum yields, could be mathematically eliminated from analyses. Thus, this data and equations presented here may help interpret Lidar data from canopies if data from leaf position subsets I and II are resolved mathematically.

CONCLUSIONS

High resolution imaging spectrophotometry capable of recording leaf spectrum over two-dimensional space is useful for many purposes in the plant sciences. The enhancement of photographic images was an unusual application which may serve to increase data recovery from scientific data archives. The detection of sucrose and invertase in living section of stems has many potential plant physiological and phytopathological applications. Measurement of water using bands near 750 and 970 nm has proved useful for measuring advances of plant pathogens and decrease of water as deuterium oxide is taken up by the leaves. This technology may lead to field measurements of water in leaves of crop plants allowing closer more frugal use of irrigation. An alternate configuration of the instrument to detect fluorescence from the photosynthetic system is also useful, especially when used at close range. The investigation of the photosynthetic fluorescence of hue-domains in variegated leaf tissues may provide basic insights into the genetic control of variegation. The instrument in its fluorescence configuration used at a distance, although it provides some useful information on photosynthesis leaves with lamina plane perpendicular to the light source, is less useful to measure canopy leaves that are not in the appropriate orientation. Thus,

to measure canopy photosynthesis, the fluorescence option needs a stronger, more focused, or more coherent, light source.

BIBLIOGRAPHIC SKETCHES

Author(s): Li Ning, Walter J. Bowyer, Annie M. Chozinski, Tamas Buba, Anita Azarenko, Gerald E. Edwards, Larry S. Daley*, James B. Callis, and Gary A. Strobel.

Li Ning is a graduate research assistant in the Departments of Horticulture and Computer Engineering at Oregon State University (OSU), Corvallis. He received his MS in Horticulture from Beijing Agriculture University, in 1987, and his BS in biology from Peking University, China, 1983. Ning is preparing to take his PhD defense in the summer months of 1996 and completing his course requirements for a MS in Computer Engineering. Ning's PhD dissertation will include the construction of a novel imaging spectrometer and fluorometer, and the application of these instruments to *in vivo* biochemistry, phytopathology of diverse plant germplasm.

Walter J. Bowyer is an associate professor in the Department of Chemistry at Hobart and William Smith Colleges, Geneva, New York. He received his PhD in analytical chemistry, from the University of Vermont in 1985, his MS in biology from the University of Virginia earlier that same year, and his BS in Ecology from Johnson State and Windham Colleges in 1980. His interests include electrochemistry and diverse spectroscopies, as well as imaging spectroscopy.

Annie M. Chozinski received her MS in Horticulture from Oregon State Univ. in 1995 and her BS in Horticulture from Ohio State in 1991. She is very interested in plant

breeding to improve medicinal and edible crops. Her interest in imaging spectroscopy arose because she found it to be the quickest most efficient way to interpret her histological data, thus solving many of her research problems.

Tamas Buba is professor of pomology at the Fruit Development Station) Ujfeherto, Hungary. His research area is plant anatomy, and includes flower bud development and dormancy investigations.

Anita Azarenko is associate professor in the Department of Horticulture at OSU. She received her PhD, Horticulture-Plant Physiology, from the University of Maryland in 1987. Her research interests include whole tree physiology and the relationships between plant physiology and crop production. She conducts basic research on flower buds, flowering sporophytic self-incompatibility, and the process of development of flowers into fruit and nuts.

Gerald E. Edwards, is a professor in the Department of Botany at Washington State University, Pullman. He received his PhD in Plant Sciences from the University of California at Riverside in 1969. He frequently uses fluorescence to investigate photosynthetic phenomena, especially when it relates to his interest in photosynthetic carbon metabolism and stress in higher plants. He is one of the most respected scientist in this area of science.

Larry S. Daley is an associate professor in the Department of Horticulture at OSU. He received his PhD from the University of California at Davis in the Biochemistry and Biophysics Department in 1975. His research interest include the biochemical and biophysical interpretation of *in vivo* leaf spectra and its relationship to germplasm research.

James B. Callis is a professor of chemistry and adjunct professor of bioengineering at the University of Washington, Seattle. He earned a PhD in chemistry from the University of Washington in 1970. His research interests include the development of instruments including the video fluorometer, flash calorimeter, imaging spectrophotometer, and laptop computerized instruments. Prof. Callis's current interests include development of instrumentation for ecological surveys and *in vivo* interferometry. Prof. Callis is best known for his contributions to applied uses of spectroscopy.

Gary A. Strobel is Gray Professor in the Plant Pathology Department at Montana State University. He received his PhD from U.C., Davis in 1963, and his BS from Colorado State in 1960. Prof. Strobel is a physiological plant pathologist, well known for his elucidation of structures, physiological activities and innovative applications of fungal and bacterial toxins. His interest in visible and near-infrared imaging relates to the usefulness of this spectroscopic technology to detect pathological events in plants.

ACKNOWLEDGMENTS

We gratefully acknowledge support from the Herman Frasch Foundation (grant number: FRASCH 63-0738), The Oregon Filbert Commission and the OSU AG Research Foundation. We thank Johnson and Johnson, Inc., (Milpitas, California) for donations of a large number of Touch^R test strips for the "One Touch II" blood glucose meter, and Lucidyne Technologies Inc., (Corvallis, Oregon) for the donation of a color copier. This paper is Oregon Agricultural Experiment Station Technical paper 11034 and 11037.

REFERENCES

- (1) L. Ning, R. Ozanich, L.S. Daley and J.B. Callis, *Spectroscopy* 9(7), 41-48 (1994).
- (2) L. Ning, G. E. Edwards, G.A. Strobel, L.S. Daley, and Callis, J. B., *Applied Spectroscopy*, 48, 1381-1389 (1995).
- (3) N.J.C. Müller, *Jahrbuch wiss Botanik* 9, 42-49 (1874).
- (4) W.W. Coblenz, *Bulletin of the Bureau Standards*, 9, 283-325 (1913).
- (5) C.A. Shull, *Bot. Gaz.*, 87, 583-607 (1929).
- (6) A. Seybold, *Planta*, 18, 479-508 (1933).
- (7) H. Kautsky and A. Hirsch, *Biochem. Zeitschrift* 274, 423-434 (1934).
- (8) H. Mestre, *Cold Spring Harbor symposia on quantitative biology*. 3, 191-209 (1935).
- (9) G.S. Rabideau, C.S. French, and A.S. Holt, *Amer. J. Bot.*, 33, 769-777 (1946). (10) C. S. French, J.S., Brown, and M.C. Lawrence, *Plant Physiol.*, 48, 421-429 (1972).
- (11) G. Papageorgiou, "Chlorophyll Fluorescence: an Intrinsic Probe of Photosynthesis," in *Bioenergetics of Photosynthesis*, Govindjee Ed. (Academic Press, New York, 1975), p. 319-371.
- (12) J. Lavorel and A.L. Etienne, "*In Vivo* Chlorophyll Fluorescence," in *Topics in Photosynthesis*, 2. J. Barber Ed. (Elsevier, Amsterdam, 1977), p. 203-268.
- (13) W. Ruhle, and A. Wild, *Planta*, 146, 551-557 (1979).
- (14) L. S. Daley, *Scientia Hort.* 28, 165-176 (1986).
- (15) L.S. Daley, M.M. Thompson, W.M. Proebsting, J. Postman, and B.R. Jeong, *Spectroscopy*, 1(7), 28-31 (1986).
- (16) L.S. Daley, P.J. Breen, and P. Mohanty, *Spectroscopy*, 2(3), 32-35 (1987).
- (17) L.S. Daley, O. Jahn, and C. Guttridge, *Photosynth. Res.* 11, 183-188 (1987).
- (18) L.S. Daley, R.A. Menendez, and R.L. Stebbins, *J. Environ. Hort.*, 5, 25-28 (1987).
- (19) H.H. Fisher, R.A. Menendez, L.S. Daley, D. Robb-Spencer, and G.D. Crabtree, *Weed Sci* 35, 333-338 (1987).

- (20) W.W. Guo, W.M. Proebsting, S.W. Potter, L.S. Daley, and J.R. Potter, *Plant Physiology*, 85, 1089-1093 (1987).
- (21) D.H. Card, D.L. Peterson and P.A. Matson, *Remote Sens. Envir.*, 26, 123-147 (1988).
- (22) L.S. Daley, J.R. Powell, G.A. Strobel, R.B. Boone, J. Postman, M. Willie, and J.H. Brown, *Plant Physiol. Biochem.*, 26, 683-694 (1988).
- (23) B.R. Jeong, L.S. Daley, J. Postman, W.M. Proebsting, and F.J. Lawrence, *Photochem. Photobiol.*, 47, 91-100 (1988). (24) B.R. Jeong, L.S. Daley, D.G. Smith, R.B. Boone, and E.J. Zais, *Spectroscopy*, 3(2), 26-31 (1988).
- (25) W.W. Cure, *Proc. Amer. Soc. Photogrammetric Eng.*, 3, 181-189 (1989).
- (26) C. Chen, L.S. Daley, and W.E. Kronstad, *Plant Physiol. Biochem.* 28, 259-269 (1990).
- (27) L.S. Daley, *Plant Physiol. Biochem.* 28, 271-282 (1990).
- (28) J.M. Fenton, and A.R. Crofts, *Photosynth. Res.*, 26, 59-66 (1990).
- (29) B.J. Yoder, and L.S. Daley, *Spectroscopy* 5(8), 44-50 (1990).
- (30) G.A. Carter, *Amer. J. Bot.*, 78, 916-924 (1991).
- (31) K.K. Karukstis, Fluorescence as a physical probe of the photosynthetic apparatus, in *Chlorophylls*, H. Scheer Ed. (CRC Press, Boca Raton, Florida, 1991) pp. 769-795.
- (32) C. Chen, J.S. Cameron, S.F. Klauer, and P.W. Foote, *Plant Physiol. Biochem.*, 30, 71-80 (1992).
- (33) C.D. Elvidge, Z. Chen, and D.P. Groeneveld, *Remote Sens. Environ.*, 44, 271-279 (1993).
- (34) M.K. Hamilton, C.O. Davis, W.J. Rhea, S.H. Pilorz and K.L. Carder, *Remote Sens. Environ.* 44, 217-230 (1993).
- (35) F. Baret, V.C. Vanderbilt, M.D. Steven, and S. Jacquemoud, *Remote Sens. Environ.*, 48, 253-260 (1994)
- (36) L. Ning, L.S. Daley, Z. Lu, and J.B. Callis, *Biochem. Biophys. Res. Commun.* 205(1), 638-644 (1994).

- (37) G. Schmuck and I. Moya, *Remote Sens. Environ.*, 47, 72-76, (1994).
- (38) L. Daley, unpublished data (1994).
- (39) L.S. Daley, J.M. Montano, R.A. Menendez, A.H. Soeldner, and R.B. Boone, *Spectroscopy*, 2(9), 32-36 (1987).
- (40) A.H. Al-Abbas, A.H., R. Barr, J.D. Hall., F.L. Crane, and M.F. Baumgardner, *Agron. J.* 66, 16-20 (1974).
- (41) R.M. Smillie, "The Useful Chloroplast: a New Approach for Investigating Chilling Stress in Plants", in *Low Temperature Stress in Crop Plants*, J.M. Lyons, D. Graham and J.K. Raison Eds. (Academic Press, New York, 1979), p. 187-202.
- (42) H.K. Lichtenthaler, *J. Plant. Physiol.*, 131, 101-110 (1987).
- (43) H.R. Bolhar-Nordenkamp and E.G. Lechner, "Winter Stress and Chlorophyll Fluorescence in Norway Spruce (*Picea abies* (L.) Karst)." in *Applications of Chlorophyll Fluorescence*, H.K. Lichtenthaler Ed. (Kluwer Academic Publ., Dordrecht, Holland, 1988), pp. 173-180.
- (44) Greene, B.A., Staehelin, L.A. and Melis, A., *Plant Physiol.*, 87, 365-370 (1988).
- (45) P. Horton and A. Hague, *Biochem. Biophys. Acta* 932, 107-115 (1988).
- (46) T.W. Brakke, J.A. Smith, and J. M. Harnden, *Remote Sens. Environ.* 29, 175-183 (1989).
- (47) H.R. Bolhar-Nordenkamp and G. Oquist, "Chlorophyll Fluorescence as a Tool in Photosynthesis Research," in *Photosynthesis and Production in a Changing Environment, a Field and Laboratory Manual*, D.O. Hall, J.M.O. Scurlock, H.R. Bolhar-Nordenkamp, R.C. Leegood and S.P. Long, Eds. (Chapman and Hall, London, 1993), Chap. 12, p. 193-206.
- (48) G.E. Edwards and N.R. Baker, *Photosynthesis Research* 37, 89-102 (1993).
- (49) K.A. Mott, Z.G. Cardon and J.A. Berry, *Plant Cell Environ.* 16, 25-34 (1993).
- (50) J. A. Abbot, T.A. Campbell, and D.R. Massie, *Remote Sens. Environ.*, 47, 87-97 (1994).
- (51) S.R. Eskelsen, G.D. Crabtree, R.B. Boone, G.M. Volk, L. Ning, and L.S. Daley, *Spectroscopy*, 8(3), 34-40 (1994).
- (52) M. Krajicek and M. Vrbova, *Remote Sens. Environ.* 47, 51-54 (1994).

- (53) B.T. Mawson, P.J. Morrissey, A. Gomez and A. Melis, *Plant Cell Physiol.* 35, 341-351 (1994).
- (54) R.M. Pratt, *Florida guide to citrus insects, diseases and nutritional disorders in color* (Univ. Florida Agric. Exp. Stat., Gainesville, FL, 1958) 291 pp.
- (55) P.F. Daley, K. Raschke, J.T. Ball and J.A. Berry, *Plant Physiol.* 90, 1233-1238 (1989).
- (56) C.B. Osmond, J.A. Berry, S. Balachandra, C. Buchen-Osmond, P.F. Daley, and R.A. Hodgson, *Bot. Acta* 103, 226-229 (1990).
- (57) V.M. Albers, and H.V. Knorr, *Plant Physiol.* 12, 833-843 (1937).
- (58) W.L. Butler, and K.H. Norris, *Modern methods of plant analysis*, 5, 51-72 (1962).
- (59) W.L. Butler, *Methods in Enzymology*, 24(B), 3-25 (1972).
- (60) T. Hiyama, and B. Ke, *Biochim. Biophys. Acta*, 267, 160-171 (1972).
- (61) J.S. Brown, and S. Schoch, *Biochim. Biophys. Acta*, 63, 201-209 (1981).
- (62) J.S. Brown, *Photosynth. Res.*, 4, 375-383 (1983).
- (63) G. Vane and A.F.H. Goetz, *Remote Sens. Environ.* 44, 117-126 (1993).
- (64) J. Beck, Patchen California Inc., Los Gatos, CA, personal communication (1994).
- (65) J. O'C Hamilton, The bug that's eating wine country, *Business Week*, (November 14), pp. 14E4, 14E8 (1994).
- (66) B. Ganapol, L. Johnson, P. Hammer, D. Peterson, and F. Baret, A new within-leaf radiative transfer model: preliminary results. Poster presented at the Remote Sensing Science Workshop NASA/GSFC, February 27- March 1, 1995.
- (67) J.A. Curcio, and C.C. Petty, *J. Optical Soc. Am.* 41, 302-304 (1951).
- (68) G.S. Birth, and K.L. Olsen, *Amer. Soc. Hort. Sci.* 85, 74-84 (1964).
- (69) W.L. Butler, *Ann. Rev. Plant Physiol.* 15, 451-470 (1964).
- (70) K.H. Norris, and J.R. Hart, Direct spectrophotometric determination of moisture content of grain and seeds, in *Principles and methods of measuring moisture in liquids and solids*, vol. 4 (A. Wexler, ed., Reinhold, NY., 1965) pp. 19-25.

- (71) G.A. Carter, *Amer. J. Bot.* 78, 916-924 (1991).
- (72) P.J. Curran, J.L. Dungan, B.A. Maclee, S.E. Plummer, and D.L. Peterson, *Remote Sens. Environ.*, 39, 153-166 (1992).
- (73) B.-C. Gao, and A.F.H. Goetz, *Remote Sens. Environ.* 52, 155-162 (1994).
- (74) L. Ning, W.J. Bowyer, L.S. Daley, E.H. Piepmeier, G.A. Strobel, and J. B. Callis, *Spectroscopy* (submitted)
- (75) I. Murray, and P.C. Williams, Chemical principles of near-infrared technology. in *Near-Infrared Technology in the Agricultural and Food Industries*. (P. Williams and K. Norris, eds. Amer. Assoc. Cereal Chemists, Inc., St Paul, Minnesota, 1987) pp. 17-34.
- (76) G.P. Wiederrecht, W.A. Sveck, M.P. Niemczyk, and M.R. Wasielewski, *J. Phys. Chem.*, 99, 8918-8926 (1995).
- (77) J. Lee, X. Yang, M. Schwartz, G. Strobel, and J. Clardy, *Chemistry and Biology* 2 (11), (in press, 1995)
- (78) M.B. Ellis, *Dermatiaceous Hyphomycetes* (Commonwealth Mycological Institute, Surrey, England, 1971)
- (79) B.C. Sutton, *The Coelomycetes* (Commonwealth Mycological Institute, Surrey, England, 1980) 696 pp.
- (80) J. Lee, X. Yang, M. Schwartz, G. Strobel, and J. Clardy (unpublished, 1995)
- (81) E.N. Ashworth, *Plant Physiol.*, 70, 1473-1479 (1982).
- (82) M.R. Warmund, B.H. Barritt, J.M. Brown, K.L. Schaffer, and B.R. Jeong, *J. Amer. Soc. Hort. Sci.*, 118, 92-96 (1993).
- (83) N.E. Good, G.D. Winget, W. Winter, T.N. Connolly, S. Izawa, and R.M.M. Singh, *Biochemistry.*, 5, 467-477 (1966).
- (84) N.E. Good, and S. Izawa, *Methods in Enzymology*, 24(B), 53-68 (1972).
- (85) W.J. Ferguson, K.I. Braunschweiger, W.R. Braunschweiger, J.R. Smith, J.J. McCormick, C.C. Wasmann, N.P. Jarvis, D.H. Bell, and N.E. Good, *Analytic. Biochem.*, 104, 300-310 (1980).
- (86) N.M. Barnett, *Can. J. Bot.*, 52, 265-271 (1974).
- (87) L.S. Daley, P. Carrol, and H. Mussell, *Biochem. J.*, 179, 719-721 (1979).

- (88) L.S. Daley, and R.G.S. Bidwell, *Plant Physiol.*, 60, 109-114 (1977).
- (89) R. M. Ozanich Jr., M.I. Schrattenholzer, and J.B. Callis, Non-invasive determination of moisture and oil content of wheat-flour cookies, *Amer. Chem. Soc. Symp., Series analytic: biosensor design and application* (Eds. P.R. Mathewson and J.W. Findley, 1992) 511, 137-164.
- (90) K.R. Jacobsen, D.G. Fisher, A. Maretzki, and P.H. Moore, *Bot. Acta* 105, 70-80 (1992).
- (91) W. Bloom, and D.W. Fawcett, *A textbook of histology*, 10th edition (W.B. Saunders Co., Philadelphia, 1975). 1033 pp.
- (92) Anonymous, b-Fructosidase, in *Biochimica information*, II (Boehringer Mannheim GmbH, 1975) 69-70.
- (93) F.B. Rudolph, and H.J. Fromm, Plotting methods for analyzing enzyme rate data, in *Contemporary enzyme kinetics and mechanism*. (D. L. Purich, editor, Academic Press, New York, 1983) pp. 53-73
- (94) R.E. Dickson, Assimilate distribution and storage, in *Physiology of trees* (A.S. Raghavendra editor, John Wiley & Sons, Inc., New York, 1991) p. 51-85
- (95) L. Ning, B. Arbogast, D.F. Barofsky, and L. Daley (unpublished)
- (96) J.K. Stone, J.N. Pinkerton, and K.B. Johnson, *Mycologia* 86, 674-683 (1994).
- (97) J.A. Milburn, and J. Kallarackal, Sap exudation. in *Physiology of Trees*, (A.S. Raghavendra ed., John Wiley, NY., 1991) pp. 385-402.
- (98) S. Wold, A. Ruhe, H. Wold and W. Dunn, *SIAM J. Sci. Stat. Comput.*, 5, 735-743 (1984).
- (99) M. Otto, and W. Wegscheider, *Analyt. Chem.*, 57, 63-69 (1985).
- (100) H. Martens, and T. Naes, *Multivariate calibration* (John Wiley and Sons Ltd., London, 1989) 419 pp.
- (101) G. Ing, ReportING Wish list. *Good Fruit Grower*. 45 (14), 61 (1994) Proof reader yes it is ReportING, it is a pun on authors name.
- (102) L. Taiz and E. Zeiger, *Plant Physiology* (Benjamin/Cummings Pub. Co., Inc., Redwood City, California, 1991).

- (103) M. Havaux and R. Lannoye, *Photosynthetica* 18, 117-127 (1984).
- (104) K. Omasa, K. Shimazaki, L. Aiga, W. Larcher and M. Onoe, *Plant Physiol.* 84, 748-752 (1987).
- (105) M.L. Ghirardi and A. Melis, *Biochem. Biophys. Acta* 932, 130-137 (1988).
- (106) L.I. Tecsi, A.J. Maule, A.M Smith and R.C. Leegood, *Plant J.* 5, 837-847 (1994).
- (107) S.B. Powles, *Ann. Rev. Plant Physiol.* 35, 14-55 (1984).
- (108) R. Valentini, G. Cecchi, P. Mazzinghi, G. Scarascia Mugnozza, G. Agati, M. Bazzani, P. De Angelis, F. Fusi, G. Matteuci and V. Raimondi, *Remote Sens. Environ.* 47, 29-35 (1994).
- (109) R. J. Strasser, A. Srivastava and Govindjee (has no initial), *Photochem. Photobiol.* 61, 32-42 (1995).
- (110) D.C. Youvan, J.E. Hearst and B. L. Marrs, *J. Bacteriol.* 154, 748-755 (1983).
- (111) E. Weis and J.A. Berry, *Biochim. Biophys. Acta* 894, 198-208 (1987).
- (112) B. Genty, and S. Meyer, *Aust. J. Plant Physiol.* 22, 277-284 (1994).
- (113) K. Siebke, and E. Weis, *Planta*, 196, 155-165 (1995).
- (114) G. Cecchi, P. Mazzinghi, L. Pantani, R. Valentini, D. Tirelli and P. De Angelis, *Remote Sens. Environ.* 47, 18-28 (1994).
- (115) E.W. Chappelle and H. Lichtenthaler, *Remote Sens. Environ.* 47, 1 (1994).
- (116) K.P. Gunther, H.-G Dahn and W. Ludeker, *Remote Sens. Environ.* 47, 10-17 (1994).
- (117) J.E. McMurtrey III, E.W. Chappelle, M.S. Kim, J.J. Meisinger and L.A. Corp, *Remote Sens. Environ.* 47, 36-44 (1994).
- (118) M. Methy, A. Oliso and L. Trabaud, *Remote Sens. Environ.* 47, 2-49 (1994).
- (119) G.H. Wagniere, *Linear and nonlinear optical properties of molecules.* (Verlag Helvetica Chimica Acta, Basel, Switzerland, 1993) p. 17.

- (120) P. Hari, E. Nikinmaa, and E. Korpilahti, Canopy, photosynthesis, and growth in *Physiology of Trees* (A.S. Raghavendra, editor, John Wiley and Sons, London, 1991) pp. 419-439.
- (121) L. Barthelemy, C. Edelin, and F. Halle, Canopy architecture, in *Physiology of Trees* (A.S. Raghavendra, editor, John Wiley and Sons, London, 1991) pp. 1-20.

Test for sucrose and cell wall bound invertase on solid substrate. Tests were done using a blood sugar meter to measure, glucose by coupled reaction on filter paper disks. The plant tissue was crushed onto filter paper and when indicated washed six times with distilled water. Disks (0.385 cm^2) were then punched out of the filter paper. This determination measures glucose, in order to measure sucrose a source of invertase is required. Invertase occurs naturally in plant cell walls. Endogenous sucrose is removed by washing gently with water (6x). In separate tests we found that disks with added sucrose but no plant tissue, or disks boiled after plant tissue was crushed onto them, yield no reaction. Sucrose additions when indicated, were 50 μl of 50 mM per disk or $650 \text{ umoles dm}^{-2}$. There were 11 replications of each treatment. Data was analyzed by multiple range analysis, distinct letters indicate statistical difference at the 95% (LSD) level.

Treatment	sucrose added	umoles $\text{h}^{-1} \text{ dm}^{-2}$	added sucrose effect net umoles $\text{h}^{-1} \text{ dm}^{-2}$
unwashed	yes	12.5a	2.3
unwashed	no	10.2b	---
washed	yes	6.2c	4.5
washed	no	1.7d	---

CHAPTER 4

SPECTROSCOPIC IMAGING OF WATER IN LIVING PLANT LEAVES,
"RAYLEIGH" CORRECTIONS, AND SIGNIFICANCE FOR BEER'S LAW
BASED *IN SITU* QUANTIFICATION

Li Ning¹, W.J. Bowyer², L.S. Daley*¹, E.H. Piepmeier³, G.A. Strobel⁴, and J. B. Callis⁵

¹Dept. of Horticulture, ALS 4017, Oregon State Univ., Corvallis, OR 97331-7304.

²Dept. of Chemistry, Hobart and William Smith Colleges, Geneva, NY 14456-3397

³Dept. of Chemistry, Gilbert Hall 153A, Oregon State Univ., Corvallis, OR 97331-4003.

⁴Plant Pathology Dept., Montana State Univ., Bozeman, MT 59717.

⁵Dept. of Chemistry, Univ. of Washington, Seattle, WA 98195.

* Author to whom correspondence should be addressed.

Published in *Spectroscopy*,
Advanstar Communications, Eugene, O.R.
March/April 1996, 11(3):34-50,
and May 1996, 11(4):68-74.

SPECTROSCOPIC IMAGING OF WATER IN LIVING PLANT LEAVES,
 "RAYLEIGH" CORRECTIONS, AND SIGNIFICANCE FOR BEER'S LAW BASED *IN SITU* QUANTIFICATION

Li Ning¹, W.J. Bowyer², L.S. Daley*¹, E.H. Piepmeier³, G.A. Strobel⁴, and J. B. Callis⁵

¹Dept. of Horticulture, ALS 4017, Oregon State Univ., Corvallis, OR 97331-7304.

²Dept. of Chemistry, Hobart and William Smith Colleges, Geneva, NY 14456-3397

³Dept. of Chemistry, Gilbert Hall 153A, Oregon State Univ., Corvallis, OR 97331-4003.

⁴Plant Pathology Dept., Montana State Univ., Bozeman, MT 59717.

⁵Dept. of Chemistry, Univ. of Washington, Seattle, WA 98195.

* Author to whom correspondence should be addressed.

Determination of biochemically active light path and scattering limit the use of imaging spectroscopy in living plants. Light scattering, with "Rayleigh" characteristics was considerably reduced with a mathematical treatment of data. Reasons why, in plants, water signals are proportional to the biochemically active light path are discussed. Determination of water path using mixtures deuterium oxide and water are demonstrated in vitro for the weak water band near 970 nm. Water path in leaf slices is also investigated. Spectra of the mixed species H-O-D is calculated and tested. A "Rayleigh" scatter correction for distribution of photosystem I antenna and total light harvesting chlorophyll protein complexes (CPX) in leaves is demonstrated. Differences in structure of CPX in the different parts of a variegated leaf were determined. We expect that shade

adaption traits revealed by this CPX analyses will relate to horticultural uses and germplasm characterization.

Key words: *Aloe milotii*, cells, chlorenchyma, chlorophyll protein complexes, *Coffea arabica*, *Corylus avellana*, deuterium spectra, deuterated water spectra, *in vivo*, leaves, parenchyma, Rayleigh, scattering, *Scrofularia nodosa*, spectroscopy, water spectra.

INTRODUCTION

Imaging living plants has myriad potential applications, from basic studies of photosynthesis, the process that supports essentially all life on Earth, to very applied applications in industry and agriculture (1). Pathlength calibration and scattering are important to imaging interpretation of absorbance signals as biochemical contents by Beer's (Beer-Lambert's) (2) law. Absorbance based spectroscopy of plant tissues has a history of constant technical development (3-28). Now imaging of *in vivo* absorbance of plants is becoming important because the x-y (1,29) and z-axes (29,30) distribution of signals from plants' biochemical structures and processes characterizes events of biophysical, biochemical, physiological, phytopathological, agricultural and industrial significance. This paper is intended to provide theoretical for *in vivo* identification and characterization of phytopathologies, and photosynthetic structures in plant germplasm.

Nuclear magnetic resonance (NMR) and magnetic resonance imaging (MRI) are useful to investigating living, and thus hydrated, plant material (e.g. 31-36). However, signal strength, signal diversity, exact quantitation, and high costs of NMR and especially

MRI equipment limit their use. *In vivo* absorbance imaging lacks these disadvantages and costs less (e.g. 1).

Absorbance imaging of biochemical, biophysical and physiological variation in complex, abundantly hydrated (see sidebar 1), plant tissues has unique challenges different those of traditional reflectance studies (see sidebar 2). These challenges yield more readily to absorbance measurements (e.g. 7, 25). Spectroscopy of the images of these complex tissues places specific demands on instrumentation, with respect to pathlength, Beer's law correlations, scattering, and the variation in the Z-axis (29,30) as light penetrates the tissues. This kind of imagery needs narrow bandwidths because broad bandwidths affects Beer's law, and automated wavelength scanning (1) to allow more ready statistical resolution (37,38) of overlapping chromophores.

With an imaging spectrophotometer that yields linear absorbance response, as an essentially continuous function of wavelength of each pixel of the image, we can, within certain limitations, obtain a Beer's law linear response to each chromophore (2). This means that if the appropriate chromophore (see Materials and Instrumentation section) molar absorption coefficients are known, and, if the path length can be determined, quantification of chemical contents can be done without need of wet chemistry calibration measurements; this greatly helps investigations of time dependent processes in living systems. However, because living tissues have complex tissues and consequently complex pathlengths, we need to estimate pathlength in living tissue.

Plant tissues are not spectroscopically homogeneous because they contain both cells and the apoplast, the continuous system of cell walls and intercellular spaces in plant tissues (39). Cells are connected to each other by the transmembrane and aqueous symplast system (39 p. 85), and require large proportions of water for their biochemistry and the physiology (e.g. 39 pp. 61-64). Cells contain organelles whose membranes separate concentrated cell biochemicals. The apoplast strongly influences light penetration (e.g. 30). Especially in the leaf, apoplast structures, shaped by rigid cell walls, serve as "light guides" taking light to the interior of the plant (e.g. 39 pp. 251-252) and cause a great deal of light scattering (e.g. 30). The apoplast areas may or may not contain large proportions of liquid water. In the apoplast, spaces not filled with cell wall material, can be filled with gases which are most commonly used for photosynthetic gas exchange. Apoplastic spaces can also contain aqueous solutions when the plant suffers certain pathologies (e.g. 8,40 p. 101,41), or uses apoplastic spaces to store or transport minerals, metabolites and water (e.g. 39,42).

The non-aqueous parts of the apoplast contains standard atmospheric gases enriched or depleted in photosynthetic and respiratory gases (mainly O₂, CO₂), water vapor and ethylene. These gases have no significant absorbance at the wavelengths examined here (500-1000 nm). This is not so in remote sensing where long passage through atmospheric water vapor near 940 nm absorbance, interferes with plant liquid water signals near 975 nm (43). Biochemical processing of these gases occurs in the aqueous phases of plant tissue (e.g. 39). Therefore, for *in vivo* biochemical function of plants, and at the wavelengths considered here, the portion of the spectroscopic pathlength

that traverses air can usually be neglected. Not so the portion of the spectroscopic pathlength that traverses the aqueous phases of plant tissue.

Life as we know it exists as cells, or structures organized from cell groupings sometimes described in science fiction, as "bags of water". Thus, when we seek molar concentrations of biochemicals in living tissue using Beer's law (Beer-Lambert law e.g. 2) the pathlength we seek is the effective pathlength of the scattering light beam as it passes through the biological solvent, liquid water. Water is present in great excess in cells and extracellular compartments and in relatively constant amounts. This is because, as discussed below, plant life requires water concentrations to be relatively fixed at somewhat less than $1000\text{g}\times\text{L}^{-1}/(18\text{ g}\times\text{mole treating water as a monomer})$ or $55.55\text{ moles}\times\text{L}^{-1}$.

Ungerminated seeds are different. Since seed analyses are such a large part of applied agricultural spectroscopy (see second side bar) it is sometimes overlooked that seeds are usually processed commercially in dormant (resting) states (44). In rest seeds have maximal stored reserves which will later fuel germination biochemistry; for this reason many kinds of resting seeds have been developed as crops to provide easily, storable, portable, and nutritious sources of food (44). Resting seeds, like resting buds (35,36,45), usually have much less water than active plant tissues. Soybeans stored for feed use usually have less than 12% moisture (e.g. 46). Soybeans used for replanting are harvested at about 14.5% water, but must be dried to 13% or less for storage (e.g. 47).

Resting seeds preserve plant life during drought, cold, dispersion to other sites (e.g. 39 pp. 490-512, 44), and when light does not reach the soil where the seed is found (e.g. 48). The balance between red (680 nm max.) and far-red (735 nm max.) light (49)

helps control much of plant function, including seed germination (e.g. 39 pp. 490-512,44). Low water content usually, but not always, helps seeds survive (44). Seeds are essentially biochemically inactive until appropriate controls trigger water uptake and massive reserve-consuming biochemistry (44).

Plant metabolic function requires high proportions of water. This is true even for seeds. Seed water content increases dramatically during germination (e.g. 44), until seeds reach water levels equivalent to "any actively growing tissue 70-80%" (50). The amount of water in plant tissues is somewhat dependent on three alternate ways plants fix carbon dioxide in photosynthesis: C-3, C-4 and Crassulacean acid metabolism (CAM) (see sidebar). CAM plants, adapted to dry climates, usually have the highest water content. Thus, in the huge, thin walled cells found inside the fleshy leaves of CAM plant genus *Aloe* (51) we measured water content of 98.7% (*Aloe milotii* cf.). CAM plant leaves are at least 93% water (52). C-3 plants have between 30-80% (52), C-4 have about the same or slightly less.

Fresh weight (FW) data, the proportion of water per total weight of fresh plant, understates the actual amount of water in the living cells. For example FW for C-3 can vary from 30 to 80% (52). However, large proportions of total weight are insoluble polymers, cellulose, hemicellulose, pectin, lignin and proteins in the cell walls found outside of the living cells (39 pp. 22), in the apoplast. Trees, for instance, have large amounts of wood, which has low water content per FW unit. Wood is composed mainly of cellulose and lignin residues from discarded xylem, a vascular tissue residue which, although it once carried mainly water and dissolved minerals, is now unused. In a tree trunk only few cell layers: phloem (vascular tissue which "pumps" mainly carbohydrates),

cambium (which produces new cells) and new xylem are "alive", fully hydrated and functioning (39). Biochemically, the rest is "dead wood".

Sugarcane, a C-4 plant, loses water content, as it grows, from about 85% to about 70% FW water at maturity (53). Yet, the decrease in water per active tissue of sugarcane is much less. This is because maturing cane increases its fiber to about 16% ("bone dry bagasse") fiber at harvest (53). Bagasse is an insoluble mix of various structural components; thus, recalculating $[70/(100-16)]$ there is about 83.3% water in mature sugarcane stem water/solute systems.

The highest molar concentrations of solutes, in living, functioning, cells and apoplast are low compared to water concentrations. In most plants the vacuole is the major part of the mature plant cell and the place where greatest solute accumulation occurs (39 p. 127). Salt glands, which occur in several angiosperms such as halophytic mangroves, are an exception. However, salt glands die and fall off when they are saturated with salt (41). Thus, when these salt glands reach high solute levels they are dying, or dead, not living tissue. Apoplastic (out of cell space) storage is significant in sugarcane (54). In guard cells cytoplasmic solute storage is important (55). However, the concentrations of these solutes do not compare to the minimum concentration of water, about $[(1000 \text{ g/l})/(18 \text{ g/moles, calculated as a monomer}) * (0.83 \text{ water/soluble cell component ratio})] = 46.1 \text{ M}$, in plant cells.

CAM plants, large accumulators of organic acids, can contain at most about 0.2 M organic acids (e.g. 52,56,57) frequently less (57,58). In most plant cells maximal concentrations of K^+ , the most abundant cation in plants, are also about 0.2 M (60). Guard cells have more, as they open stomata to admit respiratory gases, they increase their

[K⁺] by about 0.3 M (61). When open these guard cells can contain almost 0.9 M K⁺ (55). Palm phloem sap, has abundant K⁺ and amino acids and up to 20% sugars, mostly sucrose while maple sap has only 2-4% solids (41).

Sugarcane's stem, a great solute accumulators, has up to 18-20% sucrose in juice or about 0.5 M; although industrial averages are less (62). Cells organelles do not exceed these solute levels since to maintaining higher solute concentrations requires too much energy. (e.g. 54,59) and these solutes are pumped to apoplastic storage outside the cell (54).

In sugarcane stem solute concentration can be estimated from industrial data (53) as $(125 \text{ Kg sucrose}/(\text{metric ton cane}-160 \text{ Kg bagasse}))= 0.435\text{M sucrose}$. Monosaccharides from molasses can be estimated as $[(0.6, \text{ the proportion of monosaccharides in dry molasses}) \times (0.5, \text{ estimate of molasses water content})] \times (35 \text{ Kg molasses})/(\text{metric ton cane} - 160 \text{ Kg bagasse})=0.058 \text{ M}$. This total sugars estimate (0.49 M) is higher than the 0.37 M sugars reported (42) for total centrifuged cell sap and $0.29\text{g}/\text{FW} \times (1\text{FW}-0.16 \text{ dry weight correction})=0.345 \text{ M}$ sugar found in central storage parenchyma (Jacobsen, 1992). However, all calculations are consistent with the 0.227-0.67 M and 0.185-0.552 M range of sugars of symplast (in living cells) and apoplast (out of cell) values given by Moore (1995) for different sugarcane nodes. Thus, the maximal amount of solutes in other plant cells about 0.8 M (Zeiger, et al., 1987) fits the data of Moore (1995). Therefore, since the minimum amount of water in functional plant tissue is about 83%, and the maximum solutes about 0.8 M maximum water/solute molar ratios at least $55.5 \times 0.83/0.8 > 57.6$ in C-3, and C-4 plants, and $55.5 \times .93/0.8 > 65.5$ in CAM plants.

Water absorbance approximates path of light in plant cell. Since in functioning cells and apoplast, solute concentration variations are relatively small compared to solvent water molarity, we are justified in considering water concentrations to be essentially constant, near 50 M, in a given tissue and photosynthetic class of plants. Determination of solute concentration by Beer's law (see Materials and Methods section) requires knowledge of two variables: absorbance and pathlength. However, since solvent (water) concentration in plants is already known with some certainty we can use Beer's law to determine the effective light path in biologically active parts of the plant knowing only the absorbance of water.

Water has a number of absorbance bands, the most appropriate for our use is the small, but significant, absorbance near 975 nm (64-66). This band has been used to determine moisture content in grain and seeds (e.g. 11). In this paper we found that, the absorbance of water near 975 nm can be used to calculate the approximate effective pathlength of living plant tissue. Some reflectance uses of this 975 nm band succeeded (43), others (65,66) have been less successful. The uneven success of the reflectance approach may be due to limitations of reflectance (see second sidebar), the need of a reference wavelength such as described by Norris and Hart (11) and as we use in this paper, or the difference in application.

For biological interpretation of spectra, there is a caveat. Although bacteria approximate a single "bag of water", other organisms are more complex. True algae, even when only a single cell, contain multiple compartments (organelles) such as mitochondria, chloroplasts, cytoplasm, and vacuoles. Multicellular life repeats this complexity in multiple cells, adding apoplastic compartments (e.g. 39,54). Thus, higher organisms are a

complex of billions of cells, each cell containing multiple organelles, each organelle a "bag of water" (e.g. Fig. 3 in ref. 35).

Using visible and near infrared spectroscopy to examine cells inside tissues in the depth (z) direction (29,30), and adding this to x and y imaging, offers unique challenges. However, in this paper we deal with two dimensional (x, y) images with the z-direction compressed into one point. Thus, chromophores of cells and organelles within the cells that overlap along the z-axis are detected as compressed into the x-y plane. Each organelle has a specialized function with specialized biochemistry and chromophores (e.g. 39), and the number and nature of the organelles in each kind of cell along the z-axis varies. Thus, measurements of cell chromophores per unit water do not necessarily reflect the concentration of the chromophore in the organelle. However, measurements of concentration of specific chromophores (e.g. chlorophyll b) per water path unit are useful because they measure the capacity of each organelle's function per water path unit and thus per unit of biologically active space. This is particularly useful when doing *in vivo* spectroscopy seeking real time biochemical information from the x-y oriented photon gathering laminar array structures of the leaf.

Imaging complex living plant tissues in the visible and near-infrared

"The absorption of light in living plant material, either in the form of living leaves or suspensions of algae is a complicated optical process" Albers, V.M. and Knorr, H.V. 1937. Absorption spectra of single chloroplasts in living cells in region from 664 nm to 704 nm. *Plant Physiol.* 12, 833-843 (4).

"It is not generally realized that monochromatic light can be transmitted through whole apples, tomatoes, bean seeds, or peanuts and thus many biochemical processes which involve light absorbing substances can thus be studied in the intact specimen" Butler and Norris, 1962 (7).

Beer-Lambert (Beer's) law (e.g. 2) *in vitro* determination of biochemicals for living systems is a standard approach. Absorbance measured in cuvettes of known pathlength is used to determine concentrations using molar absorption coefficients (extinction coefficients, absorptivities). Biochemists routinely measure 260 and 280 nm absorbance and obtain good approximations of protein and nucleic acids in semi-purified solutions (generally attributed to Chargaff and Davison, 1955 (67)). Similar chlorophyll determinations are routine (reviewed in 27). However *in vivo* plant spectroscopy, variables increase, absorbance plus other factors become attenuation (e.g. 1,9,13) because measurements are matrix dependent (e.g. 13,25,27). This makes *in vivo* approximation of concentration through Beer's Law more complex.

For plant spectroscopic analyses of plants *in situ*: reflectance and absorbance measurements are somewhat similar. Both methods: commonly use logarithmic functions to relate measurements to concentration in materials examined, both use the phenomena of absorption directly or indirectly, and both methods have to cope with light scattering. However the plant materials explored, the calibration procedures, the objectives sought, and the instruments to implement these methods usually differ. Even when the same instrument is used, reflectance and absorbance spectra differ (e.g. 13).

Near-infrared (NIR) reflectance methods have solved applied problems with much success and productive industrial use (68). Applied research following this approach

develops important commercial uses which are strictly formalized and even legislated (e.g. 69). Crop price data based on these analyses are reported daily in business sections of newspapers.

Much of the agricultural and biological research using reflectance-NIR is done with ungerminated, low water content (see side bar 1), crop seeds (e.g. wheat, soybean), and their milled products (e.g. flour, soybean meal) which are very important to agricultural commerce. Commonly spectroscopic methods for seeds and their products (e.g. 68) emphasize reflectance (e.g. 70,71). The calibrations sought usually are verified by wet chemistry, since bulk properties, not resolution of fine structure within samples, are of the greatest concern. Elaborate models of reflectance, such as Kubelka-Monk, are frequently used to approximate pathlength (72).

With hydrated plant materials (see side bar 1) reflectance studies can be less useful (6). Kubelka-Munk (K-M) theory which can be applied to absorbance data in densely scattering turbid material (6), does not apply well when scattering is less than 0.6 (73) and when not all light is absorbed or reflected by the sample (72). Perhaps this is why a weak band such as the water band near 975 nm, which we use here, is more successfully used in absorbance applications (11), than in reflectance measurements (65,66).

Absorbance methodologies are traditionally used for more hydrated plant tissues and usually include visible as well as NIR wavelengths (e.g. 10). When this approach is used to study the biochemistry of plants *in situ* and *in vivo* (e.g. 1,9,13-28) instruments capable of making linear absorbance measurements of narrow bands of chromophores and able to deal with light scattering by these tissues are most useful (e.g. 7,13). However, the greatest advantage of the absorbance methods is that it simplifies application of Beer's law,

and thus can quantify complex images with much less need of additional wet chemistry analyses. Complex tissues, because they are by definition biochemically heterogeneous, require imaging procedures and this is usually done using a Charge Coupled Device (CCD) (e.g. 1).

CCD absorbance measurements offer advantages over unprocessed CCD images when image lighting distribution is uneven and pixel responses in the CCD are variable. Direct image instruments, usually designed for production systems, require corrections such as shade image master (e.g. 74), backlighting (e.g. 75,76), etc. When data are transformed to absorbance format, each pixel is referenced to its own efficiencies and characteristics. Thus, absorbance images, less troubled by uneven illumination and pixel response variations, are frequently much clearer.

Quantification of biochemistry in complex images of plant structures. Plants have convoluted complex structures, at all levels from intact plants, through plant parts, tissues, cells to subcellular structures. The apoplast scatters light differently from cellular components, insoluble organelle structures differently from organelle contents. Each structural component has different proportions of biochemical components. Biological material is fragile. Separating structures to calibrate biochemical content of image features, many of which are microscopic, is difficult, extremely time consuming, and almost certainly causes chemical change as membranes rupture and cell compartment contents intermingle and react.

Living tissues can be examined microscopically and some biochemical information can be obtained spectroscopically in this way. However, this approach requires excision

of tissues or studies are limited to organisms small enough to place under the microscope. Yet these data are essentially equivalent to spectroscopic examination *in vivo*.

The traditional alternative, histological fixation, kills tissue very rapidly to minimize change in morphology and holds complex tissues in a stable, usually solid form, for microscopic study. In histological fixation procedures, where the path length in a given slice of tissue is approximately equal, the relative intensity of a given stain, signals the relative concentration of the chromophore observed (e.g. 77). In this kind of histological work the light path is controlled by the thickness of the microscope section and, since these sections are very thin, scattering is relatively insignificant. Histological fixation preserves morphology and cytological shapes important for many purposes, and allows histochemical analyses of great sophistication (e.g. 77). However when tissues are fixed, cell chemistry is irreversible and severely altered, consequently time sequence studies of the same tissue sections are impossible.

To avoid chemical changes and or tissue changes on dissection of samples it is possible to freeze the tissue with liquid nitrogen, and using a microscope dissect out the cells and cell components or degrade the tissue enzymatically and segregate cells by size. Then cells can be assayed one at a time, or in groups of cells of the same type by coupled spectrophotometric or fluorometric assays (78,79). This can give excellent information on biochemical circumstances at the time of preparation (78,79). However, once these procedures are done the real time biochemical interactions of the intact tissues and organisms are less certain (e.g. 80).

For these reasons it is preferable to quantify the biochemistry of the complex images found *in vivo* spectroscopy by Beer's law. To quantifying images of living

biochemical processes *in situ* by Beer's law in complex hydrated plant materials with variable light paths and uneven tissue thickness requires pathlength determination. To do this, for the reasons presented in the first sidebar, we investigated the optical path of water in plant materials.

MATERIALS AND INSTRUMENTATION

Instrumentation This work is part of a program to develop spectroscopic charge coupled device (CCD) based imaging systems for *in vivo* work on plants and their tissues (1,30,81). Rather than *a priori* define specific characteristics required for a plant imaging system, we take an empirical approach and seek specific experimental situations to develop the instrument. In this paper we use the previously reported design (Ning, et al., 1994 1), but now substitute a mirror for the fiber optic output of the monochromometer. This change allows stronger sample illumination which is important for weak signals in the 800-1000 nm range.

At present our system uses the less efficient, but much less expensive, front illuminated charge coupled device (CCD). The 12-bit thermoelectrically cooled CCD system (Lynxx PC, CCD Digital Imaging System, Westlake Village, CA) we use has a low noise range (quantum efficiency >10%) from about 450 to 980 nm with a maximal quantum efficiency of about 40% a spatial resolution of 165 x 192 (31,680 pixels). We would like to have used, but could not afford, more sensitive and much more expensive, back illuminated UV coated CCDs. These CCD have a the low noise range between 200 to 1040 nm and maximal quantum efficiency of as high as 70% (e.g. 82,83). Higher

quantum efficiencies about 87% can be obtained without UV coatings. Noise is a strongly dependent on CCD temperature. Our CCD cools, via Peltier devices, to about to about -38 °C. More expensive CCD devices cool to liquid nitrogen temperatures.

For potential applications it is useful to compare CCD wavelength sensitivity to human vision. Visible perception by the rod receptors in the human eye extends from about 400 to nearly 600 nm (Figure 4.2 of ref. 84). However, cone receptors of the dark adapted human eye (Figure 4.1 of ref 84) detect radiation from about 350 to somewhat beyond 750 nm.

We worked with a standard monochromator (Jarrel Ash single monochromator, model No. 82-410, Scientific Measurement Systems, Grand Junction, CO) driven by a step motor (HY 200, Oregon Microsystems, Beaverton, OR). For financial reasons were not able to compare this system with optical acoustical filters as a substitute for our monochromator. We were not aware of, and thus did not test, liquid crystal approaches to monochromatic light generation (85).

Other instruments The non-imaging spectrophotometer was a Shimadzu 3100 (Shimadzu Scientific Instruments, Columbia, MD) which has a wavelength range, in up to 0.05 nm steps, of 190 to 2500 nm, an absorbance range of 4-5 A and was fitted with an integrating sphere. The imaging fluorometry was done by a simple, and reversible, reconfiguration (81) of the imaging spectrophotometer (1). Refractometry was done with an Abbe refractometer (American Optical Corp, Buffalo, New York). The thickness of the *Aloe milotii* sections was measured using a digital Mitutoya (Japan) 0-1 inch micrometer model number 293-701 using a soft zero setting.

Beer-Lambert calculations The Beer-Lambert law (2) states that the intensity of radiation decreases exponentially as it passes through an absorbing medium, symbolically:

$$I = I_0 10^{-e[J]l}$$

I_0 is the incident intensity, l is the path length through the sample of molar concentration $[J]$ in the absorbing species J , and e is the molar absorption coefficient (absorptivity, formerly 'extinction coefficient'). The dimensionless quantity $e[J]l$ is called absorbance, A formerly the 'optical' density (O.D.) of the sample, and I/I_0 is the transmittance, T . Since $A = e[J]l$, it contains e a constant and l a potentially measurable length. At standardized pathlength, l , A is proportional to $[J]$ or the concentration, with some corrections for refractive index, etc. Thus, when you measure A , and you know e and l , you can determine $[J]$ without any reference.

Plant materials Plants were placed in pots of OSU mix, and grown in OSU West Greenhouses.

RESULTS AND DISCUSSION

The leaf of *Scrofularia nodosa* 'Variegata' has different hued areas of sizes appropriate for *in vivo* calibrating images from our imaging instrument with our non-imaging spectrophotometer. Figure 4.1 (left panel) shows the first author holding the plant, commonly known as knotted figwort (86). Notice the characteristic variegated (multi-hued) oval and toothed leaves which are placed opposite each other on the stem (86). This plant belongs to the genus, *Scrofularia* L., which are Dicots found in northern temperate climates and tropical America and consists of coarse foetid herbs and shrubs,

Figure 4.1. Experimental plant material. The left panel shows a potted plant of *Scrofularia nodosa* L. Variegata a multi-hued ornamental. The first author illustrates size of plant. The right panel shows a leaf; notice the abrupt transition between different hued areas.



FIGURE 4.1

some such as the figwort have putative "local medical" use (87). Figure 4.1 (right panel) shows the leaf of this plant, in this panel the different hued areas can be readily observed.

Leaf variegation in flowering plants (angiosperms) is usually a result of chloroplast mutations that segregate into different areas of tissues (88, p. 180). This matter has some importance because chloroplast function, photosynthesis, supports essentially all life on Earth (e.g. 1,39). Chloroplast mutations and their complex inheritance can be investigated readily by *in vivo* spectroscopy (e.g. 20,22).

"Rayleigh" scattering correction. "Rayleigh" is used here in quotation marks, because it is defined empirically in heterogeneous living biological material by optimal fit to a $[kA]^{-4}$ correction (90, p. 838). This putative "Rayleigh" scattering is therefore, less documented than Rayleigh scattering from a defined model system where particles of known concentration and size distribution are studied in relative isolation. When measuring absorbance *in vivo* or *in situ* samples, such as leaves, scattering becomes significant (Fig. 4.2). The uncorrected spectra is as Butler (9) states "raised above the baseline and the absorption bands are flattened". Mestre (3) thought, that the "Rayleigh" effect was attributed to the "yellow" pigments reported in Shull's work (91). Butler (9) discusses "Rayleigh" scattering corrections, however at that time it was believed that these corrections "were limited to relatively dilute solutions." In traditional spectroscopy this is commonly corrected by use of an integrating sphere (e.g. 5,9). However, this cannot be done with an imaging CCD based instrument, because each pixel of the image is collected separately.

Figure 4.2 shows the broadening effect of this scattering when comparing the "raw" unprocessed absorbances from the CCD with the overall spectra obtained using an

Figure 4.2. "Rayleigh" scattering correction. Upper panels on left and right show comparisons of raw (uncorrected) spectra of hazel (*Corylus avellana* L.) leaves obtained by CCD imaging system and by a research spectrophotometer equipped with an imaging sphere. Notice how the raw data presents spectra with broader lower peaks. The third trace is the data from the CCD imaging system corrected using our "Rayleigh" scattering procedure. The lower panels on the left and right present regression analyses comparing integrating sphere data with "Rayleigh" corrected CCD data. The upper and lower figures on the left represent data from a training set experiment used to establish the procedure and the upper and lower figures on the right present data from a second, naive, test spectra.

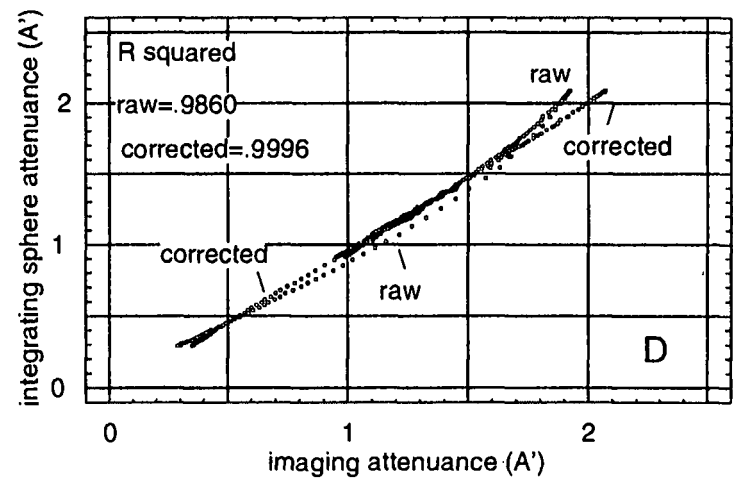
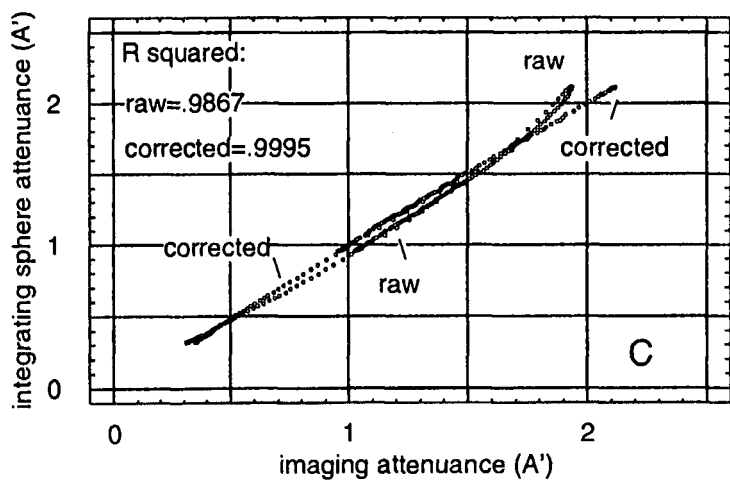
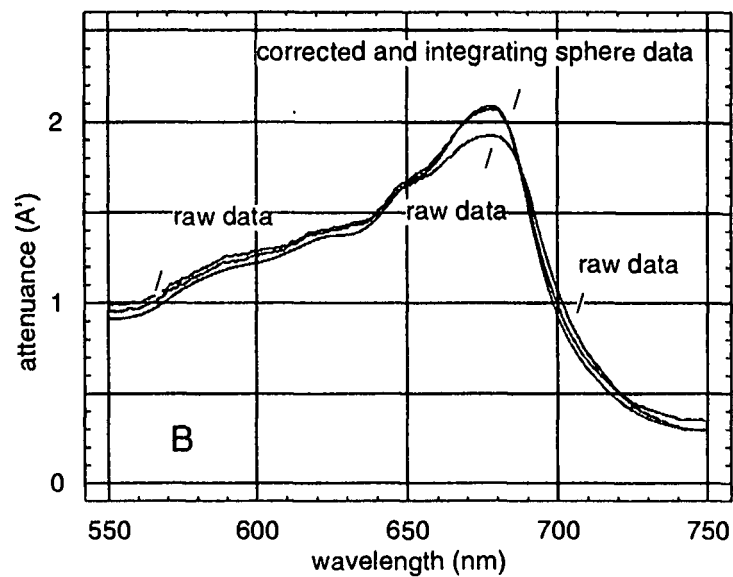
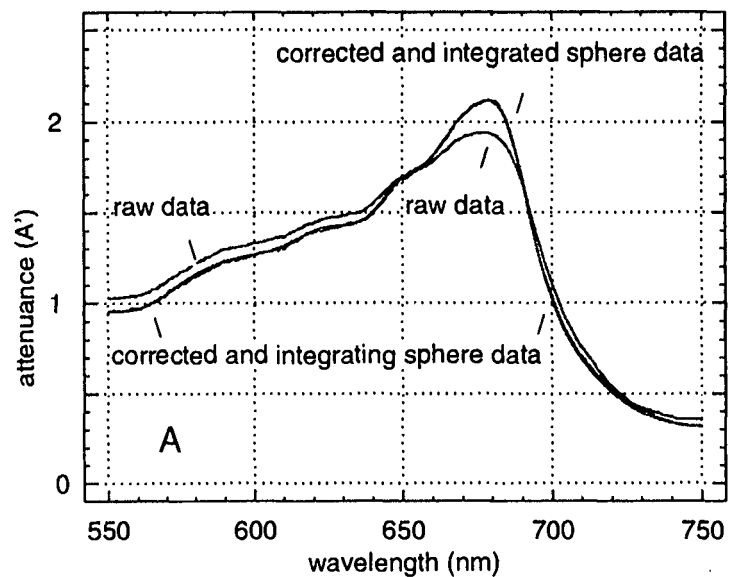


FIGURE 4.2

integrating sphere instrument. We were able to correct this absorbance (A) data to the $R^2=0.9995$ level using two successive data treatments. The first step was $A'=\log_{10}\{(I_{\text{baseline}}-I_{\text{dark}})/(I_{\text{sample}}-1.06*I_{\text{dark}})\}$. Where 1.06 is an empirical correction suggested by one of us (J.B.C) which compensates for stray light characteristics of the instrument. In the second step, developed empirically is $A''=(A'/1.86)*\{A'_{\text{longest } l}+[(A'+A'_{\text{longest } l})/A'_{\text{longest } l}]^{-4}\}$. Fits of CCD data to integrating sphere instrument data using other negative exponents (l^{-2} , l^{-3} , l^{-5} , ...) gave poorer R^2 . Thus this second step is recognizably a "Rayleigh" correction, since "experimentally, the ability to demonstrate l^{-4} is a good indication that Rayleigh scattering is being observed rather than absorbance, Raman scattering, or other effects" (90, p. 838). This scattering is somewhat different from that observed by Butler and Norris (7), who describe their effect as the "results of macroscopic and microscopic light leaks" since our detector is a CCD with 31,680 separate detectors reduces pattern or sieve effects caused by unequal absorbing areas of the sample, while retaining effects of scatter phenomena.

We chose hazel *Corylus avellana* L. for these experiments, since venation in these leaves, although present, is unobtrusive except for central vein. Thus, the visually perceptible, major, apoplastic leaf structures in the central veins of these leaves, with their light guide potential (39), can be excluded from the tissue examined using the integrating sphere equipped, non-imaging instrument. In subsequent imaging data leaf, veins are readily recognizable after "Rayleigh" correction and can be evaluated separately.

Our CCD instrument plus the corrections for apparent "Rayleigh" scattering allow imaging measurements without need of all the complex considerations used to correct

spectra in the seminal instrumental and theoretical work of Butler, Norris and Birth and others (e.g. 9,68).

Rayleigh scattering indicates that the molecules involved are smaller than the wavelengths involved. Carter (65) believes that "Rayleigh scattering by water molecules is not likely to be a significant primary effect on leaf reflectance." Butler (9) discusses the Latimer and Rabinowich hypothesis suggesting "that selective scatter might be a function of the packing and orientation of the pigment molecules" involved. More recently Latimer (12) discussed this scattering as being on the longer wavelength sides of absorbance maxima, but in our data we observe it on both sides of the maxima. In the range of the spectra illustrated the primary leaf chromophore are chlorophylls a and b, which are organized in chlorophyll protein complexes (CPX); CPX in turn are inside of the chloroplast.

Chloroplast size is roughly 30 nm^3 (Nobel, 1983, p 80) too large for "Rayleigh" scattering. The chlorophyll molecule is comprised of a complex ring structure, "head", similar to porphyrin and a long hydrocarbon "tail" called the phytol chain (e.g. 92,39). The flat porphyrin like head is about 1.5 by 1.5 nm and the tail is about 2 nm long. Thus, chlorophylls could contribute to the "Rayleigh" scattering. Since CPX can contain up to two or three hundred chlorophylls and have attached proteins, larger CPX are moieties comparable in size to the observing wavelength (e.g. 93). Therefore, for CPX, the "Rayleigh" relationship to λ^{-4} would not be expected hold (90). However since chlorophyll molecules have the appropriate absorbance, are present in large amounts (usually 0.3-3 mg per dm^2 of leaf surface area) and have suitable physical size, it is rational to consider

chlorophyll molecules as the most probable major source of the putative "Rayleigh" scattering observed in leaves.

Water Water bands are broad, due to thermal motion distorting the weak O-H·····O linkage between water molecules absorbance (e.g. 94). This yields a useful, if weak, maxima near 975 nm. Solvation in heavy water (D_2O , D-O-D) does not yield the same spectrum as water when used to hydrate biological polymers (e.g. 95,96). These spectral differences between D_2O and H_2O have potential uses in NIR spectroscopy.

Figure 4.3 (upper left) shows the spectra of deuterium oxide (D_2O , D-O-D) water mixture in visible and very short NIR. These spectra show that D-O-D absorbs much less in this region than water. This is significant to this use because wet and dry materials have different optical properties because of the air/water interphase (e.g. 30,72). Thus, it is possible dilute water with deuterium oxide and keep interphase signals constant. However, there are complications, Fig. 4.3 (upper right) shows that there is a moderate peak shift with D-O-D content.

We calculated the spectra of H-O-D (Fig. 4.3 lower left) assuming completely random attachment of deuterium/hydrogen to oxygen in each solution. Then using the data at 80% v/v D-O-D/water, assuming no absorbance for D-O-D, full absorbance for H-O-H, we calculating the residual as H-O-D. While this yields a lower molar absorption coefficient for the H-O bond of H-O-D (Fig. 4.3 lower left), than predicted by halving that of water, the H-O-D spectra (detail in Fig. 4.3 lower right) explains peak shifts occurring when diluting water with D-O-D (Fig 4.3 upper right).

Figure 4.4a tests this reconstructed spectra of H-O-D by using it to reconstructed spectra of the other D-O-D/water solutions; then comparing reconstructed to observed

Figure 4.3. Spectra of deuterium oxide (D-O-D), water (H-O-H) mixtures in visible and very short NIR. These spectra were obtained using the research instrument with the integrating sphere attachment. The liquid mixtures were placed in a 1 cm quartz cuvette; the reference beam path was air, the minima for deuterium oxide was used as a base line. The upper left panel shows the experimental data and illustrates the deuterium oxide base line. Mixtures are in volume to volume percentages. The upper right panel shows the peak shift of normalized spectra from the upper left panel, the numbers indicate the normalization factor. The lower left panel compares the spectra of water against the calculated spectra for H-O-D, this spectra was calculated from the 20% mixture of water in deuterium oxide shown in upper left figure assuming random mixing of deuterions and protons, and zero absorbance, at these wavelengths for the deuterion-oxygen bond. The normalized H-O-D bond has both slightly less than expected absorbance, a normalization factor of 2.38, not 2.00, was required. The lower right panel compares the approximately 8 nm calculated shift to shorter wavelengths of the maxima with deuteration. Which compares well to the shift observed experimentally in deuterium water mixtures shown in the upper right panel.

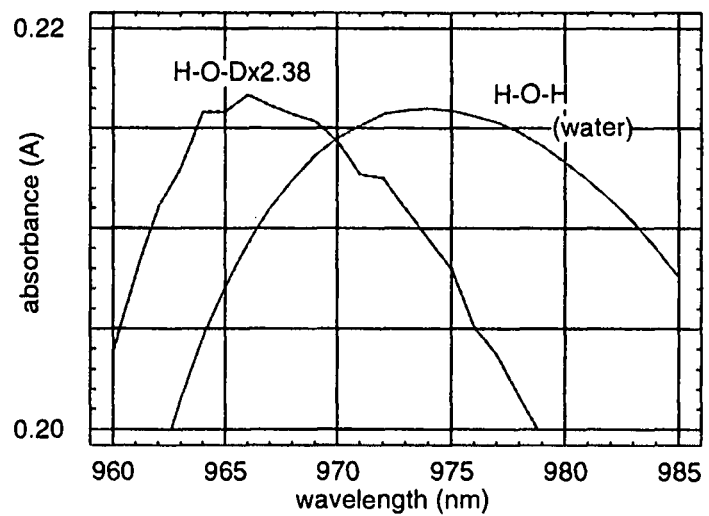
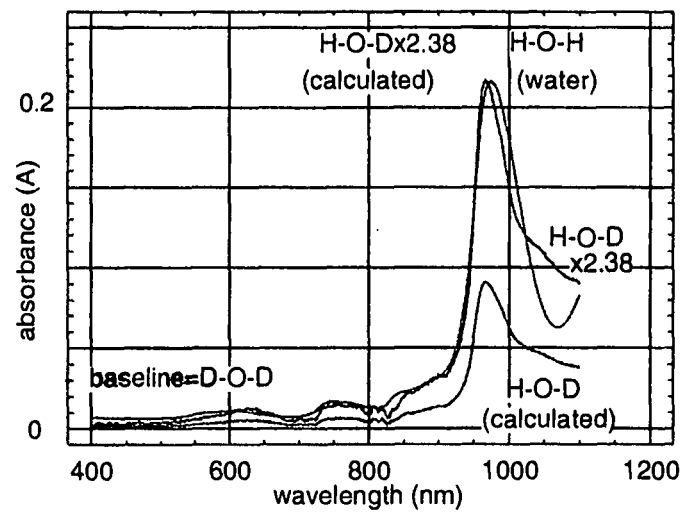
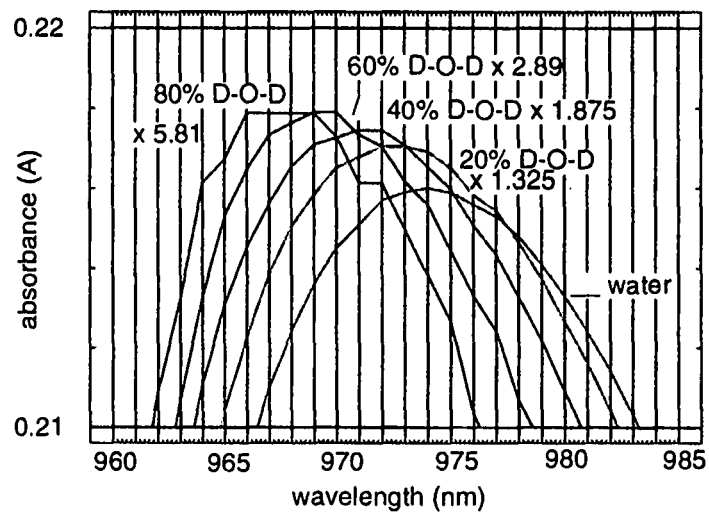
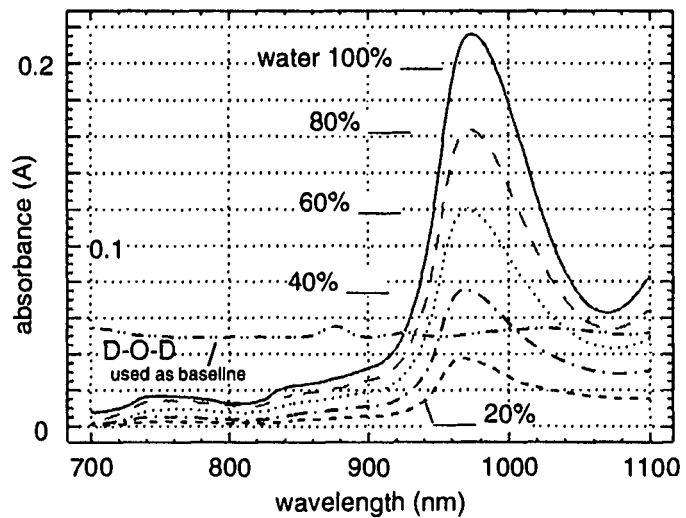


FIGURE 4.3

Figure 4.4a. Reconstruction of spectra of deuterium oxide diluted water compared to observed data. The simple random model produces reconstruction spectral ratios (rsr) showing that this simple model, described in Figure 4.2. This model assumes that only water and H-O-D contribute absorbance in this range, that the deuterium and hydrogen components randomly mix, and ignores molecule/molecule interactions and other factors. Since the deviations are small, this simple model is useful to reconstruct the spectra of the deuterium oxide water mixtures in biological context. We leave explanations of these slight deviations between measured and calculated spectra to others.

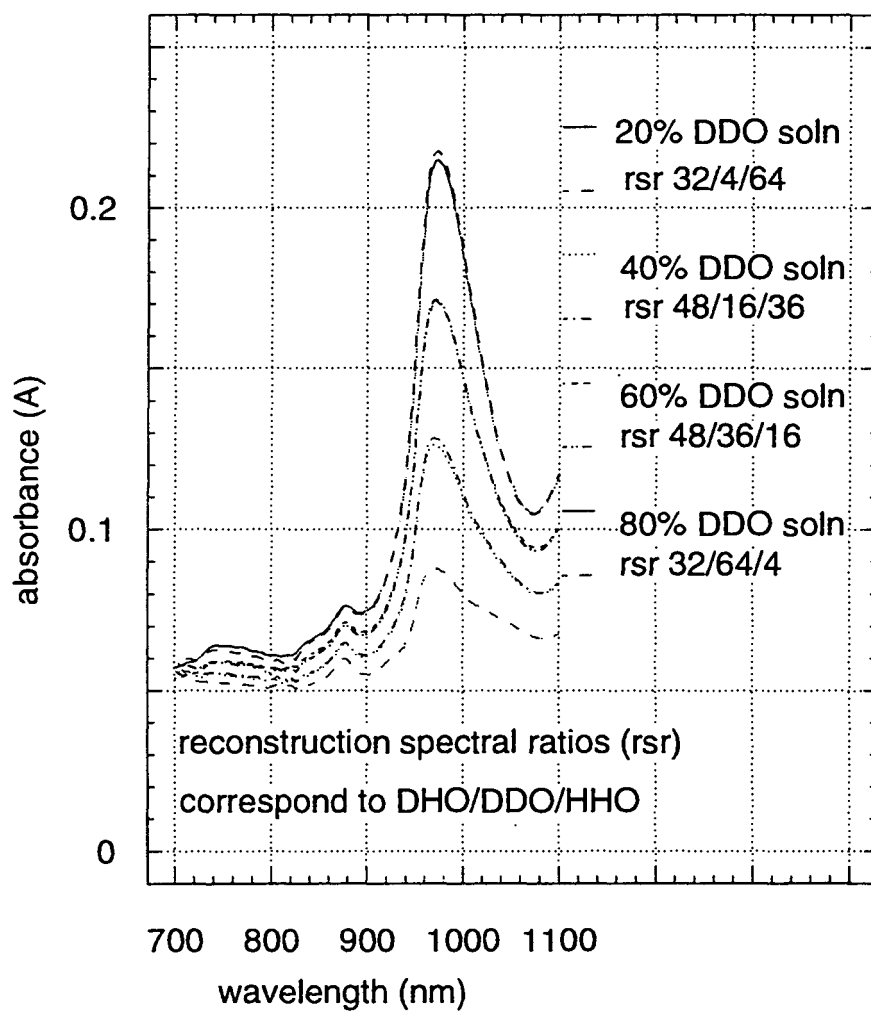


FIGURE 4.4a

Figure 4.4b. Reconstruction of a series of spectra of water/deuterium oxide mixtures using the simplified method. This figure is presented to be used as a guide for analysis of deuterium oxide/water mixtures.

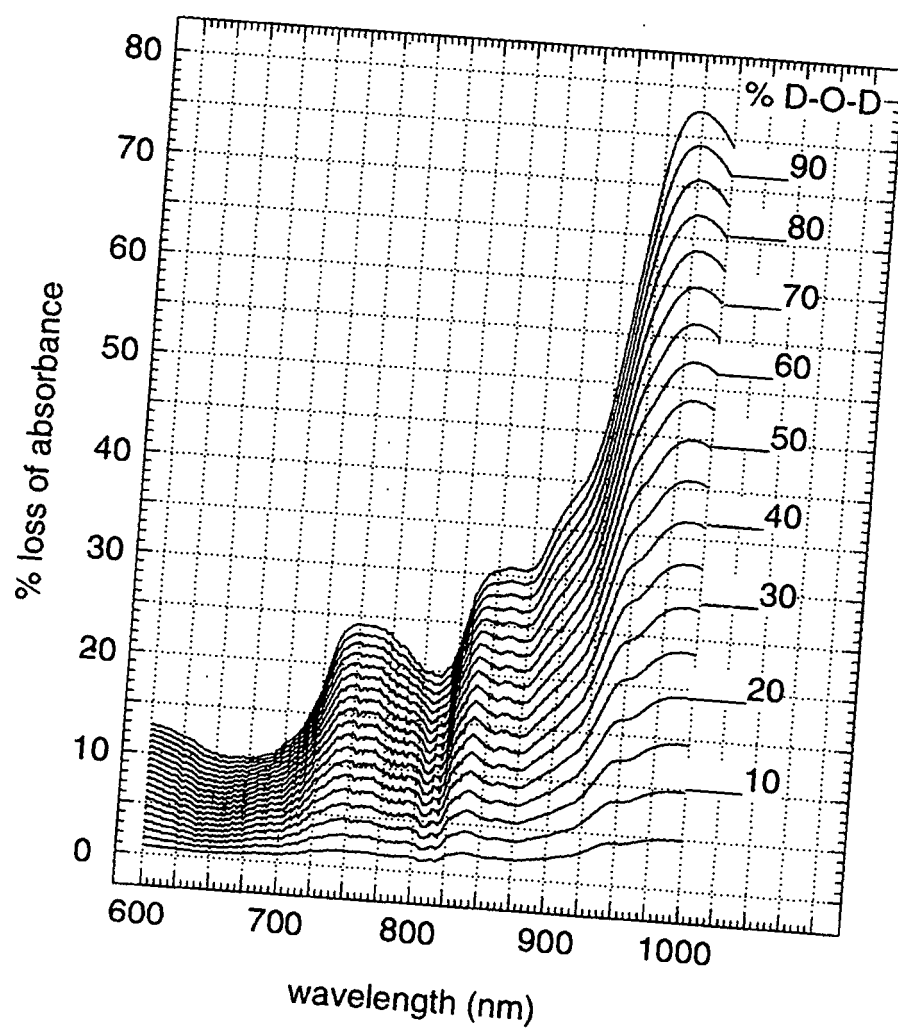


FIGURE 4.4b

spectra. There are (Fig. 4.4a) some slight deviations between observed and calculated spectra of mixes of D-O-D and water (DDO soln) (Fig. 4.3). However, these deviations are small and thus, insignificant in a biological context. Therefore, using the reconstruction method we generated spectra for a more complete series of D-O-D/water solutions (Fig. 4.4b).

Figure 4.5 tests the difference between D-O-D and water first on filter paper (left panel); then follows spectral changes of coffee and *Corylus* leaves (middle and right panel respectively) as the initially fresh leaf is freeze dried and then rehydrated.

To test our imaging instrument we used stacks of filter paper disks wetted with D-O-D/water mixes. Figure 4.6 (upper left panel) demonstrates linear response ($R^2=0.99$) of the imaging instrument to water in disks, when "Rayleigh" corrections are made. While the linearity of this response is maintained from experiment to experiment, the intensity of response varies. Factors that may contribute to variation in detectable strength of response to water content are: (i) this water band is affected by temperature (Piepmeier, unpublished); (ii) light penetration into the stacks may be difficult to control from experiment to experiment; (iii) evaporation of water from the exposed paper disks may be significant; (iv) the signal is weak (Fig. 4.6 upper right panel).

Our use of a "Rayleigh" correction for water in paper disks suggests a conflict with Gregory Carter's (65) statement that water in leaves has minimal "Rayleigh" effect. However differences in instrumentation and experimental approach between Carter's reflectance work and our own absorbance data may make what is insignificant in Carter's context, significant in our own. This can explain Carter's (65) elegant demonstration of

the lack of sensitivity of reflectance of water in the 700-1,300 nm range where our absorbance work is done. Other considerations are discussed below.

Leaves have an external waxy cuticle (39) that prevents water evaporation. The gas exchange controlling apertures in this cuticle, the stomates (39,97), close when the plant is stressed by lack of water. Therefore, during experimental work water content of leaves, and consequently our estimate of light path through biochemically active areas (see sidebar 1), can be considered constant. We use A^{800} nm, or A^{790} , as reference baselines, and A^{970} nm as water signal. Accumulating signals at these wavelengths is required to reduce noise. The notation $A^{}$ indicates "Rayleigh" corrected attenuance.

Since the concentration of water in cells of plants is essentially constant (see sidebar 1) the signal observed relates to the path of light through living cells. Thus, we investigated, by integrating sphere non-imaging spectroscopy, physically separated, uniformly hued sections from the variegated (multi-hued) leaf of *S. nodosa*. Spectra were corrected for water pathlength (Fig. 4.6 upper right). The objective was to determine whether *in vivo* spectroscopic signals from different portions of the leaf had chloroplasts with different CPX proportions (e.g. 25). This is significant for theories of light shade adaptation through CPX ratio change (93). For horticultural purposes we also wish to determine the nature of the pigmentation variation in this possibly chimeric leafed plant, and determine whether areas of lower pigmentation have differently structured chloroplasts.

Chlorophyll protein complexes and water path. Figure 4.6 (lower left panel), uses ratios of normalized spectra from the different hued sections of the leaf. The wavelength positions of the CPX are indicated by the heavy line of the fourth derivative trace. If the

Figure 4.5. Demonstration of water peak in solid substrate. These spectra were done using the research spectrophotometer. The left panel shows a comparison of water vs deuterium oxide on stacks of filter paper. The middle and right panels show spectra of leaves of coffee (*Coffea arabica*) and hazel (*Corylus avellana*) leaves respectively. These leaf spectra were taken, using the same leaves, when these leaves were fresh, freeze dried and then rehydrated. This data shows that the water peak near 970 nm is readily apparent under these conditions.

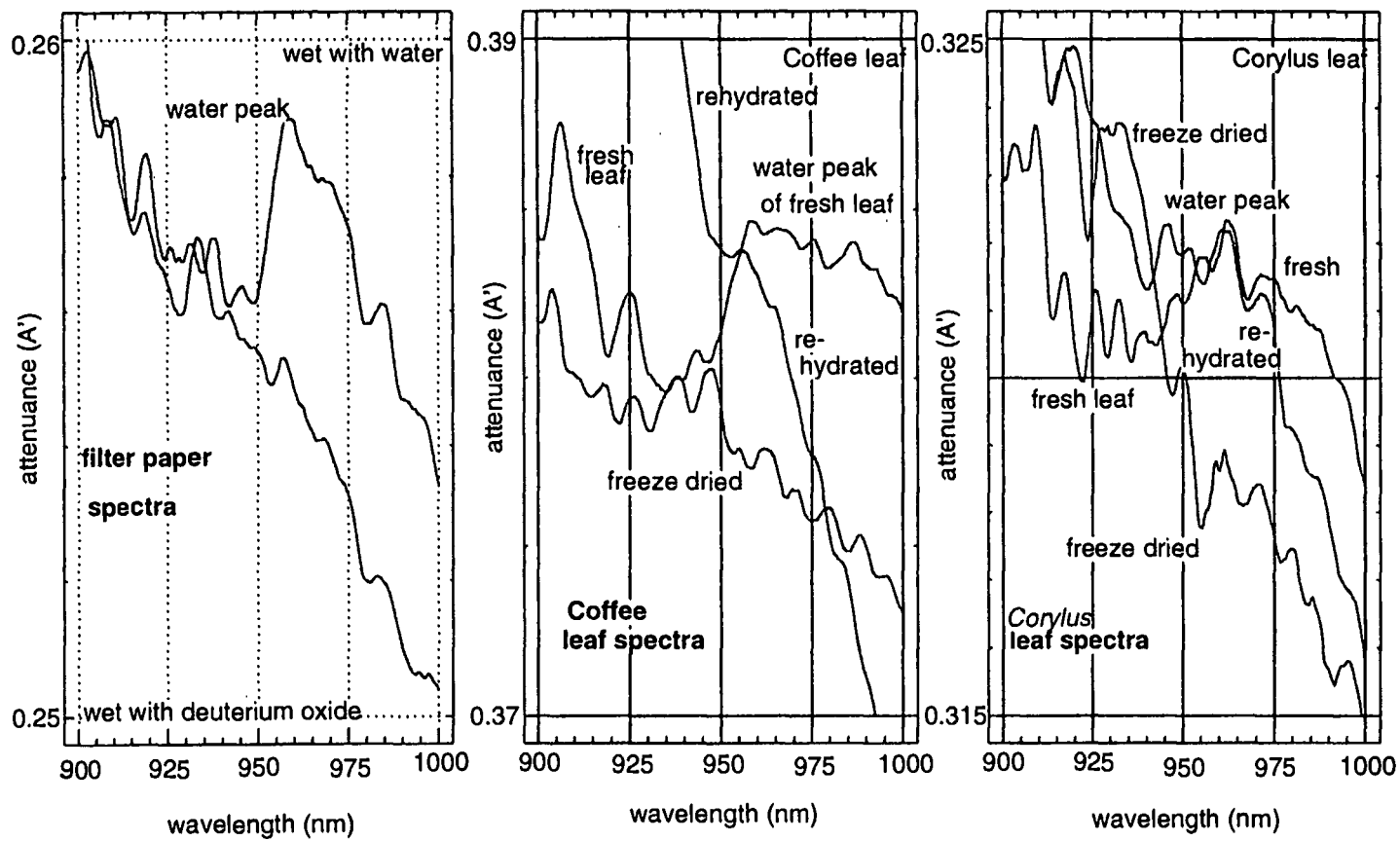


FIGURE 4.5

Figure 4.6. Utility of normalization of water in wet and living substrate. The upper left panel demonstrates linear response ($R^2=0.99$) of the imaging instrument to water in filter paper disks when analyzed by the imaging instrument when "Rayleigh" corrections are made. The upper right panel, lower left and lower right panels show research spectrophotometer data from differently hued sections of leaves of *S. nodosa* 'Variegata'. The upper right panel shows a comparison of spectra between the differently hued sections. These spectra are corrected for "Rayleigh" scattering and normalized for the 970-800 nm attenuance. Notice that both the chlorophyll protein complexes (CPX) in the leaves (strong bands at shorter wavelengths) and the weaker but distinct water bands (maxima near 970) can be observed. The panel at the lower left shows the change with wavelength (fine lines) of the ratio of absorbance of the deepest green (dark) sections to that of lightest green (light) sections. These data are compared to a normalized fourth derivative trace of the spectra (heavy trace). Fourth derivative spectra isolate signals from individual CPX (e.g. 25); and thus serve to identify the composition of the components of these complex spectra. From this data it can be seen that different CPX are present in different proportions in the differently hued sections. The fourth panel (lower right) compares the fourth derivative analyses of normalized spectra of the different sections of the leaf. The CPX which have most significance in this analyses are photosystem I (PSI) antenna which proportionally decreases in lighter-hued sections; and the light harvesting complexes which remain in about the same proportions.

A970nm - A800nm, Rayleigh corrected

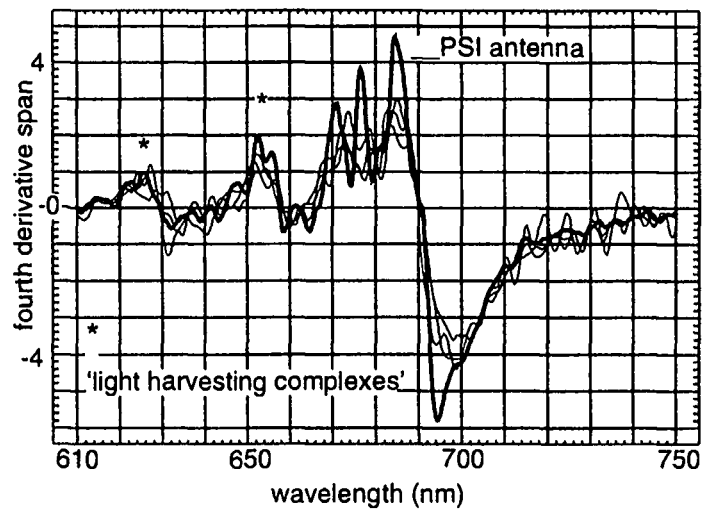
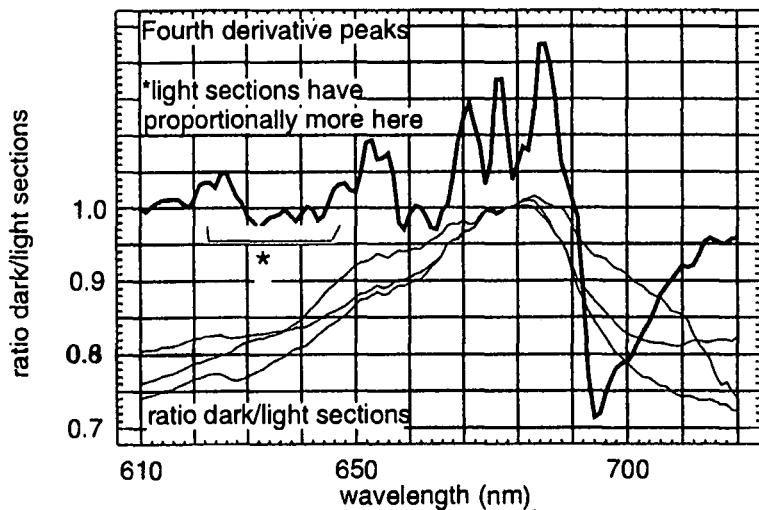
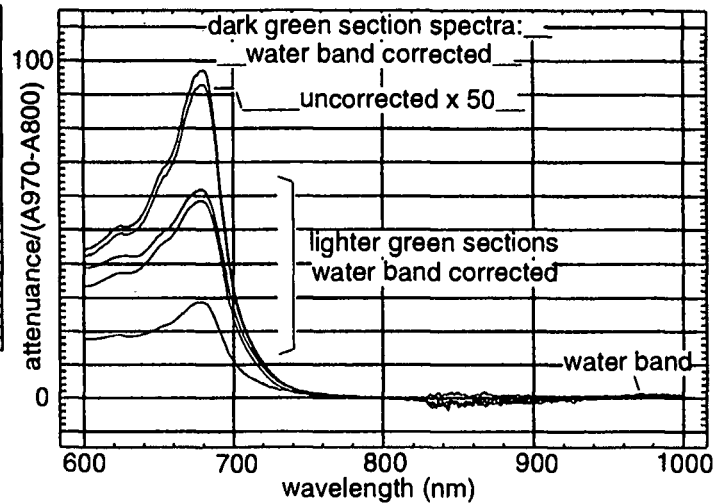
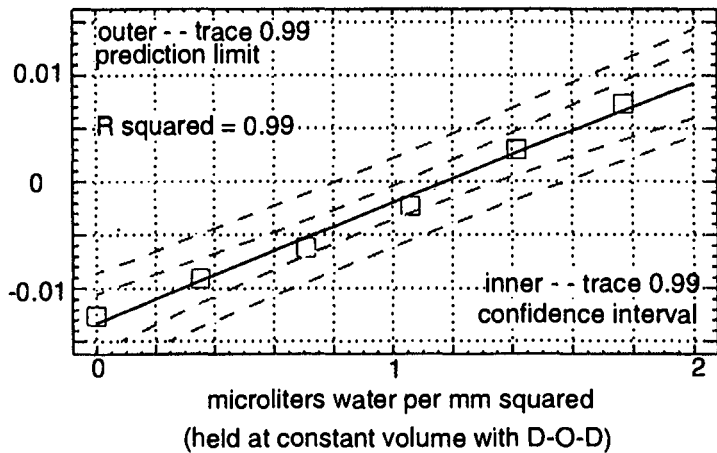


FIGURE 4.6

different sections of the leaf had the same proportions of CPX, we would expect to find the ratios a straight horizontal line, at a ratio of 1.0, across the lower left panel of Figure 4.6. This was not so. The lighter hued sections had proportionally more shorter wavelength CPX, indicated by the decreased ratio observed when dividing the normalized absorbance of the darkest hued section by that of the lighter hued sections. The decrease in absorbance above 690 nm is not interpreted because of the low absorbance of CPX in this area.

Figure 4.6 (lower right panel) shows 4th derivative analysis of the data from the different section of the *S. nodosa* leaf. The fourth derivative was smoothed using a Q-spline procedure (e.g 58) which regenerates the approximate shape of the curves from point data; compare this trace with the normalized, but unsmoothed, trace of the same data in Fig. 4.6 (lower left panel). CPX change (39,81,93), here fourth derivative analyses (Fig. 4.6 lower right) show that the PSI (photosystem I) antenna signal decreases from the deepest (heavy trace) to the lightest hued sections. Yet at the wavelengths corresponding to the light harvesting complexes (LHC) there is no perceptible decrease.

Since most commonly LHC feeds solar energy to photosystem II (PSII, e.g. 39, p. 199), this suggests that PSI/PSII ratios are higher in the lighter hued leaves. This is strongly consistent with the lighter hued sections being more light adapted. Since the different sections of this variegated leaf have been exposed to exactly the same light conditions we can explain this effect either as a result of self shading by the more abundant, or more pigmented, chloroplasts or the result of selective propagation of more light adapted chloroplasts in the lighter hued sections. In addition (data not shown) as chlorophyll content decreases from the deeper pigmented, through the less pigmented and

Figure 4.7. *In vivo* tests of water content and general distribution of chlorophyll-protein complexes in leaf sections of *Aloe milotii* and a section of living leaves of *Scrofularia nodosa* 'Variegata'. Figure 4.7, upper left plots *Aloe milotii* leaf sections of different thickness imaged at 970 nm (water band attenuation) minus 790 nm (reference attenuation). Numbers on axis indicate pixel location. The image is adjusted to the blue range. The shades of blue as indicated by color bar indicates the relative path of water. The thickness of the leaf slices is: upper and lower rows from left to right, 2.89, 2.64, 1.64 and 3.84, 5.63 and 7.17 mm respectively. There are two parts to these slices the central parenchyma and the outer, rind-like, chlorenchyma. Figure 4.7, lower left, shows plots of tissue thickness against 970-690 nm attenuation. Circles indicate chlorenchyma response, x's the response of the central parenchyma. Attenuance of different areas was determined by a median measuring graphical method in which the data was taken directly from the image. The R^2 for chlorenchyma and parenchyma were respectively 0.82 and 0.96 plots, "Rayleigh" correction decreased this R^2 to 0.72 and 0.58 suggesting that "Rayleigh" is minimal at 970 for this apparently "light piping" tissue. Figures 7 upper and lower right compare chlorophyll content images of *Aloe milotii* tissue slices and *Scrofularia nodosa* 'Variegata' leaf sections. These images were prepared by summing attenuation at 10 nm intervals from 640 to 690 nm. The relative chlorophyll absorbance of the sections are presented in shades of green superimposed on a mathematically generated yellow background as indicated by gradient color bar. Notice, although the plotting method can show subtle gradients, abrupt transitions occur between tissues and variegated sections. Figure 4.7, upper right, shows the chlorophyll absorption distribution of the *Aloe milotii* sections shown at the upper left. Notice the difference in relative chlorophyll content

between the rind-like chlorenchyma and the interior parenchyma. Figure 4.7, lower right, plots areas of high and low chlorophyll content of the variegated multi-hued section of leaf of *Scrofularia nodosa* used in Fig. 4.8. Notice the abrupt transition between variegated sections in the x-y plane of the surface of the leaf. To compare with true photographic colors see Fig. 4.1.

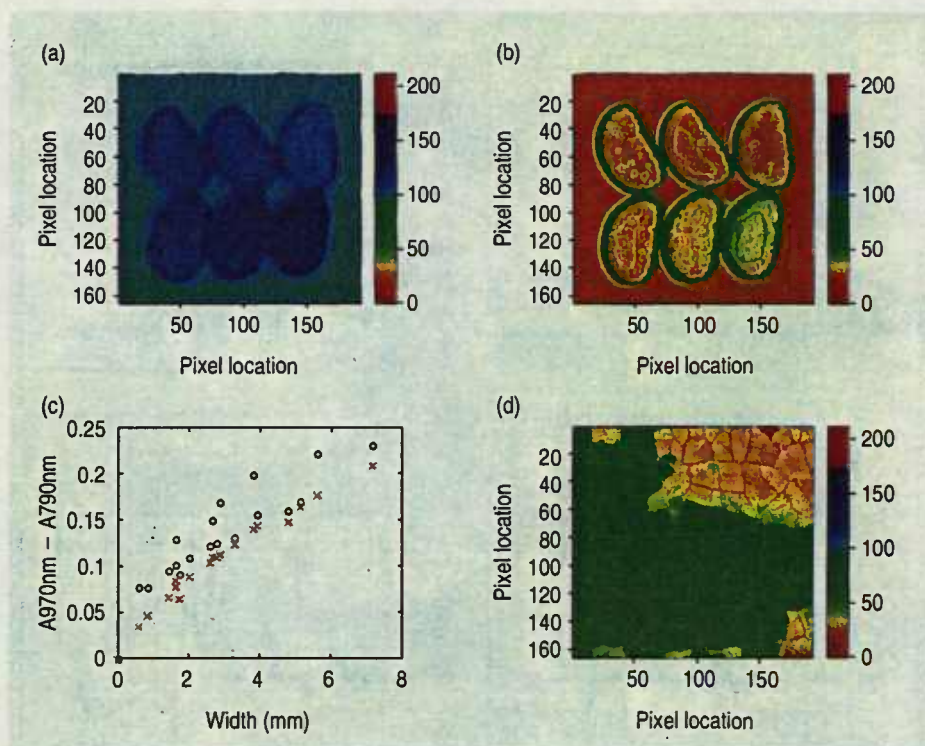


FIGURE 4.7

on to lightly pigmented areas of these *S. nodosa* leaves there is successively less quantum yield for photosynthesis (81). This suggests that what we observe is either: (i) not a true shade adaptation because we would expect greater efficiency in adapted areas; or, perhaps more logically, (ii) the strong light necessary for yield measurements has more permanent effects on these lightly pigmented, 'shade adapted' areas than on those areas of the leaf which are strongly pigmented.

Path of water *in situ*. We investigated the path of water (Fig. 4.7, upper left) in fleshy, thick but blade-like, leaves of the genus *Aloe*. The inner central part of the *Aloe* leaf consists of huge, thin walled, parenchyma cells with only very small intercellular air spaces. (51). These parenchyma cells lack chloroplasts and starch. The *Aloe* leaves are easily sliced, transversal to the long direction, with a razor blade. The resulting sections, provide a central area of parenchyma cells surrounded by a continuous band of more rigid, rind-like, tissue with chloroplasts in its cells (chlorenchyma). The lack of chloroplasts, small air spaces, and thin cell walls provide simplified and readily measured, reduced apoplast, model for the optical path of water (Fig. 4.7 upper left) in plant tissue. The rigid chlorenchyma of the thin sections allows us to readily use a micrometer to measure the thickness of the water containing cells and compare this measurement against the spectrophotometrically (970-790 nm) measured path of water (Fig. 4.7, lower left). The parenchyma of the *Aloe milotii* leaves we used had a median, mean and average deviation values for: (a) water content [estimated as % (FW-oven dried dry weight)/FW] of 98.7%, 98.4 and 0.9% of water; (b) densities relative to water at same temperature (about 23° C) of 1.009, 1.020 and 0.022; (c) refractive indices (25 °C, water was 1.3326) of 1.3341, 1.3341 and 0.00026. Thus, since these parenchyma cells lack chloroplasts and have only

small apoplastic spaces (51), they constitute a simplified *in vivo* spectroscopic model for life as bags of water (see first side bar).

Figure 4.7, upper and lower left, data allowed us to confirm, *in vivo* the correlation between 970 nm attenuance and water content. The absolute values of water absorbance were much more constant between different experiments than observed for paper disks saturated with deuterium oxide water mixes. We attribute this to the cell membranes that protect the water in the *A. milotii* tissue from evaporation during measurement and the larger amounts of water present in these experiments. The linearity of increase of the 970-790 nm water measurement to increased tissue thickness required did not benefit from "Rayleigh" correction in this non-green parenchymous tissue that lacks chloroplasts and chlorophyll, as predicted by Carter (65). This was also true for the surrounding chlorenchymous green tissues. However, this does not rule out a "Rayleigh" response to chlorophyll; since highly light conducting parenchyma is quite capable of "piping" light back into more light scattering, rind-like, chlorenchyma in such a way that it could act as a light-pipe sheath (Fig. 4.7 lower left). In addition, we note that *Aloe* parenchymous tissues have much less cell walls, and thus less cellulose/water interactions than "Rayleigh" correctable leaf (Fig. 4.2) and filter paper disks (Fig. 4.5).

To visualize the sudden transitions between areas parenchyma and chlorenchyma in *Aloe milotii* (Fig. 4.7 upper right), and between area of high, medium and low chlorophyll content of the variegated multi-hued section of leaf of *S. nodosa* (Fig. 4.7, lower right) we summing attenuance at 10 nm intervals from 640 to 690 nm. Note the abrupt transitions in both tissues. The shades of green in the color bar indicate the intensity of absorbance of chlorophyll. Yellow indicates minimal absorbance of chlorophyll. In the variegated leaf of

S. nodosa 'Variegata', each colored section is relatively uniform in chlorophyll absorbance, but transitions between sections are abrupt. This indicates the precision of genetic control between regions of the *S. nodosa* 'Variegata' leaf, as is also apparent for the two tissues of *Aloe milotii*. Interesting tissue developmental and evolutionary inferences can be inferred from these observations. Figure 4.7, upper and lower left, make the point that in plant leaves chlorophyll content can vary abruptly.

Images of CPX relative to water path. Once we were able to establish the validity of our water measurements and establish the differences in chlorophyll content between sections we were able to use the imaging spectrometer (1) to map the distribution of these different populations of chloroplasts in the intact leaf. Figure 4.8 describes the images obtained by different estimates CPX and their relationship with water path. The intensity spectrum of false color is represented as a gradient of intensity of signal proceeding smoothly from the blue, through the yellow, and on to the red range of the visible spectrum. A color bar clarifies this matter.

Proportions of CPX are given in numbers determined by the equation used. Exact quantification of CPX by absorbance is not precise because it is dependent on the relative proportions of chlorophyll a and b in the CPX, the variable size of the CPX unit, the physiologically and biophysically variable conformation of the CPX (Melis, private communic., 1995). Molar quantification of CPX *in vivo* would require a physical *in vivo* method or purification method that did not change extinction coefficient of the CPX on *in vitro* extraction; such methods do not yet exist (Melis, private communic., 1995). Thus it is possible to observe changes in relative CPX proportions, but not as yet determine molar ratios.

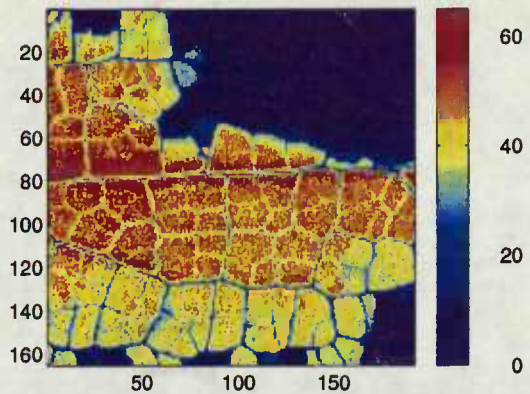
In figure 4.8, the upper left describes the pattern generated by our estimate of PSI $[psl=(2 \cdot A^{680}-A^{670}-A^{690})/2+A^{690}-A^{750}]$. This estimates a separation of PSI signal from PSII in underivatized spectra by assuming, from Daley (25) that (a) A^{670} represents a maxima for PSII with some contribution from LHC, (b) A^{680} is close to the moving maxima for the antenna of PSI (25,26), and (c) that $A^{690}-A^{750}$ represents a essentially clean signal from the remaining portion of PSI antenna. The part of the equation $2 \cdot A^{680}-A^{670}-A^{690}$ segregates from main peak (as in Fig. 4.1) the contribution of PSII and LHC (25), there by generating an estimate of the contribution of PSI below 690 nm. This estimate is then added to the $A^{690}-A^{750}$ portion of the PSI signal to generate and estimate of total PSI. Thus, panel estimates the distribution of PSI across a portion of variegated leaf lamina. This distribution generates three major sections bands consistent with the data from the separated sections generated by the non-imaging research spectrophotometer (Fig. 4.6 upper right panel).

The upper right panel of Fig. 4.8 shows a similar estimate of LHC, this was done by summing A^{630} and A^{650} maxima of chlorophyll b signals from LHC (25). This estimate of LHC is called Tlh and the equation is $(Tlh=A^{630}-A^{600}+A^{650}-A^{600})$. The pattern generated (Fig. 4.8, upper right panel) is similar to that for PSI estimate, but some what less distinct.

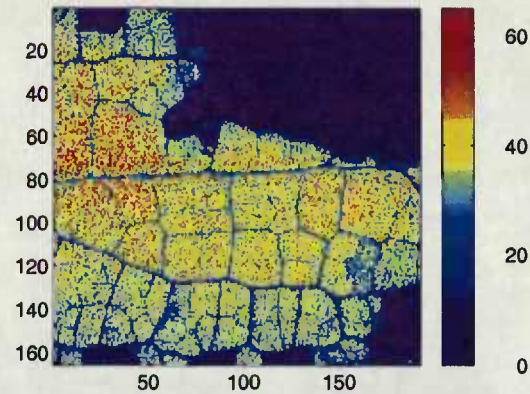
The lower two panels represent the data for PSI and LHC estimate corrected for water path ($A^{670}-A^{790}$). Water path correction generates patterns similar, but more discrete than those generated by data uncorrected for water path. Although distributions of PSI and LHC are subtly different, these differences are not readily apparent in figures

Figure 4.8. Mapping light harvesting (LH) chlorophyll-protein complexes (CPX) in the living leaf. This figure shows images of the distribution of LH CPX across the laminar plane of the multi-hued, variegated leaf section of *Scrofularia nodosa*. Numbers on x and y axis indicate pixel position. Color indicates relative intensity as in color bar at right of figure. All absorbance data are corrected by our method for "Rayleigh" scatter, as indicated by the symbol A". The area corresponds to 2.5 x 2.5 mm. The upper left panel shows the distribution generated by the "Rayleigh" corrected estimate of photosystem I (ps1"), by the formula: $ps1" = [(2 * A"680 - A"670 - A"690) / 2 - A"690 - A"750]$. The upper right panel shows the corresponding estimate of total light harvesting chlorophyll protein complex (Tlh) using the formula $Tlh" = (A"630 - A"600 + A"650 - A"600)$. The lower left panel shows ps1 data corrected for water absorbance $water = (A"970 - A"790)$; and the lower right figure Tlh corrected for water.

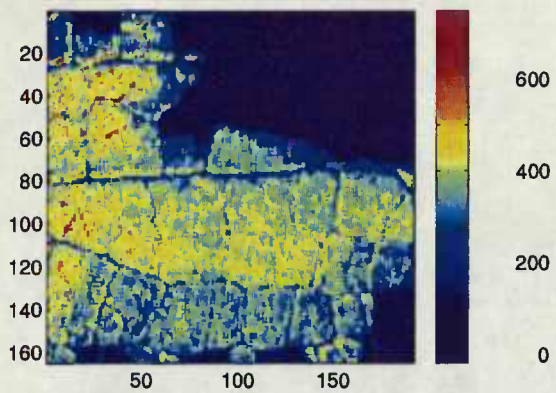
$$ps1^* = (2 \cdot A^*680 - A^*670 - A^*690) / 2 + A^*690 - A^*750$$



$$Tlh^* = A^*630 - A^*600 + A^*650 - A^*600$$



$$ps1^* / \text{water}^*$$



$$Tlh^* / \text{water}^*$$

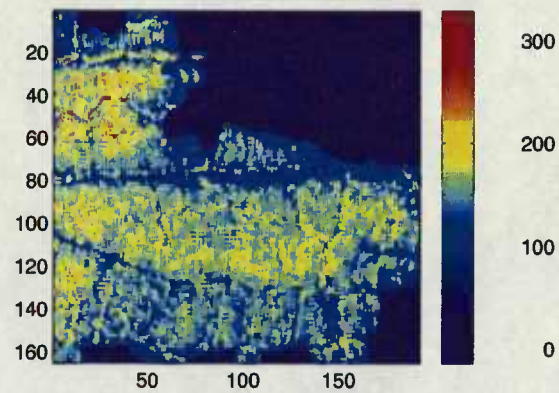


FIGURE 4.8

generated with these equations. Thus Fig. 4.8 does not allow ready inferences about light/shade adaptations (e.g. 93).

To distinguish whether the chloroplasts in the distinct regions have different proportions of LHC and PSI and thus derive inference on light shade adaptation we used two other equations. The first equation, (Fig. 4.9, upper left panel) an estimate of PSI/LHC ratio by equation $[(ps1/Th1)*15+1.6]$ shows that there are at least two regions of the leaf between which dark/shade adaption of chloroplast CPX differ. In this equation, the number 15 is used to adjust contrast, and the 1.6 is adapted from the minimum chlorophyll a/b ratio found naturally found in experimental data (e.g. 27). If we check water distribution (Fig. 4.9 upper right panel) it can be readily observed that water path in leaf does not contribute to this effect. Figure 4.9, lower left panel, shows an image generated by a second equation, a weighted difference spectra of the difference between PSI (ps1) and LHC (Th1); this difference is then divided by the water path $[13*(ps1-2*Th1)/water]$. The number 13 is an empirical contrast adjustment. This difference image divides the leaf in three general sections, and the distribution of these sections bears no apparent relation to the distribution of water, even when compared to an image of water path enhance to emphasize differences (Fig. 4.9, lower right panel). We expect that shade adaption traits revealed by this CPX analyses will relate to horticultural uses and germplasm characterization.

Figure 4.9. Mapping photosystem I (PSI) chlorophyll-protein complexes (CPX) in the living leaf. This figure shows, using the imaging spectrometer, the distribution of PSI CPX across the laminar plane of the multi-hued, variegated leaf of *Scrofularia nodosa*. Scale, conventions and correction for "Rayleigh" scattering as in Fig. 4.7. The left panel shows the distribution estimated of the estimate of photosystem I/light harvesting complex ratio $[(ps1"/Tlh")*15 + 1.6]$. This estimate implies that the highest ratio (reddest), in the upper right quadrant of the figure, is the most shade adapted. The upper right panel shows the distribution of water, $water"=A"970-A"790$. The lower left panel shows an estimate of the excess of $ps1"$ over $Tlh"$. This is a reciprocal estimate of shade adaptation, where the highest shade adaptation is the lowest color (blue in upper right quadrant). This image is water corrected. The lower right panel is an enhanced ('stretched'), image of the water distribution shown in upper right figure; notice how the water distribution is highest parallel to the central vein, and distinct from the distribution of CPX shade adaptation.

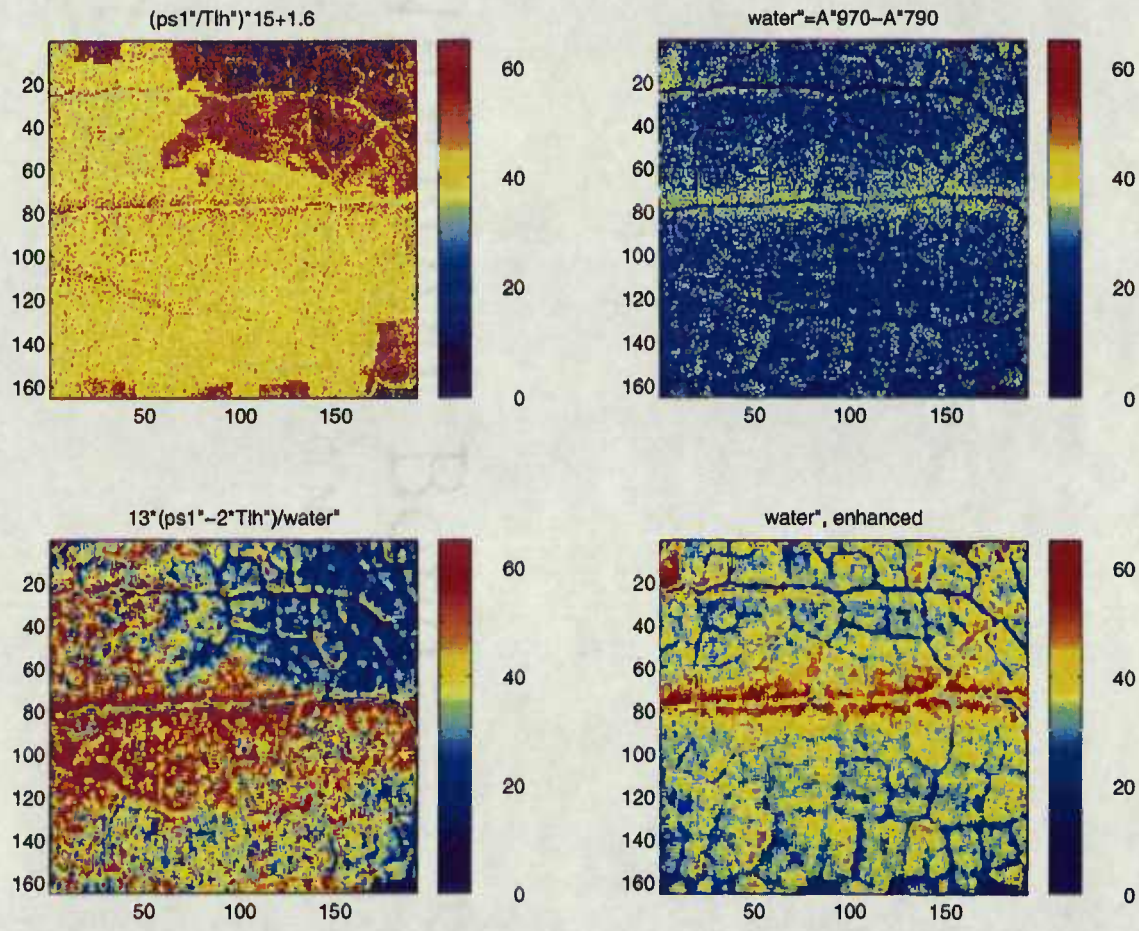


FIGURE 4.9

CONCLUSION

The use of a "Rayleigh" correction plus determination of pathlength utilizing the water signals near 970 nm are useful for *in vivo* analysis of plants. This shows it is possible to image the difference between CPX ratios in variegated living tissues. This is a matter of some significance in studies of plant development and genetics. We believe that the measurement of water path to determine pathlength of biochemically significant parts of the tissue, the "Rayleigh" correction and the use of deuterium oxide as a dilutant to determine water signals has practical and theoretical applications. Among these applications characterization of phytopathologies is a high priority.

BIBLIOGRAPHIC SKETCHES

Author(s): Ning, L., Bowyer, W.J., Daley, L.S., Piepmeier, E.H., Strobel, G.A. and Callis, J.B.

Li Ning is a graduate research assistant in the Departments of Horticulture and Computer Engineering at Oregon State University (OSU), Corvallis. He received his MS in Horticulture from Beijing Agriculture University, in 1987, and his BS in biology from Peking University, China, 1983. Ning is preparing to take his PhD defense in the winter months of 1995-1996 and completing his course requirements for a MS in Computer Engineering. Ning's PhD dissertation will include the construction of a novel imaging spectrometer and fluorometer, and the application of these instruments to *in vivo* biochemistry, phytopathology of diverse plant germplasm.

Walter J. Bowyer is an associate professor in the Department of Chemistry at Hobart and William Smith Colleges, Geneva, New York. He received his PhD in analytical chemistry, from the University of Vermont in 1985, his MS in biology from the University of Virginia earlier that same year, and his BS in Ecology from Johnson State and Windham Colleges in 1980. His interests include electrochemistry and diverse spectroscopies, as well as imaging spectroscopy.

Larry S. Daley is an associate professor in the Department of Horticulture at Oregon State University. He received his PhD from the University of California at Davis in the Biochemistry and Biophysics Department in 1975. His research interest include the biochemical and biophysical interpretation of *in vivo* leaf spectra and its relationship to germplasm research.

Edward H. Piepmeier is a professor in the Department of Chemistry at Oregon State University. He received his PhD from the University of Illinois in 1966 and his BS from North Western University, Illinois in 1960. His research interests include laser plume, atomic absorption, and near-infrared spectroscopy and high resolution spectroscopic instrumentation.

Gary A. Strobel is Gray Professor in the Plant Pathology Department at Montana State University. He received his PhD from U.C., Davis in 1963, and his BS from Colorado State in 1960. Prof. Strobel is a physiological plant pathologist, well known for his elucidation of structures, physiological activities and innovative applications of fungal

and bacterial toxins. His interest in visible and near-infrared imaging relates to the usefulness of this spectroscopic technology to detect pathological events in plants.

James B. Callis is a professor of chemistry and adjunct professor of bioengineering at the University of Washington, Seattle. He earned a PhD in chemistry from the University of Washington in 1970. His research interests include the development of instruments including the video fluorometer, flash calorimeter, imaging spectrophotometer, and laptop computerized instruments. Callis's current interests include development of instrumentation for ecological surveys and *in vivo* interferometry.

ACKNOWLEDGMENTS

The PLS program training was kindly provided to the first author by Prof. Bruce R. Kowalski, CPAC, Department of Chemistry, University of Washington. Prof. Jack Stang, Department of Horticulture, Oregon State Univ. (OSU) generously provided advice on ornamentals, Herbarium Curator Dr. Richard R. Halse, Botany and Plant Pathology, OSU kindly helped with plant identification. We also thank Prof. H. T. Hammel, Indiana Univ. School of Medicine and Dr. Thomas W. Brakke, NASA/Goddard Space Flight Center for advice on water spectra *in vivo*. Professors Gerald E. Edwards, Washington State Univ. Pullman, Anastasios Melis, U. C. Berkeley, and Edwardo Zeiger, U.C. Los Angeles for generously provided much useful advice on plant physiological concepts. We thank our OSU greenhouse manager Jim Hay and his dedicated crew for their care of our plants, Instructor Robert Schnekenburger of Bioresource Engineering

OSU for assorted technical help and computer hardware advice, and Natalie S. Daley for plant photography. We gratefully acknowledge support from the Herman Frasch Foundation (grant number: FRASCH 63-0738), and the OSU Agricultural Research Foundation, and the donation of a color printer by Lucidyne Technologies Inc. This paper is Oregon Experiment Station Technical paper #10933.

REFERENCES

- (1) L. Ning, R. Ozanich, L.S. Daley and J.B. Callis, *Spectroscopy* 9(7), 41-48 (1994).
- (2) P.W. Atkins, *Quanta: a handbook of Concepts 2nd edition*. (Oxford Univ. Press, Oxford, England 1991), p. 1.
- (3) H. Mestre, *Cold Spring Harbor symposia on quantitative biology*. 3, 191-209 (1935).
- (4) V.M. Albers, and H.V. Knorr, *Plant Physiol.* 12, 833-843 (1937).
- (5) G.S. Rabideau, C.S. French, and A.S. Holt, *Am. J. Bot.* 33, 769-777 (1946).
- (6) W.L. Butler, *J. Opt. Soc. of Amer.* 52, 292-299 (1962).
- (7) W.L. Butler, and K.H. Norris, *Modern methods of plant analysis*, 5, 51-72 (1962).
- (8) G.S. Birth, and K.L. Olsen, *Amer. Soc. Hort. Sci.* 85, 74-84 (1964).
- (9) W.L. Butler, *Ann. Rev. Plant Physiol.* 15, 451-470 (1964).
- (10) G.S. Birth, and K.H. Norris, *Techn. Bul. No. 1341, U.S.D.A* 20 pp (1965).
- (11) K.H. Norris, and J.R. Hart, in *Principles and methods of measuring moisture in liquids and solids*, vol. 4 (A. Wexler, ed., Reinhold, NY. 1965) pp. 19-25.
- (12) P. Latimer, *Photochem. Photobiol.* 40, 193-199 (1984).
- (13) L.S. Daley, *Scientia Hort.* 28, 165-176 (1986).
- (14) L.S. Daley, M.M. Thompson, W.M. Proebsting, J. Postman, and B-R. Jeong, *Spectroscopy* 1(7), 28-31 (1986).

- (15) L.S. Daley, P.J. Breen and P. Mohanty, *Spectroscopy* 2(3), 32-35 (1987).
- (16) L.S. Daley, O. Jahn, and C. Guttridge, *Photosynth. Res.* 11, 183-188 (1987).
- (17) L.S. Daley, R.A. Menendez and R.L. Stebbins, *J. Environ. Hort.* 5, 25-28 (1987).
- (18) L.S. Daley, J.M. Montano, R.A. Menendez, A.H. Soeldner and R.B. Boone, *Spectroscopy* 2(9), 32-36 (1987).
- (19) H.H. Fisher, R.A. Menendez, L.S. Daley, D. Robb-Spencer, and G.D. Crabtree, *Weed Sci* 35, 333-338 (1987).
- (20) W.W. Guo, W.M. Proebsting, S.W. Potter, L.S. Daley, and J.R. Potter, *Plant Physiology* 85, 1089-1093 (1987).
- (21) L.S. Daley, J.R. Powell, G.A. Strobel, R.B. Boone, J. Postman, M. Willie and J. H. Brown, *Plant Physiol. Biochem.* 26, 683-694 (1988).
- (22) B-R Jeong, L.S. Daley, J. Postman, W.M. Proebsting and F.J. Lawrence, *Photochem. Photobiol.* 47, 91-100 (1988).
- (23) B-R Jeong, L.S. Daley, D.G. Smith, R.B. Boone, and E.J. Zais, *Spectroscopy* 3(2), 26-31 (1988).
- (24) S.R. Eskelsen, G.D. Crabtree, R.B. Boone, and L.S. Daley, *Proc. Western Soc. Weed Sci.* 42, 44-51 (1989).
- (25) L.S. Daley, *Plant Physiol. Biochem.* 28(2), 271-282 (1990).
- (26) C. Chen, L.S. Daley and W.E. Kronstadt, *Plant Physiol. Biochem.* 28(2), 259-269 (1990).
- (27) B.J. Yoder, and L.S. Daley, *Spectroscopy* 5(8), 44-50 (1990).
- (28) S.R. Eskelsen, G.D. Crabtree, R.B. Boone, G.M. Volk, L. Ning and L.S. Daley, *Spectroscopy* 7(2), 34-40 (1994).
- (29) E. Hoque, and G. Remus, *Remote Sens. Environ.* 47, 77-68 (1994).
- (30) L. Ning, L.S. Daley, Zhao Lu and J. B. Callis, *Biochem. Biophys. Res. Communic.* 205(1), 638-644 (1994).
- (31) D.C. McCain, T.C. Selig, and Govindjee (no initials), *Proc. Natl. Acad. Sci. U.S.A.*, 81, 748-752 (1984).

- (32) G.A. Johnson, J. Brown and P.J. Kramer, *Proc. Natl. Acad. Sci. U.S.A.*, 84, 2752-2755 (1987).
- (33) N. Ishida, T. Kobayashi, M. Koizumi, and H. Kano, *Agric. Biol. Chem.*, 53, 2363-2367 (1989).
- (34) M. Faust M., D. Liu, M.M. Millard, and G.W. Stutte, *HortScience* 26, 887-890 (1991).
- (35) A.A. Gardea, L.S. Daley, R.L. Kohnert, A.H. Soeldner, L. Ning, P. B. Lombard and A.N. Azarenko, *Spectroscopy* 8(1), 27-35 (1993).
- (36) A.A. Gardea, L.S. Daley, R.L. Kohnert, A.H. Soeldner, L. Ning, P. B. Lombard and A.N. Azarenko, *Scientia Hort.* 56, 339-358 (1994).
- (37) S. Wold, A. Ruhe, H. Wold, and W. Dunn, *SIAM J. Sci. Stat. Comput.*, 5, 735-743 (1984).
- (38) M. Otto, and W. Wegscheider, *Analyt. Chem.*, 57, 63-69 (1985).
- (39) L. Taiz, and E. Zeiger, *Plant Physiology* (Benjamin/Cummings, Redwood City, California, 1991) 565 pp.
- (40) J.C. Walker, *Plant Pathology*, 2nd edition (McGraw-Hill, New York, 1957) 707 pp.
- (41) J.A. Milburn, and J. Kallarackal, *Sap exudation, in Physiology of Trees*, A.S. Raghavendra ed., John Wiley, NY. 1991) pp. 385-402.
- (42) P.H. Moore, and D.J. Cosgrove, *Plant Physiol.* 96, 794-801 (1991).
- (43) B.-C. Gao, and A.F.H. Goetz, *Remote Sens. Environ.* 52, 155-162 (1994).
- (44) J.D. Bewley, and M. Black, *Seeds: physiology of development and germination*. (Plenum Press, NY. 1994) 445 pp.
- (45) A.A. Gardea, Y.M. Moreno, A.N. Azarenko, P.B. Lombard, L.S. Daley and R.S. Criddle, *J. Amer. Soc. Hort. Sci.* 119, 756-760 (1994).
- (46) D.W. Murken, *Maintaining soybean quality, in Soybean, production, marketing and use* (Bulletin Y-69, National Fertilizer Development Center, Tennessee Valley Authority, Muscle Shoals, Alabama, 1974) pp. 98-103.
- (47) J.C. Delouche, *Maintaining soybean seed quality, in Soybean, production, marketing and use* (Bulletin Y-69 National Fertilizer Development Center, Tennessee Valley Authority, Muscle Shoals, Alabama, 1974) pp. 46-62.

- (48) A.L. Scopel, C.L. Ballare, and S.R. Radosevich, *New Phytol.* 126, 145-152 (1994).
- (49) W.L. Butler, K.H. Norris, H.W. Siegelman, and S.B. Hendricks, *Proc. Natl. Acad. Sci. USA* 45, 1703-1708 (1959).
- (50) R.G. Stanley, and W.L. Butler, *How long can a seed remain alive, in Seeds, the yearbook of agriculture* (USDA, Washington, DC, 1961) pp. 94-99.
- (51) A. Gibson, *The anatomy of succulence, in Crassulacean acid metabolism* (I.P. Ting and M. Gibbs, eds. Am. Soc. Plant Physiol., Rockville, Maryland, 1982) pp. 1-17.
- (52) U. Lüttge, and J.A.C. Smith, *Structural, biophysical and biochemical aspects of the role of leaves in plant adaptation to salinity and water stress, in Salinity tolerance of plants* (R.C. Staples and G.M. Toenniessen eds., John Wiley New York, 1984) pp. 125-150.
- (53) D.J. Heinz, R.V. Osgood, and P.H. Moore, *Sugarcane, in Encyclopedia of Agricultural Science* (Academic Press, NY, 1994) 4, 225-238.
- (54) P.H. Moore, *J. Plant Physiol.* (in press)
- (55) E.A.C. MacRobbie, *Ionic relations in guard cells, in Stomatal function* (E. Zeiger, G.D. Farquhar, I.R. Cowan, eds. Stanford Univ. Press, 1987) pp. 125-162.
- (56) H.B. Vickery, *Plant Physiol.*, 32, 220-224 (1957).
- (57) C.C. Black, N.W. Carnal, and W.H. Kenyon, *Compartmentation and regulation of CAM, in Crassulacean acid metabolism* (I.P. Ting and M. Gibbs, eds. Am. Soc. Plant Physiol., Rockville, Maryland, 1982) pp. 51-68.
- (58) W. Feng, L. Ning, L.S. Daley, Y. Moreno, A. Azarenko and R.S. Criddle, *Plant Physiol. Biochem* 32, 319-330 (1994).
- (59) W. Feng, L. Ning, L.S. Daley, Y. Moreno, A. Azarenko and R.S. Criddle, *Plant Physiol. Biochem* 32(4), 591-598 (1994).
- (60) W.D. Jeschke, *K⁺-Na⁺ exchange at cellular membranes, intracellular compartmentation of cations, and salt tolerance, in Salinity tolerance of plants* (R.C. Staples and G.M. Toenniessen eds., John Wiley New York, 1984) pp. 37-66.
- (61) W.H. Outlaw, *An introduction to carbon metabolism in guard cells, in Stomatal function* (E. Zeiger, G.D. Farquhar, I.R. Cowan, eds. Stanford Univ. Press, 1987) pp. 115-123.

- (62) G.P. Meade, and J.C.P. Chen, *Cane sugar handbook 10th edition*, Wiley, New York, 1977).
- (63) K.R. Jacobsen, D.G. Fisher, A. Maretzki, and P.H. Moore, *Bot. Acta*, 105, 70-80 (1992).
- (64) J.A. Curcio, and C.C. Petty, *J. Optical Society of America* 41, 302-304 (1951).
- (65) G.A. Carter, *Amer. J. Bot.* 78, 916-924 (1991).
- (66) P.J. Curran, J.L. Dungan, B.A. Maclee, S.E. Plummer, and D.L. Peterson, *Remote Sens. Environ.* 39, 153-166 (1992).
- (67) E. Chargaff, E. and J. N. Davison, 1955. *Nucleic acids: Chemistry and Biology* (Academic Press. New York, London 1955).
- (68) P. Williams P. and Norris, K. eds. 1987. *Near-Infrared Technology in the Agricultural and Food Industries*. (Amer. Assoc. Cereal Chemists, Inc., St Paul, Minnesota, 1987).
- (69) J.A. Panford, *Applications of near-infrared reflectance spectroscopy in North America*, in *Near-Infrared Technology in the Agricultural and Food Industries*. (P. Williams and K. Norris, eds. Amer. Assoc. Cereal Chemists, Inc., St Paul, Minnesota, 1987) pp. 201-211.
- (70) W.W. Coblentz, *Bull. Bureau Standards*, 9, 283-325 (1913).
- (71) G.S. Birth, *Agricultural Engineering* 48, 448-449 (1967).
- (72) G.S. Birth, and H.G. Hecht, *The physics of near-infrared reflectance*, in *Near-Infrared technology in the agricultural and food sciences*. (P. Williams and K. Norris, eds. Am. Assoc. Cereal Chemists, St Paul Minnesota, 1987) pp. 1-15.
- (73) B. Ganapol, L. Johnson, P. Hammer, C. Hlavka, D. Peterson, and F. Baret, *A new within-leaf radiative transfer model: preliminary results* (poster presented at the NASA Remote sensing Science Workshop, NASA/GSFC 27 Feb-1, March, 1995).
- (74) K. Omasa, *Acta Hort.* 319, 653-658 (1992).
- (75) P.P. Ling, and V.N. Ruzhitsky, *Acta Hort.* 319, 607-612 (1992).
- (76) H. Shimizu, and M. Yamazaki, *Acta Hort.* 319, 641-643 (1992).
- (77) K.R. Jacobsen, D.G. Fisher, and P.H. Moore, *Bot. Acta.* 105, 70-80 (1992).

- (78) G. Edwards, and D. Walker, *C₃, C₄: Mechanism, and Cellular and Environmental Regulation, of Photosynthesis*. (Univ. California Press, Berkeley, 1983).
- (79) W.H. Outlaw, S.A. Springer, and M.C. Tarczynski, *Enzyme assays at the single-cell level: real-time, quantitative, and using natural substrate in solution*, in *Regulation of carbon partitioning in photosynthetic tissue* (R. L. Heath and J. Preiss, eds. Amer. Soc. Plant Physiol., Rockville, Maryland, 1985) pp. 162-177.
- (80) J.M. Robinson, and C. Baysdorfer, *Interrelationships between photosynthetic carbon and nitrogen metabolism in mature soybean leaves and isolated leaf mesophyll cells*, in *Regulation of carbon partitioning in photosynthetic tissue* (R.L. Heath and J. Preiss, eds. Amer. Soc. Plant Physiol., Rockville, Maryland, 1985) pp. 333-357.
- (81) L. Ning, G.E. Edwards, G.A. Strobel, L.S. Daley and J.B. Callis, *Applied Spectroscopy* 49(10):1381-1389.
- (82) Jobin Yvon/Spex Div. of Instruments, SA, *Guide for spectroscopy* (Edison, New Jersey and Cedex, France, 1994). 264 pp.
- (83) Princeton Instruments, Inc., *Catalog for high performance digital CCD cameras* (Trenton, New Jersey, 1994). 109 pp.
- (84) M.H. Pirenne, *Vision and the Eye* (Chapman and Hall Ltd, London, 1967) p 41-56. 224 pp.
- (85) H.S. Bellamy, P.K. Dasgupta, J.L. Lopez, and E.L. Loree, *Spectroscopy* 10(6), 50-54 (1995).
- (86) F. Hay, and P.M. Syngé, *The color dictionary of garden plants with house and greenhouse plants* (Compact edition. Bloomsbury Books (Penguin), London, 1975) 584 pp.
- (87) D.J. Mabberley, *The plant-book* (Cambridge Univ. Press., Cambridge, England, 1993) 707 pp.
- (88) H.T. Hartmann, D.E. Kester, and F.T. Davies, *Plant propagation: principals and practices* (5th edition, Prentice Hall, Eaglewood Cliffs, New Jersey, 1990) 647 pp.
- (89) S. Blix, *Agric. Hort. Genet.* 19, 402-447 (1961).
- (90) C.R. Cantor, and P.R. Schimmel, *Biophysical Chemistry* (Freeman and Company, New York, 1980) 846 pp.
- (91) C.A. Shull, *Bot. Gaz.* 87, 583-607 (1929).

- (92) P.S. Nobel, *Biophysical plant physiology and ecology*. (Freeman and Company, New York, 1983) 608 pp.
- (93) M.L. Ghirardi, and A. Melis, *Biochim. Biophys. Acta* 932, 130-137 (1988).
- (94) I. Murray, and P.C. Williams, *Chemical principles of near-infrared technology, in Near-Infrared Technology in the Agricultural and Food Industries* (P. Williams and K. Norris, eds. Amer. Assoc. Cereal Chemists, Inc., St Paul, Minnesota 1987) pp. 17-34.
- (95) J.W. Ellis, and J. Bath, *J. Chem. Phys.* 6, 723-729 (1938).
- (96) M. Zhang, M. Fabian, H. Mantsch, H.H. and H.J. Vogel, *Biochemistry* 33(36), 10,833-10888 (1994).
- (97) E. Zeiger, G. Farquhar, and L. Cowan, eds., *Stomatal function* (Stanford Univ. Press, Stanford Calif. 1987).

CHAPTER 5

IMAGING FLUOROMETER TO DETECT PATHOLOGICAL
AND PHYSIOLOGICAL CHANGE IN PLANTS

Li Ning¹, Gerald E. Edwards², Garry A. Strobel³,
Larry S. Daley^{1*} and James B. Callis⁴

¹Dept. of Horticulture, ALS 4017, Oregon State Univ., Corvallis, OR 97331.

²Botany Dept., Washington State Univ., Pullman, WA 99164.

³Plant Pathology Dept., Montana State Univ., Bozeman, MT 59717.

⁴Dept. of Chemistry, Univ. of Washington, Seattle, WA 98195.

* Author to whom correspondence should be addressed.

Published in *Applied Spectroscopy*
October 1995, 49(10):1381-1389.

IMAGING FLUOROMETER TO DETECT PATHOLOGICAL AND PHYSIOLOGICAL CHANGE IN PLANTS

Li Ning¹, Gerald E. Edwards², Garry A. Strobel³, Larry S. Daley^{1*} and James B. Callis⁴

¹Dept. of Horticulture, ALS 4017, Oregon State Univ., Corvallis, OR 97331.

²Botany Dept., Washington State Univ., Pullman, WA 99164.

³Plant Pathology Dept., Montana State Univ., Bozeman, MT 59717.

⁴Dept. of Chemistry, Univ. of Washington, Seattle, WA 98195.

*Author to whom correspondence should be addressed.

Fluorescence signals from plant leaves have considerable potential for improving agricultural investigations; however, to fully interpret these signals which are distributed unevenly across the leaf it is necessary to image the signal distribution. Leaf tissues generate, complex, two dimensional, changing, time dependent, patterns of fluorescence that initiate immediately after illumination of a dark adapted leaf. These patterns are very sensitive measures of plant photosynthetic function. Thus, we built a novel, fully computer interfaced, instrument which provides two dimensional images of time dependent fluorescence in photosynthetic tissue. The instrument was built using parts of our recently constructed imaging spectrophotometer (Ning L., et al. 1994. Spectroscopy 9 (7), 41). This instrument employs a charge-coupled device (CCD) camera, which can acquire spectra for 31,680 positions per sample. Two simple filters remove excitation emission overlap. Software based on a novel approximation allows imaging of time dependent fluorescence of photosystem II across the surface of a leaf. A simple

reconfiguration of this instrument to image at a distance of seven meters was used to test potential remote sensing applications. Instrument's use in agriculture is demonstrated by: very early determination of freeze damage, herbicide effects and invasion by fungal pathogens.

Index headings: agriculture, construction, DCMU, 3-(3,4-dichlorophenyl)-1,1-dimethyl urea, fluorescence, fluorometer, freeze damage, fungus, imaging, instrument, lidar, quantum yield, pathogens, *Pestalotiopsis*, photosynthesis, plants, time dependence.

INTRODUCTION

Photosynthetic tissues generate changing patterns of fluorescence that occur immediately after illumination of a dark adapted leaf. Relationships between time dependent fluorescence maxima and minima (empirical estimate of quantum yield), very sensitive to changes in plant photosynthetic function, are important to agriculture and plant sciences because of the major biophysical, biochemical and physiological events involved. Therefore, we built an imaging fluorometer able to quantify in 2-D space fluorescence characteristics of leaves to detect changes related to photosynthetic function and pathology of plants.

Plant leaves do photosynthesis, gathering and using sun light to make the carbon food stuffs and oxygen on which almost all life on Earth depends. As sun light is gathered water is split, water's protons are used to reduced chemical compounds, and water's oxygen is released. The reduction of specific chemical compounds using photon driven mechanisms is generalized as the "light reaction"; the use of these reduced compounds to

fix CO₂ into food stuffs is the "dark reaction" (e.g. Taiz and Zeiger¹). Both the dark and the light "reactions" are comprised of many variable and complex reactions¹.

Chloroplasts, plant cell organelles¹, gather light for photosynthesis with chlorophyll containing structures called thylakoid membranes. Thylakoid membranes have highly organized, stacked, regions called grana lamellae (grana), interspersed with less organized regions called stroma lamellae (stroma). Grana are the principal sites of photosystem II (PS_{II}), the water splitting, oxygen releasing, part of the "light reaction" of photosynthesis. Stroma are the sites of photosystem I (PS_I), the other of the two linked photosynthetic systems in higher plants. PS_I reduces NADP⁺ (nicotinamide adenine dinucleotide phosphate) to NADPH. NADPH provides much of the energy used in the "dark reaction" (e.g. Taiz and Zeiger, 1991). At room temperature PS_{II} is the major and most variable source of fluorescence (e.g. Bolhar-Nordenkamp and Oquist²) and thus commonly used to measure photosynthetic parameters.

Photosynthetic processes absorb broadly across the visible range. Photosystems 'funnel' light to their reaction centers (RC)^{1,2}. When RC are maximally available (open) about 97% of absorbed light is used for photochemistry, 2.5% is transformed to heat, and fluorescence is quenched with only 0.5% re-emitted as red fluorescence². If RC are not available (closed) 90-95% of absorbed light may be 'deactivated via heat' and 2.5-5% via fluorescence². Darkening the leaf before fluorescent measurements assures open RCs; then on illumination complex, time and wavelength variable, fluorescence is produced². The strength and composition of these complex fluorescence signals in a given plant are functions of the structure and potential for activity of the photosynthetic apparatus, the demands of the "dark reaction", the health of the leaf and the plant's adaptation to

environmental conditions³⁻⁹, and vary across the leaf lamina in ways diagnostic of leaf function⁶.

Fluorescence from photosynthetic systems at the dark to light transition is photochemical quenched when the light is used to drive the electron transport chain of the photosynthetic "light reaction"¹⁰. Thus, fluorescence signals from PS_{II} increase when high temperatures, chilling, freezing, drought or excess radiation^{3,11,12} decrease photosynthesis.

In important crop plants with C-4 metabolism (see side bar in Ning, et al.¹³), such as corn (*Zea mays* L.), fluorescence can also measure the "dark reaction". This is because in C-4 plants most electron flow through PS_{II} is used, via PS_I, to make the NADPH for the "dark reactions" of carbon assimilation. Thus, fluorescence data can be closely correlated to quantum yield of CO₂ fixation¹⁴.

N.J.C. Muller¹⁵, in 1874, visually observed chlorophyll fluorescence changes in green leaves using a combination of colored glasses². By the 1920s, fluorescence microscopy allowed practical investigations of fluorescence excited by UV-A or blue light. When thin slices of leaves were examined their photosynthetic tissues emitted red fluorescence. Kautsky and Hirsch¹⁶, in 1934, exposed dark-adapted leaves to light and generating time dependent fluorescence transients. As shown in Results and Discussion section the transients are indicated by upper case letters OI₁DP₁SMT¹⁷. Letters correspond to Origin of curve or initial fluorescence, Initial rise, Dip, Peak, down Slope (or quasi-steady-state) between first maxima (P) and secondary Maximum and Terminal level respectively. Transients O, I, and D transient O occurs very rapidly, O occurring in picoseconds between "when light has been absorbed by the chlorophyll antennae" and "before the excitons have been trapped by the RCs of PS_{II}", I and D in less than a

millisecond². Since our instrument is not capable of this time resolution, extrapolated transients are labeled O', I' and D'.

Transients OI'DPSMT can be explained^{2,18,19} thus: first in a dark- adapted system emerging into light, chlorophyll antenna in light harvesting complex (LHC) II and PS_{II} antenna funnel light to PS_{II} RC generating transient O within picoseconds (10^{-12} s). Then at the PS_{II} RC the free electrons generated are taken up first by electron acceptor Q_A (transient I) and then by electron acceptor Q_B (transient D), this quenches the fluorescence. However, within less than a millisecond Q_A and Q_B are saturated slowing fluorescence quenching and fluorescence peaks at about 0.5 to 2 seconds (transient P). Next fluorescence decreases as it is quenched (transient S) by uptake of light by LHC I and PS_I. Then PS_I saturates, fluorescence peaks again (transient M), by this time the "dark" reactions of photosynthesis begin demanding reducing 'power', adding significant additional quenching which after a hundred to several hundred seconds time interval quenches fluorescence to background levels (transient T). Photochemical quenching (Q-quenching) is not the only quenching, "dark reactions" include non-photochemical quenching (E-quenching) due to an increased rate of radiationless de-excitation that occurs on "energization" of the thylakoid membrane²⁰. This energization is believed²⁰ to related to the build up of a transthylakoidal pH gradient, that occurs as chloroplast pH increases in light, in the energy generating chemiosmotic process of Nobel laureate Peter Mitchell^{21,22}.

Using the letter F, to indicate fluorescence signal intensity with the Kautsky curve transient notations, in lower case, as subscripts to indicate the photosynthetic event whose signal intensity we are measuring allows us to write equations indicating conditions or

interpretations of the fluorescent transients. The letters FI with the appropriate subscript indicate images of these transient conditions, or images of the equations generated.

Variable fluorescence (F_v) is equal to fluorescence increment between transients O to P, or $F_v = F_m - F_o$. To avoid confusion we use F_m for the maxima of time dependent fluorescence curve, not the almost synonymous F_p notation²³, we do this following custom although it may lead to confusion with the P and M transients of the Kautsky curve.

Maximum intrinsic PSII efficiency (Y) can be empirically determined from the F_v/F_m ratio². Y is a measure of the maximum efficiency of transfer of energy from light harvesting chlorophylls to the RCII. This can, but does not necessarily mean a high efficiency of quantum yield for photochemistry, since there can be other stresses limiting electron flow, or carbon assimilation reactions of photosynthesis.

F_v/F_m is typically 0.75-0.85 for a dark-adapted leaf. To find F_v we need F_o . Since F_o occurs in picoseconds it is hard to calculate from the non-linear fluorescence transients and difficult to measure directly by digital imaging technology and thus, is a source of error in F_v determinations. However, except in some specific cases such as when examining leaves treated with certain herbicides, F_o can be estimated by F_t as pointed out in Results and Discussion, $F_o \cong F_t$, where F_t is fluorescence at phase T of OIDPSMT curve. When we do this we approximate Y as Y' the empirical estimate of quantum yield [as $Y' = (F_m - F_t) / (F_m - F_{dark})$] under most, but not all, circumstances. Two cases demonstrate the usefulness of the parameter Y': (a) when some of a leaf's arrays of light harvesting systems are damaged (e.g. by freezing) and their RC are not all functional, the F_m is not as high as in a healthy leaf and both Y and Y' are lower. In this case, Y is not the maximum intrinsic PSII efficiency; however Y' (and Y) are still useful because they reveal damage to

the photosynthetic system. (b) When leaves are damaged by certain herbicides, the RC are still functional, but the damage is done to the processes after the RC. These herbicides cause electron flow inhibition, and fluorescence is not quenched. Then, F_t stays high [$F_o \ll F_t$] consequently $Y' \ll Y$. As in case (a) we don't determine maximum intrinsic P_{II} efficiency; however, here imaging Y does not reveal herbicide damage, but imaging Y' does. Experimental examples of (a) and (b) are in Results and Discussion section.

Imaging instruments help study whole body systems physiology²⁴, DNA structure and function²⁵, and calcium accumulation dynamics²⁶. In remote sensing the Airborne Visible/Infrared Imaging Spectrometer acquires images over large areas using the full solar spectrum and is very useful in ecology, hydrology, oceanography, atmospheric sciences²⁷, and biology^{28,29}. Laser distance fluorescence (Lidar) devices allow remote sensing applications (e.g. Edner et al. 18).

Fluorescence imaging devices for plant leaf function have been known for at least 5 years^{6,30}, although this is the first report of imaging of empirical estimate of quantum yield. Fluorescence and absorption spectra of leaves reveal different aspects of leaf structure and function. Both methods are useful and their capabilities overlap. Fluorescence is most frequently used to measure transitory photosynthetic functions⁶. Absorption more readily measures the more permanent structures of the photosynthetic system³¹. Fluorescence imaging can screen photosynthetic bacteria seeking highly fluorescent, low photosynthetic efficiency mutants^{30,32}. Imaged chlorophyll fluorescent transients diagnose effects of herbicides and industrial pollutants on leaves⁴. Non-photochemical quenching (q_n) is done by mechanisms²³ not directly dependent on the redox state of Q_A . This is useful because $(1-q_n)$ can positively correlate photosynthesis

rate^{33,34}, thus it is possible to image the patterns of non-photochemical quenching on leaves⁶. However, when the leaf is under stress this correlation may not hold. For example, after treatment with the powerful herbicide DCMU (3-(3,4- dichlorophenyl)-1,1-dimethyl urea) treatment, q_n is low, therefore $(1-q_n)$ is high; yet we know that high $(1-q_n)$ does not predict high photosynthesis, after all DCMU is a herbicide that interrupts photosynthesis. However, in DCMU treatments empirical estimate of quantum yield (Y'), does show changes, because although with DCMU treatments F_m is high, F_t remains almost as high, therefore the difference Y' is low. Since Y' is low we can image DCMU damage as shown in Results and Discussion section, while Y is, as described above, much less useful to image DCMU damage because it depends on F_o , not F_t .

Today leaf signals and other indicators of plant health are observed visually by a trained "field scout" in an expensive and time consuming process. Scouting, supplemented by laboratory analyses, provides information to modify spray, irrigation and fertilizer schedules to maximize productivity of individual fields. Then the modified schedule is carried out by applying agricultural inputs uniformly on entire fields.

Robotic agriculture allows supply of an individual mix of agricultural inputs to each plant in every part of the field; already devices locate and spray individual weeds³⁵. Much more could be done in the future: pesticides applied rapidly just to the affected plants, killing pests before they spread; or fertilizer mix and water supplied only as is required by each plant. This could drastically reduce amounts of pesticides used, run off of excess fertilizer, and amount of water applied. However, to do this a robot must receive and process information on the conditions of each plant. Therefore, automated interpretation of leaf function and health from leaf fluorescent images has great potential in robotic agriculture,

specially now that remote acquisition of fluorescence as well as reflectance data of vegetation has moved from first attempts²³ to more recent advances^{18,19,36-40}. Thus, interpretation of leaf fluorescent spectra from each individual plant could guide robots dispensing agricultural inputs to each plant or group of plants as needed.

EXPERIMENTAL SECTION

Instrumentation We constructed an imaging fluorometer with a simpler design than previous instruments (Fig. 5.1). It has only one light source, a 500 W, 120 volt projector lamp (model CZX/DAD, GTE Products Inc. Winchester, KY). In this simple design two filters are used (Fig. 5.1). The filtered segregated fluorescence image data is collected on a CCD chip. We used a thermoelectric cooled 12 bit CCD camera (Lynxx PC, CCD Digital Imaging System, SpectraSource Instruments, Westlake Village, CA), with a spatial resolution of 165*192 (31,680 pixels). An IBM/PC compatible computer (Pentium^R chip, 90 MHz, Intel Corp., Palo Alto, CA) controlled the CCD camera through an interface board (Lynxx PC, SpectraSource Instruments). Collected image data were stored as image files in removable 88 MByte SyQuest cartridge (Model SQ800 on the corresponding internal drive, SyQuest technology, Fremont, CA) for easy access. Adaptation to test remote sensing applications was done simply by adjusting focus on the camera, and adjust the light so it too focuses on the leaf. Since the leaf needs to be in the dark before the experiment, it is necessary to do these measurements, at night or in an enclosed space with little or no external light.

Figure 5.1. Schematics comparing CCD based imaging fluorometers. Figure 5.1a is redrawn from P. Daley⁶. Figure 1b is redrawn from Fenton and Crofts³⁰. Figures 5.1c and 5.1d show the spectral character of the filters used and schematics of the instrument presented here respectively.

Fig. 1a

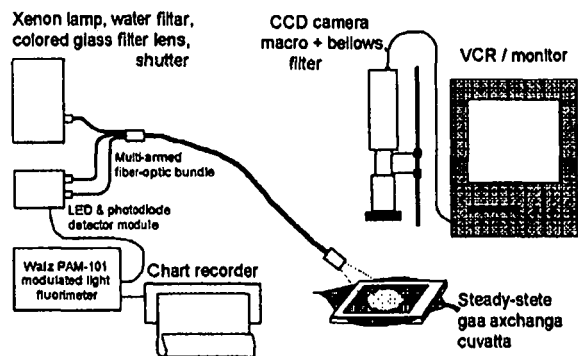


Fig. 1b

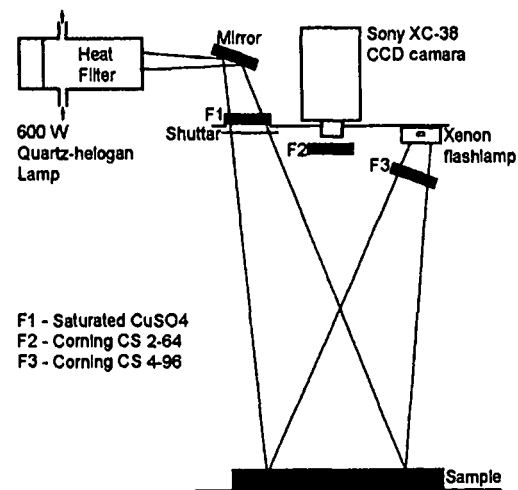


Fig. 1c

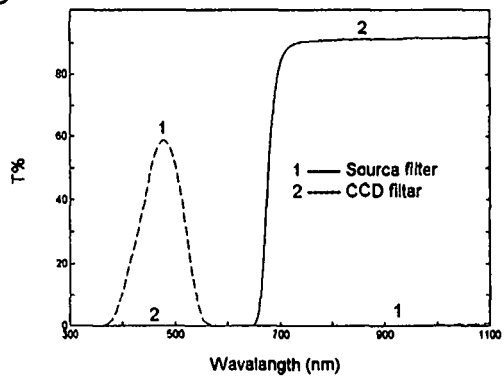
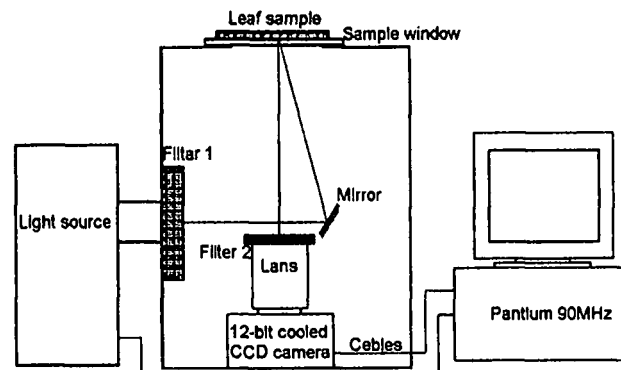


Fig. 1d



Software The program (Fig. 5.2) controlling the instrument was written using Borland C++ 3.1. The program, which is available from one of us (L.N), can be modified to achieve optimal analysis time. Data were retrieved and processed using a numerical software package called MATLAB (The MathWorks, Inc., Natick, MA).

Acquiring fluorescence images Images were taken with an exposure time of 0.1 s, however, it took about 0.6 s to completely digitize and store one image. As the light is turned on the camera captures a series of images. From the first ten images the brightest is selected as F_m . After 150 seconds the terminal image F_t is collected. A background image F_{dark} is acquired with the exciting lamp off.

We found that, under saturating light (Fig. 5.3) and with most usual treatments, $F_t \cong F_o$. Thus, from equations in Introduction, empirical estimate of quantum yield (Y') determined empirically as:

$$Y' \cong \{(F_m - F_t) / (F_m - F_{dark})\} \quad (i)$$

After images are acquired, the CCD files were translated into MATLAB files and then processed. MATLAB functions were developed so that the Y' value of one pixel of a selected area of pixels could be retrieved.

Processing of data to illustrate fluorescent photosynthetic transients. The data was collected from an area (10 pixels by 10 pixels) in the center of the leaf. The software was modified to run under directly under DOS 6.1 (Microsoft Corp., Redmond WA), rather than in Windows 3.11, Microsoft Corp.) graphical interface to accelerate the accumulation of data, data was taken every 0.1 s. The curve representing time dependence of the CCD response in the absence of the leaf (base line) was smoothed with a fifth degree polynomial fit (Statgraphic-Plus, version 7 for Dos, Manugistics, Inc., Rockville, MD). The time

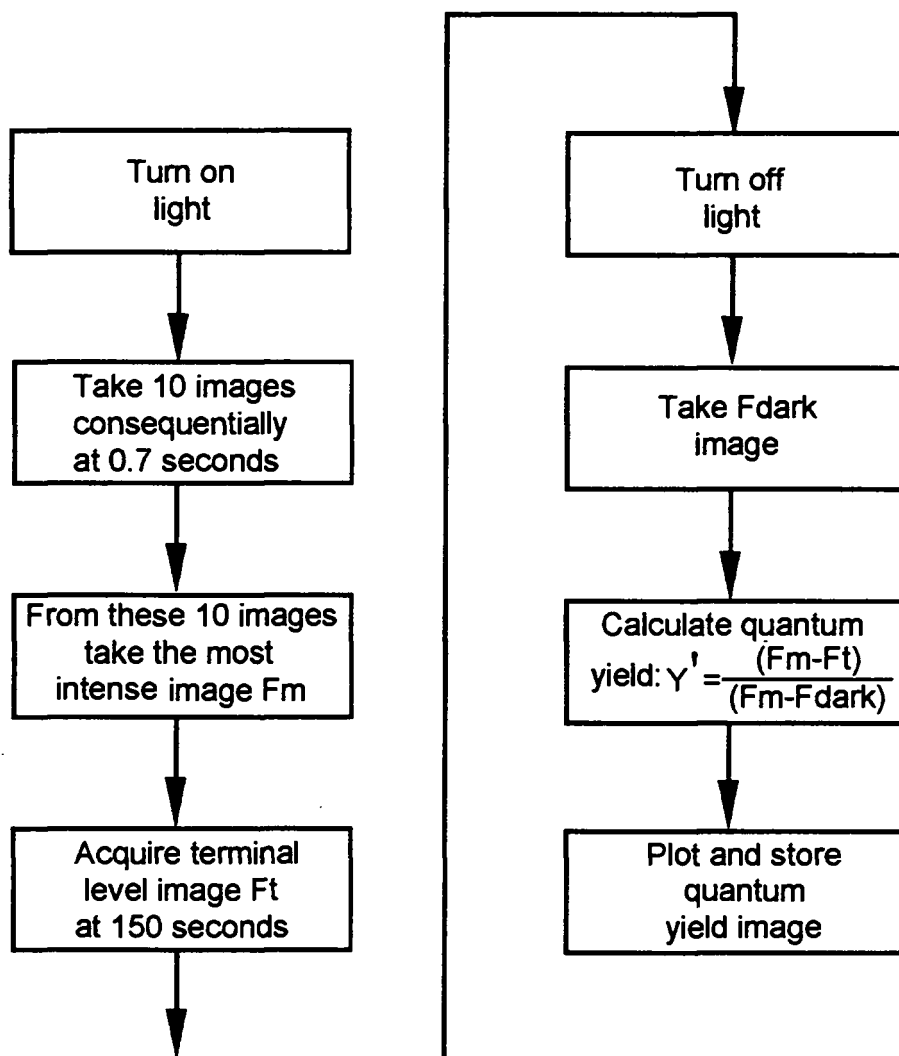


Figure 5.2. Flowchart of the software used to run the instrument.

Figure 5.3. Example of leaf fluorescent transients associated with photosynthetic apparatus. Example is taken from a coffee (*Coffea arabica* L.) leaf, measured at 11 pm at which time the leaf had been in darkness for about 5 hours. The left panel compares fluorescence transients from an untreated (live) leaf with a control sample boiled for 25 minutes. Features of interest O', I', D', P, S, M and T are indicated, the apostrophe indicates point extrapolated not measured. The right panel compares the transients from a live leaf with transients from a DCMU treated (2 mM) and a dry ice frozen and then thawed (freeze damaged) leaves. Fluorescent transient traces and DCMU treatment levels are very similar to standard conditions for point source fluorescence apparatus⁴⁴.

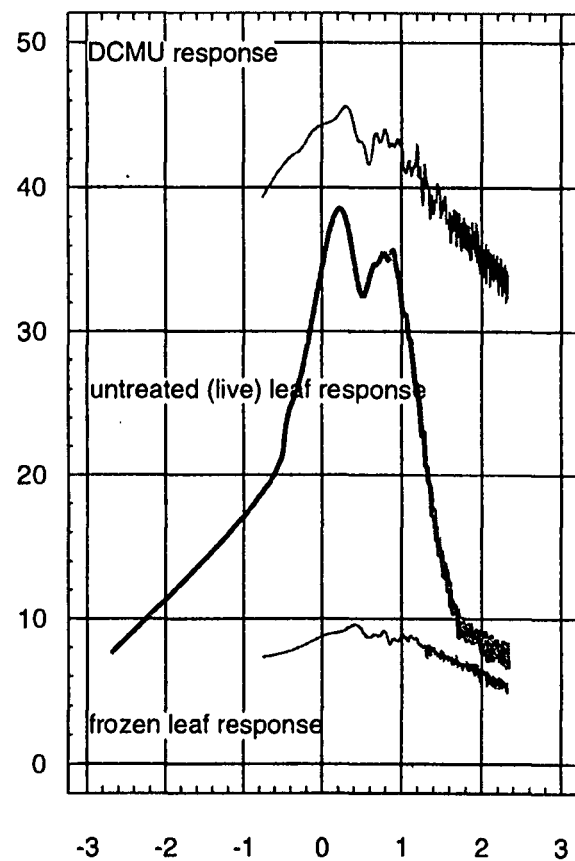
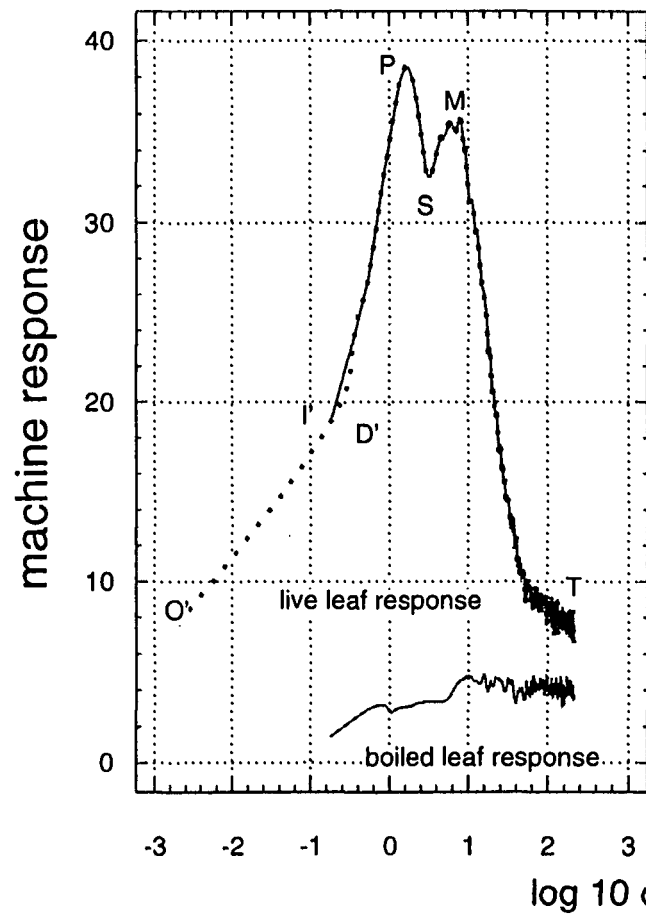


FIGURE 5.3

dependent fluorescent response of the CCD to fresh, frozen, DCMU treated and boiled leaves was fitted to a Q-spline and then a 5 unit "box car" smoothing procedure (using a program specially written for MATLAB) and then the smoothed base line was subtracted. The Q-spline fit is used because this method is capable of extrapolating peak maxima more closely in complexly curving data found in plant physiological experiments⁴¹.

Development of empirical estimate of quantum yield image for PS_{II} . The data collected by the imaging fluorometer consists of an ordered sequence of fluorescence images (FI) of the sample, each taken at a different time. The image is processed following equation (i). The first ten are evaluated for greatest intensity, the most intense is called FI_m for peak fluorescence image; the image taken at 150 seconds is FI_t for terminal fluorescence; the dark current or background fluorescence, taken without illumination, at end of experiment is symbolized by FI_{dark} . The images are processed to give fluorescent quantum images (FI_Y) thus:

$$FI_Y = \{(FI_m - FI_t) / (FI_m - FI_{dark})\} \quad (ii)$$

Plant materials The instrumentation laboratory has a door that opens directly into the greenhouse to facilitate rapid access to plant materials. Coffee (*Coffea arabica* L., var. borbon) leaves were taken immediately before use from mature-bearing coffee bushes, grown under greenhouse conditions at Oregon State University (OSU) and collected in November, 1994. The plants were potted in old OSU (before June 1994) mix which is by volume, two parts pumice, one of fine sand, one of peat (Canadian medium horticultural grade), and one of sandy loam soil and were well watered at the time of the test. *Amaranthus cruentus* L. and *Digitalis purpurea* L. was grown in same greenhouse during the fall of 1994, but in well watered new OSU mix (as above, but without sand).

The pathogen *Pestalotiopsis spp.* was isolated from the nutmeg cedar or yew (*Torreya taxifolia* Arn.) using a plating technique involving surface sterilization of stem with 70% ethanol followed by placement of stem pieces on water agar. Nutmeg trees were provided by Mark Schwartz (Univ. Calif., Davis) and were originally acquired from the Nature Conservancy of Northern Florida. Nutmeg stems were inoculated with agar blocks containing *Pestalotiopsis spp.* in a greenhouse setting, allowed to incubate for three weeks at which time the stem was harvested for spectroscopic examination, control stems received only plain water agar pieces as inoculum. Examination was done on the terminal leaves 10-12 cm removed from the site of inoculation.

RESULTS AND DISCUSSION

Figure 5.1 compares schematics of previous designs for imaging fluorometers with instrument presented here. Notice how this instrument is simpler than previous designs. The software (flowchart in Fig. 5.2) and the unique mathematical manipulations described in Experimental section allows for clear presentation of a empirical estimate of quantum yield (Y') image an ability not previous described. This program, by seeking the maximally fluorescent image, has the novel advantage of measuring actual FI_m , rather than measuring FI_x , where x is an estimate of the time when transient P will occur. Since, in leaves in stress fluorescence levels in various patches of the leaf differ^{6,42}, and the time at which transient peaks appear at varies with pathology, physiology and species^{2,9}, our software by choosing the FI_m automatically allows more ready comparisons of pathological, physiological and species (germplasm) differences.

Figure 5.3 illustrates the fluorescence transients generated by the interaction of light on photosynthetic apparatus of the previously darkened leaf. Discussion of transients is found in Introduction, processing of this data is explained in Experimental section. Figure 5.3 can be compared with standard schematics (e.g. Fig 12.4 of Bolhar-Nordenkamp and Oquist²) which generalize fluorescence transients for common physiological conditions of leaf and species responses. The Origin data point is estimated from the Terminal data point. Transients O, I, and D are estimated by Q-spline fit extrapolation and shown uncorrected for time lags. These lags occur, because of the speed limitations of digital CCD response and thus these transients are indicated in primed notation in Fig. 5.3. Transients P, S, M and T are at their expected positions. The right frame of this figure makes the point that there are different ways that damage to the photosynthetic system can affect the Kautsky curve making it possible, as shown below, to distinguish by fluorescence transient imaging causes of damage at distance.

Figures 5.4 and 5.5 show the usefulness of the instrument. Figure 5.4a shows rapid determination of freeze damage. This has the potential to be important in agriculture. In the volatile agricultural futures market, such as in the rapid quantification of frost damage to citrus, it could promote market stability by more rapidly preparing harvest size predictions. Notice how the freeze damage is partially delayed by vascular tissue while in the following figure DCMU damage is spread via these same vascular tissues. Figure 5.4b demonstrates rapid and localization and detection of herbicide damage by DCMU. Figure 5.4c shows the spread of DCMU damage via the vascular tissue of the leaf. Since DCMU is used, electron transfer is blocked at Q_B , and the

Figure 5.4. Y' images (Empirical estimation of quantum yield) of freezing damaged, DCMU treated and fungal pathogen infected leaves. Figure 5.4a (upper left panel) shows effect of freezing damage on PS_{II} empirical estimate of quantum yield [$Y' = (F_m - F_t) / (F_m - F_{dark})$] of a leaf of *Digitalis purpurea* L. To get this effect, the leaf was held 15 minutes in the dark, then still keeping the leaf in the dark, small pieces (about 3 mm diameter) of dry ice were placed on the leaf for two minutes, then removed and the leaf, still in the dark, was left at room temperature for five minutes before measurement. In these figures the reddest color corresponds to the highest and the darkest blue to the lowest Y' as indicated in the color bar on the side of each panel. Figure 4b (upper right panel) shows effect on PS_{II} empirical estimate of quantum yield [$Y' = (F_m - F_t) / (F_m - F_{dark})$] of DCMU herbicide (50 mM) treated leaves of *Amaranthus cruentus* L. This plant is more sensitive to DCMU than coffee. The leaf was also preincubated in the dark for 15 minutes and Fig. 5.4b shows effects at 15 minutes exposure to droplets. Figure 5.4c (lower right panel) shows the effects 12 hours after allowing the petiole of the leaf to take up the DCMU solution. Figure 5.4d (lower left panel) shows differences [$Y' = (F_m - F_t) / (F_m - F_{dark})$] between leaves (needles) of the endangered species nutmeg cedar or yew (*Torreya taxifolia* Arn.) leaves infected with (left) and free (right) of *Pestalotiopsis spp.* fungal pathogen. Leaves were held in dark for 20 minutes, after unpacking from cold shipping container, before fluorescent measurements.

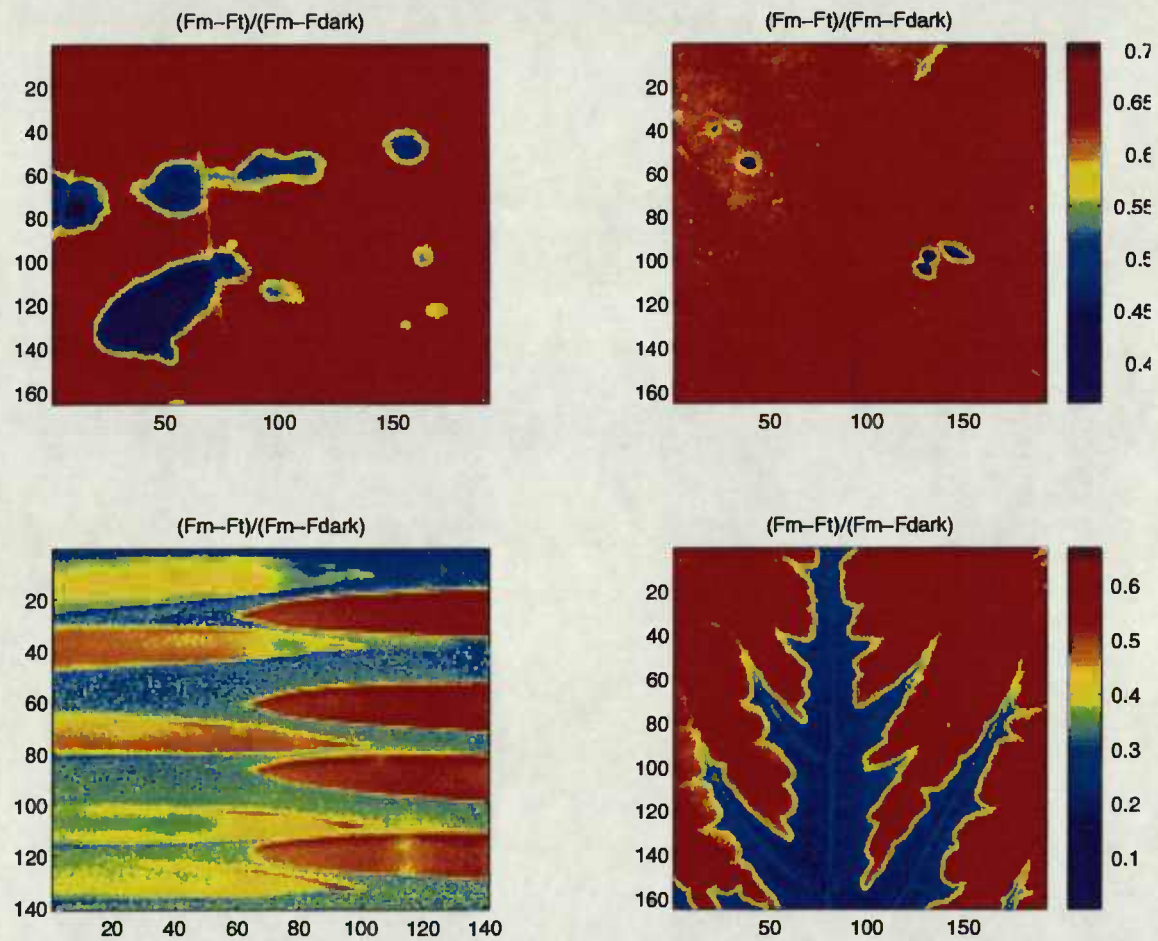


FIGURE 5.4

fluorescence will decrease because no re-oxidation of Q_A can occur². The advantages of measuring Y' and not Y or q_n are discussed in Introduction.

Figure 5.4d shows the utility of the instrument for the detection of stresses induced in plants under attack by disease causing plant pathogens. In this case damage to the leaves of the nutmeg (Florida) yew can be detected before symptoms are visible to human eye. The yellowish needles on the left are showing fungal toxin induced effects. These needles are free of the fungus which has colonized stem tissues at least 10 cm below these needles. The reddish needles on the right are from a healthy (non-infected) plant. The slight yellow band on the lowest healthy leaf was caused by folding damage to this leaflet when it was transported for assay. This relatively simple experiment demonstrates the power and practical utility of this instrument and this technique. It will certainly be interesting to learn if other more common diseases of field, garden and forest species are also associated with early physiological changes that can be readily detected by imaging of empirical estimate of quantum yield. Knowledge of this type would prove extremely useful in carrying out early control measures thereby resulting in substantial savings to growers.

Figure 5.5, false colored in a special "jet scale", shows how the instrument can measure fluorescence at a moderate distance. This is done to test the limits of our instrumentation, the utility of our equations and imaging systems and evaluate different physiological responses, but our instrument in its present form is not intended for field use. Three leaves are illuminated in each of these four image treatments. The leaf on the left is freeze treated and is a barely visible "ghost" image. The fluorescence transient maxima image (F_m) reveals little difference between untreated and DCMU treated leaves. The

Figure 5.5. Imaging fluorometer used at a distance of 7 meters. The figure shows use of the instrument configured for use at a distance of 7 meters. There are three coffee leaves in each image panel. The leaf at the left side of each panel was treated by freezing with dry ice and then thawed. This freeze damaged leaf has a barely perceptible ghost image. The center leaf is the untreated control. The leaf on the right side of the panel is treated by partially dipping in 2 mM DCMU. The panels at the upper left, upper right, lower left and lower right show: response at the time of maximal fluorescence^{44,45} (F_m); response at time of minimal fluorescence (F_t); response ($F_m - F_t$); and response $Y' = (F_m - F_t) / (F_m - F_{dark})$. In the upper left panel (F_m), one can distinguish the non-fluorescing freeze damaged leaf from the untreated and DCMU dipped leaf. However, when measuring fluorescence maxima one has difficulty distinguishing the DCMU effects from the control leaf's response. In the upper right panel the persistence of the fluorescence of the DCMU treated leaf is apparent. Subtracting F_t from F_m , lower left panel, distinguishes the DCMU treatment, but the image of the control leaf is not very uniform. The normalization procedure of the lower right panel [$Y' = (F_m - F_t) / (F_m - F_{dark})$] the untreated leaf yields a quite uniform false color, while on the DCMU leaf, the area that has been dipped is not visible and the effect of DCMU on the undipped portion of the leaf is beginning to spread via the vascular tissue of the leaf veins. Combining the responses of F_m (upper left) and that of Y' (lower right) we can distinguish healthy, freeze damaged and DCMU treatments.

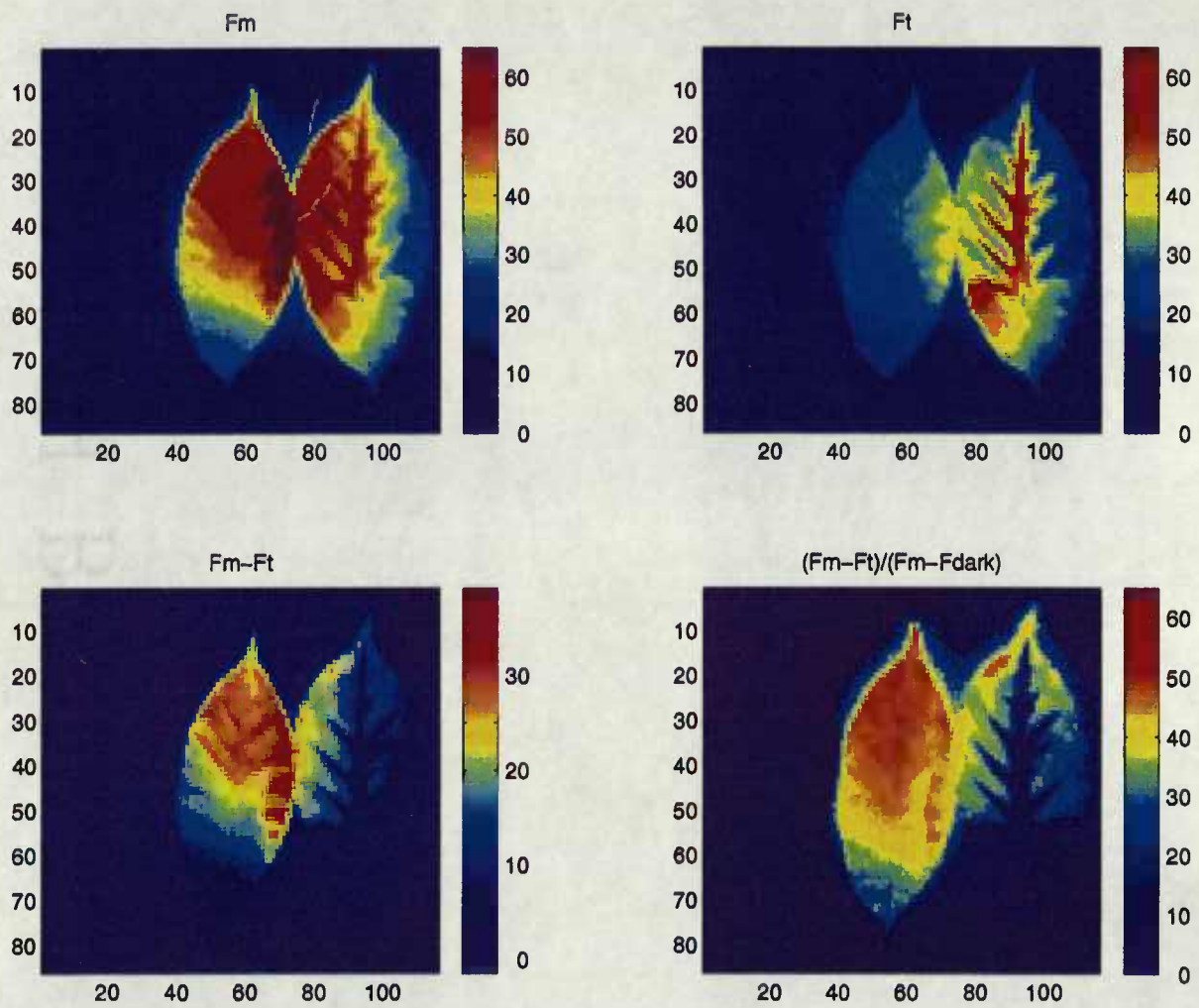


FIGURE 5.5

terminal fluorescence image (F_t) shows as expected (see Fig 5.3) a brighter image for the DCMU treated leaf. The F_m-F_t image shows some differences between untreated control and DCMU treated leaves. However, the best distinction between control and DCMU treated is obtained using the Y' equation (quantum yield estimate) image. Notice that in the DCMU treated leaf the herbicide has spread from the lower, completely dark, part of the leaf that was dipped in DCMU to the untreated area following the leaf's vascular tissue.

This data and equations may help interpret lidar data from photosynthetically challenged plants. Notice in Fig. 5.5 because of the distance from the light source, the fluorescence signals are weaker, than those illuminated from a shorter distance; however, this is easily remedied using a more powerful light source or a laser. This effect of lack of saturating exciting light is more readily seen in image equations F_m , F_t and F_m-F_t data, but is relatively well compensated for when the image equation is $(F_m-F_t)/(F_m-F_{\text{dark}})=Y'$. Thus Y' , may prove more useful than other fluorometric measures⁴³ for Lidar applications.

CONCLUSION

The imaging fluorometer we constructed works well for the plant pathological and physiological uses and opens up a large number of applied uses. Its construction, simpler than previous designs, lends itself to commercial production. This instrument's unique ability to estimate empirical estimate of quantum yield makes it specially useful in situations when the plant is in stress and the non-photochemical quenching is not inversely

related to photosynthesis. The software has a novel approach to estimation of empirical estimate of quantum yield which has potential in lidar based remote sensing.

ACKNOWLEDGMENTS

We note the resemblance, but not the equivalency, between the Karukstis's elegant equation for "vitality index", used in a non-imaging context⁴⁴, and our use of the Y' equation to prepare images. We gratefully acknowledge support from the Herman Frasch Foundation (grant number: FRASCH 63-0738), The Oregon Filbert Commission and the OSU Agricultural Research Foundation. This paper is Oregon Agricultural Experiment Station Technical paper 10758.

REFERENCES

1. L. Taiz and E. Zeiger, *Plant Physiology* (Benjamin/Cummings Pub. Co., Inc., Redwood City, California, 1991), Chap. 8-10, p. 177.
2. H.R. Bolhar-Nordenkamp and G. Oquist, "Chlorophyll Fluorescence as a Tool in Photosynthesis Research," in *Photosynthesis and Production in a Changing Environment, a Field and Laboratory Manual*, D.O. Hall, J.M.O. Scurlock, H.R. Bolhar-Nordenkamp, R.C. Leegood and S.P. Long, Eds. (Chapman and Hall, London, 1993), Chap. 12, p. 193.
3. M. Havaux and R. Lannoye, *Photosynthetica* 18, 117 (1984).
4. K. Omasa, K. Shimazaki, L. Aiga, W. Larcher and M. Onoe, *Plant Physiol.* 84, 748 (1987).
5. H.R. Bolhar-Nordenkamp and E.G. Lechner, "Winter Stress and Chlorophyll Fluorescence in Norway Spruce (*Picea abies* (L.) Karst)." in *Applications of Chlorophyll Fluorescence*, H.K. Lichtenthaler Ed. (Kluwer Academic Publ., Dordrecht, Holland, 1988), 173.

6. P.F. Daley, K. Raschke, J.T. Ball and J.A. Berry, *Plant Physiol.* 90, 1233 (1989).
7. (a) M.L. Ghirardi and A. Melis, *Biochem. Biophys. Acta* 932, 130 (1988); (b) B.T. Mawson, P.J. Morrissey, A. Gomez and A. Melis, *Plant Cell Physiol.* 35, 341 (1994).
8. C.B. Osmond, J.A. Berry, S. Balachandra, C. Buchen-Osmond, P.F. Daley, and R.A. Hodgson, *Bot. Acta* 103, 226 (1990).
9. L.I. Tecsí, A.J. Maule, A.M. Smith and R.C. Leegood, *Plant J.* 5, 837 (1994).
10. G. Papageorgiou, "Chlorophyll Fluorescence: an Intrinsic Probe of Photosynthesis," In *Bioenergetics of Photosynthesis*, Govindjee Ed. (Academic Press, New York, 1975), p. 319.
11. R.M. Smillie, "The Useful Chloroplast: a New Approach for Investigating Chilling Stress in Plants", in *Low Temperature Stress in Crop Plants*, J.M. Lyons, D. Graham and J.K. Raison Eds. (Academic Press, New York, 1979), p. 187.
12. S.B. Powles, *Ann. Rev. Plant Physiol.* 35: 14 (1984).
13. L. Ning, R. Ozanich, L.S. Daley and J.B. Callis, *Spectroscopy* 9(7), 41 (1994).
14. G.E. Edwards and N.R. Baker, *Photosynthesis Research* 37, 89 (1993).
15. N.J.C. Möller, *Jahrbuch wiss Botanik* 9, 42 (1874).
16. H. Kautsky and A. Hirsch, *Biochem. Zeitschrift* 274, 423 (1934).
17. J. Lavorel and A.L. Etienne, "In Vivo Chlorophyll Fluorescence," in *Topics in Photosynthesis*, 2. J. Barber Ed. (Elsevier, Amsterdam, 1977), p. 203.
18. H. Edner, J. Johansson, S. Svanberg and E. Wallinder, *Applied Optics*, 33, 2471 (1994).
19. M. Methy, A. Oliso and L. Trabaud, *Remote Sens. Environ.* 47, 42 (1994).
20. U. Schreiber, U. Schiliwa and W. Bilger, *Photosynth. Res.* 10, 51 (1986).
21. E. Racker, *A new look at mechanisms in bioenergetics*, (Academic Press, New York, 1976), Chap. 1, p. 22.
22. W.A. Cramer and D.B. Knaff, *Energy Transduction in Biological Membranes* (Springer- Verlag, New York, 1991), Chap. 3, p. 93.
23. G.H. Kraus and E. Weis, *Annu. Rev. Plant Physiol. Molec. Biol.* 42, 313 (1991).

24. R.F.E. Wolf, K.H. Lam, E.L. Mooyaart, R.P. Bleichrodt, P. Nieuwenhuis and J.M. Schakenraad, *Laboratory Animals* 26(3), 222 (1992).
25. E.G. Jordan, O.V. Zatsepina and P.J. Shaw, *Chromosoma* 101(8), 478 (1992).
26. A. Borst and M. Egelhaaf, *Proc. Natl. Acad. Sci. USA* 89, 4139 (1992).
27. G. Vane and A.F.H. Goetz, *Remote Sens. Environ.* 44, 117 (1993).
28. C.D. Elvidge, Z. Chen and D.P. Groeneveld, *Remote Sens. Environ.* 44, 271 (1993).
29. M.K. Hamilton, C.O. Davis, W.J. Rhea, S.H. Pilorz and K.L. Carder, *Remote Sens. Environ.* 44, 217 (1993).
30. T.M. Fenton and A. R. Crofts, *Photosynth. Res.* 26, 59 (1990).
31. L.S. Daley, *Plant Physiol. Biochem.* 28, 271 (1990).
32. D.C. Youvan, J.E. Hearst and B. L. Marrs, *J. Bacteriol.* 154, 748 (1983).
33. E. Weis and J.A. Berry, *Biochim. Biophys. Acta* 894, 198 (1987).
34. P. Horton and A. Hague, *Biochem. Biophys. Acta* 932, 107 (1988).
35. J. Beck, Patchen California Inc., Los Gatos, CA, personal communication (1994).
36. G. Cecchi, P. Mazzinghi, L. Pantani, R. Valentini, D. Tirelli and P. De Angelis, *Remote Sens. Environ.* 47, 18 (1994).
37. E.W. Chappelle and H. Litchenthaler, *Remote Sens. Environ.* 47, 1 (1994).
38. K.P. Gunther, H.-G Dahn and W. Ludeker, *Remote Sens. Environ.* 47, 10 (1994).
39. J.E. McMurtrey III, E.W. Chappelle, M.S. Kim, J.J. Meisinger and L.A. Corp, *Remote Sens. Environ.* 47, 36 (1994).
40. R. Valentini, G. Cecchi, P. Mazzinghi, G. Scarascia Mugnozza, G. Agati, M. Bazzani, P. De Angelis, F. Fusi, G. Matteuci and V. Raimondi, *Remote Sens. Environ.* 47, 29 (1994).
41. W. Feng, L. Ning, L.S. Daley, Y. Moreno, A. Azarenko and R.S. Criddle, *Plant Physiol. Biochem* 32, 319 (1994).
42. K.A. Mott, Z.G. Cardon and J.A. Berry, *Plant Cell Environ.* 16, 25 (1993).

43. J.E. Corlett, H.G. Jones, J.M. Masojidek and A. Massacci, *Photosynthetica* 27, 257 (1992).
44. Karukstis, K. K., Fluorescence as a physical probe of the photosynthetic apparatus, in *Chlorophylls*, H. Scheer Ed. (CRC Press, Boca Raton, Florida, 1991) pp. 769-795.
45. Strasser, R.J., A. Srivastava and Govindjee (has no initial), *Photochem. Photobiol.* 61, 32 (1995).

CHAPTER 6

IN VIVO PLANT LEAF PHOTOSYNTHETIC
APPARATUS CAN STORE DIGITAL INFORMATION
AS FLUORESCENCE SIGNALS

Li Ning¹, Bent E. Petersen²,
Gerald E. Edwards³, Larry S. Daley^{1*},
and James B. Callis⁴

¹Department of Horticulture, ALS 4017, Oregon State University, Corvallis, OR
97331-7304

²Department of Mathematics, Kidder Hall 368, Oregon State University, Corvallis, OR
97331-4605

³Botany Dept., Washington State Univ., Pullman, WA 99164

⁴Department of Chemistry, University of Washington, Seattle, WA 98195.

* Author to whom correspondence should be addressed, (541) 757-7456 am., (541)
737-5476 main office and pm; e-mail daleyl@ava.bcc.orst.edu, or daleyl@bcc.orst.edu.

To be published in *Applied Spectroscopy*
This paper is Oregon Agricultural experiment station paper 10990

IN VIVO PLANT LEAF PHOTOSYNTHETIC
APPARATUS CAN STORE DIGITAL INFORMATION
AS FLUORESCENCE SIGNALS

Li Ning¹, Bent E. Petersen², Gerald E. Edwards³, Larry S. Daley^{1*}, and James B. Callis⁴

¹Department of Horticulture, ALS 4017, Oregon State University, Corvallis, OR

97331-7304

²Department of Mathematics, Kidder Hall 368, Oregon State University, Corvallis, OR

97331-4605

³Botany Dept., Washington State Univ., Pullman, WA 99164

⁴Department of Chemistry, University of Washington, Seattle, WA 98195.

*Author to whom correspondence should be addressed, (541) 757-7456 am., (541)

737-5476 main office and pm; e-mail daleyl@ava.bcc.orst.edu, or daleyl@bcc.orst.edu.

Imaging plant tissue fluorescence can be done with a new, CCD (charge coupled device) equipped, imaging spectroscopic instrument (Ning, *et al.*, Spectroscopy, 9 (7), 41-48, 1994), which can be reversible and rapidly reconfigured as an imaging fluorometer (Ning *et al.*, Applied Spectroscopy 48 (10), 1381-1389, 1995). In the fluorescence configuration two dimensional spatial distribution of estimates of quantum yield fluorescence (Y') can be imaged (Ning *et al.*, 1995). Y' images of leaf areas with immediately functional photosynthetic apparatus appear smooth and uniform to the human eye since they are much less affected by variations in chlorophyll content and light path through the leaf. However, areas of the leaf where the chlorophyll-protein complex (CPX) structures of the leaf's photosynthetic apparatus, have different light history,

pathology, or other damage generate different Y' value images. Using this principle we were able to store and recover images from leaves. Examples of these images are shown here and were used on the cover of *Applied Spectroscopy*, volume 48, number (10). In an extension of this finding, we prepared binary data coding for the value of p to 99 decimal places (100 digits), on living leaves. The images containing the binary codes for these digits can be "read" by eye because the human brain interprets visual data with great skill. However, the images containing these codes cannot be "read" (recognized) as readily by instrumentation. Thus, it was necessary to enhance the images to facilitate instrument "reading". A program was developed to enhance the images and "read" the data. This program was able to "read" the images with no errors. The photosynthetic mechanism involved (non-photochemical quenching), role of leaf age and germplasm variation, and the potential applications of this finding in terms of bioelectronics are discussed. Other future applied applications such as to: diagnose in individual leaves, photosynthetic functionality and senescence, measures useful in agricultural applications, and to track and time passage of animals in wild life studies are brought to the readers attention.

INTRODUCTION

Here we report storage of digital data using the photosynthetic apparatus inside living leaves. This is a novel finding. Our finding that living leaves can store binary information is distinct from, but related to, use of chloroplast components in electronic systems. The construction of electronic devices from biomolecular components is known as "biomolecular electronics"¹.

Biomolecular electronics are not the same as semiconductor electronics. The "desired device producing properties of semiconductors are derived from the bulk properties of appropriately doped materials"¹. Radically different from semiconductors, in biomolecular electronic devices "the inputted device producing property and the potential for density packing are intrinsic characteristics of individual molecules or ensembles of molecules"¹.

To discuss the relationship of our results to bioelectronics some background on instrumentation, photosynthetic fluorescence and use of chloroplast components in electronic systems is helpful. The instrumentation used was described previously^{2,3}; pertinent details are found in Instrumentation, Materials and Methods section.

Photosynthetic fluorescence details are quite complex³⁻⁹. Plants gather energy from solar photons. Photons, of course, move at the speed of light. Therefore, somehow photosynthetic systems of plants must trap the photonic energy, long enough and in the appropriate forms to do biochemical work. At the same time the more rapid processes of photonic energy conversion to heat and fluorescence must be minimized for maximum efficiency of photosynthesis. This channeling of photonic energy to chemical energy is done in the chloroplasts, cellular organelles found almost exclusively in the leaves⁹. The chloroplast structures used for this are chlorophyll-protein complexes (CPX) assembled into photosystems I and II (PSI and PSII) and the supporting light harvesting chlorophyll protein complexes (LHC)⁹.

Absorbing broadly across the near UV and visible range, and with the aid of various accessory pigments and LHC, PSI and PSII 'funnel' light to their reaction centers (RC) where photochemistry occurs⁸⁻¹¹. The conversion of photonic energy to biochemical

energy, takes time and the RC are not always ready to accept light. This is particularly the case when light is present in excess of the plants' capacity to use light for biochemistry.

The state of the RC influences the amount of fluorescence (Table 6.1). Under limiting light when RC are functioning at maximal efficiency, about 97% of absorbed light is used for photochemistry, 2.5% is transformed to heat, and fluorescence is quenched with only 0.5% re-emitted as red fluorescence⁸. When closed under excess light reduction, RC produce maximum fluorescence, 90-95% of absorbed light may be lost through heat deactivation and 2.5-5% through fluorescence⁸. Thus, when the RC are closed much higher fluorescence is observed (Table 6.1).

Darkening the leaf ensures open, resting, RCs. During the transition from dark to light in this process of activation, complex time and wavelength variable, fluorescence signals are generated e.g. ^{3,4,8}. The intensity and timing of these complex fluorescence signals strongly reflect the structure and potential for activity of the photosynthetic apparatus, the demands of the "dark reaction", the health of the leaf and the plant's adaptation to environmental conditions e.g. ^{3,6-8,11-19}.

On illumination, light energy is transmitted to the RCs, which can become temporarily closed and over reduced until quenching mechanisms are activated (Table 6.1). Photochemical quenching occurs as electron flow is initiated oxidizing electron acceptors. Non-photochemical mechanisms of chlorophyll fluorescence quenching can be activated under excess light. Non-photochemical quenching mechanisms relate to raising the pH of chloroplast thylakoid membranes, which establishes a pH differential within the chloroplast. This pH gradient then can be used, via Mitchell (chemiosmotic) type

mechanisms(e.g. Skulachev²⁰), to generate energy used to physically separate photosynthetic components (Table 6.1).

When light energy is in excess of that which can be effectively used productively, two events can occur (Table 6.1). These two events are: non-photochemical fluorescence quenching in which the separated photosynthetic components dissipate energy from the LHC²¹⁻²³ into heat (down-regulating photoprotection); and RC damage by photoinhibition. In photoinhibition the initial electron flow of the system is reversed causing singlet oxygen generation; this singlet oxygen then damages the RC (Table 6.1).

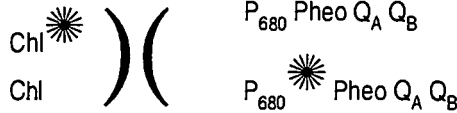
In intact leaves e.g. ^{3,14,24} the functional photosynthetic apparatus generate characteristic changing patterns of fluorescence immediately after these tissues are illuminated. The train of fluorescent signals emitted from photosynthetic apparatus as the light activation process is initiated can be considered roughly analogous to the diagnostic process that a computer or other complex apparatus undergoes as it is turned on. Analogously to computer diagnostics, the variation in intensity and timing of the sequence fluorescence signals emitted by the photosynthetic apparatus in this process are diagnostic of leaf function e.g. ^{3,14,18}, leaf environmental history and damage e.g. ^{12,25-30}.

From among these changing fluorescence patterns emitted^{3,4-7} during the light activation of the photosynthetic apparatus we select a few important signal phases to image³. The selected fluorescence pattern phases imaged include maxima (Fm) and the time estimated minima (Fs). The distribution of intensity of these two pattern phases across the image can be used, as described in Instrumentation, Materials and Methods section, to generate images of estimated quantum yield of photosynthesis using the Y'

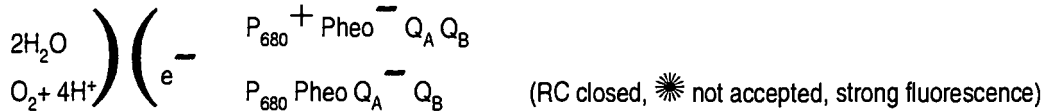
Table 6.1. Schematic representation of open and closed reaction centers (RC) of photosystem II (PSII) relative to chlorophyll fluorescence and machine response. Reaction center (RC) is represented as P_{680} Pheo Q_A Q_B . Pheophytin (Pheo) is a chlorophyll in which the central Mg atom has been replaced by two H atoms, Q_A Q_B are bound quinone and second receptor quinone respectively. When a leaf is in the dark all PSII RCs are open; when the leaf is transferred to bright light Q_A becomes fully reduced resulting in maximum fluorescence. By convention when Q_A is negatively charged (Q_A^-) RC is defined as closed. In a closed RC (P_{680} Pheo Q_A^-) excitation of P_{680} cannot result in stable charge separation. Following illumination with light, and a rise in fluorescence, quenching of fluorescence can occur through processes which re-establish open RC. This is done through induction of photosynthesis which re-establish open RC. This is done through induction of photosynthesis which establishes a sink for electrons and increases electron flow (photochemical quenching); and/or through down regulation (non-photochemical quenching) of PSII by high membrane energization which results in dissipation of energy from light membrane energization which results in dissipation of energy from light harvesting chlorophyll and limits transfer of energy to RC. In addition, fluorescence can be quenched by photoinhibition.

Normal conditions

- (1) Photons (☀) excite antenna chlorophyll (Chl) to Chl^* and pass to P_{680} in reaction center (RC)
 $\text{Chl}^* \rightarrow \text{Chl} \rightarrow \text{P}_{680}^* \text{Pheo} \text{Q}_\text{A} \text{Q}_\text{B}$ (RC open to accept ☀, weak fluorescence)



- (2) Bound quinone (Q_A) reduced to quinone Q_A^- ; then electron hole ($^+$) is filled from oxidation of water as water is split to provide electrons (e^-). RC closes and more ☀ are released as fluorescence



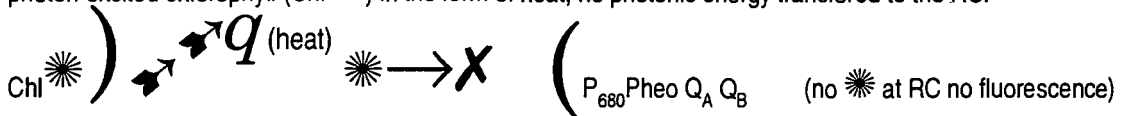
- (3) consumption of electrons by photochemical processes, represented here by the transfer of an electron to second quinone acceptor (Q_B), restores open centers. Less ☀ released as fluorescence



Result When suddenly illuminated, untreated, healthy darkened leaves yield a fluorescence pulse which peaks at maxima F_m , decreasing to a low F_s . Our instrument detects this as a high Y' [$Y' = (F_m - F_s) / (F_m - F_{\text{dark}})$].

Non-photochemical quenching (adaptation to excess light)

Under excess light a rise in pH across the thylakoid membranes mediates dissipation of energy from photon excited chlorophyll (Chl^*) in the form of heat, no photonic energy transferred to the RC.



Result Fluorescence pulse is quenching under excess light (low Y'), but pulse phenomena rapidly returns if leaf allowed to rest for about five minutes under low light, which results in a rapid recovery of high Y' .

Photoinhibition (damage by high light)

- (1) excess photons enter RC $\text{P}_{680}^* \text{Pheo} \text{Q}_\text{A}^- \text{Q}_\text{B}$ (☀ added to closed RC)
- (2) charge separation occurs between P_{680}^+ and Pheo^- $\text{P}_{680}^+ \text{Pheo}^- \text{Q}_\text{A}^- \text{Q}_\text{B}$ (RC has excess e^-)
- (3) recombination to excited triplet state $^3\text{P}_{680} \text{Pheo} \text{Q}_\text{A}^- \text{Q}_\text{B}$ (RC in excited triplet state)
- (4) RC in excited triplet state transfers energy to O_2 making singlet oxygen $^3\text{O}_2 \rightarrow ^1\text{O}_2$ (Singlet oxygen made)
- (5) Singlet oxygen damages another photon excited RC $\text{P}_{680}^* + ^1\text{O}_2 \rightarrow \text{X} \text{P}_{680}$ (RC damaged no fluorescence)

Result Fluorescence pulse is quenched (low Y') under high light due to RC damage. Leaf's ability to respond to light with a fluorescence pulse returns slowly (over hours) as RC is repaired to again produce high Y' .

estimator of quantum yield³. The distribution of Y' values in these images are very sensitive indicators of changes in plant photosynthetic functions³.

Fluorescence quantum efficiency measures how well photosynthetic systems function (reviewed by Ning *et al.*³). In plants photosynthetic function is closely regulated by the interaction of each plant's genetically coded germplasm variables with the environmental variables that act on the plant. These variables are often distributed in a diagnostic way across the two-dimensional x-y plane of the leaf lamina. Thus, imaging of estimates of quantum yield in this x-y plane has plant physiological, pathological and agricultural uses e.g. ^{3,14,31-34}. However, this paper suggests another use: to seek in the abundant variation of plant germplasm the plant photosynthetic systems most useful for bioelectronic applications.

Two examples of potential electronic uses are: (a) coupling of chloroplast components to electronic systems³⁵⁻⁴⁰ and (b) re-engineering of photosynthetic reaction systems for bioelectronic applications⁴¹.

The pigment protein complex bacteriorhodopsin and the photosynthetic apparatus are two main sources of materials for biomolecular electronics. The bacteriorhodopsin system and its biomolecular electronic differences with the photosynthetic apparatus are discussed by Greenbaum⁴⁰. Here we deal with the use of intact photosynthetic units *in vivo*. To understand these potential bioelectronic applications it is helpful to think of photosynthetic systems as photoelectronic devices: "Photosynthesis is vectorial photochemistry. Light quanta that are captured in photosynthetic reaction centers initiate a primary electron-transfer reaction resulting in a spatial separation of electrostatic charge across the photosynthetic membrane. The vectorial nature of photosynthesis lies in the

intrinsic orientation of the reaction centers embedded in the membranes. Electron flow is from the inner membrane surface of the flattened saclike vesicles to the outer membrane"³⁷. "This unidirectionality of electron transfer is an excellent example of exquisite molecular-level control of electron movement through an insulating medium... (a photosynthetic system is) an elementary component in a molecular electronic device"⁴¹.

Photosynthetic reaction centers, and potentially whole photosynthetic systems may be re-engineered for technological applications⁴². In addition, given the many millions of years of plant development and the natural variation in photosynthetic apparatus of plant and bacterial germplasm, there is much natural material to explore for bioelectronic applications. Therefore to biologically oriented scientists, such as ourselves, it seems logical that it should be much less expensive to bioengineer existing germplasm to make bioelectronic components or bioelectronic component precursors than to start to assemble these molecular components from simple synthesized molecules. Thus natural germplasm promises to be a potentially useful resource from which to select reaction centers and other photosynthetic apparatus components useful to assemble bioelectronic apparatus. Perhaps further into the future through the progress of bioengineering, growing intact bioelectronic apparatus in green plants may become a reasonable enterprise.

INSTRUMENTATION, MATERIALS AND METHODS

Hardware We used an imaging spectrophotometer /fluorometer described previously²³. The imaging fluorometer configuration has a simpler design than previous instruments. It has only one light source, a 500 W, 120 volt projector lamp (model

CZX/DAD, GTE Products Inc. Winchester, KY). Two filters are used, one filter removes long wavelength light from the excitation beam and the other short wavelength light from the detecting system. Time sequenced image data is collected, as in the imaging spectrophotometer, on a thermoelectric cooled 12 bit CCD camera (Lynxx PC, CCD Digital Imaging System, SpectraSource Instruments, Westlake Village, CA), with a spatial resolution of 165×192 (31,680 pixels). An IBM/PC compatible computer (PentiumR chip, 90 MHz, Intel Corp., Palo Alto, CA) controls the CCD camera through an interface board (Lynxx PC, SpectraSource Instruments). Collected image data are stored, for easy access, as image files in removable 88 MByte SyQuest cartridge (Model SQ800 on the corresponding internal drive, SyQuest technology, Fremont, California)

Acquiring fluorescence images Fluorescence quantum yield (Y) is estimated as (Y') ³. To obtain Y' a background, "dark", signal plus two selected fluorescence signals are required. The detector, here the CCD camera, captures a timed series of signal samples which represent points along the complex time dependent fluorescence transients of the Kautsky curve^{3,4}. From the first ten signals the brightest is selected as Fm. After this a signal at 150 seconds (Fs) is collected to represent the terminal signal. The background signal (Fdark) is acquired with the exciting lamp off. Fs is used to estimate the initial fluorescence signal (Fo), which occurs and changes too rapidly to detect with most equipment (e.g. Wiederrecht *et al.*⁴³. This is done because we found that, under saturating light³ and with most usual treatments, $F_s \cong F_o$. Thus, from equations in previous paper³, an estimate of quantum yield (Y') determined empirically as:

$$Y' \cong \{(F_m - F_s) / (F_m - F_{\text{dark}})\} \quad (i)$$

The data collected from the CCD consists of a time ordered sequence of fluorescence images (FI) of the sample, each taken at a different time. Images were taken with an exposure time of 0.1 s, however, it took about 0.6 s to completely digitize and store one image. The image of estimated quantum yield (FIY') is processed by equation ii (below) which is an image matrix version of equation (i). The first ten images collected by the instrument are evaluated for greatest intensity, the most intense is called FIm for peak fluorescence image; the image taken at 150 seconds is FIs the estimated of terminal fluorescence; the dark current or background fluorescence, taken without illumination, at end of experiment is symbolized by FIdark.

The images FIm, FIs, and FIdark are processed by equation ii to the yield estimated quantum yield image (FIY') thus:

$$FIY' = \{(FIm - FIs) / (FIm - FIdark)\} \quad (ii)$$

After images are acquired, the CCD files were translated into MATLAB files (The MathWorks, Inc., Natick, MA) and then processed. MATLAB functions were developed so that the Y' value of one pixel of a selected area of pixels could be retrieved.

Software for image acquisition, processing and developing correlations Image acquisition and processing software have been described previously^{2,3}. The program controlling the instrument was written using Borland C++ 4.0. This program, which is available from one of us (L.N.), can be modified to achieve optimal analysis time. Data were retrieved and processed using MATLAB a numerical software package.

Image enhancement software for machine vision (e.g. D. Kaill⁴⁴) was developed specifically for this purpose. The principles of this program are found in Results and Discussion section [details are available from one of us (LN)].

Plant materials Tobacco plants (*Nicotiana tabacum* L.) were grown in pots containing OSU mix and kept in OSU greenhouses. Ginkgo biloba leaves were obtained from trees grown on campus.

RESULTS AND DISCUSSION

While examining plants for quantum efficiency reactions to certain insults³ we found we could generate images (cover of Applied Spectroscopy, volume 48, number (10)). These images are generated by placing a colored transparency mask over a leaf (cover legend of Applied Spectroscopy, volume 48, number (10), p. 6A). The mask is a colored transparency of the selected image. The leaf is illuminated through the mask using the fluorometer lamp for 0.5-3.5 minutes at a light intensity of about 5,000 mEinstein.s.m⁻².s⁻¹ at the surface of the leaf. The exact time of illumination is determined by the characteristics of the particular leaf's germplasm, and its physiological age and history of light exposure. The mask is then removed, and immediately the series of fluorescence images are acquired as described in Instrumentation, Materials and Methods section.

Figure 6.1 image, illustrates a detail from Sandro Botticelli's (1445-1510) renaissance painting, the birth of Venus, as recorded on a tobacco leaf's photosynthetic arrays. The image mask was 1.5 by 1.5 cm. The panels at the upper left, upper right, lower left and lower right show respectively: response at the time of maximal fluorescence (F_m); response at time of minimal fluorescence (F_s); response (F_m-F_s); and response for

Figure 6.1. Demonstrating the sensitivity of the imaging fluorometer: photo-induced “Birth of Venus” image on a living tobacco leaf. The false color images in these figure follow the convention red greatest intensity, yellow less and blue little of activity measured. Images of detail from Sandro Botticelli's "Birth of Venus" demonstrating the image storage capabilities of a living tobacco leaf. This figure shows data obtained by the instrument when it is configured to measure photosynthetic fluorescence and the image is acquired perpendicular to the plane of the leaf and at close range. The panels at the upper left, upper right, lower left and lower right show respectively: response at the time of maximal fluorescence (F_m); response at time of minimal fluorescence (F_s); response ($F_m - F_s$); and response for quantum yield estimate $Y' = (F_m - F_s) / (F_m - F_{dark})$. Panel legends show these equations, however, the imaging program does not allow for subscripts. Compare resolution of image panel at upper left with image panel at lower right.

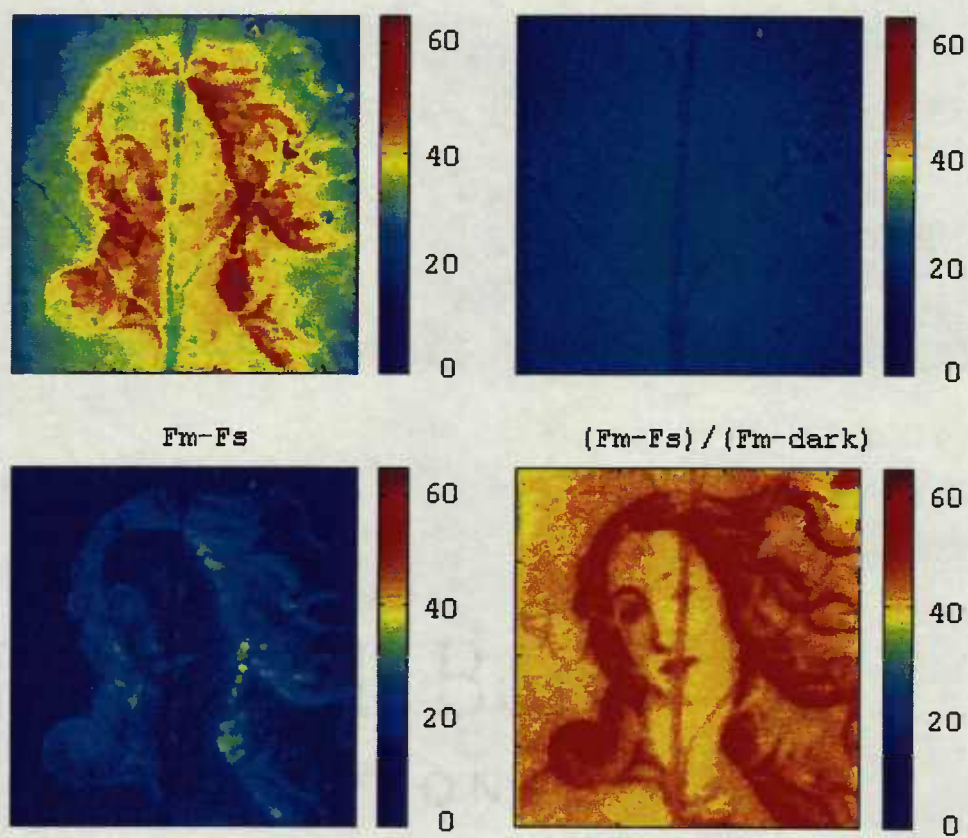


FIGURE 6.1

quantum yield estimate $Y'=(F_m-F_s)/(F_m-F_{dark})$. Panel legends show these equations, however, the imaging program does not allow for subscripts. The leaf is perpendicular to the light source direction.

To interpret our image data certain conventions are used. The instrument's CCD array covers two dimensions, commonly the x-y plane of the leaf lamina. The intensity of the instruments response, a third dimension, is represented as a color gradient.

The variable coloring of the two-dimensional space of the figure, represents the intensities of the instrument's signal or signal equation. For instance a gradient of increasing intensity of fluorescence (or absorbance) is commonly represented in colors, smoothly increasing wavelength from the blue, through the yellow, and on to the red range of the visible spectrum. To make this convention clearer to the reader a color gradient bar is usually included adjacent to the figure. For example in Fig. 6.1, the darkest, most intensely red, areas indicate highest level of the appropriate parameter [F_m , F_s , (F_m-F_s) , or Y'], colors change through orange to yellow areas indicate decreasing parameter levels, and light blue (turquoise) and deep blue indicate areas with the very low or not measurable levels of the parameter. Thus, in the lower right of Fig. 6.1 these colors indicate estimates of relative quantum efficiencies (Y'). When necessary "stretching" color images is accomplished by mathematical manipulations of image generating equations.

Notice in Fig. 6.1, how in this leaf the distribution of maximal fluorescence (F_m), upper left, yields an imperfect image. The imperfections are attributed to variations in the relative distribution of chlorophyll especially near leaf veins⁴⁵. The terminal fluorescence (F_s), upper right, is of low intensity, yielding a dark image in which details are hard to see.

The difference between maximal fluorescence and minimal fluorescence ($F_m - F_s$) still retains the effects of chlorophyll content. However, the image equation, lower right, which estimates quantum yield Y' , $(F_m - F_s)/(F_m - \text{dark})$ shows the image quite clearly. Comparing the upper left image with the lower right image, one can see how the Y' equation presents relatively uniform surfaces in which the image features can then be seen quite clearly.

The lower right panel image is now recognizable as a detail of Botticelli's "Birth of Venus". The photosynthetic efficiency is most affected in those CPX domains on the leaf that are most exposed to light. Those parts of the leaf that had been most protected from the light, by the most deeply colored parts of the mask before it was removed, such as the flowing hair of the Venus have the highest Y' .

In vigorous mature leaf tissues, the image lasts about eight minutes. Tissues in the early process of senescence much less. Ginkgo leaves in the fall, although not yet showing visible signs of senescence, no longer produce good images. As discussed in Introduction, three potential image forming mechanisms (Table 6.1) are available for this effect (A. Melis, personal communic., 1995): (i) non-photochemical quenching related to transthylakoid pH change²¹⁻²³, (ii) photoinactivation^{21-23,46}, and (iii) gross photobleaching. Gross photobleaching (iii) is unlikely cause of image formation since our images fade. Photoinactivation (ii) recovery is an order of magnitude slower (~90 minutes) than the time we observe (~8 minutes); and photoinactivation does not occur in the dark. This suggests that the most probable mechanism of image formation is non-photochemical quenching. Non-photochemical quenching (Table 6.1) occurs when a large pH gradient is built up across the thylakoid membranes of the chloroplast under excess light²¹⁻²³. Under

appropriate light conditions this pH gradient is used to generate ATP for photosynthetic processes. However, under excess light the gradient becomes too large and causes membrane separations (Table 6.1) and photochemical quenching of fluorescence occurs mediated by xanthophylls²¹⁻²³. Other image data, not shown here, relates to mechanisms ii and iii.

Once it was apparent that a living leaf could store information, we prepared different masks to test limits of the system. Using π digits⁴⁷ we generated mask presenting the sequence of π in decimal form. From this we learned that resolution of the system was not yet adequate for decimal data storage. Thus, we prepared a binary mask showing π to 99 decimal places. The mask consists of twenty x twenty "rectangles".

Figure 6.2 illustrates design of the original mask in which a binary coded map shows the constant π taken to 99 decimal places. The binary code for each digit is represented as rows of "rectangles" which are read in the horizontal direction from left to right, starting at the first horizontal row and continuing in consecutive rows. The digits are represented in binary code, each digit taking up four "rectangle"s. The sequence starts with 3.1415..., and the decimal "point" is not coded. The data is read from left to right using four "rectangles" for each digit, then continuing to the next four "rectangles" without spacers for the next digit. In each group of four rectangles, here the superscripts reflect mathematical notation, the positions represent 23 (8), 22 (4), 21 (2), 20(1) respectively. If the rectangle is dark we multiply this position by one, if it is light we multiply the position by 0. Thus we read the first four "rectangles" pixels as light=8x0=0; light=4x0=0; dark=2x1=2; dark 1x1, for a total of 3. The second four pixels read: light=8x0=0; light=4x0=0; light=2x0=0; dark=1x1=1, for a total of 1. The third four

Figure 6.2. The mask used to code 100 digits of π apparent quantum efficiency of photosynthesis. The lower axis shows the sequence of data rectangle width (five across). The left axis shows the sequence of rows. The numbers across the upper border show, in digital form, the digits of π for the upper row of each group of four "rectangles". The numbers on the rectangles themselves represent the digital representation of each rectangle.

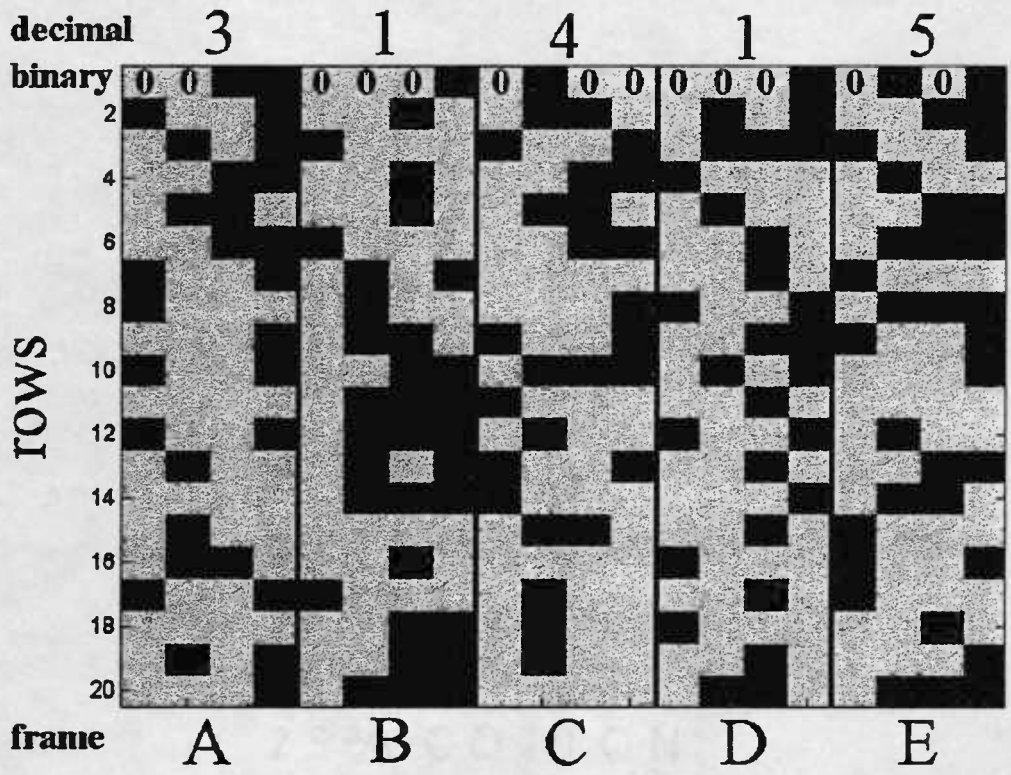


FIGURE 6.2

pixels read: light=8x0=0; dark=4x1=4; light=2x0=0; light=1x0=1, for a total of 4. The next four pixels read light=8x0=0; light=4x0=0; light=2x0=0; dark 1x1=1 for a total of 1. The last four pixels of row read light=8x0=0; dark 4x1=4; light=2x0=0; dark 1x1=1 for a total of 5. The first four, of the next row also left to right, read dark 8x1=8; light 4x0=0; light =2x0=0; dark 1x1=1 for a total of 9. This reads 314159 which when the decimal is placed after the first digit becomes 3.14159, which is recognizable as the beginning of the π sequence ($p=3.14159$). In Figure 6.3 upper left, we can, reading by eye, see the first 100 digits of p . This demonstrates that the living leaf can store binary notation. Machine reading of this data is discussed below. There was considerable variation in the storage abilities of leaves of various species, so far the best leaf source is greenhouse grown tobacco. Ginkgo leaves are also useful³, however, the ability to store binary information is degraded when the Ginkgo leaves senesce in the fall.

Although the trained human eye can read the coded images produced by the Y' equation, these images are not readily decoded (read) by instrumentation. Instrumentation reading of images is called machine vision, and "Vision algorithms implemented on expensive hardware...have severely limited the options of the application developer and user"⁴⁴. To avoid these problems we developed a program to facilitate machine vision in the general MATLAB system.

The development of this program is shown in Fig. 6.3. The upper left panel of Fig. 6.3 shows the Y' based image generated on the leaf. This panel shows several features which limit machine reading. These features include: (a) uneven intensities of maxima (red and dark red) and minima (blue and yellow) attributed to slightly different physiology of different regions of the leaf, variations in CCD pixel sensitivities and variations in leaf

Figure 6.3. The process of preparation of the image for machine reading. The panels at the upper left, upper right, lower left and lower right show advancing levels of preparation for machine reading.

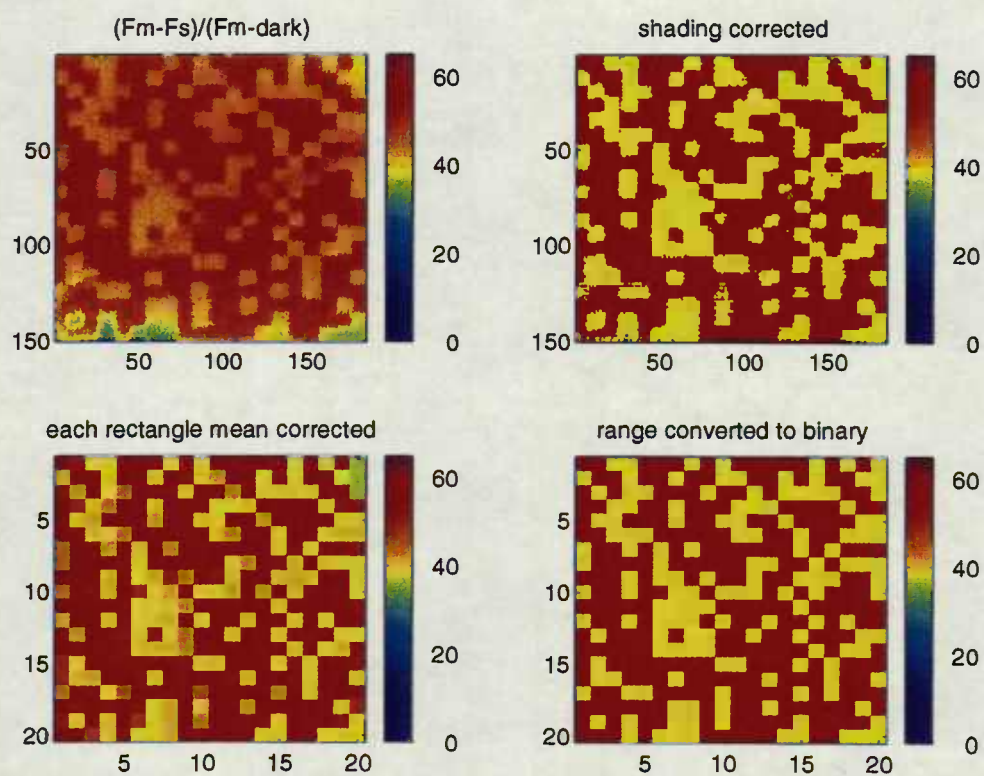


FIGURE 6.3

illumination. This means that those parts of the code that will become the active 1's of the binary notation are yellow in some regions of the image; in other parts of the image, such as in the lower part, these minima are blue. Machine vision reading is best done after these uneven intensities are corrected. (b) The essentially continuous (analog) nature of the plant's fluorescent signals is conserved in the image by the 12 bit range of the CCD. The width (~10-60) of this continuous color range can easily be seen by comparing this upper left panel to the color bar on its right side. This needs to be changed because for machine vision a two color, binary, format is preferred. (c) The interference of leaf veins and microscopic structures modifies the exact reproduction of the rectangular binary codes of the mask. This can be seen by the faint diagonal traces, caused by leaf venation, which appear in the right middle and lower parts of this image panel. Uniform colored code for all dark and a different uniform color code for all light "rectangles" facilitate machine vision reading.

The upper right panel of Fig. 6.3 has been corrected for range differences in different sections of the image. This was done in two steps. First the image was divided into four horizontal strips, each of these strips was about 38 CCD pixels (or five "rectangles") wide and extended the width of the image. The maxima of each of these strips was determined. Then, using this maxima, the range of each of these strips were normalized to the three other strip's range. Second this process was repeated using four vertical strips. As this panel shows the lower values, which will become the 1s of the binary code, are now a uniform color. The color bar still shows the continuous nature of the image; however one can see that by comparison with the color bar the range of colors in the upper right image is now much more restricted.

Notice that in the upper panel left of Fig. 6.3, the rectangles are not uniformly rectangular. The edges of the "rectangles" representing are still ragged as in the upper right panel. And the effects of leaf venation, perceived in this image as a diagonal line of imperfect "rectangle"s, descending from upper right to lower left, are still detectable. However this be corrected in the lower left panel, since although the color or numeric value of the "rectangle" is not known, the size of the "rectangle"s, containing the binary code, is uniform and known. Therefore a program was designed to correct this. The color of each "rectangle" of the lower left panel were assigned the color of mean of all the pixels of a regular "rectangle" section if it were superimposed on the irregular "rectangles" of the upper right panel. Note that the pixel notation on the right and lower axes of the upper panels is now replace, in the lower panels, by smaller numbers which indicating the positions of the "rectangles".

However, the lower left panel, because of the correction making the "rectangles" uniform, now has a wider range of color than observed in the image of the upper right. This needed correction. Therefore the data of the lower left panel of Fig. 6.3 is shown after yes/no logic was fitted to a threshold and the continuous function of range was reduced to two domains 0s (red) and 1s (bluish green). Notice by observing the color bar that there are only two colors in the panel. Now this panel only has two well separated color "points" from the wide range of "color points" found in the bar to right of the panel; this demonstrates the binary nature of the image in the lower left panel. This lower left image allows ready machine vision recovery of all the information in the original mask, and the 99 decimal place value of π can be determined by machine reading.

CONCLUSION

It is possible to store and recover digital data from living plant leaves utilizing the fluorescence properties of the photosynthetic apparatus. The mechanism most consistent with this effect is photochemical quenching. However, while the demonstration of the recovery of digital data from a leaf is in itself interesting; we do not expect direct, immediate, use of leaves as memory storage; although the eventual use of such media should not be ruled out. We expect that more immediate utility of this method will arise in the *in vivo* selection of best and most appropriate plant germplasm for given bioelectronic purposes. The utilization of this methodology to determine level of physiological integrity, photosynthetic functionality and onset of senescence in crop plants is another potential use. This instrument is expected to measure recovery, via remote fluorescence sensing, of transitory images of plant damage caused by the passage of wild game through a given area, this is expected to be useful for game management and related purposes.

BIBLIOGRAPHIC SKETCHES

Author(s): Li Ning, Bent E. Petersen, Gerald E. Edwards, Larry S. Daley*, and James B. Callis

Li Ning is a graduate research assistant in the Departments of Horticulture and Computer Engineering at Oregon State University (OSU), Corvallis. He received his MS in Horticulture from Beijing Agriculture University, in 1987, and his BS in biology from Peking University, China, 1983. Ning is preparing to take his PhD defense in the Fall of 1996 and completing his course requirements for a MS in Computer Engineering. Ning's

PhD dissertation will include the construction of a novel imaging spectrometer and fluorometer, and the application of these instruments to *in vivo* biochemistry, phytopathology of diverse plant germplasm.

Bent E. Petersen, is a professor in the Department of Mathematics at OSU. He received his PhD. in Mathematics at Massachusetts Institute of Technology, in 1968, and his BS in Mathematics in 1964 at the Univ. British Colombia. Professor Petersen specializes in partial differential equations and is author of the mathematics graduate text Introduction to the Fourier transform and pseudo-differential operators.

Gerald E. Edwards, is a professor in the Department of Botany at Washington State University, Pullman. He received his PhD in Plant Sciences from the University of California at Riverside in 1969. He frequently uses fluorescence to investigate photosynthetic phenomena, especially when it relates to his interest in photosynthetic carbon metabolism and stress in higher plants. He is one of the most respected scientist in this area of science.

Larry S. Daley is an associate professor in the Department of Horticulture at OSU. He received his PhD from the University of California at Davis in the Biochemistry and Biophysics Department in 1975. His research interest include the biochemical and biophysical interpretation of *in vivo* leaf spectra and its relationship to germplasm research.

James B. Callis is a professor of chemistry and adjunct professor of bioengineering at the University of Washington, Seattle. He earned a PhD in chemistry from the University of Washington in 1970. His research interests include the development of instruments including the video fluorometer, flash calorimeter, imaging

spectrophotometer, and laptop computerized instruments. Prof. Callis's current interests include development of instrumentation for ecological surveys and *in vivo* interferometry. Prof. Callis is best known for his contributions to applied uses of spectroscopy.

ACKNOWLEDGMENTS

We gratefully acknowledge support from the Herman Frasch Foundation (grant number: FRASCH 63-0738). We thank Lucidyne Technologies Inc., (Corvallis, Oregon) for the donation of a color copier. This paper is Oregon Agricultural Experiment Station Technical paper 10990.

REFERENCES

1. E. Greenbaum, "Biomolecular electronics and applications", in Molecular biology and biotechnology, R.A. Meyers, Ed. (VCH Publishers, Inc, New York, New York, 1995), pp. 98.
2. L. Ning, R. Ozanich, L.S. Daley and J.B. Callis, Spectroscopy 9(7), 41-48 (1994).
3. Ning, L., G. E. Edwards, G.A. Strobel, L.S. Daley, and Callis, J. B., Applied Spectroscopy, 48, 1381(1995).
4. H. Kautsky and A. Hirsch, Biochem. Zeitschrift 274, 423-434 (1934).
5. G. Papageorgiou, "Chlorophyll Fluorescence: an Intrinsic Probe of Photosynthesis," In Bioenergetics of Photosynthesis, Govindjee Ed. (Academic Press, New York, 1975), p. 319.
6. H.R. Bolhar-Nordenkamp and E.G. Lechner, "Winter Stress and Chlorophyll Fluorescence in Norway Spruce (*Picea abies* (L.) Karst)." in Applications of Chlorophyll Fluorescence, H.K. Lichtenthaler Ed. (Kluwer Academic Publ., Dordrecht, Holland, 1988), 173.
7. K.K. Karukstis, "Fluorescence as a physical probe of the photosynthetic apparatus", in

- Chlorophylls, H. Scheer Ed. (CRC Press, Boca Raton, Florida, 1991) pp. 769-795.
8. H.R. Bolhar-Nordenkamp and G. Oquist, "Chlorophyll Fluorescence as a Tool in Photosynthesis Research," in *Photosynthesis and Production in a Changing Environment, a Field and Laboratory Manual*, D.O. Hall, J.M.O. Scurlock, H.R. Bolhar-Nordenkamp, R.C. Leegood and S.P. Long, Eds. (Chapman and Hall, London, 1993), Chap. 12, p. 193.
 9. L. Taiz and E. Zeiger, *Plant Physiology* (Benjamin/Cummings Publishing Company, Redwood City, California, 1991).
 10. T. Hiyama, and B. Ke, *Biochim. Biophys. Acta.*, 267, 160 (1972).
 11. B.T. Mawson, P.J. Morrissey, A. Gomez and A. Melis, *Plant Cell Physiol.* 35, 341 (1994).
 12. M. Havaux and R. Lannoye, *Photosynthetica* 18, 117 (1984).
 13. H.K. Lichtenthaler, *J. Plant. Physiol.*, 131, 101 (1987).
 14. P.F. Daley, K. Raschke, J.T. Ball and J.A. Berry, *Plant Physiol.* 90, 1233 (1989).
 15. C.B. Osmond, J.A. Berry, S. Balachandra, C. Buchen-Osmond, P.F. Daley, and R.A. Hodgson, *Bot. Acta* 103, 226 (1990).
 16. G.E. Edwards and N.R. Baker, *Photosynthesis Research* 37, 89 (1993).
 17. J. A. Abbot, T.A. Campbell, and D.R. Massie, *Remote Sens. Environ.*, 47, 87 (1994).
 18. B. Genty, and S. Meyer, *Aust. J. Plant Physiol.* 22, 277 (1994).
 19. M. Methy, A. Olivoso and L. Traubaud, *Remote Sens. Environ.* 47, 42 (1994).
 20. Skulachev, V.P., "Chemiosmotic systems and the basic principles of cell energetics", in *Molecular mechanisms in bioenergetics* (L. Ernster, Ed.) (Elsevier, Amsterdam, 1992) p. 37-73.
 21. S.P. Long, S. Humphries and P.G. Falkowski, *Annu. Rev. Plant Physiol. Plant Mol. Biol.* 45, 633 (1994).
 22. A.M. Gilmore, T.L. Hazlett, and Govindjee (no initial) *Proc. Natl. Acad. Sci. USA* 92, 2273 (1995).
 23. B. Demmig-Adams and W.W. Adams, *Trends in Plant Sciences*, 1, 21 (1996).
 24. G. Schmuck and I. Moya, *Remote Sens. Environ.*, 47, 72, (1994)

25. S.B. Powles, *Ann. Rev. Plant Physiol.* 35: 14 (1984).
26. K. Omasa, K. Shimazaki, L. Aiga, W. Larcher and M. Onoe, *Plant Physiol.* 84, 748 (1987).
27. M.L. Ghirardi and A. Melis, *Biochem. Biophys. Acta* 932, 130 (1988).
28. L.I. Tecsi, A.J. Maule, A.M Smith and R.C. Leegood, *Plant J.* 5, 837 (1994).
29. R. Valentini, G. Cecchi, P. Mazzinghi, G. Scarascia Mugnozza, G. Agati, M. Bazzani, P. De Angelis, F. Fusi, G. Matteuci and V. Raimondi, *Remote Sens. Environ.* 47, 29 (1994).
30. Strasser, R.J., A. Srivastava and Govindjee (has no initial), *Photochem. Photobiol.* 61, 32 (1995).
31. D.C. Youvan, J.E. Hearst and B. L. Marrs, *J. Bacteriol.* 154, 748 (1983).
32. E. Weis and J.A. Berry, *Biochim. Biophys. Acta* 894, 198 (1987).
33. J.M. Fenton, and A.R. Crofts, *Photosynth. Res.*, 26, 59 (1990).
34. K. Siebke, and E. Weis, *Planta*, 196, 155 (1995).
35. E. Greenbaum, *Science* 230 (4732), 1373 and cover (1985).
36. E. Greenbaum, *J. Phys.Chem.* 92, 4571 (1988).
37. E. Greenbaum, *J. Phys.Chem.* 94, 6151 (1990).
38. E. Greenbaum, *J. Phys.Chem.* 96, 514 (1992).
39. J.W. Lee, I. Lee, P.D. Laible, T.G. Owens, and E. Greenbaum, *Biophys. J.* 69, 652 (1995). 40. J.W. Lee, I. Lee, and E. Greenbaum, *Biosensors & Bioelectronics*, (in press, 1996)
41. E. Greenbaum, "Biomolecular electronics and applications", in *Molecular biology and biotechnology: a comprehensive desk reference* R.M. Meyers Ed., (VCH Publishers Inc, New York, 1995) pp. 98-103.
42. S.G. Boxer, J. Stocker, S. Franzen and J. Salafsky, "Re-engineering photosynthetic reaction centers", in *Molecular electronic science and technology*,. A. Aviram Ed (Amer. Inst. Physics, New York, 1992) pp. 226-236

43. G.P. Wiederrecht, W.A. Sveck, M.P. Niemczyk, and M.R. Wasielewski, J. Phys. Chem., 99, 8918 (1995).
44. D. Kaill, Photonics Spectra, 29 (11), 93 (1995)
45. L. Ning, W.J. Bowyer, L.S. Daley, E.H. Piepmeier, G.A. Strobel, and J. B. Callis, Spectroscopy 11 (2) (in press, 1996).
46. Y-I Park, W.S. Chow and J. M. Anderson, Plant Cell Physiol. 36, 1163 (1995)
47. David Turner, 1995, Project Gutenberg/IBC, Illinois, Benedictine College, Lisle, Illinois. Mathematical credits digits follow the work of Scott Hemphill, with comparisons to the work of Bailey and Kanada, e-mail publication at chipmonk@eagle.ibc.edu (To proofreader this is a e-mail publication, thus we are uncertain of format and credits).

CHAPTER 7

In vivo IMAGING OF THE INTERIOR OF *Tradescantia zebrina* LEAVES BY
OPTICAL CROSS CORRELATION INTERFEROMETRY.

Li Ning¹, Zhao Lu², Larry S. Daley¹ and J. B. Callis²

¹ Dept. of Horticulture, ALS 4017, Oregon State University, Corvallis, OR 97331.

² Dept. of Chemistry, University of Washington, Seattle, WA 98195

Published in Biochemical and Biophysical Research Communications
November 1994, 205(1):638-644.

This paper is Oregon Agricultural Experiment Station Technical Paper 10588.

IN VIVO IMAGING OF THE INTERIOR OF *TRADESCANTIA ZEBRINA* LEAVES BY OPTICAL CROSS CORRELATION INTERFEROMETRY.

Li Ning¹, Zhao Lu², Larry S. Daley¹ and J. B. Callis²

¹ Dept. of Horticulture, ALS 4017, Oregon State University, Corvallis, OR 97331. ²Dept. of Chemistry, University of Washington, Seattle, WA 98195

SUMMARY

Using optical correlation interferometry, a novel method for plant sciences, we imaged *in vivo* the z-direction, perpendicular to the leaf surface, through *Tradescantia zebrina* leaves. Non-invasively we: determined number of major cell layers, followed the time sequence of decrease in cell z-axis after exposure of tissues to high salt, and observed disruption of cells caused by freezing and thawing.

INTRODUCTION

We seek non-invasive measurement inside plant leaves. Our ultimate objective is to study the biochemistry of plants *in vivo* in three dimensions (3-D) by UV, visible and near infrared spectroscopy. Since Coblenz (1) to recent times (2-8) *in situ* plant leaf spectra, has been done in quasi one dimensional form (1-D) with the x-y plane perpendicular to the light source axis plus the z-axis, depth axis, collapsed into one point. Since the 1-D approach cannot resolve patterns of structures across the lamina of the leaf

which have applied and theoretical significance we developed a two (2-D) dimensional (x-y image) spectrophotometer (9,10). 2-D images have great utility; however z-axis spectra is also important because leaf cell biochemistry is most frequently specialized in tissues perpendicular to this axis. Thus, complete optical characterization of leaves requires z-direction data.

Low-coherence reflectometry is used by some medical scientists (11-13), but novel to plant sciences. *Tradescantia* has large, well defined cells, where Robert Brown (1828) first observed protoplasmic streaming (14). *Tradescantia zebrina*, has leaves well suited to this method, since its leaves have few leaf cell layers, regularly formed and distinct, that vary in number between the silver and green bands that extend along the length of the leaf (described below).

Many approaches are available to image along the z-axis as well as the conventional x and y axes. To mechanically slice the sample into sections perpendicular to the z-axis is destructive and thus, reveals data from only one instant in time for each set of tissue slices. This, because of biological variability between tissue samples, introduces unwanted variables into the composite time sequences generated from the pooled samples. In optical tomography (e.g. 15), the straight forward use of parallel sheets of light becomes problematic for small objects. Therefore, using a microscope, one captures a series of optical slices by simply varying the focal distance; then one corrects the images for above and below plane out of focus contributions (16). The resulting stack of 2-D images can then be rendered into 3-D images using the same techniques that MRI (17) uses to make 3-D images.

One can get z-axis data by tracing photon flow through samples. A way to do this is to give a pulse of light and time photon arrival. This requires super fast electronics to measure small objects, i.e. to resolve one micron requires 4×10^{-15} s timing. Light pulses of a duration this short require very expensive, and not easily portable, laser technology (e.g. 18).

There is an alternative way: non-monochromatic light undergoes random fluctuations on a time scale set by the inverse bandwidth of the light source (19). These fluctuations can be characterized by their correlation time τ given by the equation:

$$\tau = \lambda^2 (\pi * \Delta\lambda * c)^{-1}$$

Here λ is wavelength, * indicates multiplication, and c is the speed of light, which in a vacuum is 2.998×10^8 meters per second, approximated here as $3 \times 10^8 \text{ m*s}^{-1}$. Thus, for a center wavelength of 450 nm, and a band width of 90 nm, $\Delta\lambda = 90 \text{ nm}$; we can approximate: τ as $(450 \text{ nm})^2 / (\pi * 90 \text{ nm} * 3 \times 10^8 \text{ m*s}^{-1}) = 2.38 \times 10^{-15} \text{ s}$, which is enough time resolution for a spatial resolution of better than a micron.

A fluctuating light source can replace pulse light as the probe. From linear systems theory (e.g. 20), it can be shown that one can do the equivalent to an impulse response experiment, by cross correlating the random probe beam with the output beam. It is not yet possible to perform the cross correlation in the time domain because detectors of sufficiently wide bandwidth and means to record the waveforms do not exist. Instead we use the spatial domain with a Michelson interferometer (19) as an analog computer of the cross correlation function. Such a device is available commercially (Precision Reflectance Interferometer, Model 8504A, Hewlett-Packard Co, Palo Alto, CA) implemented in a

convenient fiber optic form. This device, developed to test fiber optic instrumentation, can profile human skin in depth (13).

The sample is placed at the end of the interferometer, and replaces the usual mirror. In this case, the light will strongly constructively interfere whenever, the path lengths of the moving reference mirror and a reflecting surface in the test object are equal. This matching condition, known as the center burst, appears as a spike ("peak") in the waveform (interferogram) of intensity vs position of the reference arm. One therefore obtains a series of peaks each corresponding to a specific reflecting surface of the object. And, as the photons transverse a highly scattering medium, back scattering of light exhibits an exponential decay in space, corresponding to the exponentially declining probability that the photons penetrate a specific distance without being scattered.

MATERIALS AND METHODS

Materials and leaf manipulations *Zebrina* (*Tradescantia zebrina* Bosse, Commelinaceae), grown in a Univ. of Washington, Seattle, Botany Dept. greenhouse was picked in late August and September. Polystyrene spheres (Polysciences Inc., Warrington, PA) diameters were 0.2 microns (μm). To test the effects of hypertonicity the leaf slivers were bathed in appropriate solutions during assay. To test cell integrity conductivity measurements were taken with a standard multimeter, with the electrodes separated by 1.2 mm, then calibrated relative to NaCl solutions. Freezing experiments were done while samples were in the instrument by holding a chip of dry ice to the slide that supports the cuvette. Before and during freezing, and after thawing measurements were taken without

moving the sample. Verification of freeze damage was done in parallel experiments, as is standard, by conductivity measurements. Multiple replications of experiments were done to assure reproducibility of cross correlation data.

Instrumentation The light microscope used was a Nikon Microphot-FXA obtained from Meridian Instrument Co, Inc. (Kent, WA). A 91.4 micron diameter wire was used to calibrate tissue width. A newly constructed imaging fluorometer (Ning, et al., unpublished) was used to image fluorescence yield. The optical autocorrelation interferometer (Precision Reflectance Interferometer, Model 8504A, Hewlett-Packard Co, Palo Alto, CA) was operated at 1300 nm (21-23) illuminating the leaf from the lower surface. Data was signal averaged by instrument, and processed using MATLAB (The Math-Works, Natick, MA), Statgraphics Plus (Manugistics Inc., Rockville, MD) and PhotoFinish (Softkey International Corp., Marietta, GA).

RESULTS AND DISCUSSION

To test of the optical autocorrelative interferometer and illustrate the nature of the cross correlation functions we made a cuvette as shown in upper part of Fig. 7.1. Below this in Fig. 7.1, three sets of traces show the peaks in the cross correlation function numbered to correspond to the numbered surfaces of the cuvette. The peaks labeled with numbers without primed superscripts define the object and its dimensions, if one knows the index of refraction of the cuvette materials. The peaks labeled with numbers with primed superscripts represent multiple secondary reflections within the object. The top trace shows the cross correlation function obtained with air in the cuvette. The middle

Figure 7.1. Optical cross correlation interferometer response in model system. The model is diagramed in upper left of figure; a second diagram of the model, upper middle of the figure, shows the numbered locations of the reflection sites which correspond to peaks in the data traces; secondary reflections are indicated by numbers with superscripts ' , " , and "' . The three examples of data traces from the instrument are immediately below the diagrams of the model. The spans of the traces are indicated on x-axes. The cavities are located between peaks 2 and 3. The uppermost, middle and lowest traces correspond, respectively, to cavities filled with air, water and a suspension of 0.2 micron polystyrene spheres in water. The lowest set of traces illustrates data from two scans, with the second scan derived from analysis of a model with a longer cell length. The longer cell length displaces peak 3 to peak 3. Notice that the replacement of air by water removes the secondary reflections and also increases the apparent distance between peak 2 and peak 3, due to the increase in time that light takes to pass through water, about 1.33 x the time in air.

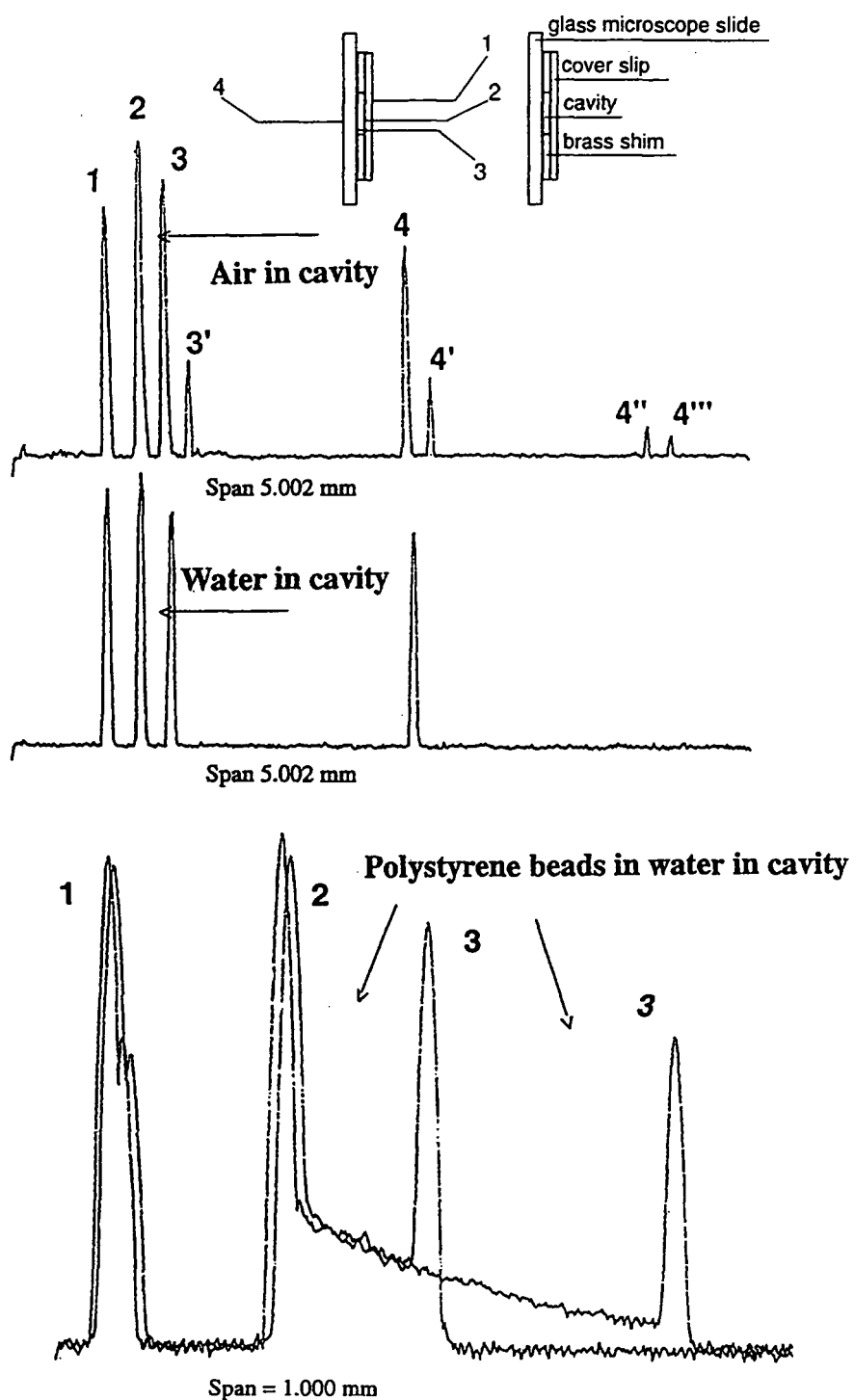


FIGURE 7.1

trace shows the cross correlation function after the cuvette has been filled with water. Now the secondary reflections are suppressed due to decrease reflectivity at glass water boundary compared to the glass air boundaries of the previous trace. The distance between peaks 2 and 3 is greater, because light travels more slowly in water than air. The lowest set of traces is from a cuvette filled with a water suspension of polystyrene microspheres; here the length scale has been expanded to show the data more clearly. In these traces, photon density declines exponentially as light transverses this scattering medium. The second, longer, trace in this part of the figure was generated using a cuvette in which the cavity dimensions have been expanded as indicated by the shift of peak 3 to peak 3'; here the decline in light follows the same exponential form, but over a longer distance.

Light micrographs show the structural differences in the transverse sections of silver and green tissues of *T. zebrina* (Fig. 7.2 left and right respectively); above the micrographs are the corresponding cross correlation images. Note the greater width of the middle layer of tissue that contains the bulk of the photosynthetic apparatus, and the doubling of upper cell layers in the green, as opposed to the silver, sections of the leaf. Notice how the cross correlation images correspond to the different structures found in these leaves. Since we get the same cross correlation images in intact leaves (not shown) it is apparent we can determine cell layers non-invasively. Fluorescence activity measurements (not shown) demonstrated that the green section is photosynthetically active and the low chlorophyll (silver) section is almost inactive.

Figure 7.3 shows a time sequence of effects of hypertonic solutions on cross correlation images. The data shown is for silver tissue and is presented in the MATLAB

Figure 7.2. Optical image fit to optical cross correlation interferometer response of *Tradescantia zebrina* leaves. This plant has well marked low chlorophyll 'silver' bands (left in figure), that extend parallel to the central vein in the direction we have assigned as y. These silver bands are separated by high chlorophyll 'green' areas which have one additional upper layer of large cells (right in figure). Leaf width is assigned to the x-direction, leaf thickness, showing different layers of cells is the z-axis. Left figure shows light micrograph of leaf x-z plane showing a cross section of a silver band; the corresponding optical cross correlation interferometer trace is superimposed. The right figure shows a light micrograph of leaf x-z plane showing a cross section of a green area, with the corresponding optical cross correlation interferometer trace. In this micrograph, cell walls not in the plane of the image appear blurred. The wire standard (and the liquid portions of the cells in the traces) appear to be larger on interferometry scale because there is no correction ($\times 1.33$) for the change of the speed of light in aqueous solutions.

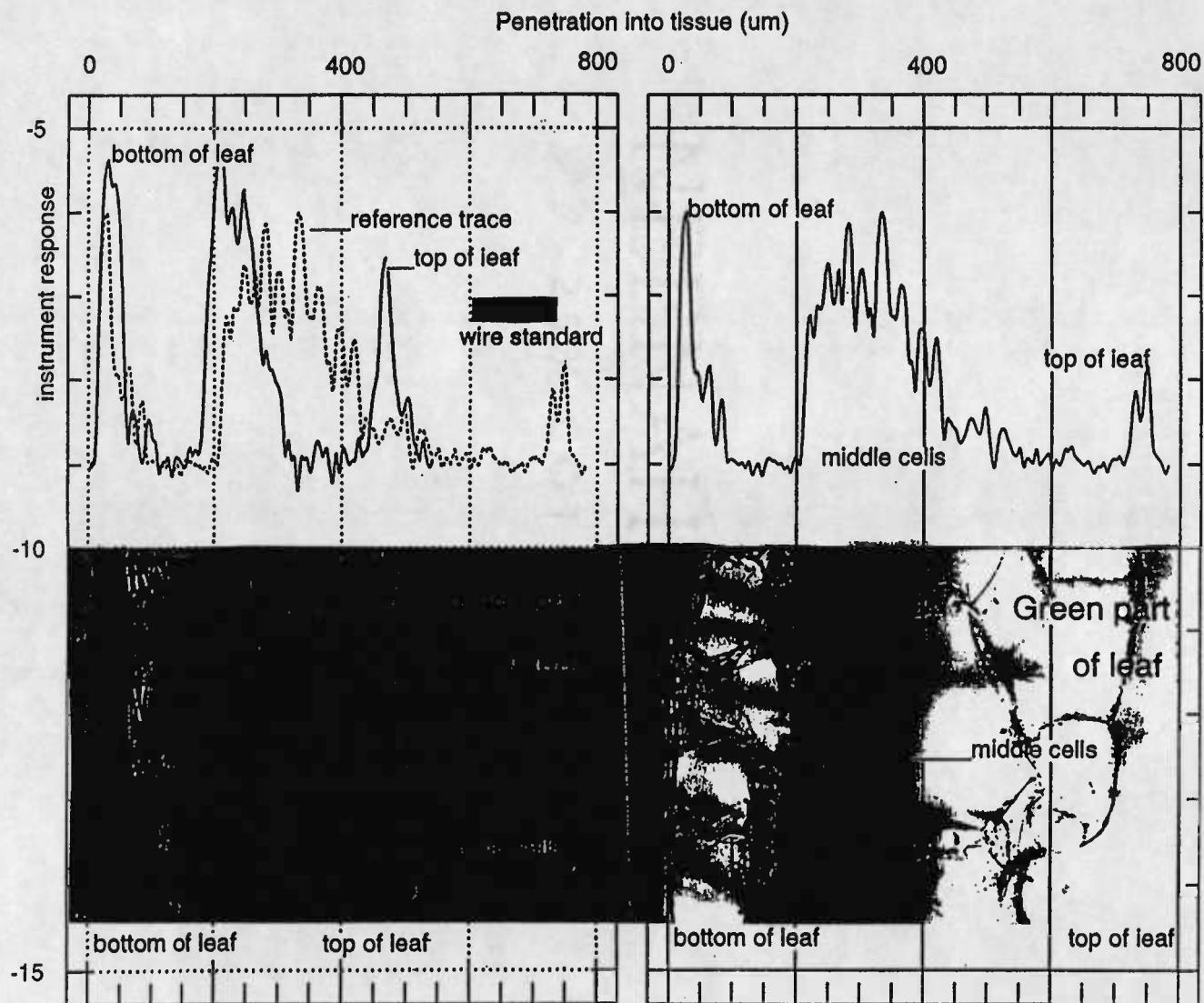


FIGURE 7.2

Figure 7.3. Time sequence histogram of optical cross correlation images (z-axis) as a silver section of the leaf immersed in 15% sodium chloride solution. The plot was prepared using Mat-lab image function and PhotoFinish.

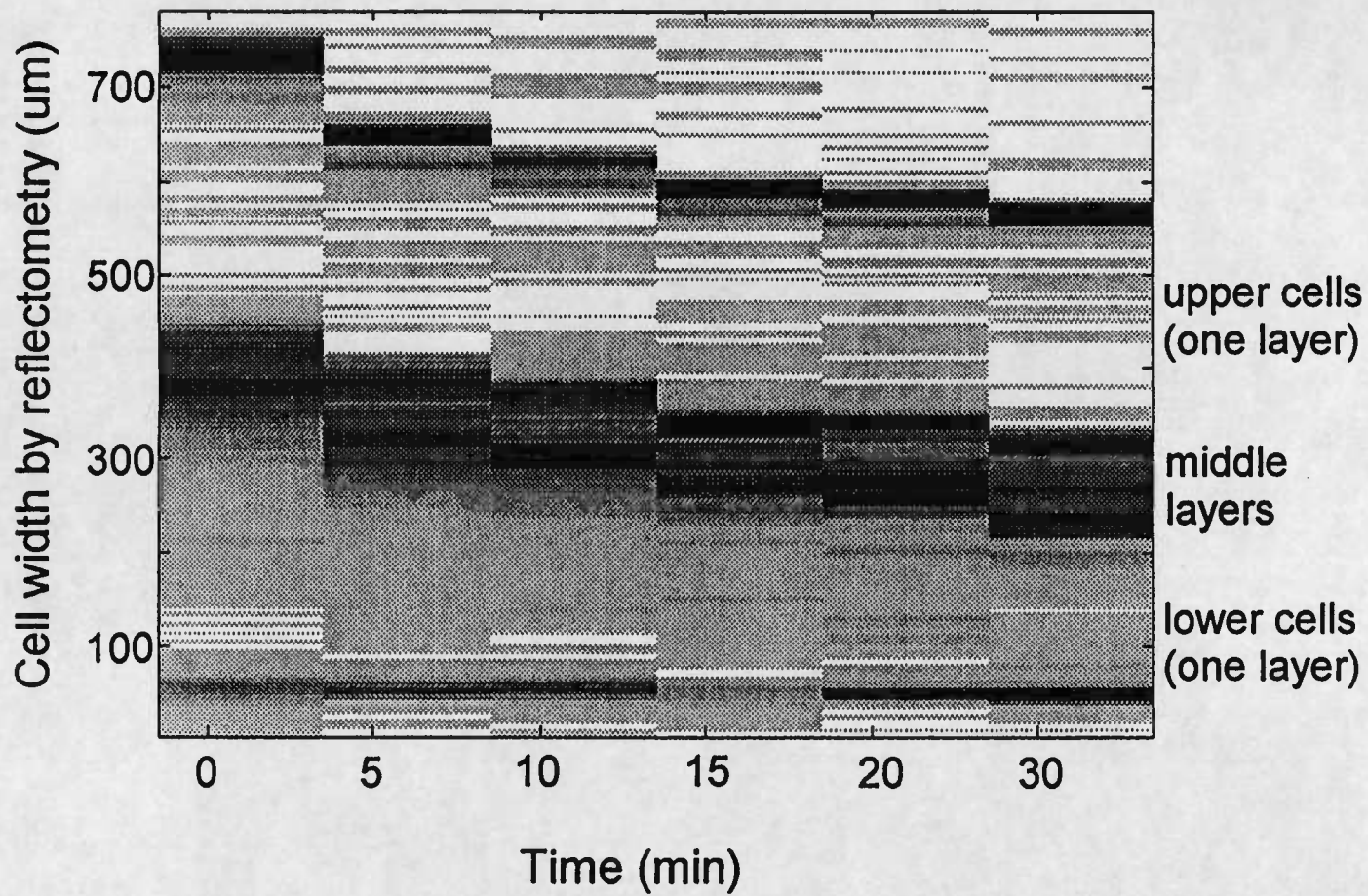


FIGURE 7.3

image function format which generates a histogram illustrating depth change with time. The darkest lines represent the most intense reflections, and correspond to peaks in Figs. 7.2 and 7.4, and thus separate the leaf depth profile into upper cells, middle layer cell, and lower cell regions. The upper unlabeled space which increases sequentially, with time, from left to right is free liquid solution above the upper layer of cells, and can be used to indicate the total loss of leaf depth. The time sequences are separated by the sequential abrupt changes in cell depth, which are referenced to lowest part of lower cells. Since the experimental variable is external high salt which takes water out of the cells, and we know that these changes require immersion in high salt solutions, it is most logical to assume that depth loss is a function of loss of cell water. Thus, we can determine that lower cells lose water more readily than upper cells, and middle cells resist dehydration. We expect this technology to be useful in our *in vivo* spectroscopic drought stress investigations.

Figure 7.4 shows optical cross correlation images of silver tissue describing the effects of freezing leaf tissue on cell z-axis. The upper part of the figure shows tissue before freezing and when frozen, notice the increase in reflectance of the lower layer of cells where the light enters, and the decrease in light reaching the upper part of the leaf. The lower part of the figure compares the fresh tissue signals with signals after thawing, illustrating the effects of mechanical damage on the middle cell layers. The increase in reflectance from the upper part of the leaf indicates that the disruption of the middle layer has allowed more light to reach the lower cells. In this process the conductivity of the external solution increased significantly as a result of spilling cell contents of thaw ruptured cells into surrounding solution. It may be possible to use this technology to

Figure 7.4. Optical cross correlation images (z-axis) of a silver section of the leaf before and after freezing, and then when thawed. The upper figure shows compares traces when fresh and frozen; the lower figure compares the fresh and thawed traces. The traces were prepared using Statgraphics Plus Q-spline plot.

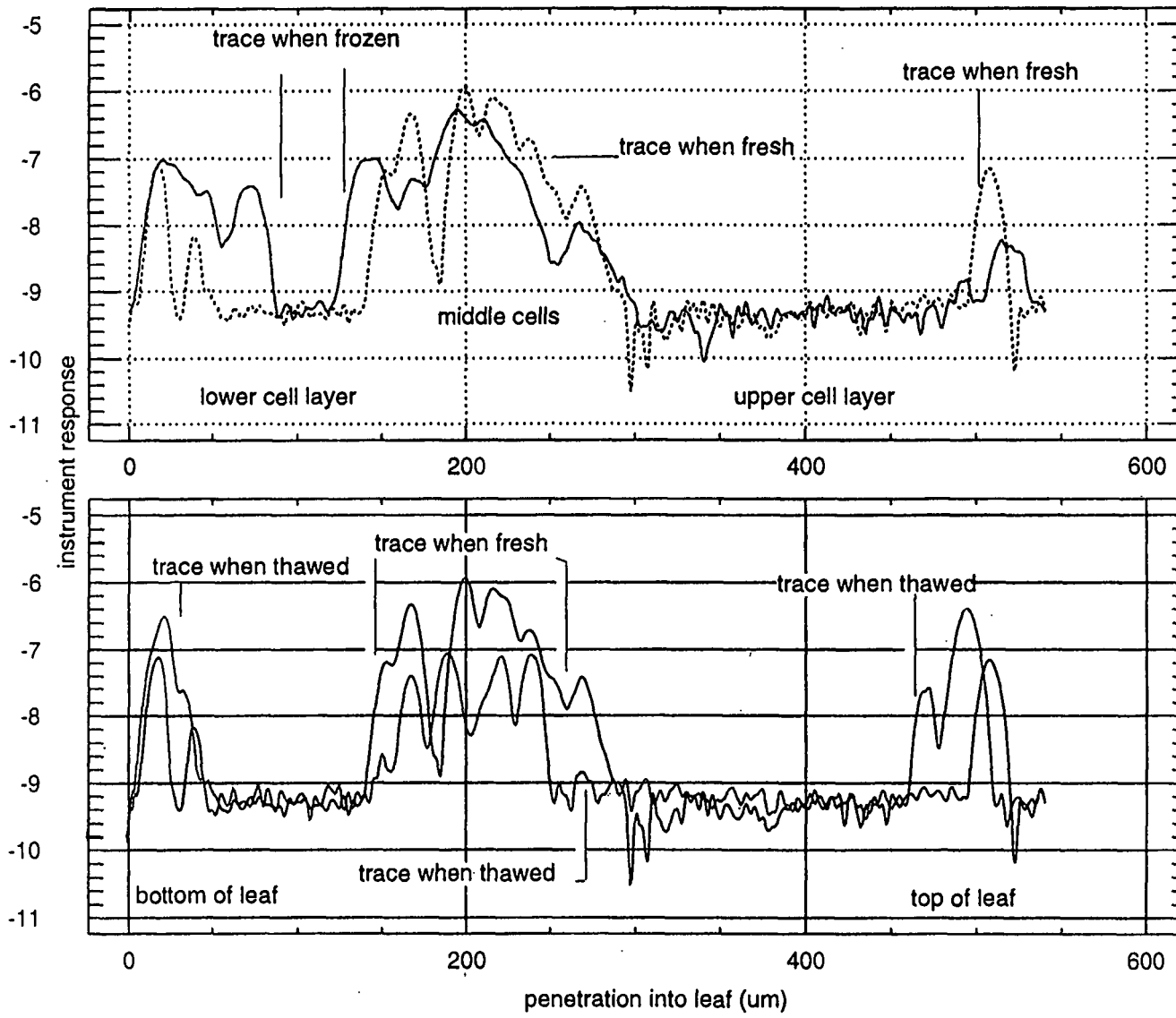


FIGURE 7.4

determine freeze damage in the field, a matter of some importance to the important plant nursery industry of Oregon.

ACKNOWLEDGMENTS

This work was supported by a grant from the Herman Frasch Foundation (332-HF92). We are grateful to Lloyd Burgess, Paul Shelly and Ines Ferreira of the Center for Process Analytical Chemistry (Chemistry Dept., Univ. of Washington, Seattle) for the loan of the instrument and instruction in its use. The instrument, a Precision Reflectance Interferometer (Model 8504A) was a generous gift from Hewlett-Packard Co (Palo Alto, CA). Stan Gartler (Medical School, Univ. of Washington, Seattle) provided instruction and use of the light microscope. We thank Douglas Ewing (Botany Dept., Univ. of Washington, Seattle) who grew and help select the experimental plant material, Gerald E. Edwards (Botany Dept., Washington State University, Pullman) for kind advice, and Natalie S. Daley for model diagrams. This paper is Oregon Agricultural Experiment Station Technical paper 10588.

REFERENCES

1. Coblentz, W.W. (1913). *Bulletin of the Bureau Standards*, 9, 283-325.
2. Shull, C.A. (1929). *Bot. Gaz.*, 87, 583-607.
3. Seybold, A. (1933). *Planta*, 18, 479-508.
4. Rabideau, G.S., French, C.S. and Holt, A.S. (1946). *Amer. J. Bot.*, 33, 769-777.
5. Butler, W.L. (1972). *Methods in Enzymology*, 24(B), 3-25.

6. Ruhle, W. and Wild, A. (1979). *Planta*, 146, 551-557.
7. Daley, L.S. (1986). *Scientia Hort.* 28, 165-176.
8. Daley, L.S. (1990). *Plant Physiol. Biochem.*, 28, 271-282.
9. Ning, L., Ozanich, R., Daley, L.S. and Callis, J. B. (1994). *Spectroscopy*, 97, 41-48.
10. Ning, L., Chozinski, A., Buban, T., Azarenko, A.N., Daley, L.S., Callis, J.B., and Strobel, G.A. (1996). *Spectroscopy* (in press).
11. Huang, D., Swanson, E.A., Lin C.P., Schumann, J.S., Stinson, W.G., Chang, W., Hee, M.R., Flotte, T., Gregory K., Puliafito, C.A. and Fujimoto J.G. (1991). Optical coherence tomography. *Science* 254, 1178- 1181
12. Hitzengerger, C.K. (1992). *Applied Optics*, 31, 6637-6642.
13. Schmitt, J.M., Knuttell, A and Bonner R.F. (1993). *Applied Optics*, 32, 6032-6042.
14. Mabberley, D.J. (1987). *The plant book*, Cambridge Univ. Press, Cambridge, England.
15. Burns, D. H. (1994). *Appl. Spectrosc.* 48(5), 12A-19A.
16. Castleman, K.R. (1979). *Digital image processing*, Prentice-Hall, Inc, Englewood Cliffs, NJ.
17. Treado, P.J., I.W. Levin and E.N. Lewis. (1994). *Appl. Spectrosc.* 48(5), 607-615.
18. Savikhin, S., Zhu, Y., Lin, S., Blankenship, R.E. and Struve, W.S. (1994). *J. Phys. Chem.* (in press).
19. Chamberlain, J. (1979). *The principals of interferometric spectroscopy*, John Wiley, New York, NY.
20. Yu, F.T.S. (1973). *Introduction to diffraction, information processing and holography*, MIT Press, Cambridge, MA.
21. Beck, P.A. (1993). *Hewlett-Packard J.* 1993 (February), 49-51.
22. Chou, H. and Sorin W.V. (1993). *Hewlett-Packard J.* 1993 (February), 52-59.
23. Booster, D.H., Chou, H., Hart, M.G., Mifsud, S.J. and Rawson, R.F. (1993). *Hewlett-Packard J.* 1993 (February), 39-48.

CHAPTER 8

CONCLUSION

The three imaging instruments used were successfully employed in novel ways to investigate biophysical, biochemical, physiological and plant pathological properties of plant germplasm *in vivo*. Two of these instruments, the imaging spectrophotometer and imaging fluorometer, were constructed for this purpose and one, the imaging interferometer, adapted from other uses. The first two instruments image in x-y planes, such as the lamina of the leaf, the third in the z-axis, perpendicular to the plane of the leaf lamina. The information obtained is summarized below.

Imaging spectrophotometer

This instrument proved capable of acquiring spectra for 31,680 positions per sample in a range of 450 to 1000 nm. Excellent quality images were obtained by application of signal averaging techniques, for instance by signal averaging ten times absorbance differences of 0.05 attenuation ($\sim A$) units can be resolved. Such resolution was found critical in the examination of plant germplasm for the effects of such stresses as plant disease.

In the future, using multivariate calibration methods such as partial least squares, calibration models of spectral properties of discrete components taken from the literature

could be used to target, and thus investigate, important germplasm properties *in vivo*. In this work it has been found that suitable subjects for these kinds of investigations are the many different kinds of chlorophyll-protein complexes (CPX) which have published spectral properties and are known to change in proportions during light adaptation, changes in plant nutritional sources, and disease. Since the instruments optical technology is non-invasive, it allows continuous examination of physiological change in the same sample. This greatly simplifies the critically important and commonly used time course experiments. Thus, it is possible that imaging spectroscopy will become a routine laboratory tool to measure plant pathological, plant physiological, biochemical and biophysical parameters and their associated histochemical change, in addition to the instruments potential in applied robotic and precision agriculture.

There are several things that could be done to improve the imaging spectrophotometer. A better CCD camera would improve spatial resolution and dynamic range, this would help especially for examination of weakly absorbing bands in the near-infrared (IR) range. With an IR sensitive camera the 900-1700 nm bands for water, starch and protein could be examined. As measurements are dependent on the speed of processing a faster computer would accelerate data acquisition.

However, in the present configuration the instrument very satisfactorily carried out the following tasks:

- **Determination of the location of mesophyll and bundle sheath *in vivo*** In sugarcane (*Saccharum officinarum* L.), a C-4 plant, patterns consistent with the resolution of bundle sheath from mesophyll cells were found using a specific image

equation. In this image equation $((A_{684\text{ nm}} - A_{700\text{ nm}}) - (A_{650\text{ nm}} - A_{638\text{ nm}})) / A_{680\text{ nm}}$, each component represents attenuance ($\sim A$) at each given wavelength.

- ***In vivo* chlorophyll b deficiency determination** This was carried out by comparisons of CPX structure and function between different hue domains of variegated leaves in imaging and standard research spectrophotometers. The plant germplasm used for this study was the ornamental perennial grass *Milium effusum* L var. *aureum* and reference was made to published spectra of OY-OG chlorophyll b deficient mutant of *Zea mays* L.

- ***In vivo* determination of root respiration** Relative respiration rates of excised plant roots was determined by measuring pH dependent absorbance of a dye-impregnated agar in which the roots were placed. The pH sensitive dye, reazurin (7-hydroxy-3H-phenoxazin-3-one 10-oxide), changed color to reveal the localized pH changes around soybean (*Glycine max* var. Yuusuzumi) root. These pH changes are consistent with the expected respiratory activities of the different parts of the root.

- ***In situ* detection of xylem development** This was done through the spectroscopic resolution of the xylem tracer dye in microphotographs of apple (*Malus domestica* Borkh. var. Red Rome) flower buds. These buds contain pigments that make the tracing of the presence of dye in the xylem impossible to detect by visual observation.

- ***In situ* determination of glucose and sucrose** This was done using as a chromophore a glucose oxidase dye coupled system, in which the sucrose was converted to glucose with the use of exogenous invertase. The plant material used was hazel (*Corylus avellana* L.) stems.

- ***In situ* determination of invertase** This was done with the same biochemicals and plant materials as immediately above, except for the addition of exogenous sucrose and the lack of addition of exogenous invertase.
- ***In vivo* effects of a pathogen** The progress of the effects of the spread of toxin during infection of the foliage of the rare and endangered nutmeg (stinking) cedar or yew of Florida (*Torreya taxifolia* Arn.) by the fungal pathogen *Pestalotiopsis microspora* was followed spectrophotometrically, the most statistically significant chromophore was water.
- **Water transportation** The time course of displacement of water by heavy water (deuterium oxide) was followed spectrophotometrically in roselle (Jamaican sorrel *Hibiscus sabdariffa* L.) leaves.
- **Measurement of biologically active light path inside leaf** The water content of actively growing plant tissues is relatively constant, thus the use of a “Rayleigh” correction plus the determination of path length utilizing the water signals near 970 nm were found useful to estimate biologically active component concentrations *in vivo*. It was shown by this method that it is possible to image the difference between CPX concentrations in living tissues.

Imaging fluorometer

A novel instrument was constructed to record the complex, two dimensional, time dependent, patterns of photosynthetically derived fluorescence that initiate immediately after illumination of a dark adapted leaf. The instrument was designed as a reversibly reconfigurable modification of the imaging spectrophotometer, in which two filters remove excitation emission overlap and the software is based upon a novel approximation of quantum yield of the fluorescence of photosystem II. A simple further reconfiguration of the instrument, which allowed imaging leaf photosynthetic fluorescence at a distance of seven meters, was used to test potential remote sensing applications. This instruments unique ability to empirically estimate quantum yield makes it specially useful in situations when the plant is in stress and the non-photochemical quenching is not inversely related to photosynthetic activity.

Using this instrument it was also demonstrated that it is possible to store, and recover digital data from living plant leaves, by utilizing the time dependent properties of the fluorescence yield of activated photosynthetic reaction centers. The mechanism most likely responsible for this phenomenon is photochemical quenching. However, while the demonstration of the recovery of digital data from a leaf is in itself interesting, we do not expect, direct, immediate, use of leaves as memory storage; although eventual use of such media should not be ruled out. We expect that more immediate utility of this method will arise in the *in vivo* selection of the best and most appropriate plant germplasm for given bioelectronic purposes. This instrument is expected to be useful to measure recovery, via

remote sensing, of transitory images of plant damage caused by the passage of wild game through a given area and thus to be useful for game management and related purposes.

Results obtained with this instrumentation include:

- **Quantum efficiency estimation.** Quantum efficiency estimation (Y') was obtained with a novel algorithm. This algorithm allows generation of a uniform image field when a undamaged leaves are used, only leaves or areas of the leaves where the photosynthetic apparatus have been impaired show damage as decrease in Y' and an interruption of the uniform image field. Unlike many previous methods leaf thickness or lack of uniformity of distribution chlorophyll have very little effect. The use of Y' will allow for more ready automated analyses of damage by such procedures as neural networks, etc.

- **Photoinduced images and storage of digital information on living leaves**

Light controls both the “light” and “dark” reactions of the photosynthetic process. Excess light causes activation of several adaptive protective mechanisms including non-photochemical quenching. Strong light, because of the time dependence of recovery from non-photochemical quenching of the photosynthetic reaction centers, significantly, but temporally, reduces photosystem II quantum yield in the area of the leaf receiving the strong light. Thus a mask with patterns of transparent and opaque areas can be used to imprint an image on a leaf. The areas of the leaf which were under the more transparent part of the mask receive excess light, suffer non-photochemical quenching, and thus have much less quantum yield; those areas of the leaf that were under the opaque areas of the mask retain most of their reaction centers unimpaired and with high quantum efficiency. On removal of the mask and measurement of fluorescence by the instrument images or

patterns of quantum efficiency can be seen. With this procedure images and data can be stored on a leaf.

- **Rapid determination of freeze damage** The imaging fluorometer can readily and immediately detect freeze damage because freezing severely affects the function of the photosynthetic apparatus. In the volatile agricultural futures market, quantitative data on the extent of freeze damage to citrus or coffee crops could promote market stability by enabling more rapid and reliable harvest size predictions.
- **Rapid determination of herbicide damage** Many herbicides act directly on the photosynthetic function others commonly have strong secondary effects on this essential process. Measurement and avoidance of herbicide drift and measurement of effectiveness of herbicide treatment are important to agricultural productivity.
- **Detection of fungal pathogen damage** Most pathogens attacking leaves rapidly affect leaf photosynthetic function and these effects are readily detected using the fluorometric instrument.
- **Measurement of fluorescence at a distance** For applied use it is important that fluorescence be detected at a distance. The instrument, with minor modifications, was able to detect changes in photosynthetic fluorescence at a distance of 7 meters.

Optical correlation interferometry

Using a commercially manufactured instrument, for a novel purpose, it was found possible to image *in vivo* in the z-direction through *Tradescantia zebrina* Bosse leaves.

With this instrument it was found possible to:

- **determine the number of major cell layers**
- **follow the time sequence of decrease in cell z-axis after the exposure of tissue to high salt**
- **observe disruption of cells caused by freezing and thawing**

Summery

From these investigations it was concluded that constructing and using instruments capable of imaging plant tissue in the x, y and z-directions is well within present technology; and use of such instruments yields much useful information about the physiology, pathology, biochemistry and biophysics of plant germplasm.

BIBLIOGRAPHY

- Abbot J. A., T.A. Campbell, and D.R. Massie, 1994, *Remote Sens. Environ.* 47:87.
- Afromowitz M.A., J.B. Callis, D.M. Heimbach, L.A. Desoto, and M.K. Norton, 1988, *IEEE Transactions on Biomedical Engineering* 35:842.
- Al-Abbas A.H., A.H., R. Barr, J.D. Hall., F.L. Crane, and M.F. Baumgardner, 1974, *Agron. J.* 66:16.
- Albers V.M., and H.V.Knorr, 1937, *Plant Physiol.* 12:833.
- Aldridge P.K., J.B. Callis, and D.H. Burns, 1990, *J. Liq. Chrom.* 13:2829.
- Anonymous, 1975, b-Fructosidase, in *Biochimica Information, II*, Boehringer Mannheim GmbH. pp. 69.
- Ashworth E.N., 1982, *Plant Physiol.*, 70:1473.
- Atkins P.W., 1991, *Quanta: a handbook of Concepts 2nd edition*. Oxford Univ. Press, Oxford, England, pp. 1.
- Baret F., V.C. Vanderbilt, M.D. Steven, and S. Jacquemound, 1994, *Remote Sens. Environ.*, 48:253.
- Barnett N.M., 1974, *Can. J. Bot.*, 52:265.
- Barthelemy L., C. Edelin, and F. Halle, 1991, Canopy architecture, in *Physiology of Trees* (A.S. RagHAVendra, ed.), John Wiley and Sons, London, pp. 1-20.
- Beck J., 1994, Patchen California Inc., Los Gatos, CA, personal communication.
- Beck P.A., 1993, *Hewlett-Packard J.* 2:49.
- Bellamy H.S., P.K. Dasgupta, J.L. Lopez, and E.L. Loree, 1995, *Spectroscopy* 10(6):50.
- Bewley J.D., and M. Black, 1994, *Seeds: physiology of development and germination*, Plenum Press, NY. pp. 445.
- Birth G.S., 1967, *Agricultural Engineering* 48:448.
- Birth G.S., and H.G. Hecht, 1987, *The physics of near-infrared reflectance, in Near-Infrared technology in the agricultural and food sciences*. (P. Williams and K. Norris, eds.) Am. Assoc. Cereal Chemists, St Paul Minnesota, pp. 1-15.
- Birth G.S., and K.H. Norris, 1965, Techn. Bul. No. 1341, *U.S.D.A* 20 pp.

- Birth G.S., and K.L. Olsen, 1964, *Amer. Soc. Hort. Sci.* 85:74.
- Black C.C., Biochemistry Department, University of Georgia, personal communication.
- Black C.C., N.W. Carnal, and W.H. Kenyon, 1982, *Compartmentation and regulation of CAM, in Crassulacean acid metabolism*, (I.P. Ting and M. Gibbs, eds.), Am. Soc. Plant Physiol., Rockville, Maryland, pp. 51-68.
- Blix S., 1961, *Agric. Hort. Genet.* 19:402.
- Bloom K., and D.W. Fawcett, 1975, *A textbook of histology*, 10th edition, W.B. Saunders Co., Philadelphia. 1033 pp.
- Bolhar-Nordenkamp H.R. and G. Oquist, 1993, "Chlorophyll Fluorescence as a Tool in Photosynthesis Research," in *Photosynthesis and Production in a Changing Environment, a Field and Laboratory Manual*, (D.O. Hall, J.M.O. Scurlock, H.R. Bolhar- Nordenkamp, R.C. Leegood and S.P. Long, Eds.), Chapman and Hall, London, Chap. 12, pp. 193:206.
- Bolhar-Nordenkamp H.R., and E.G. Lechner, 1988, "Winter Stress and Chlorophyll Fluorescence in Norway Spruce (*Picea abies* (L.) Karst)", in *Applications of Chlorophyll Fluorescence*, (H.K. Lichtenthaler Ed.), Kluwer Academic Publ., Dordrecht, Holland, pp. 173:180.
- Booster D.H., H. Chou, M.G. Hart, S.J. Mifsud and R.F. Rawson, 1993. *Hewlett-Packard J.* 2:39.
- Borggaard C., and H.H. Thodberg, 1992, *Anal. Chem.* 64:645.
- Borst A., and M. Egelhaaf, 1992, *Proc. Natl. Acad. Sci. USA* 89:4139.
- Boxer S.G., J. Stocker, S. Franzen and J. Salafsky. 1992. Molecular electronic science and technology: Re-engineering photosynthetic reaction centers. *New York: Amer. Inst. Physics.*
- Brakke T.W., J.A. Smith, and J. M. Harnden, 1989, *Remote Sens. Environ.* 29:175.
- Brown J.S. and S. Schoch, 1981, *Biochim. Biophys. Acta* 63:20.
- Brown J.S., 1983, *Photosynth. Res.*, 4:375.
- Burns D.H., J.B. Callis, and G.D. Christian, 1986, *Anal. Chem.* 58:2805.
- Burns, D. H, 1994, *Appl. Spectrosc.* 48(5):12A.
- Butler W.L., 1962, *J. Opt. Soc. of Amer.* 52:292.
- Butler W.L., 1964, *Ann. Rev. Plant Physiol.* 15:451.

- Butler W.L., 1972, *Methods in Enzymology*, 24(B):3.
- Butler W.L., and K.H. Norris, 1962, *Modern methods of plant analysis*, 5:51.
- Butler W.L., K.H. Norris, H.W. Siegelman, and S.B. Hendricks, 1959, *Proc. Natl. Acad. Sci. USA* 45:1703.
- Callis J.B., and A.P. Burkner, 1983, *ACS Symp. Ser.* 236:233.
- Cantor C.R., and P.R. Schimmel, 1980, *Biophysical Chemistry* (Freeman and Company, New York, 1980) 846 pp.
- Card D.H., D.L. Peterson and P.A. Matson, 1988, *Remote Sens. Envir.*, 26:123.
- Carter G.A., 1991, *Amer. J. Bot.* 78:916.
- Castleman K.R., 1979, *Digital image processing*, Prentice-Hall, Inc, Englewood Cliffs, NJ.
- Cecchi G., P. Mazzinghi, L. Pantani, R. Valentini, D. Tirelli and P. De Angelis, 1994, *Remote Sens. Environ.* 47:18.
- Chamberlain J., 1979, *The principals of interferometric spectroscopy*, John Wiley, New York, NY.
- Chappelle E.W., and H. Litchenthaler, 1994, *Remote Sens. Environ.* 47:1.
- Chargaff E. and J. N. Davison, 1955, *Nucleic acids: Chemistry and Biology* (Academic Press. New York, London).
- Chen C., J.S. Cameron, and S.F. Klauer, 1990a, *HortScience* 25:1166.
- Chen C., J.S. Cameron, S.F. Klauer, and P.W. Foote, 1992, *Plant Physiol. Biochem.*, 30:71.
- Chen C., L.S. Daley and W.E. Kronstadt, 1990b, *Plant Physiol. Biochem.* 28(2):259.
- Chou H. and Sorin W.V., 1993, *Hewlett-Packard J.* 2:52.
- Coblentz W.W., 1913, *Bull. Bureau Standards*, 9:283.
- Cockburn W., 1981, *Plant Cell. Envir.*, 4:417.
- Corlett J.E., H.G. Jones, J.M. Masojidek and A. Massacci, 1992, *Photosynthetica* 27:257.
- Cramer W.A., and D.B. Knaff, 1991, Energy Transduction, in *Biological Membranes*, Springer- Verlag, New York, Chap. 3, p. 93.

- Curcio J.A., and C.C. Petty, 1951, *J. Optical Society of America* 41:302.
- Cure W.W., 1989, *Proc. Amer. Soc. Photogrammetric Eng.* 3:181.
- Curran P.J., J.L. Dungan, B.A. Maclee, S.E. Plummer, and D.L. Peterson, 1992, *Remote Sens. Environ.* 39:153.
- Daley L.S., 1994, unpublished data.
- Daley L.S., 1986a, *Scientia Hort.* 28:165.
- Daley L.S., 1990, *Plant Physiol. Biochem.* 28(2):271.
- Daley L.S., and K.C. Nichols, 1987a, *Plant Physio. Biochem.* 25:467.
- Daley L.S., and R.G.S. Bidwell, 1977, *Plant Physiol.*, 60:109.
- Daley L.S., J.M. Montano, R.A. Menendez, A.H. Soeldner, and R.B. Boone, 1987b, *Spectroscopy* 2(9):32.
- Daley L.S., J.R. Powell, G.A. Strobel, R.B. Boone, J. Postman, M. Willie, and J.H. Brown, 1988, *Plant Physiol. Biochem.* 26:683.
- Daley L.S., M.M. Thompson, W.M. Proebsting, J. Postman, and B.R. Jeong, 1986b, *Spectroscopy* 1(7):28.
- Daley L.S., O. Jahn, and C. Guttridge, 1987c, *Photosynth. Res.* 11:183.
- Daley L.S., P. Carrol, and H. Mussell, 1979, *Biochem. J.*, 179:719.
- Daley L.S., P.J. Breen and P. Mohanty, 1987d, *Spectroscopy* 2(3):32.
- Daley L.S., R.A. Menendez and R.L. Stebbins, 1987e, *J. Environ. Hort.* 5:25.
- Daley L.S., 1986c, *Scientia Hort.* 28:165.
- Daley P.F., K. Raschke, J.T. Ball, and J.A. Berry, 1989, *Plant Physiol.* 90:1233.
- David T., 1995, Project Gutenberg/IBC, Illinois, Benedictine College, Lisle, Illinois. Mathematical credits digits follow the work of Scott Hemphill, with comparisons to the work of Bailey and Kanada, e-mail publication at chipmonk@eagle.ibc.edu (To proofreader this is a e-mail publication, thus we are uncertain of format and credits).
- Debye P., 1947, *J. Phys. Colloid. Chem.* 51:8.

- Delouche J.C., 1974, *Maintaining soybean seed quality*, in *Soybean, production, marketing and use* (Bulletin Y-69 National Fertilizer Development Center, Tennessee Valley Authority, Muscle Shoals, Alabama) pp. 46-62.
- Demmig A.B. and W.W. Adams, 1996, *Trends in Plant Sciences* 1:21.
- Dickson R.E., 1991, Assimilate distribution and storage, in *Physiology of trees* (A.S. Raghavendra ed.), John Wiley & Sons, Inc., NY. p. 51-85
- Edner H., J. Johansson, S. Svanberg and E. Wallinder, 1994, *Applied Optics*, 33:2471.
- Edwards G., and D. Walker, 1983, *C₃, C₄: Mechanism, and Cellular and Environmental Regulation, of Photosynthesis*. (Univ. California Press, Berkeley).
- Edwards G.E., and N.R. Baker, 1993, *Photosynthesis Research* 37:89.
- Ehleringer J.R., and R.K. Monson, 1993, *Ann. Rev. Ecol. Sys.*, 24:411.
- Ellis J.W., and J. Bath, 1938, *J. Chem. Phys.* 6:723.
- Ellis M.B., 1971, *Dermatiaceous Hyphomycetes*, Commonwealth Mycological Institute, Surrey, England.
- Elvidge C.D., Z. Chen, and D.P. Groeneveld, 1993, *Remote Sens. Environ.* 44:271.
- Eskelsen S.R., G.D. Crabtree, R.B. Boone, and L.S. Daley, 1989, *Proc. Western Soc. Weed Sci.* 42:44.
- Eskelsen S.R., G.D. Crabtree, R.B. Boone, G.M. Volk, L. Ning and L.S. Daley, 1994, *Spectroscopy* 7(2):34.
- Faust M., D. Liu, M.M. Millard and G.W. Stutte, 1991, *HortSci* 26:887.
- Feng W., L. Ning, L.S. Daley, Y. Moreno, A. Azarenko and R.S. Criddle, 1994a, *Plant Physiol. Biochem* 32:319.
- Feng W., L. Ning, L.S. Daley, Y. Moreno, A. Azarenko and R.S. Criddle, 1994b, *Plant Physiol. Biochem* 32(4):591.
- Fenton T.J., and A. R. Crofts, 1990, *Photosynth. Res.* 26:59.
- Ferguson W.J., K.I. Braunschweiger, W.R. Braunschweiger, J.R. Smith, J.J. McCormick, C.C. Wasmann, N.P. Jarvis, D.H. Bell, and N.E. Good, 1980, *Analytic. Biochem.*, 104:300.
- Fisher H.H., R.A. Menendez, L.S. Daley, D. Robb-Spencer, and G.D. Crabtree, 1987, *Weed Sci* 35:333.

- French C.S., J.S. Brown, and M.C. Lawrence, 1972, *Plant Physiol.* 48:421.
- Ganapol B., L. Johnson, P. Hammer, C. Hlavka, D. Peterson, and F. Baret, 1995, *A new within-leaf radiative transfer model: preliminary results* (poster presented at the NASA Remote sensing Science Workshop, NASA/GSFC 27 Feb-1, March, 1995).
- Gao B.C., and A.F.H. Goetz, 1994, *Remote Sens. Environ.* 52:155.
- Gardea A.A., L.S. Daley, R.L. Kohnert, A.H. Soeldner, L. Ning, P.B. Lombard, and A.N. Azarenko, 1993, *Spectroscopy* 8(1):27.
- Gardea A.A., L.S. Daley, R.L. Kohnert, A.H. Soeldner, L. Ning, P.B. Lombard, and A.N. Azarenko, 1994a, *Scientia Hort.* 56:339.
- Gardea A.A., Y.M. Moreno, A.N. Azarenko, P.B. Lombard, L.S. Daley and R.S. Criddle, 1994b, *J. Amer. Soc. Hort. Sci.* 119:756.
- Genty B., and S. Meyer 1994, *Aust. J. Plant Physiol.* 22:277.
- Ghirardi M.L., and A. Melis, 1988, *Biochim. Biophys. Acta* 932:130.
- Gianelli M.L., D.H. Burns, J.B. Callis, G.D. Christian, and N.H. Andersen, 1983, *Anal. Chem.* 55:1858.
- Gibson A., 1982, *The anatomy of succulence, in Crassulacean acid metabolism* (I.P. Ting and M. Gibbs, eds.) Am. Soc. Plant Physiol., Rockville, Maryland, pp. 1-17.
- Gilmore A.M., T.L. Hazlett, and Govindjee, 1995, *Proc. Natl. Acad. Sci. USA* 92:2273.
- Good N.E., and S. Izawa, 1972, *Methods in Enzymology*, 24(B):53.
- Good N.E., G.D. Winget, W. Winter, T.N. Connolly, S. Izawa, and R.M.M. Singh, 1966, *Biochemistry.*, 5:467.
- Greenbaum E. J., 1988, *Phys.Chem.* 92:4571.
- Greenbaum E. J., 1990, *Phys.Chem.* 94:6151.
- Greenbaum E. J., 1992, *Phys.Chem.* 96:514.
- Greenbaum E., 1985, *Science* 230(4732):1373 and cover.
- Greenbaum E., 1995, *Molecular biology and biotechnology: Biomolecular electronics and applications*, VCH Publishers, Inc. NY.
- Greene B.A., L.A. Staehelin, and A. Melis, 1988, *Plant Physiol.* 87:365.
- Griffiths H., 1992, *Plant Cell. Envir.*, 15:1051.

- Gunther K.P., H.-G Dahn and W. Ludeker, 1994, *Remote Sens. Environ.* 47:10.
- Guo W.W., W.M. Proebsting, S.W. Potter, L.S. Daley, and J.R. Potter, 1987, *Plant Physiology* 85:1089.
- Hamilton J.O.C., 1994, The bug that's eating wine country, *Business Week*, (November 14), pp. 14E4-14E8.
- Hamilton M.K., C.O. Davis, W.J. Rhea, S.H. Pilorz, and K.L. Carder, 1993, *Remote Sens. Environ.* 44:217.
- Hari P., E. Nikinmaa, and E. Korpilahti, 1991, *Canopy, Photosynthesis, and Growth in Physiology of Trees* (A.S. Raghavendra, editor, John Wiley and Sons, London) pp. 419-439.
- Hartmann H.T., D.E. Kester, and F.T. Davies, 1990, *Plant propagation: principals and practices* (5th edition, Prentice Hall, Eaglewood Cliffs, New Jersey) 647 pp.
- Havaux M., and R. Lannoye, 1984, *Photosynthetica* 18:117.
- Hay F., and P.M. Syngé, 1975, *The color dictionary of garden plants with house and greenhouse plants* (Compact edition. Bloomsbury Books (Penguin), London) 584 pp.
- Heinz D.J., R.V. Osgood, and P.H. Moore, 1994, *Sugarcane, in Encyclopedia of Agricultural Science* (Academic Press, NY) 4:225.
- Hitzenberger C.K. 1992. *Applied Optics*, 31:6637.
- Hiyama T., and B. Ke, 1972, *Biochim. Biophys. Acta*, 267:160.
- Hoque E., and G. Remus, 1994, *Remote Sens. Environ.* 47:77.
- Horton P., and A. Hague, 1988, *Biochem. Biophys. Acta* 932:107.
- Huang D., E.A. Swanson, C.P. Lin, J.S. Schumann, W.G. Stinson, W. Chang, M.R. Hee, T. Flotte, K. Gregory, C.A. Puliafito, and J.G. Fujimoto, Optical coherence tomography. *Science* 254:1178.
- Hunt R., 1982, *Plant Growth Curves* (Edward Arnold Ltd, London), p.115.
- Ing G., ReportING Wish list, 1994, Good Fruit Grower. 45(14):61, Proof reader yes it is ReportING, it is a pun on authors name.
- Ishida N., T. Kobayashi, M. Koizumi, and H. Kano, 1989, *Agric. Biol. Chem.*, 53:2363.
- Jacobsen K.R., D.G. Fisher, A. Maretzki, and P.H. Moore, 1992, *Bot. Acta*, 105:70.

- Jeong B.R., L.S. Daley, D.G. Smith, R.B. Boone, and E.J. Zais, 1988a, *Spectroscopy* 3(2), 26.
- Jeong B.R., L.S. Daley, J. Postman, W.M. Proebsting and F.J. Lawrence, 1988b, *Photochem. Photobiol.* 47:91.
- Jeschke W.D., 1984, K^+ - Na^+ exchange at cellular membranes, intracellular compartmentation of cations, and salt tolerance, in *Salinity tolerance of plants* (R.C. Staples and G.M. Toenniessen eds.), John Wiley NY., pp. 37-66.
- Johnson G.A., J. Brown and P.J. Kramer, 1987, *Proc. Natl. Acad. Sci. U.S.A.*, 84:2752.
- Jordan E.G., O.V. Zatsepina, and P.J. Shaw, 1992, *Chromosoma* 101(8):478.
- Kaill D., 1995, *Photonics Spectra*, 29(11):93.
- Karukstis K. K., 1991, Fluorescence as a physical probe of the photosynthetic apparatus, in *Chlorophylls*, (Scheer H. ed.), CRC Press, Boca Raton, Florida, pp. 769-795.
- Kautsky H. and A. Hirsch, 1934, *Biochem. Zeitschrift* 274:423.
- Krajicek M., and M. Vrbova, 1994, *Remote Sens. Environ.* 47:51.
- Kraus G.H., and E. Weis, 1991, *Annu. Rev. Plant Physiol. Molec. Biol.* 42:313.
- Latimer P., 1984, *Photochem. Photobiol.* 40:193.
- Lavorel J., and A.L. Etienne, 1977, "In Vivo Chlorophyll Fluorescence," in *Topics in Photosynthesis*, 2. (Barber J. ed.), Elsevier, Amsterdam, p. 203-268.
- Lee J., X. Yang, M. Schwartz, G. Strobel, and J. Clardy, 1995, *Chemistry and Biology* 2(11):721.
- Lee J.W. I. Lee, P.D. Laible, T.G. Owens, and E. Greenbaum, 1995, *Biophys. J.* 69:652.
- Lee J.W., I. Lee, and E. Greenbaum, 1996, *Biosensors & Bioelectronics* (in press).
- Lichtenthaler H.K., 1987, *J. Plant. Physiol.*, 131:101.
- Ling P.P., and V.N. Ruzhitsky, 1992, *Acta Hort.* 319:607.
- Long S.P., S. Humphries and P.G. Falkowski, 1994, *Annu. Rev. Plant Physiol. Plant Mol. Biol.* 45:633.
- Luttge U., 1993, *New Phytol.* 125:59.
- Luttge U., and J.A.C. Smith, 1984, *Structural, biophysical and biochemical aspects of the role of leaves in plant adaptation to salinity and water stress*, in *Salinity tolerance*

- of plants* (R.C. Staples and G.M. Toenniessen eds.), John Wiley New York, pp. 125-150.
- Mabberley D.J., 1993, *The plant-book*, Cambridge Univ. Press., Cambridge, England, 707 pp.
- MacRobbie E.A.C., 1987, *Ionic relations in guard cells*, in *Stomatal function*, E. Zeiger, G.D. Farquhar, I.R. Cowan, eds.), Stanford Univ. Press, pp. 125-162.
- Martens H., and T. Naes, 1989, *Multivariate calibration*, John Wiley and Sons Ltd., London, 419 pp.
- Mawson B.T., P.J. Morrissey, A. Gomez and A. Melis, 1994, *Plant Cell Physiol.* 35:341.
- McCain D.C., T.C. Selig, and Govindjee, 1984, *Proc. Natl. Acad. Sci. U.S.A.*, 81:748.
- McMurtrey J.E., E.W. Chappelle, M.S. Kim, J.J. Meisinger and L.A. Corp, 1994, *Remote Sens. Environ.* 47:36.
- Meade G.P., and J.C.P. Chen, 1977, *Cane sugar handbook 10th edition*, Wiley, New York.
- Mestre H., 1935, *Cold Spring Harbor symposia on quantitative biology.* 3:191.
- Methy M., A. Olivoso and L. Trabaud, 1994, *Remote Sens. Environ.* 47:42.
- Milburn J.A., and J. Kallarackal, 1991, *Sap exudation*, in *Physiology of Trees*, (A.S. Raghavendra ed.), John Wiley, NY., pp. 385-402.
- Moore P.H., and D.J. Cosgrove, 1991, *Plant Physiol.* 96:794.
- Mott K.A., Z.G. Cardon and J.A. Berry, 1993, *Plant Cell Environ.* 16:25.
- Müller N.J.C., 1874, *Jahrbuch wiss Botanik* 9:42.
- Murken D.W. 1974, *Maintaining soybean quality*, in *Soybean, production, marketing and use*, Bulletin Y-69, National Fertilizer Development Center, Tennessee Valley Authority, Muscle Shoals, Alabama, pp. 98-103.
- Murray I., and P.C. Williams, 1987, Chemical principles of near-infrared technology, in *Near-Infrared Technology in the Agricultural and Food Industries* (P. Williams and K. Norris, eds. Amer. Assoc. Cereal Chemists, Inc., St Paul, Minnesota) pp. 17-34.
- Ning L, L.S. Daley, Zhao Lu and J. B. Callis, 1994a, *Biochem. Biophys. Res. Communic.* 205(1):638.

- Ning L., G. E. Edwards, G.A. Strobel, L.S. Daley, and Callis, J. B., 1995a, *Applied Spectroscopy*, 48:1381.
- Ning L., R. Ozanich, L.S. Daley and J.B. Callis, 1994b, *Spectroscopy* 9(7):41.
- Ning L., L.S. Daley, W.J. Bowyer, E.H. Piepmeier, G.A. Strobel, and J. B. Callis, 1996a, *Spectroscopy* 11(3):34 and 11(4):68. .
- Ning, L., J.D.S. Danielson, A. Chozinski, T. Buban, A. N. Azarenko, L.S. Daley, J.B. Callis, and G.A. Strobel, 1995b, *Spectroscopy* (in press).
- Nobel P.S., 1983, *Biophysical plant physiology and ecology*, Freeman and Company, New York, 608 pp.
- Norris K.H., and J.R. Hart, 1965, in *Principles and methods of measuring moisture in liquids and solids*, vol. 4 (A. Wexler, ed., Reinhold, NY.) pp. 19-25.
- Omasa K., 1992, *Acta Hort.* 319:653.
- Omasa K., K. Shimazaki, L. Aiga, W. Larcher and M. Onoe, 1987, *Plant Physiol.* 84:748.
- Osmond C.B., J.A. Berry, S. Balachandra, C. Buchen-Osmond, P.F. Daley, and R.A. Hodgson, 1990, *Bot. Acta* 103:226.
- Otto M., and W. Wegscheider, 1985, *Analyt. Chem.*, 57:63.
- Outlaw W.H., 1987, *An introduction to carbon metabolism in guard cells, in Stomatal function*, (E. Zeiger, G.D. Farquhar, I.R. Cowan, eds.), Stanford Univ. Press, pp. 115-123.
- Outlaw W.H., S.A. Springer, and M.C. Tarczynski, 1985, *Enzyme assays at the single-cell level: real-time, quantitative, and using natural substrate in solution, in Regulation of carbon partitioning in photosynthetic tissue* (R. L. Heath and J. Preiss, eds.), Amer. Soc. Plant Physiol., Rockville, Maryland, pp. 162-177.
- Ozanich R.M., M.I. Schrattenholzer, and J.B. Callis, 1992, Non-invasive determination of moisture and oil content of wheat-flour cookies, *Amer. Chem. Soc. Symp.*, Series analytic: biosensor design and application (P.R. Mathewson and J.W. Findley ed.) 511:137.
- Panford J.A., 1987, *Applications of near-infrared reflectance spectroscopy in North America, in Near-Infrared Technology in the Agricultural and Food Industries*. (P. Williams and K. Norris, eds.), Amer. Assoc. Cereal Chemists, Inc., St Paul, Minnesota, pp. 201-211.

- Papageorgiou G., 1975, "Chlorophyll Fluorescence: an Intrinsic Probe of Photosynthesis," In *Bioenergetics of Photosynthesis*, (Govindjee ed.), Academic Press, New York, p. 319-371.
- Park Y., W.S. Chow and J. M. Anderson, 1995, *Plant Cell Physiol.* 36:1163.
- Pirenne M.H., 1967, *Vision and the Eye*, Chapman and Hall Ltd, London, p. 41-56. 224 pp.
- Powles S.B., 1984, *Ann. Rev. Plant Physiol.* 35:14.
- Pratt R.M., 1958, Florida guide to citrus insects, diseases and nutritional disorders in color, *Univ. Florida Agric. Exp. Stat.*, Gainesville, FL.
- Princeton Instruments, Inc., 1994, *Catalog for high performance digital CCD cameras*, Trenton, New Jersey, 109 pp.
- Rabideau G.S., C.S. French, and A.S. Holt, 1946, *Amer. J. Bot.*, 33:769.
- Racker E., 1976, *A new look at mechanisms in bioenergetics*, Academic Press, New York, Chap. 1, p. 22.
- Robinson J.M., and C. Baysdorfer, 1985, R.L. Heath and J. Preiss, eds. *Amer. Soc. Plant Physiol.*, Rockville, Maryland, pp. 333-357.
- Rosenthal R.D., 1994, Futrex inc., Gaithersburg, Maryland, personal communication.
- Rudolph F.B., and H.J. Fromm, 1983, Plotting methods for analyzing enzyme rate data, in *Contemporary enzyme kinetics and mechanism*. (D. L. Purich, ed.), Academic Press, New York, pp. 53-73
- Ruhle W. and A. Wild, 1979, *Planta*, 146:551.
- Savikhin S., Y. Zhu, S. Lin, R.E. Blankenship, and W.S. Struve, 1994, *J. Phys. Chem.* (in press).
- Schmitt J.M., A. Knuttell, and R.F. Bonner, 1993, *Applied Optics*, 32:6032.
- Schmuck G. and I. Moya, 1994, *Remote Sens. Environ.* 47:72.
- Schreiber U., U. Schiliwa and W. Bilger, 1986, *Photosynth. Res.* 10:51.
- Scopel A.L., C.L. Ballare, and S.R. Radosevich, 1994, *New Phytol.* 126:145.
- Seybold A., 1933, *Planta*, 18:479.
- Shimizu H., and M. Yamazaki, 1992, *Acta Hort.* 319:641.

- Shull C.A., 1929, *Bot. Gaz.*, 87:583.
- Siebke K., and E. Weis, 1995, *Planta*, 196:155.
- Sinadze P.S., National Academy of Sciences, Tbilisi, Georgia, personal communication, 1977..
- Skulachev V.P., 1992, *Molecular mechanisms in bioenergetics: Chemiosmotic systems and the basic principles of cell energetics*, Elsevier, Amsterdam.
- Slocombe S.P., G.C. Whitelam and W. Cockburn, 1993, *Plant Cell. Envir.*, 16:403.
- Smillie R.M., 1979, "The Useful Chloroplast: a New Approach for Investigating Chilling Stress in Plants", in *Low Temperature Stress in Crop Plants*, (J.M. Lyons, D. Graham and J.K. Raison ed.), Academic Press, New York, p. 187-202.
- Stanley R.G., and W.L. Butler, 1961, *How long can a seed remain alive, in Seeds, the yearbook of agriculture* (USDA, Washington, DC) pp. 94-99.
- Stone J.K., J.N. Pinkerton, and K.B. Johnson, 1994, *Mycologia* 86:674.
- Strasser R.J., A. Srivastava and Govindjee (has no initial), 1995, *Photochem. Photobiol.* 61:32.
- Sutton B.C., 1980, *The Coelomycetes* (Commonwealth Mycological Institute, Surrey, England) 696 pp.
- Taiz L. and E. Zeiger, 1991, *Plant Physiology*, Benjamin/Cummings Pub. Co., Inc., Redwood City, California, Chap. 8-10, p. 177.
- Tecsi L.I., A.J. Maule, A.M Smith and R.C. Leegood, 1994, *Plant J.* 5:837.
- Ting I.P., 1995, Botany Department, University of California, Riverside, personal communication.
- Treado P.J., I.W. Levin and E.N. Lewis, 1994, *Appl. Spectrosc.* 48(5):607.
- Valentini R., G. Cecchi, P. Mazzinghi, G. Scarascia Mugnozza, G. Agati, M. Bazzani, P. De Angelis, F. Fusi, G. Matteucci and V. Raimondi, 1994, *Remote Sens. Environ.* 47:29.
- Vane G., and A.F.H. Goetz, 1993, *Remote Sens. Environ.* 44:117.
- Vernon D.M., J.A. Ostrem and H.J. Bohnert, 1993, *Plant Cell. Envir.*, 16:437.
- Vickery H.B., 1957, *Plant Physiol.*, 32:220.

- Wagniere G.H., 1993, *Linear and nonlinear optical properties of molecules*, Verlag Helvetica Chimica Acta, Basel, Switzerland, pp. 17.
- Walker J.C., 1957, *Plant Pathology*, 2nd edition, McGraw-Hill, New York, 707 pp.
- Warmund M.R., B.H. Barritt, J.M. Brown, K.L. Schaffer, and B.R. Jeong, 1993, *J. Amer. Soc. Hort. Sci.*, 118:92.
- Weis E., and J.A. Berry, 1987, *Biochim. Biophys. Acta* 894:198.
- Wiederrecht G.P., W.A. Sveck, M.P. Niemczyk, and M.R. Wasielewski, 1995, *J. Phys. Chem.*, 99:8918.
- Williams P. and K. Norris, 1987, *Near-Infrared Technology in the Agricultural and Food Industries*. (Amer. Assoc. Cereal Chemists, Inc., St Paul, Minnesota) 333 pp.
- Wold S., A. Ruhe, H. Wold, and W. Dunn, 1984, *SIAM J. Sci. Stat. Comput.*, 5:735.
- Wolf R.F.E., K.H. Lam, E.L. Mooyaart, R.P. Bleichrodt, P. Nieuwenhuis and J.M. Schakenraad, 1992, *Laboratory Animals* 26(3):222.
- Wyatt P.J., 1994, *American Lab.* 1994(3):25.
- Yoder B.J. Daley L.S., 1990, *Spectroscopy* 5(8):44.
- Youvan D.C., J.E. Hearst and B. L. Marrs, 1983, *J. Bacteriol.* 154:748.
- Yu F.T.S., 1973, *Introduction to diffraction, information processing and holography*, MIT Press, Cambridge, MA.
- Yvon J. 1994, Div. of Instruments, SA, *Guide for spectroscopy*, Edison, New Jersey and Cedex, France, 264 pp.
- Zeiger E., G. Farquhar, and L. Cowan, 1987, *Stomatal function*, Stanford Univ. Press, Stanford, CA 503 pp.
- Zhang M., M. Fabian, H. Mantsch, H.H. and H.J. Vogel, 1994, *Biochemistry* 33(36), 10:833.